



UNIVERSITEIT VAN PRETORIA  
UNIVERSITY OF PRETORIA  
YUNIBESITHI YA PRETORIA

**SLOW RELEASE OF MOSQUITO REPELLENTS FROM  
MICROPOROUS POLYOLEFIN STRANDS**

by

**António Benjamim Mapossa**

Thesis submitted in partial fulfilment of the requirements for the degree of

**Doctor of Philosophy**

**in**

**Chemical Technology**

In the Faculty of Engineering, Built and Environment and Information

Technology

University of Pretoria

Pretoria

2019

## **DECLARATION**

**I, António Benjamim Mapossa, student No. 16389523,** do hereby declare that this research is my original work and that to the best of my knowledge and belief, it has not been previously in its entirety or in part been submitted and is not currently being submitted either in whole or in part at any university for a degree or diploma, and that all references are acknowledged.

**SIGNED** on 6th June 2019

A handwritten signature in black ink, consisting of a large, stylized 'A' followed by a 'B' and a horizontal line extending to the right.

---

AB. Mapossa



UNIVERSITEIT VAN PRETORIA  
UNIVERSITY OF PRETORIA  
YUNIBESITHI YA PRETORIA

# **SLOW RELEASE OF MOSQUITO REPELLENTS FROM MICROPOROUS POLYOLEFIN STRANDS**

**Author:** António Benjamim Mapossa

**Supervisor:** Prof. Walter W. Focke

**Degree:** PhD (Chemical Technology)

**Department:** Chemical Engineering

## **SYNOPSIS**

Malaria is a principal cause of illness and death in countries where the disease is endemic. The indoor residual sprays of insecticides and indoor use of long-lasting insecticide-treated nets (LLINs) are practical methods of the prevention of malaria recommended by WHO. However, the elimination of malaria is creating difficulties as the current methods do not protect against mosquitoes biting outdoors. The purpose of this study was to develop a new product by incorporating repellents into inexpensive thermoplastic polymer namely poly(ethylene-co-vinyl acetate) (EVA) and linear low-density polyethylene (LLDPE) to control the release rate of mosquito repellents from microporous polyolefin strands, e.g. repellent bracelets and anklets which can be used for longer periods of time, say for three to six months. Four approaches were

considered in this research. In the first study, the evaporation rate of repellents was determined using thermogravimetric analysis (TGA). The duration of protection against mosquitoes by the repellent is partially affected by the rate of loss of repellent due abrasion, penetration and evaporation. Therefore, the repellent evaporation rate can be regarded as one of the physical properties of repellents which might affect repellent efficiency. The results showed that three repellents, namely Icaridin, IR3535 and DEET, had a low volatility compared to the other repellents investigated. These three repellents are indicators of long protection time against mosquitoes. The second approach was to use the open-cell microporous strands as reservoirs for relatively large quantities of mosquito repellent. Repellents of interest include DEET, Icaridin, ethyl anthranilate and IR3535. Microporous polymer strands containing mosquito repellent were prepared by twin-screw extrusion compounding. A co-continuous phase structure was achieved by rapid quenching in an ice-water bath of the homogeneous polymer-repellent melt exiting the extruder. Phase separation occurred through spinodal decomposition which trapped the liquid repellent in the microporous polymer matrix. The extraction and TGA results corresponded well to the amount of repellent added in the compounding step, showing that very little repellent was lost during processing. The third approach showed that control of the repellent-release rate was possible with a skin-like membrane at the surfaces of the open-cell polymer-repellent strands extruded. The presence of a skin-like membrane of the polymer strands was studied using scanning electron microscopy and estimated by a mathematical model. It was found that some of the microporous polymer strands released the repellents at an almost constant rate. The experimental and predicted data fitted very well, showing the accuracy of the mathematical model developed. The last study demonstrated that the polyolefin strands that contained up to 30 wt% of either DEET or Icaridin provided effective protection against bites from the *Anopheles arabiensis* mosquito even after 12 weeks of ageing at 50 °C. This means that the bracelets or anklets made with polyolefin impregnated with DEET or Icaridin may offer a new effective control strategy which is cost effective for outdoor mosquito bites.

**Keywords:** malaria; mosquitoes; repellents; polyolefin strands; evaporation rate; permeability; release rate; TIPS method.

# **DEDICATION**

**Dedicated to**

**My parents and siblings**

## **ACKNOWLEDGMENTS**

I wish to sincerely thank my supervisor Prof. Walter W. Focke for his encouragement and guidance with this work and throughout my time at the University of Pretoria.

I would also like to thank the following people for their assistance:

Prof. Leo Braack (Insectary)

Mr Joseph Sebekedi (Compounding)

Mr Alcides Siteo (Compounding and Bioassay testing)

Dr Eudri Venter (Scanning Electron Microscopy)

Ms Erna van Wilpe (Scanning Electron Microscopy)

Mr Victor (Thermogravimetric analysis)

Mr Cyril Ndonyane (Bioassay testing of selected polymer-repellent systems)

Dr Isbe van der Westhuizen (Thermogravimetric analysis)

Mr Robert Tewo (Compounding, FTIR analysis, bioassay testing and review of the thesis)

Mr Tatenda Madzorera (Bioassay testing)

Dr Homa Izadi (Thermogravimetric analysis)

Ms Chanita Sungkapreecha (Thermogravimetric analysis)

Mr Jiten Mistry (Payne Permeability test)

Dr Gimo Daniel “Vhamambo Tuks” (Review of manuscript, a part of the thesis)

Ms Suzette Seymore (Administration)

Dr Mthokozisi Sibanda (Experimental discussion)

Mr Sifiso Nsibande (Chemical structures discussion)

Mr Sifiso Skosana (Compounding)

This research was financially supported by the Deutsche Forschungsgemeinschaft (DFG) (Grant AN 212/22-1) (Funding). The author is grateful to UP-IAM for the experimental work and to UP-ISMC for the bioassay using foot-in-cage tests on the prototype formulation produced.

I would like to extend my sincere gratitude to my parents, Benjamim Mapossa and Angelina Filimone, and my brothers Américo (mais velho), Jorge (Falêncio), Carlitos (Khalos), Jacob (Jako), Agostinho (Txatxa) and my sister Elisa Mapossa (Mbia), for encouraging me and affording me this opportunity to further my studies. I would also like to thank my girlfriend Quetinha Soares and friends Patrícia, Géssica and Matusse.

# TABLE OF CONTENTS

<b>DECLARATION</b> .....	i
<b>SYNOPSIS</b> .....	ii
<b>DEDICATION</b> .....	iv
<b>ACKNOWLEDGMENTS</b> .....	v
<b>LIST OF FIGURES</b> .....	xii
<b>LIST OF TABLES</b> .....	xviii
<b>LIST OF ACRONYMS AND ABBREVIATIONS</b> .....	xx
<b>LIST OF SYMBOLS</b> .....	xxiii
<b>THESIS OUTLINE</b> .....	xxv
<b>CHAPTER 1 INTRODUCTION</b> .....	1
1.1 Background.....	1
1.2 Objectives.....	4
1.3 Methodology.....	5
<b>CHAPTER 2 LITERATURE REVIEW</b> .....	8
2.1 Mosquito-borne diseases.....	8
2.2 Vector control measures.....	13
2.2.1 Indoor residual insecticide spraying (IRS).....	13
2.2.2 Long-lasting insecticide impregnated nets (LLINs).....	14
2.3 Brief history of insect repellents.....	16
2.4 Characteristics of the ideal repellent.....	17
2.5 Repellent categories.....	18
2.5.1 Plant-derived repellents.....	18
2.5.2 Limitations of the use of plant-derived repellents.....	19
2.5.3 Synthetic repellents.....	19
2.5.4 N,N-Diethyl-3-methylbenzamide (DEET).....	20
2.5.5 Ethyl 3-[acetyl(butyl)amino] propanoate or (IR3535).....	24
2.5.6 Icaridin (KBR3023: sec-butyl 2-(2-hydroxyethyl) piperidine-1) carboxylate.....	27
2.5.7 Ethyl anthranilate (EA).....	29
2.6 Factors affecting the efficacy of repellents.....	30
2.7 Evaporation rate of repellents determined using thermogravimetric analysis (TGA).....	31



2.8 Mathematical models used to estimate the volatility of repellents .....	32
2.8.1 Evaporation rate .....	32
2.8.2 Vapour pressure equations for pure compounds .....	33
2.8.3 The Wagner equation .....	33
2.8.4 The Antoine equation .....	34
2.8.5 The Cox equation .....	35
2.8.6 The Myrdal and Yalkowsky equation .....	36
2.9 Diffusion coefficients ( $D_{AB}$ ) .....	37
2.10 Estimating air permeability .....	41
2.11 Polyolefin-clay nanocomposites .....	41
2.11.1 Permeability of nanocomposites .....	45
2.12 Microporous polymers .....	49
2.12.1 The thermally induced phase separation (TIPS) method .....	49
2.13 Controlled-release system .....	53
2.13.1 Modelling for repellent release from polymer strands .....	56
<b>CHAPTER 3 EXPERIMENTAL</b> .....	<b>63</b>
3.1 Materials .....	63
3.1.1 Chemicals .....	63
3.1.2 Polymers .....	64
3.1.3 Nanofillers .....	65
3.2 Sample preparation .....	66
3.2.1 Preparation of the polymer-clay nanocomposite films .....	66
3.3 Mosquito repellent polyolefin strands .....	67
3.3.1 Preparation of mosquito repellent LLDPE strands without a nanofiller .....	67
3.3.2 Preparation of repellent polyolefin strands with added nanofiller .....	68
3.4 Methods of characterizing repellents .....	69
3.4.1 Thermal-oxidative stability of repellents by FTIR analysis .....	69
3.4.2 Determination of chemical composition by X-ray fluorescence (XRF) .....	70
3.4.3 Thermogravimetric analysis and analytical conditions .....	70
3.5 Methods of characterizing nanocomposite films .....	70
3.5.1 Fourier transform infrared (FTIR) analysis .....	70
3.5.2 Thermogravimetric analysis (TGA) .....	71

3.5.3 Measurements of thicknesses.....	71
3.6 Polymer film permeability tests .....	72
3.6.1 Determination of permeability .....	73
3.7 Characterization methods of the polymer strands.....	74
3.7.1 Diameter measurement of the polymer strands.....	74
3.7.2 Extraction of repellent from the polymer strands .....	74
3.7.3 Estimation of membrane thickness covering the polymer strand .....	75
3.7.4 Absorption of repellent by the polymers.....	76
3.7.5 Shrinkage of polymer strand.....	77
3.7.6 Thermogravimetric analysis (TGA).....	77
3.7.7 Scanning electron microscopy (SEM) .....	78
3.8 Repellent release rate studies .....	78
3.9 Efficacy studies of the repellents .....	79
3.9.1 Volunteers.....	79
3.9.2 Ethics approval.....	79
3.9.3 Mosquitoes.....	79
3.9.4 Exposure of mosquitoes and conditions of insectary in terms of temperature and humidity ....	80
3.9.5 Application of polyolefin repellent strands on the leg .....	80
3.9.6 Determination of degree of protection .....	82
3.9.7 Statistical analysis.....	83
<b>CHAPTER 4 RESULTS AND DISCUSSION.....</b>	<b>84</b>
4.1 Characterization of repellents .....	84
4.1.1 Thermo-oxidative stability of repellents .....	84
4.1.2 Chemical composition determined by X-ray fluorescence (XRF).....	89
4.2 Determination of the volatility of repellents by thermogravimetric analysis (TGA).....	89
4.2.1 Vapour pressure correlations with experimental data in the literature.....	89
4.2.2 The Myrdal and Yalkowsky equation .....	90
4.2.3 Repellent evaporation .....	92
4.2.4 Diffusion coefficient of repellents .....	93
4.3 Characterization of polymer films .....	97
4.3.1 Thermogravimetric analysis (TGA).....	97
4.3.2 Fourier transform infrared spectroscopy (FTIR).....	99

4.3.4 Determination of permeability of films to repellents.....	100
4.4 Release of repellents from microporous polymer strands.....	102
4.4.1 Effect of repellent on swelling and shrinkage of the polymers.....	102
4.4.2 Repellent content of the extruded strands by TGA and solvent extraction.....	104
4.4.3 Structure of the internal region of the extruded polymer strands.....	111
4.4.4 Outer surfaces of LLDPE strands .....	122
4.4.5 Estimation of the membrane thickness .....	126
4.4.6 Factors affecting the release behaviour.....	131
4.5 Repellence testing .....	138
4.5.1 Statistical analysis .....	144
<b>CHAPTER 5 CONCLUSIONS AND RECOMENDATIONS.....</b>	<b>145</b>
<b>REFERENCES.....</b>	<b>149</b>
<b>PUBLICATIONS .....</b>	<b>175</b>
<b>Journal Articles.....</b>	<b>175</b>
<b>Conferences participated in .....</b>	<b>175</b>
<b>APPENDICES.....</b>	<b>177</b>
<b>Appendix I: FTIR spectra of neat decanoic acid and decanoic acid heated for 30 min at 200 °C in an open container .....</b>	<b>177</b>
<b>Appendix II: Vapour pressure values reported in the literature for all pure compounds studied .....</b>	<b>178</b>
<b>Appendix III: Parameters calculated to predict diffusion coefficient for repellents.....</b>	<b>182</b>
DEET .....	182
Dimethyl phthalate.....	183
Ethyl anthranilate.....	184
Decanoic acid.....	185
IR3535 .....	186
Icaridin.....	187
<b>Appendix IV: Isothermal repellent evaporation from open cups .....</b>	<b>188</b>
<b>Appendix V: Calibration of setting feeder for LLDPE and pump feed for (a) DEET; (b) Icaridin; (c) IR3535; and (d) ethyl anthranilate .....</b>	<b>189</b>
<b>Appendix VI: Conditions of compounding of the LLDPE strands impregnated with repellent without clay.....</b>	<b>191</b>

<b>Appendix VII: Typical compounder settings, i.e. temperature profiles from hopper to die and screw speed used to compound polymer strands.....</b>	<b>192</b>
<b>Appendix VIII: Thermogravimetric analysis (TGA) of neat DEET and Icaridin, neat LLDPE and LLDPE nanocomposite strands impregnated with repellents .....</b>	<b>197</b>
<b>Appendix IX: Repellent content by solvent extraction and thermogravimetric analysis ..</b>	<b>198</b>
<b>Appendix X: Diameter size of the LLDPE strands measured by Mutotoyo Vernier caliper .....</b>	<b>199</b>
<b>Appendix XI: Strand diameters, release model parameters (<math>\kappa_1</math>, <math>\kappa_2</math>, <math>\kappa_3</math>) and estimated membrane thickness (<math>z_{\text{membrane}}</math>) for LLDPE microporous strands aged at 50 °C .....</b>	<b>200</b>
<b>Appendix XII: Modelling for IR3535 released from LLDPE strands. Release model parameters are also listed.....</b>	<b>201</b>
<b>Appendix XIII: Microporous structures of LLDPE impregnated with repellents and Dellite 43B organoclay .....</b>	<b>203</b>
LLDPE microporous structures formed with 20 wt.% DEET .....	203
LLDPE microporous structures formed with 30 wt.% DEET .....	204
LLDPE microporous structures formed with 20 wt.% Icaridin .....	205
LLDPE microporous structures formed with 30 wt.% Icaridin .....	206
LLDPE microporous structures formed with 30 wt.% IR3535.....	207
LLDPE microporous structures formed with 30 wt.% ethyl anthranilate.....	208
<b>Appendix XIV: Comparison of the inner and outer surfaces of the polymer strands .....</b>	<b>209</b>
<b>Appendix XV: DEET released from polymer strands aged at 50 °C. Initially 5 wt.% Dellite 43B organoclay was added to the strand .....</b>	<b>210</b>
<b>Appendix XVI: Protection Analysis.....</b>	<b>211</b>
ANOVA Models .....	213
Kruskal-Wallis Test .....	214
Analysing pre-post data .....	214
Data.....	217
<b>Appendix XVII: Specification sheets of polymers, fumed silica and Dellite 43B organoclay considered in this study .....</b>	<b>219</b>
Specification of LLDPE (HR411).....	219
Specification of Pyrogenic Silica (HDK® N20).....	221
Specification of Organoclay DELLITE® 43B .....	223
<b>Appendix XVIII: Physical properties of mosquito repellents .....</b>	<b>223</b>

## LIST OF FIGURES

<b>Figure 1.1:</b> Preferred bite sites of <i>Anopheles arabiensis</i> , <i>Anopheles gambiae</i> and <i>Anopheles funestus</i> on the human body. Darkened areas represent the preferred areas of the species for biting on human body: (A) standing or seated humans, and (B) lying flat on the ground (Braack et al., 2015) .....	2
<b>Figure 2.1:</b> (■) Countries endemic for malaria, 2016; (■) Countries endemic for in 2000, no longer endemic in 2016; (□) Countries not endemic for malaria, 2000; (■) Not applicable (source: WHO, 2016) .....	12
<b>Figure 2.2:</b> Molecular structure of DEET (Adapted from Leal, 2014).....	20
<b>Figure 2.3:</b> Molecular structure of IR3535 adapted from (Leal, 2014) .....	24
<b>Figure 2.4:</b> Molecular structure of Icaridin (adapted from Leal, 2014).....	27
<b>Figure 2.5:</b> Molecular structure of ethyl anthranilate .....	29
<b>Figure 2.6:</b> Structure of montmorillonite (phyllosilicate clay) (taken from Duncan, 2011) .....	43
<b>Figure 2.7:</b> (a) Tactoid; (b) intercalated, and (c) exfoliated polymer nanocomposites (Duncan, 2011).....	44
<b>Figure 2.8:</b> Arrangement of parallel platelets causing a tortuous pathway (Choudalakis and Gotsis, 2009).....	47
<b>Figure 2.9:</b> Effect of the degree of delamination on the tortuosity factor and the aspect ratio of nanoplatelets. $W$ is the thickness of the stacks (Choudalakis and Gotsis, 2009, Bharadwaj, 2001) .....	48
<b>Figure 2.10:</b> Phase diagram of a typical miscible polymer-repellent system. The solid line defines the binodal phase boundary and the broken line the spinodal envelope (Akhtar and Focke, 2015) .....	52
<b>Figure 2.11:</b> Model of the microporous strand showing the liquid core location, the vapour-filled microporous region and the outer skin layer that functions like a membrane that limits the rate at which the repellent is released .....	56

<b>Figure 3.1:</b> Chemical structure of the organic modifier intercalated in Dellite 43B organoclay (Majeed et al., 2013) .....	65
<b>Figure 3.2:</b> Thickness measurement using a Mitutoyo Digital micrometer .....	72
<b>Figure 3.3:</b> Payne permeability cups, rings and polymer nanocomposite films used to study the permeability of the repellents through polymer film .....	73
<b>Figure 3.4:</b> Mitutoyo Digital Vernier calliper.....	74
<b>Figure 3.5:</b> A treated foot prepared for a foot-in-cage test .....	81
<b>Figure 3.6:</b> Photo of the foot-in-cage test .....	82
<b>Figure 4.1:</b> (a) FTIR spectra for the mosquito repellents DEET and Icaridin before and after thermal-oxidative stability testing by exposure to air at either 50 °C for four months or for 30 min at 200 °C. (b) Expanded view of the carbonyl absorption region proving the statement of the thermal stability of DEET and Icaridin. ....	86
<b>Figure 4.2:</b> (a) FTIR spectra for the mosquito repellents ethyl anthranilate before and after thermal-oxidative stability testing by exposure to air at either 50 °C for four months or for 30 min at 200 °C. (b) Expanded view of the carbonyl absorption region proving the statement of the thermal stability of ethyl anthranilate.....	87
<b>Figure 4.3:</b> (a) FTIR spectra for the mosquito repellent ethyl butylacetylaminopropionate (IR3535) and dimethyl phthalate before and after thermal-oxidative stability testing by exposure to air at either 50 °C for four months or for 30 min at 200 °C. (b) Expanded view of the carbonyl absorption region for IR3535 and dimethyl phthalate showing the development of a new band near 1690 cm <sup>-1</sup> and 1685 cm <sup>-1</sup> , respectively. ....	88
<b>Figure 4.4:</b> (a) Comparison of the experimental vapour pressure values reported by Baccanari et al. (1968), Weast and Grasselli (1989) and Lide and David (2009) with the values theoretically determined by equations (2.2), (2.3) and (2.6) for decanoic acid. (b) Comparison of the experimental vapour pressure values reported by Roháč et al. (1999), O'Neil (2013) and Daubert, (1989) with the values theoretically obtained by equations (2.4), (2.5) and (2.6) for dimethyl phthalate. ....	90

<b>Figure 4.5:</b> The experimental vapour pressure values for (a) DEET reported by Drapeau et al. (2011), Haynes (2014) and Blaine (1976); (b) ethyl anthranilate reported by Lide (2004), Api et al. (2015), Weast and Grasselli (1989), Milwaukee (1990), Islam et al. (2017b); (c) IR3535 reported by O'Neil (2013) and (d) Icaridin reported by O'Neil (2013) are compared with the values estimated by equation (2.6).....	91
<b>Figure 4.6:</b> Comparison of experimentally determined TGA evaporation rates by equation (2.1) and theoretically predicted rates (solid line) by equation (2.19) for: (a) IR3535; and (b) Icaridin .....	92
<b>Figure 4.7:</b> Comparison of experimentally determined TGA evaporation rates by equation (2.1) and theoretically predicted rates (solid line) by equation (2.19) for: (a) decanoic acid; (b) dimethyl phthalate; (c) DEET; (d) ethyl anthranilate. ....	93
<b>Figure 4.8:</b> Air permeabilities of the repellents Icaridin, ethyl butylacetylaminopropionate (IR3535), decanoic acid, DEET, dimethyl phthalate, Citriodiol and ethyl anthranilate measured at 50 °C using Payne cups. ....	94
<b>Figure 4.9:</b> Comparison of theoretically predicted diffusion coefficients (solid line) obtained by equation (2.9) and experimentally determined TGA diffusion coefficients calculated by equation (2.20) for: (a) decanoic acid; (b) dimethyl phthalate; (c) DEET; and (d) ethyl anthranilate.....	96
<b>Figure 4.10:</b> Comparison of theoretically predicted diffusion coefficients (solid line) obtained by equation (2.9) and experimentally determined TGA diffusion coefficients obtained by equation (2.20) for: (a) IR3535; (b) Icaridin.....	97
<b>Figure 4.11:</b> TGA and DTG profiles of (a) the neat LLDPE and LLDPE-43B nanocomposite films; and (b) the neat EVA and EVA-43B nanocomposite films.....	98
<b>Figure 4.12:</b> FTIR spectra of (a) the neat LLDPE and LLDPE-43B nanocomposite films, and (b) the neat EVA and EVA-43B nanocomposite films .....	100
<b>Figure 4.13:</b> TGA mass loss traces for DEET, Icaridin, neat polymers and (a) and (b) LLDPE, and (c) and (d) EVA-based strands containing 5 wt.% Dellite 43B clay and either 20 or 30 wt.% DEET and 20 or 30 wt.% Icaridin .....	106

**Figure 4.14.** TGA mass loss traces for IR3535, ethyl anthranilate and neat LLDPE. (a) LLDPE-based strands contained 5 wt.% Dellite 43B clay and either 30 or 40 wt.% IR3535. The formulation 40 wt.% IR3535 was loaded with 5 wt.% fumed silica. (b) LLDPE-based strands contained 5 wt.% Dellite 43B clay and either 30 wt.% ethyl anthranilate and formulation 40 wt.% ethyl anthranilate only contained 5 wt.% fumed silica. .... 107

**Figure 4.15:** TGA curves of LLDPE strands initially containing: (—) 20 wt.% Icaridin and loaded with 5 wt.% Dellite 43B organoclay; and (—) 20 wt.% Icaridin with the absence of nanofillers. .... 109

**Figure 4.16:** TGA traces of LLDPE strands initially containing: (a) 30 wt.% DEET; (b) 30 wt.% Icaridin; (c) 20 wt.% DEET; and (d) 20 wt.% Icaridin at 0 month and 6 months. All strands initially contained 5 wt.% Dellite 43B organoclay ..... 110

**Figure 4.17:** SEM micrographs of LLDPE strands impregnated with: (a) 41 wt.% of DEET; and (b) 42 wt.% of Icaridin. No fillers were added in the LLDPE strands. .... 112

**Figure 4.18:** SEM micrographs of LLDPE strands impregnated with: (a) 41 wt.% of IR3535; and (a) 44 wt.% of ethyl anthranilate. No fillers were added in the LLDPE strands. .... 113

**Figure 4.19:** SEM micrographs showing the effect of silica and insect repellent type on the structure of the internal microporous region of extruded LLDPE strands. (a) 30 wt.% Icaridin; and (b) 30 wt.% DEET. All strands contained 5 wt.% fumed silica. .... 115

**Figure 4.20:** SEM micrographs showing the effect of silica and insect repellent type on the structure of the internal microporous region of extruded LLDPE strands. (a) 30 wt.% IR3535, and (b) 30 wt.% ethyl anthranilate. All strands contained 5 wt.% fumed silica. .... 116

**Figure 4.21:** SEM micrographs showing the effect of insect repellent type and concentration on the structure of the internal microporous region of extruded LLDPE strands. (a) 20 wt.% DEET; and (b) 30 wt.% DEET. All strands contained 5 wt.% Dellite 43B clay..... 118

**Figure 4.22:** SEM micrographs showing the effect of insect repellent type and concentration on the structure of the internal microporous region of extruded LLDPE strands. (a) 20 wt.% Icaridin; and (b) 30 wt.% Icaridin. All strands contained 5 wt.% Dellite 43B clay. .... 119



- Figure 4.23:** SEM micrographs showing the effect of insect repellent type on the structure of the internal microporous region of extruded LLDPE strands. (a) 30 wt.% IR3535; and (b) 30 wt.% ethyl anthranilate. All strands contained 5 wt.% Dellite 43B clay..... 120
- Figure 4.24:** SEM micrographs showing the internal structure region of extruded EVA strands. (a) 30 wt.% DEET; and (b) 30 wt.% Icaridin. All strands contained 5 wt.% Dellite 43B clay..... 121
- Figure 4.25:** Cross-section evidently showing an outside skin covering of the strand: (a) 20 wt.% Icaridin; (b) 30 wt.% Icaridin; (c) 20 wt.% DEET; and (d) 30 wt.% DEET. All LLDPE strands contained 5 wt.% Dellite 43B clay. .... 123
- Figure 4.26:** Side views of the outer surface structure of the strand: (a) 20 wt.% Icaridin; (b) 20 wt.% DEET and (c) and (d) initially containing 30 wt.% DEET. All LLDPE strands contained 5 wt.% Dellite 43B clay. .... 124
- Figure 4.27:** The outer surface appearance of the skin of the LLDPE strands: (a) and (b) 30 wt.% DEET and (c) and (d) 20 wt.% Icaridin. All the LLDPE strands contained 5 wt.% Dellite 43B clay. .... 125
- Figure 4.28:** Release of 30 wt.% DEET (BM103), 30 wt.% Icaridin (BM206), 30 wt.% IR3535 (BM208) and 30 wt.% ethyl anthranilate (BM207) from strands. The LLDPE-based strands initially contained 5 wt.% Dellite 43B organoclay..... 132
- Figure 4.29:** Effect of concentration of the DEET on release from the LLDPE strands. The amount of repellent initially incorporated into the LLDPE strands was: (▲) 40wt.% DEET (BM101) and (●) 30wt.% DEET (BM102). Both strands contained 5 wt.% fumed silica. .... 133
- Figure 4.30:** Effect of nanofiller on repellent release from LLDPE strands. (a) The LLDPE strands initially containing: (▲) 30 wt.% DEET and 5 wt.% fumed silica (BM102); and (●) 30 wt.% DEET and 5 wt.% Dellite 43B clay (BM103); (b) The LLDPE strands initially containing: (▲) 20 wt.% Icaridin and 5 wt.% fumed silica (BM504) and (●) 20 wt.% Icaridin and 5 wt.% Dellite 43B clay (BM300A). .... 134

**Figure 4.31:** Effect of diameter sizes of LLDPE-strands on release of the repellent. (a) (●) 20 wt.% DEET (BM302B) - diameter size ( $3.42 \pm 0.16$  mm); (●) 20 wt.% DEET (BM302A) - diameter size ( $4.61 \pm 0.17$  mm); (▲) 20 wt.% Icaridin (BM300B) - diameter size ( $2.26 \pm 0.05$  mm); and (▲) 20 wt.% Icaridin (BM300A) - diameter size ( $4.54 \pm 0.23$  mm). (b) (●) 30 wt.% DEET (BM303B) - diameter size ( $2.87 \pm 0.15$  mm); (●) 30 wt.% DEET (BM303A) - diameter size ( $4.66 \pm 0.21$  mm); (▲) 30 wt.% Icaridin (BM301B) - diameter size ( $2.15 \pm 0.06$  mm); and (▲) 30 wt.% Icaridin (BM301A) - diameter size ( $4.63 \pm 0.25$  mm). All strands contained 5 wt.% Dellite 43B clay. .... 135

**Figure 4.32:** Effect of temperature on release of DEET-containing LLDPE strands. (a) LLDPE initially containing (▲) 20 wt.% DEET aged at 50 °C and (●) 20 wt.% DEET aged at 30 °C; (b) LLDPE initially containing (▲) 30 wt.% DEET aged at 50 °C and (●) 30 wt.% DEET aged at 30 °C..... 136

**Figure 4.33:** Effect of temperature on release of Icaridin-based LLDPE strands. (a) LLDPE initially containing (▲) 20 wt.% Icaridin aged at 50 °C and (●) 20 wt.% Icaridin aged at 30 °C; (b) LLDPE initially containing (▲) 30 wt.% Icaridin aged at 50 °C and (●) 30 wt.% Icaridin aged at 30 °C. .... 136

**Figure 4.34:** Repellent release curves during oven ageing at 50 °C. The LLDPE- and EVA-based strands contained 5 wt.% Dellite 43B clay and either DEET or Icaridin as a repellent. (a) 30 wt.% DEET (BM403), 20 wt.% DEET (BM402), 30 wt.% DEET (AS403), 20 wt.% DEET (AS402). (b) 30 wt.% Icaridin (BM401), 20 wt.% Icaridin (BM400), 30 wt.% Icaridin (AS504) and 20 wt.% 30 wt.% Icaridin (AS503)-based strands..... 137

**Figure 4.35:** Bar plot of results of foot-in-cage repellent tests for polymer strands containing either DEET or Icaridin as repellents. All the compositions utilized Dellite 43B clay as the thickening agent. The repellents-based polymer strands used are: 30 wt.% DEET (BM403), 20 wt.% DEET (BM402), 30 wt.% DEET (AS403), 20 wt.% DEET (AS402), 30 wt.% Icaridin (BM401), 20 wt.% Icaridin (BM400), 30 wt.% Icaridin (AS504) and 20 wt.% 30 wt.% Icaridin (AS503)-based strands. The strands were aged at 50 °C in a convection oven and the bioassay tests were done every two weeks for up to 12 weeks..... 144

## LIST OF TABLES

<b>Table 2.1:</b> Previous studies showing the efficacy of DEET against mosquitoes .....	22
<b>Table 2.2:</b> Previous studies showing the efficacy of IR3535 against mosquitoes .....	25
<b>Table 2.3:</b> Previous studies showing the efficacy of Icaridin against mosquitoes.....	28
<b>Table 2.4:</b> Parameters of the Wagner equation used for decanoic acid (Ambrose and Ghiassee, 1987) .....	34
<b>Table 2.5:</b> Antoine equation constants and temperature range used for decanoic acid (Kahlbaum, 1894) and dimethyl phthalate (Roháč et al., 1999).....	35
<b>Table 2.6:</b> Parameters of the Cox equation and range of temperature used for dimethyl phthalate (Roháč et al., 1999, Gobble et al., 2014). .....	35
<b>Table 2.7:</b> Names of repellents, critical temperature, critical volume and critical pressure and sources.....	39
<b>Table 2.8:</b> Parameters of the collision integral $\Omega_D$ (Poling et al., 2001).....	40
<b>Table 3.1:</b> List of chemicals, their properties and suppliers .....	64
<b>Table 3.2:</b> Nanocomposite film samples prepared by melt extrusion method.....	67
<b>Table 3.3:</b> TX28P extrusion conditions used for compounding LLDPE strands.....	69
<b>Table 3.4:</b> TGA instruments and pans used to predict the evaporation rate of the repellents ....	70
<b>Table 4.1:</b> Chemical composition in (%) of Dellite 43B organoclay.....	89
<b>Table 4.2:</b> Thickness of neat polymer and polymer-clay nanocomposite films in units of $\mu\text{m}$	100
<b>Table 4.3:</b> Permeability of the neat polymer and polymer-clay nanocomposite films to the repellents in units of $\text{g}\cdot\mu\text{m}\cdot\text{day}^{-1}\cdot\text{m}^{-2}$ . Both properties were evaluated at 50 °C.....	102
<b>Table 4.4:</b> Polymer swelling by repellents expressed in wt.% evaluated at 30 and 50 °C .....	103
<b>Table 4.5:</b> Shrinkage of polymer strands expressed in wt.% evaluated at 50 °C .....	104

<b>Table 4.6:</b> Nominal repellent content (in wt.%) and values estimated using solvent extraction and thermogravimetric analysis (TGA) .....	108
<b>Table 4.7:</b> Nominal repellent content in (wt.%) and estimated values of repellent trapped in LLDPE strands after oven aging for 6 months at 50 °C using thermogravimetric analysis (TGA) and mass loss of repellents from strands.....	111
<b>Table 4.8:</b> Repellent content (wt-%), polymer strand diameters, release model parameters ( $\kappa_1$ and $\kappa_2$ ), initial evaporation rate (dX/dt) and estimated membrane thicknesses ( $z_{\text{membrane}}$ ) of microporous EVA and LLDPE strands aged at 50 °C.....	129
<b>Table 4.9:</b> Results of foot-in-cage mosquito repellent tests .....	140

## LIST OF ACRONYMS AND ABBREVIATIONS

ATR	Attenuated total reflection
ANOVA	Analysis of variance
AS	Repellent-based EVA strand samples
BET	Brunauer-Emmett-Teller
BM	Repellent-based LLDPE strand samples
CHIKV	Chikungunya virus
D <sub>B</sub>	Double bond
DDT	Dichloro-diphenyl-trichloroethane
DEET	N,N-Diethyl-3-methylbenzamide
DMP	Dimethyl phthalate
D <sub>pan</sub>	Diameter of pan
D <sub>i</sub>	Diameters before shrinkage process of strands
D <sub>f</sub>	Diameters after shrinkage process of strands
EA	Ethyl anthranilate
EOs	Essential oils
EVA	Poly(ethylene-co-vinyl acetate)
E (%)	Estimated repellent amount in mass percent
FTIR	Fourier Transform infrared spectroscopy
HBN	Hydrogen bond number
H <sub>pan</sub>	Height of pan
IR3535	Ethyl 3-[acetyl(butyl)amino] propanoate
Icaridin	KBR3023: sec-butyl 2 – (2-hydroxyethyl piperidine -1) carboxylate
IRS	Indoor residual spraying
LLINs	Long-lasting insecticide impregnated nets
κ <sub>1</sub> , κ <sub>2</sub> , κ <sub>3</sub>	Model parameters used for repellent release from strands
LOI	Loss on Ignition

LLDPE	Linear low-density polyethylene
LLIN	Long-lasting insecticide-treated net
MFI	Melt flow index
NICD	National Institute for Communicable Diseases
NIPS	Non-solvent induced phase separation
$N_T$	Number of mosquitoes landing on and/or probing the treated leg
$N_C$	Number of mosquitoes landing on and/or probing the control leg
$N_C$	Number of carbon atoms
$N_H$	Number of hydrogen atoms
$N_O$	Number of oxygen atoms
$N_N$	Number of nitrogen atoms
$N_{Cl}$	Number of chlorine atoms
$N_{Br}$	Number of bromine atoms
$N_F$	Number of fluorine atoms
$N_I$	Number of iodine atoms
$N_S$	Number of sulphur atoms
$n(-OH)$	Number of functional group of alcohols
$n(-COOH)$	Number of functional group of carboxylic acid
$n(-NH_2)$	Number of functional group of primary amines
$p$ (%)	Protection in percentage
pH	Scale of acidity
$Q$ (%)	Estimated polymer matrix swelling by repellents in percentage
RING	$\Sigma$ independent single, fused or conjugated ring system
SEM	Scanning Electron Microscopy
SIPS	Solvent-induced Phase Separation
SP3	$\Sigma$ non-ring, non-terminal $sp^3$ atoms
SP2	$\Sigma$ non-ring, non-terminal $sp^2$ atoms
$S_R$ (%)	Shrinkage of polymer strands in percentage
TAEPS	Thermally assisted evaporation phase separation

$T_B$	Triple bond
TIPS	Thermally induced phase separation
TGA	Thermogravimetric analysis
UCST	Upper critical solution temperature
UK	United Kingdom
US	United States
VA	Vinyl acetate
XRF	X-ray fluorescence
$X(t)$	Total amount of repellent remaining
WHO	World Health Organization
$W_i$	Weight of the strands before extraction
$W_f$	Weight of the strands after extraction
$W_s$	Weight of swollen polymer pellets
$W_d$	Weight of dry polymer pellets
$\tau$	Molecular structure representing the torsional bond
$\Omega_D$	Collision integral
$Z_c$	Critical compressibility factor

## LIST OF SYMBOLS

$A$	Vaporization surface area [ $\text{m}^2$ ]
$b$	Slope of the linear mass loss vs. time plot [ $\text{g}\cdot\text{day}^{-1}$ ]
$C_L$	Concentration [ $\text{mol}\cdot\text{dm}^3$ ]
$d_{mA}/d_t$	TGA-measured rate of mass loss [ $\text{mPa}\cdot\text{m}^2\cdot\text{s}^{-1}$ ]
$D_{AB}$	Diffusion coefficient of repellent [ $\text{mm}^2\cdot\text{s}^{-1}$ ]
$D_{eff}$	Effective diffusion coefficient [ $\text{mm}^2\cdot\text{s}^{-1}$ ]
$J$	Repellent flux [ $\text{g}\cdot\text{day}^{-1}\cdot\text{mm}^{-2}$ ]
$M_{wA}$	Molar mass of the vaporizing repellent [ $\text{g}\cdot\text{mol}^{-1}$ ]
$M_{wB}$	Molar mass of the air [ $\text{g}\cdot\text{mol}^{-1}$ ]
$m_o$	Initial mass [g]
$m(t)$	Mass at time [g]
$P_A$	Vapour pressure of repellent [kPa]
$P$	Permeability coefficient [ $\text{g}\cdot\mu\text{m}\cdot\text{day}^{-1}\cdot\text{mm}^{-2}$ ]
$P_r$	Reduced vapour pressure [kPa]
$P_c$	Critical pressure [kPa]
$P_0$	Constant pressure [kPa]
$R$	Gas constant [ $\text{J}\cdot\text{mol}^{-1}\cdot\text{K}^{-1}$ ]
$R_P$	Diameter of the porous region [mm]
$S_A$	Air permeability [ $\text{mPa}\cdot\text{m}^2\cdot\text{s}^{-1}$ ]
$L_f$	Film thickness [ $\mu\text{m}$ ]
$L$	Length of filament [mm]
$t$	Time [days]
$t_f$	Release time [days]
$T$	Absolute temperature [K]
$T_r$	Reduced temperature [K]
$T_c$	Critical temperature [K]



$T_0$	Constant temperature [K]
$T_b$	Boiling temperature [K]
$T_m$	Melting temperature [ $^{\circ}\text{C}$ ]
$\rho$	Density of compound [ $\text{g}\cdot\text{cm}^{-3}$ ]
$\rho_{eq}$	Equilibrium mass density [ $\text{g}\cdot\text{cm}^{-3}$ ]
$V_b$	Liquid molar volume [ $\text{cm}^3\cdot\text{mol}^{-1}$ ]
$V_c$	Critical volume [ $\text{m}^3\cdot\text{kg}\cdot\text{mol}^{-1}$ ]
X	Amount of repellent released [g]
$z_{membrane}$	Membrane thickness that covers polymer strand [ $\mu\text{m}$ ]

## THESIS OUTLINE

The thesis comprises five chapters and references. Appendices are included.

*Chapter 1* is an introduction to the study, research objectives and descriptions of the sample preparation and characterization methods.

*Chapter 2* presents a literature review of the study. A brief description is given of mosquito-borne diseases, vector control measures, the history of insect repellents and natural and synthetic repellents. Previous studies of repellents that are effective against mosquitoes are reported. The volatility of mosquito repellents, the equations that describe evaporation rate, diffusion coefficient, vapour pressure and the permeability of repellents in air are discussed. The nanocomposite theory and equations that describe permeability through films and how to measure them are presented. The literature on the preparation of microporous polymer strands using the thermally induced phase separation (TIPS) method is discussed. Finally, the controlled-release technology and the mathematical model for repellent release from polymer strands are highlighted.

The raw materials and experimental procedures used in this study are described in *Chapter 3*. The instruments and methods used in the laboratory are also described in this chapter.

*Chapter 4* presents the results and discussions of the thermo-oxidative stability of repellents. Secondly, the determination of the evaporation rate and permeation kinetics mosquito repellents are reported and discussed. The results of the thermal stability of polymer-nanocomposite films and the chemical interaction of the clay and polymer were obtained by TGA and FTIR methods.

This chapter also presents and discusses the results of the thermal stability and morphological properties of polymer nanocomposite strands containing repellent. The results of polymer matrix swelling by repellents and shrinkage of polymer strands are presented. The effect of the type and concentration of repellents and the nanofiller (fumed silica and clay) in the microporous polymer structure are discussed. The membrane thickness of the strands was estimated and are reported. The experimental data of the release of repellents and the modelling of the kinetics of the release rate of repellent from microporous polymer strands are presented and discussed. Furthermore, the conditions that affected the repellent release rate such as temperature, nature and concentrations of repellent, diameter of strand, nanofiller (fumed silica and clay) and nature of the polymer are discussed. Finally, the results of the repellence bioassays carried out with polymer strands containing repellent and loaded with clay Dellite 43B are discussed.

*Chapter 5* presents the overall conclusions of the study together with recommendations for possible future work.

The *References* provide a record of the literature consulted during this study, which was also used to elucidate the findings of the study.

The *Appendices* include complementary and supplementary data generated during the study.

# CHAPTER 1

## INTRODUCTION

### 1.1 Background

Mosquito-borne diseases such as malaria, yellow fever, chikungunya, Zika virus and dengue fever are major public health problems due to their effects on humans. According to the World Health Organization, in 2017 alone around 219 million malaria cases were reported with an estimated 435 000 malaria deaths (WHO, 2018). Most of the reported cases occurred in sub-Saharan Africa (WHO, 2017; WHO, 2018). Apart from this, mosquito bites can also cause secondary infections, pain, discomfort and allergic reactions in sensitive individuals, and systemic reactions such as urticaria and angioedema of the skin (Islam et al., 2017b, Gillij et al., 2008, Peng et al., 2004).

Over the years, malaria control has been increasingly aimed at eliminating or reducing mosquito populations. Several methods are available for controlling the malaria vectors. Among them, Long-Lasting Insecticide-Treated Nets (LLINs) and Indoor Residual Spraying are the most important control strategies recommended by WHO. However, these methods are not effective in an outdoor environment, where people spend more time during the day and early evening.

Braack et al. (2015) reported the biting behaviour of African malaria vectors to identify where they bite on the human body. The vectors used in the study were *Anopheles arabiensis* from Malahlapanga in South Africa and *Anopheles gambiae* and *Anopheles funestus* from northern Uganda. The results showed that 93% of mosquito bites occur on the ankles and feet of people seated or standing outdoors. Additionally, the study reported that mosquitoes are attracted to the smell of the feet and ankles. However, if the feet and ankles are protected or covered, the

mosquitoes won't bite above the ankle but seek alternative hosts with non-covered ankles and feet.

Figure 1.1 shows preferred bite sites of *Anopheles arabiensis*, *Anopheles gambiae* and *Anopheles funestus* on the human body.

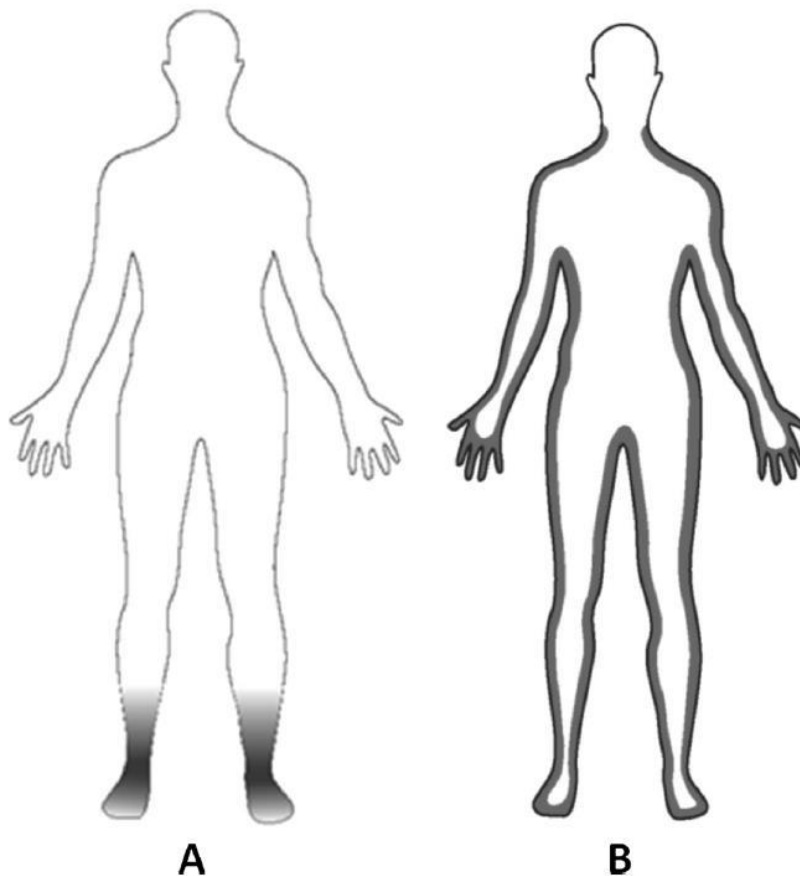


**Figure 1.1:** Preferred bite sites of *Anopheles arabiensis*, *Anopheles gambiae* and *Anopheles funestus* on the human body. Darkened areas represent the preferred areas of the species for biting on human body: (A) standing or seated humans, and (B) lying flat on the ground (Braack et al., 2015)

Additionally, Reddy et al. (2011) studied the behaviour of *Anopheles gambiae* and *Anopheles melas* outdoors on Bioko Island, Equatorial Guinea. The study showed that high levels of outdoor biting by mosquitoes occurred at night and during the early evening and morning. These findings

highlight the need for further studies regarding the importance and urgency of developing new methods to control mosquito-borne diseases when humans are outdoors.

Personal protection against mosquitoes by the use of repellents has become a useful method that can reduce and/or prevent transmission of many insect-borne diseases. Repellent products, such as creams, roll-ons and sprays, are available on the market for outdoor protection. However, most of these applications have a very short period of protection. In the case of topical skin applications, they have shorter protection periods and frequent applications are necessary. Thus, repeated application is required due to environmental effects such as excessive sweating, humidity and insect activity. Besides, frequent use of repellent products would not be affordable to poorer communities.

Longer periods of protection from insect bites are thus required. Izadi et al. (2017) reported on a particularly effective binary repellent blend of ethyl butylacetylaminopropionate (I3535) and nonanoic acid against mosquito. Akhtar (2015) developed a natural mosquito repellent-based polymer matrix and evaluated the repellent release from polymer matrix. Sibanda (2016) developed an Insecticide Treated Wall Lining (ITWL) or Netlon<sup>®</sup> by impregnation polyethylene (LDPE and HDPE) with insecticide. In addition, Sibanda et al. (2018) investigated bicomponent fibres for controlled release of volatile mosquito repellents. The methods developed by authors aimed to provide a longer protection period against mosquito. However, in the present study, the aim of the investigation is to develop a new product (such as an anklet or bracelet) incorporating mosquito repellents in a polymer to repel mosquitoes for an extended period while at the same time keeping the product cost effective. Such a product will be especially valuable in outdoor situations. The final product should not only be effective against mosquito-borne malaria, but also

reduce the biting frequency of other mosquitoes transmitting diseases such as dengue fever, chikungunya, yellow fever and Zika virus. In this way it will contribute to the improvement in overall public health and social well-being.

A possible method of achieving this is to use polyolefin strands filled with a repellent. Polyolefins were chosen because they are widely available and cost effective. This would make the total cost of the final product affordable, an important consideration in this project. Xu et al. (2006) reported that intercalated or incomplete exfoliated structures and dispersed tactoids with several layers can effectively enhance the barrier properties of the polymer matrix. This concept of a tortuous diffusion pathway, achieved by dispersing exfoliated clay nanoplatelets in the polymer matrix, was also explored. The aim of having exfoliated clay present is to reduce the release rate of the active ingredient, i.e. the volatile repellent, through the polymer membrane. Therefore, when impermeable nanoparticles are added to a polymer, the permeating molecules are forced to wiggle around them in a random fashion, and consequently diffuse by a tortuous pathway (Pavlidou and Papaspyrides, 2008). Furthermore, in this work, important factors were considered when selecting the repellents, such as their thermal-oxidative stability, volatility and efficiency at repelling mosquitoes.

## **1.2 Objectives**

- ❖ Investigate the thermal-oxidative stability of mosquito repellents with Fourier Transform Infrared Spectroscopy (FTIR).
- ❖ Determine the volatility of mosquito repellents by thermogravimetric analysis (TGA).
- ❖ Prepare polymer-clay nanocomposite films.

- ❖ Determine the permeation rate of repellents through polymer-clay nanocomposite films.
- ❖ Develop a process for generating an open-cell structure in polymer strands suitable for internally accommodating a liquid mosquito repellent by melt compounding (extruder).
- ❖ Characterize the raw materials and products extruded using X-ray fluorescence (XRF), Scanning Electron Microscopy (SEM), thermogravimetric analysis (TGA) and Fourier Transform Infrared Spectroscopy (FTIR) analysis.
- ❖ Evaluate the amount of repellents entrapped by polymer strands using the extraction method and thermogravimetric analysis.
- ❖ Measure the polymer swelling caused by repellents and the shrinkage of polymer strands impregnated with repellents.
- ❖ Track the repellent release rate from microporous polymer strands as a function of oven ageing temperature and time.
- ❖ Model the kinetics of the repellent release rate from microporous polymer strands.
- ❖ Perform repellent bioassays using foot-in-cage tests on the prototype formulation produced.

### **1.3 Methodology**

Ten main phases were followed in the present study:

- (1) The volatility of repellents was quantified through thermogravimetric analysis and with Payne permeability cups in a convection oven. The evaporation parameters were determined using the equation that describes diffusion-controlled evaporation through a stagnant gas. In addition, the vapour pressure, air permeability and the diffusion coefficient of the repellents as a function of temperature were estimated.



- (2) Nanocomposite polymer films were prepared. The thickness of the polymer nanofilms was determined by a Mutotoyo digital Vernier. The permeability coefficient of the repellents through polymer-clay nanocomposite films was measured. The thermal stability of the nanocomposite films was studied using TGA. The chemical interactions of polymer and organoclay Dellite 43B formulations was studied using FTIR analysis. Furthermore, the elemental analysis of organoclay Dellite 43B was done using X-ray fluorescence (XRF).
- (3) The thermo-oxidative stability of repellents was evaluated using FTIR.
- (4) Selected polymer-repellent systems were processed into strands by extrusion into an ice-water bath. The extruded strands were characterized by TGA and SEM.
- (5) The microstructure of the microporous polymer strands was observed with SEM. The skin-like membrane was also observed or confirmed using SEM.
- (6) The swelling and shrinkage of polymer strands impregnated with DEET and Icaridin were evaluated.
- (7) The release rate of the repellents from microporous polymer strands was studied, as was the effect of various parameters on the repellent release rate for these strands. The parameters evaluated included temperature, type and concentration of the repellent, the nature of the polymer, and the nature of the nanofiller, e.g. fumed silica or organoclay Dellite 43B.
- (8) Models for the mosquito repellent release kinetics were developed. They were used to estimate the nominal thickness of the outer skin covering the microporous polymer strands.

(9) Bioassays of the polymer strands filled with repellents namely as DEET and Icaridin were carried out over a period of 12 weeks to determine their repellent activity against *Anopheles arabiensis* mosquitoes. Foot-in-cage tests were carried out.

(10) A statistical analysis was used to check the reliability of the results.

## CHAPTER 2

### LITERATURE REVIEW

#### 2.1 Mosquito-borne diseases

Mosquito-borne diseases are a serious health problem for people living in endemic regions, mainly sub-Saharan Africa. Diseases transmitted by mosquitoes include malaria, dengue fever, yellow fever, Zika virus and chikungunya. In the recent past up to three million people have died every year from mosquito-borne diseases, including one child every thirty seconds (Fasulo, 2008). The numbers have since decreased, and in 2017, 219 million cases of malaria occurred globally resulting in 435 000 deaths (WHO, 2018). Mosquito bites can also cause secondary effects such as pain, allergic reactions in sensitive individuals, discomfort and systemic reactions such as urticaria and angioedema of the skin (Islam et al., 2017b, Gillij et al., 2008, Peng et al., 2004). However, strategies of vector control continue to be a major challenge to the World Health Organization (WHO) as they try to reduce the risk of epidemics and outbreaks of these diseases in endemic regions. In the following paragraphs mosquito-borne diseases and their symptoms are described.

**Dengue fever** is a major public health concern throughout tropical and sub-tropical regions of the world. This disease is caused by four closely related dengue viruses that belong to the genus *Flavivirus* (family *Flaviviridae*). Dengue fever is transmitted mainly by the *Aedes aegypti* mosquito (Ooi et al., 2006). The disease is the most rapidly spreading mosquito-borne viral disease, with a 30-fold increase in global incidence over the past 50 years (WHO, 2012). The Dengue virus is thought to have emerged about 1 000 years ago in an infectious cycle involving

non-human primates and mosquitoes, with transmission to humans having occurred about 100 years ago (Messina et al., 2014). Although outbreaks of diseases with symptoms similar to those of Dengue fever have been reported for centuries, it was only in 1943 in Japan and 1945 in Hawaii that the first two Dengue viruses were isolated (Messina et al., 2014). The symptoms of Dengue are: (i) fever lasting 2 to 7 days; (ii) haemorrhagic tendencies; (iii) severe headache, (iv) pain behind the eyes, (v) muscle and joint pains, (vi) nausea, and (vii) vomiting (WHO, 2014).

**Chikungunya virus (CHIKV)** is an arthropod-borne virus transmitted to human beings by *Aedes* spp. mosquitoes (Rezza et al., 2007). It is believed the virus originated in Africa (Weaver, 2014) and it was isolated specifically in Tanzania in 1953 (Rezza et al., 2007). After isolation, a number of outbreaks of CHIKV infection have been reported in several African countries, in India and in Southeast Asia (Rezza et al., 2007). The mosquito-borne chikungunya virus causes a febrile illness (chikungunya fever), typically accompanied by a rash and severe, debilitating arthralgia (Weaver, 2014).

**Yellow fever** is an endemic mosquito-borne *flavivirus* (family Flaviviridae) disease that occurs in tropical areas of South America and Africa (Monath and Vasconcelos, 2015, Barnett, 2007, Monath, 2001). This disease continues to be a threat to travellers to and residents of endemic areas, despite the availability of an effective vaccine for nearly 70 years (Monath and Vasconcelos, 2015). A series of epidemics and smaller outbreaks of yellow fever that occurred in West African countries were mainly responsible for the rapid spread of yellow fever on the continent, but the first epidemic was reported in Kenya more than two decades ago (Barnett, 2007). In humans, yellow fever is a severe acute illness accompanied by fever, nausea, vomiting and epigastric pain, hepatitis with jaundice, renal failure, haemorrhaging and shock (Monath, 2001).

**Zika virus** is a disease believed to be transmitted to humans by infected mosquitoes and has been isolated from *Aedes africanus*, *Aedes luciocephalus* and *Aedes aegypti* (Duffy et al., 2009). Zika virus was first identified in Africa (Uganda) in 1947 (Benelli and Mehlhorn, 2016, Duffy et al., 2009). In 2007, the first documented outbreak of Zika virus was noted by physicians on Yap Island, Federated States of Micronesia (Hennessey et al., 2016, Duffy et al., 2009). Approximately 73% of the population aged  $\geq 3$  years were infected with Zika virus (Duffy et al., 2009). In 2015, new cases of Zika virus were reported in South America, especially in Brazil (Dyer, 2015, Zammarchi et al., 2015). According to the Brazilian Ministry of Health, this was the first documented outbreak in Brazil (Dyer, 2015). Since then, the virus has quickly spread within Brazil and to other countries in South America (Petersen et al., 2016). With the spread of Zika virus in Brazil, there has been a marked reported increase of cases of infants born with microcephaly (Hennessey et al., 2016). Some studies have reported that the cause of microcephaly is closely associated with Zika virus (Ventura et al., 2016, Cauchemez et al., 2016). The symptoms of Zika virus are mild and are characterised by acute onset of fever, arthralgia (Hennessey et al., 2016) and sometimes muscle or joint pain (Dyer, 2015). There is as yet no vaccine for Zika virus.

**Malaria** is a parasitic disease caused by infection with protozoan parasites of the *Plasmodium* species (Nkumama et al., 2017). There are four known species of *Anopheles* mosquitoes that are most prevalent in Africa that transmit malaria, namely: (i) *Anopheles gambiae*; (ii) *Anopheles fectus*, (iii) *Anopheles arabiensis*, and (iv) *Anopheles melas* (Sinka et al., 2010). Although mosquito-borne malaria is considered as a disease affecting people living in sub-tropical and tropical regions, outbreaks can occur anywhere in the world (Nogueira Barradas et al., 2016,

Fasulo, 2008). For example, a study done in the UK showed that falciparum malaria infection infects about 20% of travellers from Africa (Lalloo et al., 2016).

The symptoms are often non-specific. They include fever/sweats/chills, malaise, myalgia, headache, diarrhoea and cough. The majority of these symptoms will not require hospitalization (Nkumama et al., 2017, Lalloo et al., 2016). Nowadays malaria still remains the main cause of morbidity and mortality among pregnant women and children up to five years of age (Bardají et al., 2011, Bhattarai et al., 2007, Makono and Sibanda, 1999). Children older than six months of age are particularly susceptible because they have lost their maternal antibodies and also have not yet developed protective immunity (Phillips et al., 2017). Pregnant women are more susceptible to *Plasmodium* spp. infection because the placenta itself selects for the emergence of parasites that express receptors that recognise the placental vasculature. These receptors are antigens to which pregnant women have not yet become partially immune (Phillips et al., 2017).

According to the latest estimates of WHO, between 2000 and 2015 malaria incidence rates reduced by 41% and death due to malaria decreased by 62% worldwide. In Africa for example, the malaria incidence rate fell by 42% and the mortality rate by 66% during the same period (WHO, 2016). Despite this remarkable progress, malaria continues to be a health problem for people. However, efforts to boost the eradication of malaria worldwide continue to be made. The global target set for 2030 is to reduce the incidence and mortality rates of malaria globally by at least 90% compared to the 2015 statistics, to eliminate malaria from at least 35 countries in which the disease was transmitted in 2015, and to prevent the re-establishment of malaria in all countries that are malaria free (WHO, 2016).

Figure 2.1 shows malaria-endemic countries in 2000 and 2016 worldwide. According to Figure 2.1, malaria continues to be a major disease that affects people in Africa, Asia and Central and South America. The African continent continues to have the highest incidence of malaria compared to other countries (WHO, 2016).



**Figure 2.1:** (■) Countries endemic for malaria, 2016; (■) Countries endemic for in 2000, no longer endemic in 2016; (□) Countries not endemic for malaria, 2000; (■) Not applicable (source: WHO, 2016)

Figure 2.1 shows that there is no country in the European region that reported cases of malaria in 2015. Therefore, countries with three consecutive years of zero indigenous cases are considered to have eliminated malaria (WHO, 2016). Vector control methods are an important strategy for the control of mosquito-borne diseases, in particular malaria.

## **2.2 Vector control measures**

Vector control plays a significant role in the current global strategy of control of the major vector-borne diseases, mainly in the prevention of malaria (Zaim and Guillet, 2002). The most commonly used vector control interventions to prevent mosquito bites recommended by WHO are indoor residual insecticide spraying and long-lasting insecticide impregnated nets (LLINs). These methods are used in endemic regions such as sub-Saharan Africa (Okumu and Moore, 2011, Pluess et al., 2010, Tanser et al., 2007). The methods were responsible for preventing two-thirds of malaria cases in Africa between 2000 and 2015 (Phillips et al., 2017). Despite the demonstrated success in reducing human-mosquito interactions, the methods are effective only against endophilic vectors (Reddy et al., 2011).

### **2.2.1 Indoor residual insecticide spraying (IRS)**

IRS has long been recognised as the most commonly used method of malaria control. The use of dichloro-diphenyl-trichloroethane (DDT) against malaria has eliminated or greatly reduced the disease, malaria being a public health problem in almost all countries on all continents (Pluess et al., 2010, Shiff, 2002). Nowadays, IRS continues to be applied in many regions of the world, mainly Africa. In most cases the services are provided by the public health system or by commercial companies (Pluess et al., 2010).

Indoor residual insecticide spraying with DDT has been the most effective chemical strategy against mosquitoes. However, DDT has its limitations which include the following: DDT does not last long, and its use has become uncertain because DDT, which is an organic pollutant, can persist for many years in the environment and can cause problems for public health (Sibanda, 2016). The



possible effects of DDT exposure are low sperm counts, testicular anomalies, premature delivery of fetus and small for gestational age fetuses (Jaga and Dharmani, 2003). The IRS method requires more complex and costly operational delivery systems than LLINs and claims of sustained high coverage often remain unproven (Kleinschmidt et al., 2009).

### **2.2.2 Long-lasting insecticide impregnated mosquito nets (LLINs)**

The use of mosquito nets as protection against harmful insects has been practiced since historical times (Lengeler, 2004). The WHO recommends coverage by LLINs for all people who live in regions at-risk for malaria. The most cost-effective way to achieve this is by providing LLINs free of charge so as to ensure equal access of the nets for all. Effective behaviour changes in communication strategies are also required to ensure that all people at risk of malaria sleep under a LLINs every night, and that the net is properly maintained.

The LLINs interventions are used mostly in Africa. Unlike IRS they are low cost and easy to implement (Sibanda, 2016). In addition, these methods are very efficacious and effective (Lengeler, 2004). However, the principal limitation is that protection is only offered during sleeping time. It is also necessary to wash the nets from time to time, which gradually reduces their insecticidal property (Sibanda, 2016). In some countries in Africa, there is already evidence suggesting the emergence of vector resistance to insecticides, especially pyrethroids (Phillips et al., 2017).

The use of only indoor-based interventions has greatly reduced mosquito-borne diseases such as malaria. However, methods to control malaria in an outdoor environment need to be urgently

developed as another alternative since people stay outdoors for lengthy periods during the day and early evening.

One of the limitations of the current vector control methods is insecticide resistance (especially pyrethroids). Insecticide resistance is the reduction of insecticide activity in an insect population. This resistance can be observed when an insecticide repeatedly fails to achieve the expected level of control when used according to the recommendations for the insect species. The growing development of insecticide resistance exhibited by various mosquito species poses a threat to malaria control programmes (Alou et al., 2012).

Mosquitoes are developing resistance to groups of insecticides. In a study carried out on *An. arabiensis* from an area known as Gwave, a malaria endemic area in Zimbabwe, permethrin resistance in mosquito populations was discovered (Munhenga et al., 2008). In Côte d'Ivoire, resistance towards permethrin, deltamethrin and  $\lambda$ -cyhalothrin was observed to be largely present in *An. gambiae* (Alou et al., 2012). In Sudan, WHO susceptibility tests with *An. arabiensis* showed resistance to DDT and pyrethroids (Abdalla et al., 2014).

Resistance to insecticides develops when insects find ways to overcome the toxins. In biochemical resistance, enzyme detoxification deactivates the insecticide before it reaches the target site (Ranson et al., 2011). In physiological resistance, the toxin is not necessarily broken down but instead it is accommodated by altering one or more physiological functions, e.g. an increase in the rate of insect metabolism. The growing trend of pyrethroid resistance constitutes a serious threat to malaria control programmes. Thus, the development of environmentally safe insect control methods and the rise of insecticide resistance have prompted research into repellents in recent years (Islam et al., 2017b, Diaz, 2016, Deletre et al., 2016). Conducting research into repellents is

challenging for several reasons, such as: (1) the different repellent phenomena are not well defined; (2) it is difficult to test and quantify repellence; (3) the physiological mechanisms are poorly known; and (4) the field efficacy appears to be highly variable (Deletre et al., 2016). Previous studies have proved and emphasized the application of repellents that can potentially prevent mosquito-human interactions, thereby playing a significant role in reducing disease transmission (Islam et al., 2017b, Diaz, 2016, Alpern et al., 2016, Auysawasdi et al., 2016). In addition, the use of devices that repel mosquitoes from a distance have gained popularity in the recent past. These include impregnated plastic strips, coils and candles (Alpern et al., 2016). Sibanda (2016) obtained promising results incorporating repellents into polymer matrices to increase the time of repellence activity against mosquitoes.

Vaccines against yellow fever, Japanese encephalitis and tick-borne encephalitis are available in some places of the world (Ishikawa et al., 2014, Heinz and Stiasny, 2012). However, their limited access by the poor in endemic areas has prompted the development of alternative preventive measures to control the risk of the vectors (Islam et al., 2017b). Therefore, in the absence of vaccines against malaria, one of the most effective and ancient prophylactic measures is the use of volatile mosquito repellents that may provide an additional line of defence against mosquito-borne diseases when used correctly and consistently (Islam et al., 2017b, Leal, 2014).

### **2.3 Brief history of insect repellents**

The use of insect repellents has been known since antiquity. Burning plant leaves was a common technique used to keep mosquitoes away from houses, and herbs were prepared and used on the skin as repellent substances (Lupi et al., 2013). Insect repellents are known as volatile chemicals which, when applied on human skin, repel insects in the opposite direction from its source, thus

discouraging contact and bites (Diaz, 2016). It is also believed that most insect repellents act by producing a vapour barrier, which prevents contact of the insect with the human skin (Nogueira Barradas et al., 2016, Nerio et al., 2010). Repellents are available on the market in many different chemical formulations such as aerosols, pump sprays, lotions, creams, suntan oils, powders, grease sticks and cloth impregnation laundry emulsions. Some of the factors that determine the suitability and the applicability of a repellent include: (i) type of repellent (e.g. active ingredient, formulations); (ii) environmental factors (temperature, humidity, wind), and (iii) inherent repellent properties (vapour pressure, boiling point, odour, solubility). According to Islam et al. (2017b) repellents tend to dissipate rapidly and readily and may fail to protect against arthropods. For instance, repellents with low boiling points tend to be less effective as they vaporize too rapidly, providing a barrier only for a short period of time. Moreover, compounds with high boiling points tend to have low repellence as they do not vaporize readily and consequently do not produce sufficient vapours to form barriers (Brown and Hebert, 1997).

#### **2.4 Characteristics of the ideal repellent**

The characteristics of the ideal insect repellent (Diaz, 2016, Katz et al., 2008) are the following:

- ❖ They must have good efficacy against a wide range of insects.
- ❖ They must be able to be used on the skin without side-effects.
- ❖ They must not damage clothing after application (i.e. staining, bleaching or weakening of fibre).
- ❖ They must be chemically stable, economically available and accessible for widespread use.
- ❖ They must be nontoxic.
- ❖ There must be no bad odour, or they must have a pleasant odour.

- ❖ No oily residues must be left on the skin that are difficult to remove by washing, wiping and sweating.
- ❖ They must be inert to most commonly used plastics.
- ❖ They must provide a sufficiently long period of insect repellent effect.

## **2.5 Repellent categories**

There are two basic chemical groups of repellents: (1) synthetic repellents, which include DEET, IR3535, Icaridin (trade name Saltidin<sup>®</sup>), dimethyl phthalate, ethyl anthranilate or ethyl 2-aminobenzoate which nowadays dominate the market, and (2) plant-derived repellents such as citronella oil and lemon eucalyptus oil (Diaz, 2016). Citriodiol may also be considered as a potential natural active ingredient for repellents in the future.

### **2.5.1 Plant-derived repellents**

Essential oils (EOs) are complex mixtures of volatile organic compounds produced as secondary metabolites in plants. They are composed of hydrocarbons (terpenes and sesquiterpenes) and other oxygenated compounds (alcohols, esters, ethers, aldehydes, phenols, lactones) (Nerio et al., 2010, Toloza et al., 2008).

For centuries plants have been used worldwide as medications to treat some diseases. Relatively few plants have gained significant attraction for use in controlling malaria-bearing mosquitoes and other arthropods. This could be due to an absence of scientific data rather than an absence of plant activity (Tisgratog et al., 2016). Nowadays, the use of essential oils from plants as insect repellents has a high of consumer acceptance. This is due to the perception that natural repellents are safer than synthetic ones and also natural repellents are easier to acquire by people who live in the rural

areas (Tisgratog et al., 2016). Various EOs extracted from different plant families have been shown to have high repellence against arthropod species. For example, the monoterpenes, limonene, citronellal, camphor, eugenol, terpinolene and thymol are commonly described in the literature as presenting with mosquito repellent activity (Nerio et al., 2010, Yang et al., 2004, Jantan and Zaki, 1998, Gillij et al., 2008). Among sesquiterpenes,  $\beta$ -caryophyllene is most cited as a strong repellent against *A. aegypti* (Nerio et al., 2010, Gillij et al., 2008). The repellence of several essential oils appears to be associated with the presence of one or more volatile constituent substances (monoterpenes and sesquiterpenes) (Trongtokit et al., 2005, Gonçalves et al., 2012). According to Tawatsin et al. (2001), Trigg, (1996) and Odalo et al. (2005) some repellents from plants are also effective against Anopheles mosquitoes.

### **2.5.2 Limitations of the use of plant-derived repellents**

Although repellents derived from plants are effective when freshly applied, most essential oils volatilize quickly. Hence, they tend to provide a shorter time of protection than synthetic repellents (Trongtokit et al., 2005, Carroll and Loye, 2006, Barasa et al., 2002). This accounts for the market dominance of formulations based on longer-lasting synthetic repellents (Barasa et al., 2002). Their low boiling points also limit their incorporation into most polymers because during compounding large amounts of repellent can be lost by volatilization.

### **2.5.3 Synthetic repellents**

Before World War II and the emergency of synthetic chemical repellents, primarily plant-based compounds with oil of citronella were the most widely used compounds and the standard against which others were tested (Islam et al., 2017a, Bissinger and Roe, 2010). There were also three

synthetic repellents, namely: (i) dimethyl phthalate (DMP) discovered in 1929; (ii) Indalone (butyl-3,3-dihydro-2,2-dimethyl-4-oxo-2H-pyran-6-carboxylate) patented in 1937; and (iii) ethyl hexanediol, also known as Rutgers 612 which was first used in 1939. These were the important repellents during World War II. After the War, three chemicals known as formulation 6-2-2 or M-250 (a combination of six parts DMP and two parts each Indalone and Rutgers 612) were later introduced for use by the military (Islam et al., 2016, Brown and Hebert, 1997, Bissinger and Roe, 2010).

#### 2.5.4 N,N-Diethyl-3-methylbenzamide (DEET)

N,N-diethyl-3-methylbenzamide is the most effective and most widely used insect repellent because it is inexpensive. N,N-diethyl-3-methylbenzamide was first discovered by the US Department of Agriculture and patented by the US Army in 1946. It was approved for public use in 1959 and since then has been considered a standard repellent (Fradin, 1998, Lupi et al., 2013). Although DEET is considered very effective, its use in children has been limited because some medical cases have been reported. These include dermatitis, allergic reactions, neurological (seizures) and cardiovascular side-effects, as well as encephalopathy, especially when the repellent is used inappropriately (Fradin, 1998, Koren et al., 2003). DEET's molecular structure is shown in Figure 2.2.

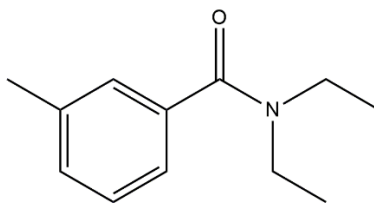


**Figure 2.2:** Molecular structure of DEET (Adapted from Leal, 2014)

Previous studies have revealed most satisfactory performance of DEET against mosquitoes compared to other repellents such as IR3535 soybean oil and citronellal (Fradin and Day, 2002). The bioassay demonstrated that the product based on DEET provided longer-lasting protection of almost 5 hours when compared to IR3535, which provided 23 mins of protection, soybean oil at least 95 min and citronellal almost 20 min of protection. A study done by Frances et al. (1996) demonstrated that the use of DEET formulations against *Culex vishnui*, *Culex gelidus* and *Culex tritaeniorhynchus* mosquitoes provided 87% protection for up to 5 hours, and with 50% of DEET formulation 95% protection was provided for 8 hours. Table 2.1 lists works published on the efficacy of DEET against mosquitoes.

This present study considered the use of DEET incorporated into polyolefin slow-release devices on the basis of the effectiveness of DEET as a mosquito repellent.



**Table 2.1:** Previous studies showing the efficacy of DEET against mosquitoes

Mosquitoes	Product, active ingredient and concentration	Protection (%)	Time (h)	References
<i>Aedes albopictus</i>	Skinsations® Spray-DEET 7%	-	5	(Barnard and Xue, 2004a)
	Off! Spray DEET 15%	-	7.2	
<i>Aedes aegypti</i>	DEET 20%	82.7	5	(Trongtokit et al., 2004)
<i>Aedes communis</i>	DEET	98	4	(Debboun et al., 2000)
		74	6	
		56	8	
	DEET+AI3-37220	98	4	
		95	6	
		76	8	
<i>Aedes aegypti</i>	OFF! Deep Woods-DEET 23.8%	-	5.02	(Fradin and Day, 2002)
	Sawyer Controlled Release®-DEET 20%	-	3.9	
	OFF! Skintastic-DEET 6.65%	-	1.9	
	OFF! Skintastic for Kids-DEET 4.75%	-	1.5	
<i>Aedes aegypti</i>	DEET 25%	100	6	(Tawatsin et al., 2001)
	DEET 25% + Vanillin 5%	100	6	

---

<i>Aedes aegypti</i>	DEET 20% in ethanol	100	7	(Thavara et al., 2001)
		100	8	
<i>Aedes vigilax</i>	DEET 34.6% Army repellent personal	>95	5	(Frances et al., 2009)
<i>Aedes albopictus</i>	DEET 10%	100	4	(Misni et al., 2009)
		88.8	6	
		77.1	8	
<i>Aedes aegypti</i>	DEET 12% Cream	96.2	6.75	(Mittal et al., 2011)
<i>Anopheles</i> spp.	DEET 20%	88.9	4	(Frances et al., 2004)
		74.5	5	
<i>Anopheles gambiae</i>	DEET 30%	88.17	7	(Kweka et al., 2012)
<i>Anopheles stephensi</i>	DEET 12% Cream	100	11	(Mittal et al., 2011)
<i>Anopheles culicifacies</i>	DEET 12% Cream	100	11	(Mittal et al., 2011)
<i>Anopheles annularis</i>	DEET 12% Cream	100	11	(Mittal et al., 2011)
<i>Anopheles subpictus</i>	DEET 12% Cream	100	11	(Mittal et al., 2011)
<i>Anopheles arabiensis</i>	Socks-DEET	>90	3360	(Sibanda et al., 2018)

---

### 2.5.5 Ethyl 3-[acetyl(butyl)amino] propanoate or (IR3535)

IR3535 is a synthetic repellent with a chemical structure like that of the amino acid alanine. IR3535 has been available in Europe for more than 20 years. At a concentration of 20%, IR3535 is effective against *Anopheles* and *Aedes* mosquitoes for a period of four to six hours (Sorge et al., 2007). Previous studies carried out in Liberia showed that IR3535 can repel more than 92% of biting *Anopheles gambiae* and *Anopheles funestus* for six hours (Marchio, 1996). In addition, other studies suggest that IR3535 is an effective repellent for *Anopheles*, *Aedes* and *Culex* mosquitoes (Barnard and WHO, 2000). There are no recommendations for its use or avoidance in children or during pregnancy (Diaz, 2016). Figure 2.3 shows the chemical structure of IR3535.

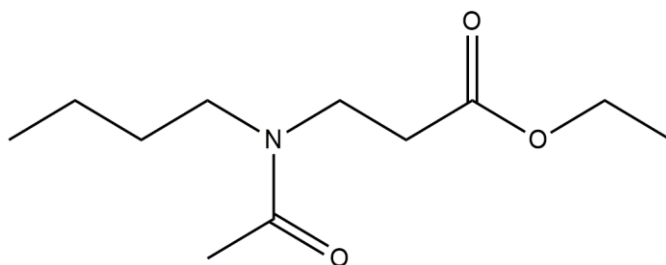


**Figure 2.3:** Molecular structure of IR3535 adapted from (Leal, 2014)

Table 2.2 lists the studies published on the efficacy of IR3535 against mosquitoes.

**Table 2.2:** Previous studies showing the efficacy of IR3535 against mosquitoes

<b>Mosquitoes</b>	<b>Product, active ingredient and concentration</b>	<b>Protection (%)</b>	<b>Time (h)</b>	<b>References</b>
<i>Aedes albopictus</i>	IR3535 20% in ethanol solution	-	5.0	(Thavara et al., 2001)
<i>Aedes aegypti</i>	IR3535 20% in ethanol solution	-	9.8	(Thavara et al., 2001)
<i>Aedes albopictus</i>	IR3535 10%	-	7.8	(Tawatsin et al., 2006)
<i>Anopheles dirus</i>	IR3535 10%	-	8.0	(Tawatsin et al., 2006)
<i>Aedes aegypti</i>	IR3535 10%	-	6.7	(Tawatsin et al., 2006)
<i>Culex quinquefasciatus</i>	IR3535 10%	-	8.0	(Tawatsin et al., 2006)
<i>Anopheles dirus</i>	IR3535 20% in ethanol solution	-	3.8	(Thavara et al., 2001)
<i>Culex quinquefasciatus</i>	IR3535 20% in ethanol solution	-	13.7	(Thavara et al., 2001)
<i>Culex tritaeniorhynchus</i>	IR3535 20% in ethanol solution	-	14.8	(Thavara et al., 2001)
<i>Aedes aegypti</i>	IR3535 10% Spray <sup>®</sup>	95	6.0	(Naucke et al., 2007)
		90	6.0	
		85	7.0	
<i>Aedes aegypti</i>	IR3535 15% Spray <sup>®</sup>	95	6.0	(Naucke et al., 2007)
		90	6.0	
		85	6.0	

---

<i>Aedes aegypti</i>	IR3535 10% Lotion <sup>®</sup>	95	4.0	(Naucke et al., 2007)
		90	5.0	
		85	6.0	
<i>Aedes aegypti</i>	IR3535 15% Lotion <sup>®</sup>	95	6.0	(Naucke et al., 2007)
		90	6.0	
		85	6.0	
<i>Aedes aegypti</i>	IR3535 20% Spray <sup>®</sup>	95	6.0	(Naucke et al., 2007)
		90	7.0	
		85	7.0	
<i>Aedes</i> spp. <i>Culex</i> spp. and <i>Anopheles</i> spp.	IR3535 10 % Lotion			(Carroll, 2008)
	IR3535 20% Pump spray	-	>7.0	
	IR3535 20% Aerosol			

---

### 2.5.6 Icaridin (KBR3023: sec-butyl 2-(2-hydroxyethyl) piperidine-1) carboxylate

Icaridin, also known as Saltidin<sup>®</sup>, was developed in Europe in the 1990s and released into the USA (Diaz, 2016). Icaridin is available in various markets worldwide for use against many types of insect such as mosquitoes, black flies and ticks. At a concentration of 20%, Icaridin has an effectiveness against *Anopheles* and *Aedes* mosquitoes for at least four to six hours (Sorge et al., 2007). Table 2.3 lists the studies published on the efficacy of Icaridin against different mosquitoes. The residual repellent effectiveness of Icaridin on skin is reported to exceed that of DEET in some cases. In addition, previous studies carried out on acute toxicity, irritant effect and skin penetration show KBR 3023 to be acceptable for human use (Barnard and WHO, 2000). The physical properties of Icaridin show that it is a colourless, clear, viscous liquid that is stable in light and heat (Barnard and WHO, 2000). The chemical structure of Icaridin is shown in Figure 2.4.

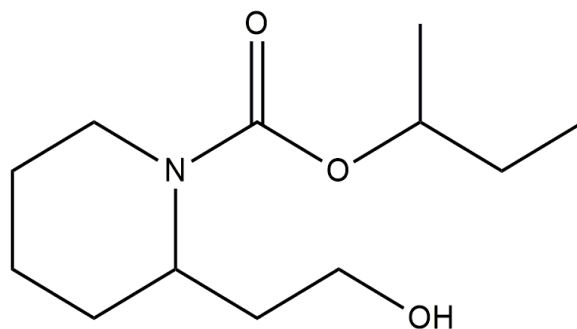


**Figure 2.4:** Molecular structure of Icaridin (adapted from Leal, 2014)

**Table 2.3:** Previous studies showing the efficacy of Icaridin against mosquitoes

<b>Mosquitoes</b>	<b>Product, active ingredient and concentration</b>	<b>Protection (%)</b>	<b>Time (h)</b>	<b>References</b>
<i>Aedes albopictus</i>	Icaridin 10% Autan <sup>®</sup> spray	-	5.7	(Barnard and Xue, 2004a)
<i>Aedes aegypti</i>	Icaridin 10% Lotion	95	6	(Naucke et al., 2007)
		90	7	
		85	8	
<i>Aedes aegypti</i>	Icaridin 20% Spray	95	6	(Naucke et al., 2007)
		90	7	
		85	9	
<i>Anopheles</i> spp.	Icaridin 19.2% in ethanol	86.7	6	(Frances et al., 2004)
	Bayrepel Army <sup>®</sup>	71.5	7	
<i>Anopheles stephensi</i>	Bayrepel 20% in complex solvent	100	8	(Amer and Mehlhorn, 2006)
<i>Culex quinquefasciatus</i>	Bayrepel 20% in complex solvent	100	8	(Amer and Mehlhorn, 2006)
<i>Culex annulirostris</i>	Icaridin <sup>®</sup> 19.2% in ethanol	99.2	5	(Frances et al., 2004)
	Bayrepel Army <sup>®</sup>	85.0	6	

### 2.5.7 Ethyl anthranilate (EA)

Ethyl anthranilate, also known as ethyl 2-aminobenzoate, has attracted significant attention in repellent research in recent years. Despite few studies having been reported on its efficacy against mosquitoes, EA is considered an improved alternative to DEET (Islam et al., 2017a, Afify et al., 2014, Kain et al., 2013). Islam et al. (2017c) investigated the effectiveness of the ethyl anthranilate against mosquito vectors *Aedes aegypti*, *Anopheles stephensi* and *Culex quinquefasciatus*. The results showed that the ethyl anthranilate had an effectiveness against *Aedes aegypti*, *Anopheles stephensi* and *Culex quinquefasciatus* for at least two to four hours. The chemical structure of ethyl anthranilate is shown in Figure 2.5.

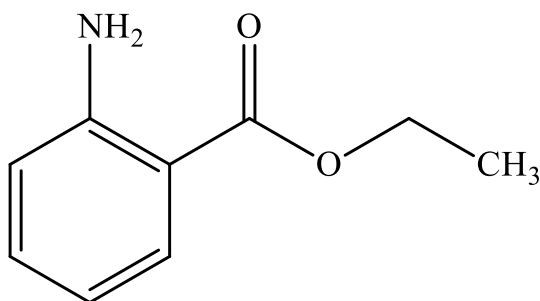


**Figure 2.5:** Molecular structure of ethyl anthranilate

Table 2.1, Table 2.2 and Table 2.3 show that the repellent-based products available on the market continue to have problems related to the short time of protection. The studies showed that the time of protection for topical formulations of DEET, IR3535 and Icaridin against several mosquitoes range from 1 to 11 hours. However, DEET-filled bicomponent fibres knitted into socks provided effectiveness against *Anopheles arabiensis* for up to 20 weeks (Sibanda et al., 2018). Furthermore, DEET remains the most efficient and effective mosquito repellent. Due to some cases of toxicity



of related to the use of DEET reported in literature, IR3535 and Icaridin are considered as alternative mosquito repellents.

## **2.6 Factors affecting the efficacy of repellents**

One of the key issues when trying to improve the effectiveness of an insect repellent is to control the volatility (readiness to evaporate) of the active ingredients. Optimum topical application is dependent on vapour phase repellence and prolonged duration (Maibach et al., 1974). In order to predict the effectiveness of repellents, it is important to understand the external factors that affect the repellents, particularly when they are applied on the skin. The external factors include: abrasion, evaporation and temperature (Maibach et al., 1974, Gabel et al., 1976, Smith, 1963, Bernard, 2005).

**Abrasion.** This occurs through friction with clothing and other objects. This can also occur through other physical activities, which allows the repellent to be lost (Maibach et al., 1974, Smith, 1963, Rueda et al., 1998).

**Evaporation.** This also plays a major role in repellent loss. This depends on the vapour pressure at ambient temperature and is related to the boiling points of the repellents. Compounds that have a lower boiling point may allow better vapour repellence, but they may dissipate faster. Compounds with higher boiling points have a low vapour pressure and would be ineffective in repelling at a distance. This may allow mosquitoes to land but not bite. Generally, most repellents are effective up to a distance of about 4 cm from the skin (Maibach et al., 1974, Smith, 1963).

**Temperature.** This goes hand-in-hand with evaporation and concerns the effect of ambient temperature on the evaporative loss of the repellent (Maibach et al., 1974). Khan et al. (1973) studied the effect of temperature on protection time of N,N-Diethyl-m-toluamide (DEET) and other repellents. They found that the protection time was halved with every 10 °C rise in ambient temperature. The authors also found that more repetitive application of the repellent was needed at temperatures over 26 °C. Other factors such as wind velocity, loss from water wash-off and sweating also affected protection time.

The effective protection periods offered by current creams and sprays are affected by the factors of evaporation, temperature, wind and abrasion. Polymer-based controlled-release repellent devices could help to avoid the need for frequent application of topical repellents. They could be worn as anklets or bracelets around the ankle or wrist. A longer protection time will prove advantageous to rural communities.

## **2.7 Evaporation rate of repellents determined using thermogravimetric analysis (TGA)**

As previously described, the evaporation rate can be regarded as one of the important physical properties of repellents which may affect efficiency. Previous studies considered the link between the evaporation rate of repellents in relation to the protection period achieved against mosquitoes (Kasman et al., 1953, Smith, 1963, Gabel et al., 1976). These results demonstrated that the protection time was inversely proportional to the evaporation rate of the repellent. The present study also compiled repellent vapour pressure data available in the literature. In addition, the aim of the present study was to investigate the rate of evaporation of repellents using thermogravimetric analysis (TGA). The repellent vapour pressure is a most important property as

it is useful for predicting the release of volatiles of repellents from polymer strands and for predicting the protection time of repellents against mosquitos. In addition, there is a paucity of evaporation rate data for repellents in the literature. The TGA method is a useful tool for determining the vapour pressure. Its advantages are the small amounts of substance required, the simplicity of the experimental set-up and the short experimental times, compared with conventional methods of vapour pressure measurement, which usually require a large amount of samples, and long sample preparation and measurement times (de Oliveira and Cremasco, 2014, Pieterse and Focke, 2003, Rong et al., 2012). In consequence, a number of articles in the literature have reported the use of TGA analysis to estimate the volatility and/or vapour pressure-temperature relationship of pure compounds (Beverley et al., 1999, de Oliveira and Cremasco, 2014, Pieterse and Focke, 2003, Hazra et al., 2002, Wright et al., 2004, Phang and Dollimore, 2001, da Silva Portela et al., 2012, Price, 2001, Rong et al., 2012).

## **2.8 Mathematical models used to estimate the volatility of repellents**

### **2.8.1 Evaporation rate**

Equation 2.1 describes the evaporation rate when it is controlled by diffusion through a stagnant gas layer (Pieterse and Focke, 2003).

$$\frac{dm_A}{dt} = \left( \frac{M_{wAA}}{zRT} \right) P_A D_{AB} \quad (2.1)$$

where  $dm_A/dt$  ( $\text{g}\cdot\text{s}^{-1}$ ) is the TGA measured rate of mass loss;  $P_A$  (kPa) is the vapour pressure of repellent at absolute temperature  $T$  (K);  $R$  ( $\text{J}\cdot\text{mol}^{-1}\cdot\text{K}^{-1}$ ) is the gas constant;  $D_{AB}$  ( $\text{m}^2\cdot\text{s}^{-1}$ ) is the

diffusion coefficient of the repellent;  $M_{wA}$  ( $\text{kg}\cdot\text{kmol}^{-1}$ ) is the molar mass of the vaporizing repellent; and  $A$  ( $\text{m}^2$ ) is the vaporization surface area.

### **2.8.2 Vapour pressure equations for pure compounds**

Vapour pressure is an important thermo-physical property in numerous chemical processes and product design applications (Mohammadzadeh and Zahedi, 2008). It can be determined experimentally using different techniques. However, with the increasing number of compounds, the calculations require a considerable investment in time and cost. Many correlations for estimating vapour pressure can be used to complement existing experimental measurements – numerous correlations are available that can be used to estimate or correlate the vapour pressure of pure liquids as a function of temperature. The present study addresses the four best-known equations namely: (i) the Wagner equation (Poling et al., 2001); (ii) the Antoine equation; (iii) the Cox equations (Roháč et al., 1999, Gobble et al., 2014); and (iv) the Myrdal and Yalkowsky equation (Myrdal and Yalkowsky, 1997).

### **2.8.3 The Wagner equation**

The Wagner equation has contributed greatly to vapour pressure data reduction. This is attributed to the fact that it can represent, with a very high accuracy, the experimental data for many substances over the entire liquid-vapour range, from the triple point to the critical point (Wu and Liu, 2005, Forero and Velásquez, 2011). The vapour pressure of decanoic acid was reported in the form of the Wagner equation (Ambrose and Ghiassaei, 1987). The Wagner equation also extrapolates well with temperature and it is represented by equation (2.2) as follows:

$$\ln P_r = (A\tau + B\tau^{1.5} + C\tau^{2.5} + D\tau^5)/T_r \quad (2.2)$$

where  $P_r = P/P_c$  is the reduced vapour pressure;  $T_r = T/T_c$  is the reduced temperature;  $\tau = 1 - T_r$ ;

$A$ ,  $B$ ,  $C$  and  $D$  are the Wagner parameters and are listed in the Table 2.4 for decanoic acid.

**Table 2.4:** Parameters of the Wagner equation used for decanoic acid (Ambrose and Ghiassee, 1987)

Temperature range (K)	Pc/kPa	Tc/K	A	B	C	D
246-726	2229.784	726.0	-9.0706	2.77535	-11.10141	-2.43545

#### 2.8.4 The Antoine equation

The Antoine equation is considered most appropriate for correlating vapour pressures over the so-called medium-pressure region that spans the pressure range from approximately 1 to 200 kPa (Roháč et al., 1999). The equation is stated in equation (2.3) for decanoic acid and in equation (2.4) for dimethyl phthalate.

$$\log_{10}(P_A) = A - [B/(T + C)] \quad (2.3)$$

$$\ln(P_A) = A - [B/(T + C)] \quad (2.4)$$

where  $P_A$  is the vapour pressure in (kPa);  $T$  is the absolute temperature in (K);  $A$ ,  $B$  and  $C$  are the Antoine constants which depend on both the compound and the measurement temperature range.

The Antoine equations were used to correlate the vapour pressures of decanoic acid (Kahlbaum, 1894) and dimethyl phthalate (Roháč et al., 1999). The constants for decanoic acid and dimethyl phthalate are listed in Table 2.5.

**Table 2.5:** Antoine equation constants and temperature range used for decanoic acid (Kahlbaum, 1894) and dimethyl phthalate (Roháč et al., 1999).

Compound	Equation form	Temperature range (K)	A	B	C
Decanoic acid	2.3	426.0 - 460.3	2.4645	733.581	-256.708
Dimethyl phthalate	2.4	466 - 552	14.82359	4660.937	-99.1086

### 2.8.5 The Cox equation

The Cox equation was previously used to correlate the vapour pressure of dimethyl phthalate (Gobble et al., 2014, Roháč et al., 1999). The Cox equation (equation (2.5)) is also known to extrapolate well with temperature (Gobble et al., 2014).

$$\ln(P/P_o) = [1 - (T_o/T)\exp\{A_0 + A_1 T + A_2 T^2\}] \quad (2.5)$$

where  $P$  is the vapour pressure in (kPa);  $T$  is the absolute temperature in (K);  $T_o$  is a constant reference temperature (K);  $P_c$  is the critical pressure in (kPa);  $A_0$ ,  $A_1$  and  $A_2$  are the Cox parameters listed in Table 2.6.

**Table 2.6:** Parameters of the Cox equation and range of temperature used for dimethyl phthalate (Roháč et al., 1999, Gobble et al., 2014).

Temperature range (K)	$T_o$ /K	$P_0$ /kPa	$A_0$	$A_1$	$A_2$
324 - 552	555.799	101.325	3.076854	-0.001650657	1.17163E-06

### 2.8.6 The Myrdal and Yalkowsky equation

Recent research findings have indicated that the available vapour pressure values of compounds in the literature have some inconsistencies. Therefore, the reproducibility of the data depends on the experiments and the method used to determine the vapour pressure (Nhlapo, 2013). The method proposed by Myrdal and Yalkowsky is widely used to estimate the vapour pressure of liquid compounds (Myrdal and Yalkowsky, 1997). In this work, the Myrdal and Yalkowsky method was used to estimate the vapour pressure of the repellents. The formula is given by equation (2.6) as follows:

$$\log_{10}(P) = -\frac{[86.0+0.4\tau+1421HBN](T_b-T)}{19.1T} + \frac{[-90.0-2.1\tau]}{19.1T} + \left(\frac{T_b-T}{T} - \ln\frac{T_b}{T}\right) \quad (2.6)$$

where  $T_b$  is the boiling point in (K); the parameters  $\tau$  and  $HBN$  characterize the molecular structure representing the torsional bond and the hydrogen bond number. The parameters  $\tau$  and  $HBN$  are determined using the semi-empirical equations described in equation (2.7) and equation (2.8).

$$HBN = \frac{\sqrt{n(-OH)+n(-COOH)+0.33\sqrt{n(-NH_2)}}}{M_w} \quad (2.7)$$

where  $n(-OH)$ ,  $n(-COOH)$  and  $n(-NH_2)$  represent the number of functional groups of alcohols, carboxylic acids or primary amines respectively,  $M_{WA}$  is the molecular weight of the repellent.

$$\tau = SP3 + 0.5SP3 + 0.5RING - 1 \quad (2.8)$$

where  $SP3$  is the  $\Sigma$  non-ring, non-terminal  $sp^3$  atoms (e.g.  $CH_2$ ,  $CH$ ,  $C$ ,  $NH$ ,  $N$ ,  $O$ ,  $S$ );  $SP2$  is the  $\Sigma$  non-ring, non-terminal  $sp^2$  atoms ( $=CH$ ,  $=C$ ,  $=N$ ,  $C=O$ ); and  $RING$  is the  $\Sigma$  independent single, fused or conjugated ring system (Jain and Yalkowsky, 2006).

In the torsional bond, terminal groups such as -CH<sub>3</sub>, -NH<sub>2</sub>, -OH, -CN<sup>-</sup>, -F<sup>-</sup>, -Cl<sup>-</sup>, Br<sup>-</sup>, -I<sup>-</sup>, = O, = CH<sub>2</sub> and 2N as well as non-terminal *sp*. Hybrid carbons are not included. Also not included are carbon atoms with three identical groups. Compounds with a negative value of  $\tau$  are assigned a value of zero, and for compounds containing aliphatic cyclic rings such as cyclohexane, a value of -2 per ring is added (Jain et al., 2004).

## 2.9 Diffusion coefficients ( $D_{AB}$ )

Several methods are used for estimating diffusion coefficient in low-pressure for binary gas systems such as the equations proposed by Arnold, Gilliland, Fuller, Wilke and Lee, Bairley, Chen and Othmer (Poling et al., 2001). However, in this work, the procedure proposed by Wilke and Lee equation was used to estimate the diffusion coefficient in air of liquid repellents. The Wilke-Lee equation proposed was used due its reliability (Wilke and Lee, 1955). The equation is presented in equation (2.9) as follows:

$$D_{AB} = \frac{\left[ 3.03 - \left( \frac{0.98}{2\sqrt{M_{wAB}}} \right) \right] (10^{-3}) T^{\frac{3}{2}}}{P^2 \sqrt{M_{wAB}} \sigma_{AB}^2 \Omega_D} \quad (2.9)$$

where  $D_{AB}$  (cm<sup>2</sup>·s<sup>-1</sup>) is the binary diffusion coefficient;  $T$  (K) is the temperature;  $M_{wA}$  and  $M_{wB}$  are molecular weights of substances A (repellent) and B (air) represented in g·mol<sup>-1</sup>;  $P$  is the pressure in bar.  $M_{wAB}$  is obtained from equation (2.10).

$$M_{wAB} = 2 \left[ \frac{1}{M_{wA}} + \frac{1}{M_{wB}} \right]^{-1} \quad (2.10)$$

The scale parameter  $\sigma_{AB}$  is obtained from equation (2.11).



$$\sigma_{AB} = \frac{(\sigma_A + \sigma_B)}{2} \quad (2.11)$$

where each component is written by equation (2.12)

$$\sigma = 1.18 V_b^{1/3} \quad (2.12)$$

$V_b$  is the liquid molar volume at the normal boiling temperature ( $T_b$ ), which can be obtained from experimental data or estimated using empirical methods. For decanoic acid, dimethyl phthalate, DEET and ethyl anthranilate, the method proposed by Rackett (Poling et al., 2001) to determine the pure saturated-liquid molar volume was used. The equation used is presented by equation (2.13).

$$V_b = V_c z_c^{(1-T_b/T_c)^{2/7}} \quad (2.13)$$

where  $V_c$  is the critical volume;  $z_c$  is the critical compressibility factor;  $T_c$  is the critical temperature in (K). The molar volumes  $V_b$  and  $V_c$  have units of  $\text{cm}^3 \cdot \text{mol}^{-1}$ .

The critical compressibility factor is obtained by equation (2.14):

$$Z_c = \frac{P_c V_c}{R T_c} \quad (2.14)$$

where  $R$  is the gas constant and the critical parameters ( $T_c$ ,  $V_c$  and  $P_c$ ) were found in the literature and are listed in Table 2.7.

**Table 2.7:** Names of repellents, critical temperature, critical volume and critical pressure and sources

Repellent	$T_c$ /(K)	$V_c$ /(m <sup>3</sup> ·kg·mol <sup>-1</sup> )	$P_c$ /(kPa)	Source
DEET	778.19	0.620	2 517.59	Cheméo ( <a href="https://www.chemeo.com">https://www.chemeo.com</a> )
Ethyl anthranilate	812.12	0.484	3 615.89	Cheméo ( <a href="https://www.chemeo.com">https://www.chemeo.com</a> )
Dimethyl phthalate	831.50	0.540	3 191.93	Cheméo ( <a href="https://www.chemeo.com">https://www.chemeo.com</a> )
Decanoic acid	726.0	0.621	2 161.74	Cheméo ( <a href="https://www.chemeo.com">https://www.chemeo.com</a> )

The liquid molar volume at the normal boiling temperature for Icaridin and IR3535 was estimated using the additive method suggested by Schroeder (Poling et al., 2001). This method was used for these two repellents (Icaridin and IR3535) because the critical parameters ( $T_c$ ,  $V_c$  and  $P_c$ ) were not found in the literature.

The method uses the analogy of counting the numbers of carbon, hydrogen, oxygen, and nitrogen atoms, and then adding one (1) for each double bond ( $D_B$ ), two (2) for each triple bond ( $T_B$ ) and multiplying the sum by seven. The formula used is described by equation (2.15):

$$V_b = 7(N_C + N_H + N_O + N_N + N_{D_B} + 2N_{T_B}) + 31.5N_{Br} + 24.5N_{Cl} + 10.5N_F + 38.5N_I + 21N_S - 7^{\#} \quad (2.15)$$

The additive method has been extended to include halogens and sulphur. The last value in equation (2.15) given by ( $\#$ ) is counted once if the compound has one or more rings (Poling et al., 2001).  $V_b$  is represented by cm<sup>3</sup>·mol<sup>-1</sup>.

The collision integral  $\Omega_D$  calculated from the accurate relation proposed by Neufield (Poling et al., 2001) is given in equation (2.16):

$$\Omega_D = \frac{A}{(T^*)^B} + \frac{C}{\exp(DT^*)} + \frac{E}{\exp(FT^*)} + \frac{G}{(HT^*)} \quad (2.16)$$

where  $T^* = kT/\varepsilon_{AB}$  and  $A, B, C, D, E, F, G$  and  $H$  are parameters of the collision integral (Poling et al., 2001). All parameters are listed in Table 2.8.

For each component  $(\varepsilon/k)_{AB}$  is calculated using equation (2.17), while  $\varepsilon_{AB}$  is determined using a simple equation (2.18):

$$\varepsilon/k = 1.15T_b \quad (2.17)$$

$$\varepsilon_{AB} = \sqrt{\varepsilon_A \varepsilon_B} \quad (2.18)$$

where  $T_b$  is the normal boiling point (at 1 atm) in (K). For systems in which one component is air,  $\sigma_{air} = 3.62 \text{ \AA}$  and  $\varepsilon/k_{air} = 97.0 \text{ K}$ .

**Table 2.8:** Parameters of the collision integral  $\Omega_D$  (Poling et al., 2001).

A	B	C	D	E	F	G	H
1.06036	0.15610	0.19300	0.47635	1.03587	1.52996	1.76474	3.89411

## 2.10 Estimating air permeability

The release rate of a pure volatile compound into air is determined by its air permeability. The release rate parameter is the product of the vapour pressure of the compound and its diffusion coefficient in air as described in equation (2.19) (Pieterse et al., 2006).

$$S_A = P_A D_{AB} \quad (2.19)$$

where  $S_A$  is the air permeability represented by ( $\text{mPa} \cdot \text{m}^2 \cdot \text{s}^{-1}$ );  $P_A$  (kPa) is the vapour pressure; and  $D_{AB}$  is the diffusion coefficient in ( $\text{m}^2 \cdot \text{s}^{-1}$ ).

However, from equation (2.19) it was possible to calculate the experimental diffusion coefficient through the relation to air permeability. In this regard the experimental values of the evaporation rates of repellents obtained by TGA and Payne cups and vapour pressure were considered. The simple equation is given by equation (2.20) as follows:

$$D_{AB} = S_A / P_A \quad (2.20)$$

## 2.11 Polyolefin-clay nanocomposites

Annually, it is estimated about 250 million tons of plastics are produced worldwide (Hong and Rhim, 2012). Polyolefins constitute the most widely used group of thermoplastics due to acceptable strength, light weight, low cost, easy processability and good water barrier properties. They are prepared by polymerization of simple olefins such as ethylene, propylene, butenes, isoprenes and pentenes, as well as their copolymers (Subramanian, 2017). An inherent characteristic common to all polyolefins is a nonpolar, nonporous, low-energy surface that is not

receptive to inks and lacquers without special oxidative pre-treatment (Sadiku et al., 2017, Hammen, 2014, Chrissopoulou and Anastasiadis, 2010). Polyolefin-based materials can be tailor-made for a wide range of applications, from rigid thermoplastics to high-performance elastomers (Chrissopoulou and Anastasiadis, 2011).

Since the first production of polyolefins following the development of Ziegler-type catalysts, commercial exploitation has been very rapid because of their attractive characteristics. However, polyolefins are notch sensitive and brittle on exposure to severe conditions, such as low temperature and high rate of impact (Chrissopoulou and Anastasiadis, 2010, Chrissopoulou and Anastasiadis, 2011). In order to improve the application of polyolefins, fillers are incorporated into polyolefins to increase the stability, heat distortion, stiffness, strength and impact resistance without sacrificing their processability and barrier property (Hong and Rhim, 2012, Marchante and Beltrán, 2015, Chrissopoulou and Anastasiadis, 2011).

As an introductory concept, nanocomposite materials are two-phase systems that consist of a polymer matrix and dispersed inorganic particles of nanometer scale. The inorganic particles usually come from the family of 2:1 phyllosilicate, which consists of an aluminium or magnesium hydroxide octahedral sheet sandwiched between two silicon oxide tetrahedral sheets. The layer thickness of each platelet is around 1 nm, and their lateral dimensions may vary from 30 nm to several microns as briefly described in Figure 2.6 (Choudalakis and Gotsis, 2009).

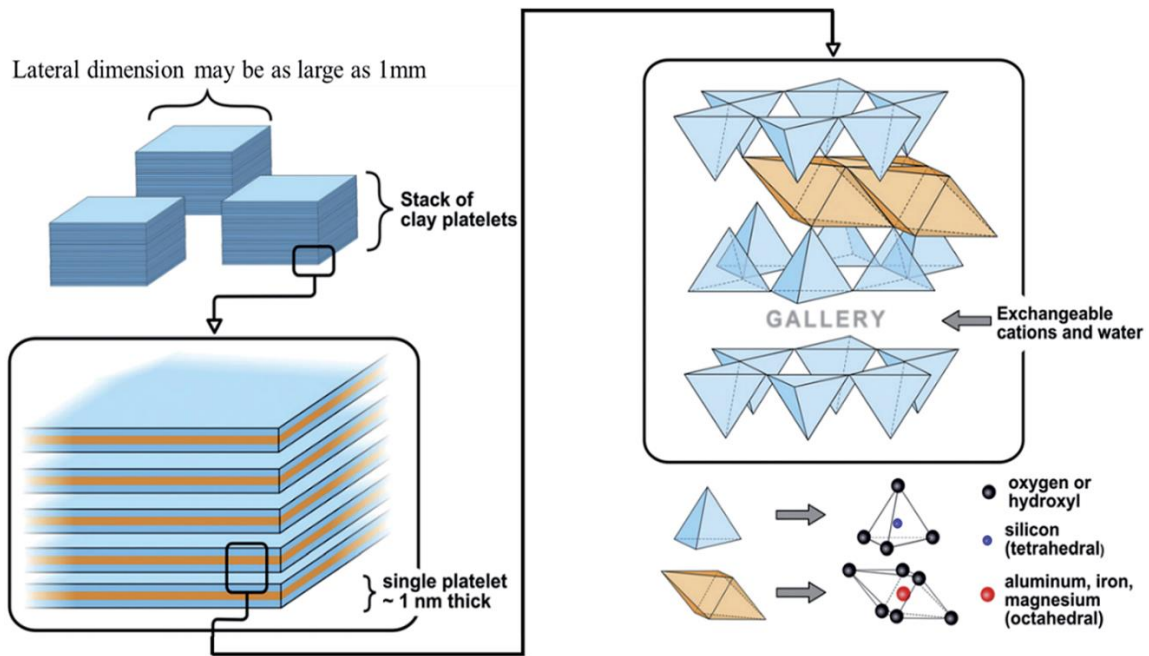


**Figure 2.6:** Structure of montmorillonite (phyllosilicate clay) (taken from Duncan, 2011)

Three types of nanocomposite morphology are possible depending on the strength of the interfacial interaction. These are: (i) phase-separated; (ii) intercalated; and (iii) exfoliated as shown in Figure .7. For phase-separated nanocomposites, clay tactoids are obtained throughout the matrix. The polymer chains surround nanoclay platelets but do not penetrate between the clay layers. However, the lack of platelet separation may form large, micron-sized agglomerates (Pavlacky et al., 2012). Intercalation involves the insertion of polymer chains in the galleries of the initial layered tactoids, which leads to a longitudinal expansion of the galleries. Exfoliation implies the formation of a complete breakage of the initial layer stacking order and homogeneous dispersion of the layers in the polymer matrix. Complete exfoliation of the layered silicate in the polymer matrix is often aimed at developing clay-based nanocomposites (Cui et al., 2015).

There are three methods typically used when preparing a polymer-nanocomposite (Choudalakis and Gotsis, 2009):

- ❖ Intercalation in a suitable monomer and subsequent in situ polymerization which leads to exfoliation
- ❖ Intercalation of the polymer from the solution and exfoliation
- ❖ Polymer melt intercalation and exfoliation.

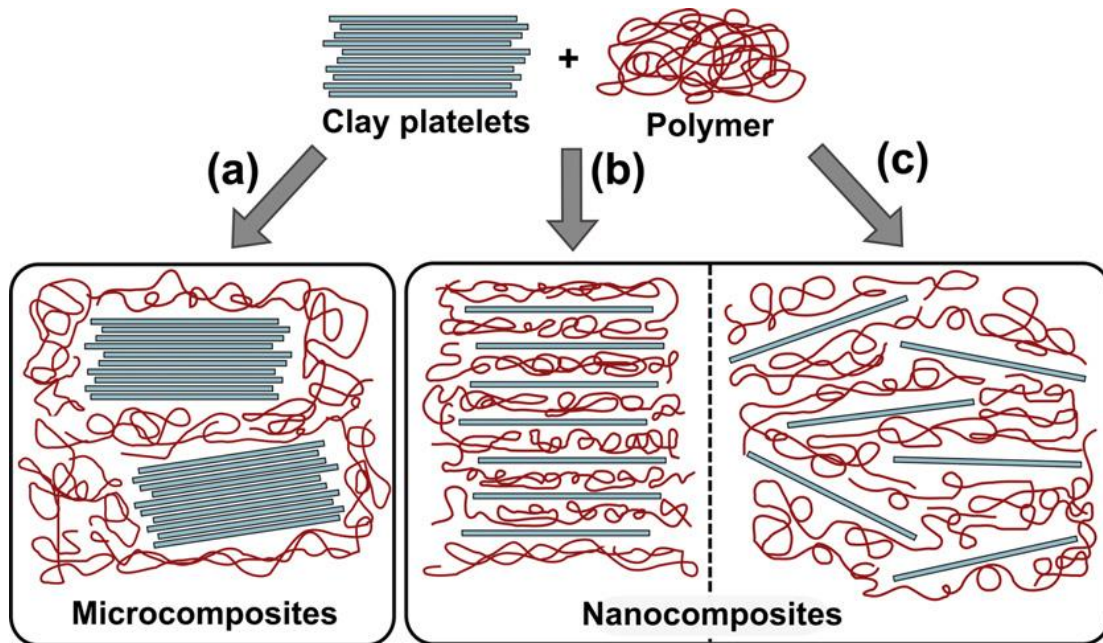


**Figure 2.7:** (a) Tactoid; (b) intercalated, and (c) exfoliated polymer nanocomposites (Duncan, 2011)

Layered inert silicate nanoclays (such as montmorillonite and kaolinite) seem to be the most effective nanoscale fillers due to their rich intercalation chemistry and high strength (Cui et al., 2015). Furthermore, there is great interest in montmorillonite because it is abundant, relatively inexpensive and easy to modify (to make it more compatible with polymers) and has shown good results (Marchante and Beltrán, 2015). Exfoliation of nanofillers can yield individual platelets dispersed in a polymer matrix. Small molecules cannot pass through the nanoplatelets and therefore their presence enforces a tortuous diffusion path which constitutes a barrier structure for

gases (Cui et al., 2015). It has been found that gas permeability through polymer films can be reduced by 50 – 500 times even at low clay loadings (Choudalakis and Gotsis, 2009).

Nanocomposites that incorporate the exfoliation method produce the highest surface area interaction between clay nanoplatelets and the polymer, and thus they have improved performance. Homogeneous dispersion of clay in polymers is not easy because of the preferential parallel sticking of the clay nanoplatelets and hydrophilicity of its surface (Pavlacky et al., 2012). In fact, the incompatibility between hydrophilic clay and hydrophobic polymer often causes agglomeration of clay mineral particles in the polymer matrix (LeBaron et al., 1999).

In situ polymerization has been found to be the most effective technique to obtain well-exfoliated clay nanoplatelets in a polymer matrix compared with melt and solution intercalation methods (Bouzouita et al., 2017, Cui et al., 2015). Unfortunately, this method is not always practicable from the industrial viewpoint. The alternative melt intercalation technique is most versatile and less environmentally harmful and is therefore an efficient method of preparing polymer nanocomposite in an industrial setting (Bouzouita et al., 2017).

### **2.11.1 Permeability of nanocomposites**

The permeability of barrier polymer films can be defined as the ability to allow gases and vapours to pass through them (Feldman, 2001). The barrier properties of polymer films are dependent on the nature of the polymer (density, solubility, morphology, filler concentration), the fluid nature and concentration, the area and thickness of the film, permeation time and temperature (Feldman, 2001). During the permeability process through a polymer film, the solution is first absorbed onto the high-pressure surface of the polymer. The dissolved fluid then diffuses through the polymer



according to the concentration gradient towards the lower-pressure opposite surface. Lastly, the fluid on the other side of the film desorbs (Feldman, 2001).

For a steady state diffusion across the film, gas or fluid measurements can be made using the constant volume, changing pressure approach. This approach involves applying a vacuum to both sides of the film, with thickness  $L_f$ , situated inside the permeability cell, and calculating the permeability coefficient  $P$  (the permeation of penetrate molecules thought the film) from equation (2.21) (Cui et al., 2015).

$$P = \frac{VL_f}{ART\Delta p} \frac{dp}{dt} \quad (2.21)$$

where  $P$  is the permeability coefficient in ( $\text{g}\cdot\mu\text{m}\cdot\text{day}^{-1}\cdot\text{mm}^{-2}$ );  $V$  is the total amount of gas permeation through the film into a cell;  $A$  is the film area,  $R$  the universal gas constant;  $T$  the absolute temperature;  $\Delta p$  the pressure gradient across the film; and  $dp/dt$  the transmission rate.

The permeability coefficient of a polymer is also equal to the product of the diffusion coefficient  $D$  (movement of the penetrated molecules inside the film) and the solubility coefficient  $S$  (dissolution of a permeant molecule into a film). This relation, which is often used to describe the gas transport properties of composites reinforced with nanofillers in a polymer matrix, only holds true if the value of  $D$  is independent of concentration and  $S$  follows Henry's law. This is clearly described by equation (2.22) (Cui et al., 2015).

$$P = DS \quad (2.22)$$

As part of the second step in the polymer permeability process, diffusion through a film includes permeation or passing through the voids and gaps between macromolecules. The diffusion rate in general can be described by Fick's secondary law shown in equation (2.23) (Feldman, 2001).

$$\frac{dc}{dt} = -D \frac{d^2c}{dx^2} \quad (2.23)$$

where  $dc/dt$  is the concentration variation over time in days.

Nanocomposites show better barrier properties (Cui et al., 2015) than homogeneous films owing to the tortuous diffusion pathways. This phenomenon is illustrated in Figure 2.8. The effective path length for gas diffusion is increased in this way while the diffusion coefficient decreases. Therefore, a decrease in the solubility is also expected in the nanocomposite due to the reduced polymer matrix volume.

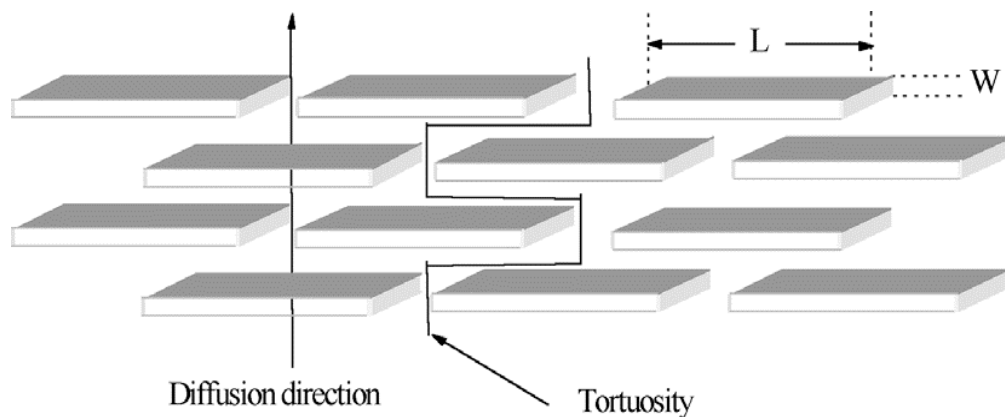


**Figure 2.8:** Arrangement of parallel platelets causing a tortuous pathway (Choudalakis and Gotsis, 2009).

Thus, it can be noted that the volume fraction of the nanoplatelets (degree of dispersion), their orientation relative to the diffusion direction and their aspect ratio have an impact on the permeability (Choudalakis and Gotsis, 2009). The delamination of the clay affects the degree of

dispersion of the nanofiller. Fully delaminated (exfoliated) sheets with a high aspect ratio in the nanocomposite present much higher values for the tortuosity factor than those with partially delaminated nanocomposite platelets (i.e. intercalated). Figure 2.9 shows the effect of the degree of delamination on the tortuosity factor and the aspect ratio of the nanoplatelets.

Many mass transfer models assume that the platelets have a regular and uniform shape (rectangular or circular) and form a regular array in space (Choudalakis and Gotsis, 2009). Their orientations are either parallel to one another and perpendicular to the diffusion direction (Figure 2.8) or a distribution of orientations with the average orientation at an angle to the main direction of diffusion.

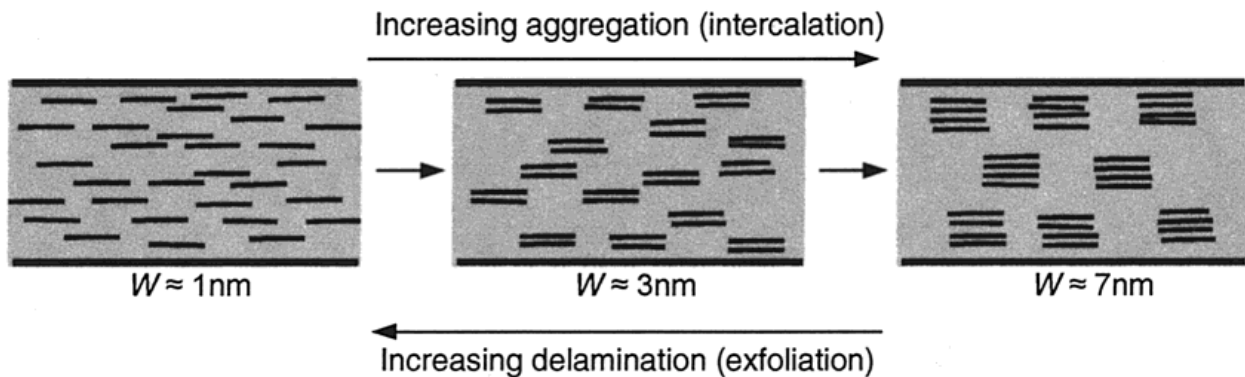


**Figure 2.9:** Effect of the degree of delamination on the tortuosity factor and the aspect ratio of nanoplatelets.  $W$  is the thickness of the stacks (Choudalakis and Gotsis, 2009, Bharadwaj, 2001)

A number of studies have reported on how to develop intercalated or exfoliated nanocomposite structures with polyolefin/montmorillonite (MMT) (Yano et al., 1993, Meng et al., 2008, Durmus et al., 2007, Nikkhah et al., 2009, Corcione et al., 2008, Hong and Rhim, 2012, Rahnama et al., 2014, Hotta and Paul, 2004, Golebiewski et al., 2008). These studies revealed that the incorporation procedure into a polymer matrix is important in order to obtain complete nanoclay

dispersion. To the best of our knowledge, there has been no work reported about the effect of organo-montmorillonite (OMMT) in the barrier property of polyolefin nanocomposite matrices against volatile mosquito repellents. However, two trials of this work were devoted to evaluating the barrier properties of polyolefin nanocomposite films against repellents and the use of exfoliated clay to reduce the repellent release rate from polyolefin strands.

## **2.12 Microporous polymers**

Microporous polymer structures have been prepared by different methods, including non-solvent-induced phase separation (NIPS) (Xin et al., 2012), solvent-induced phase separation (SIPS) (Chen and Shanks, 2007), thermally induced phase separation (TIPS) (Castro, 1981) and thermally assisted evaporation phase separation (TAEPS) (Hellman et al., 2004).

### **2.12.1 The thermally induced phase separation (TIPS) method**

The TIPS method was introduced by Castro (Castro, 1981). Among all the methods mentioned above, TIPS has become one of the most useful for the preparation of microporous polymer structures (Liu et al., 2011, Lloyd et al., 1990). Due to its advantages such as ease of control and a low tendency towards production defects, TIPS is able to produce a variety of relatively thick isotropic microporous microstructures capable of producing suitable controlled release (Cha et al., 1995, Liang et al., 2013). Microporous materials have been of great interest in many potential membrane applications in the fields of microfiltration, ultrafiltration, reverse osmosis, gas separation, clean energy, catalysis and storage media due to their extraordinarily high porosity and surface area (Kim and Lee, 2015). Various polymers were used to prepare microporous structures via the TIPS method. They included: (i) Polypropylene (PP) (Kim and Lloyd, 1991, Lim et al.,

1991, Lloyd et al., 1990, Yang et al., 2006); (ii) Polyvinylidene fluoride (PVDF) (Li et al., 2008, Yang et al., 2008, Lin et al., 2009, Rajabzadeh et al., 2009); (iii) Poly(ethylene-co-vinyl alcohol) (EVOH) (Zhou et al., 2009, Shang et al., 2003); (iv) Polystyrene (Matsuyama et al., 2001, Kim et al., 2007); and (v) polyethylene (PE) (Wang et al., 2015, Lloyd et al., 1990, Akhtar and Focke, 2015, Matsuyama et al., 2003, Liu et al., 2011, Shen et al., 2008, Yang et al., 2006, Israel et al., 1995, Gong et al., 2012). Therefore, the preparation of microporous structures using polyolefins has been extensively studied owing to their good thermal and solvent resistance as well as their low cost. Generally, for the preparation of microporous polymer structures by the TIPS method, the steps listed below are followed (Lloyd et al., 1990, Wang et al., 2015, Liu et al., 2011):

- ❖ In the TIPS process, a homogeneous solution is obtained at an elevated temperature by blending the polymer with the diluent or liquid. The liquid is usually a low molecular weight and high boiling point diluent in which the polymer is effectively insoluble at room temperature (Akhtar and Focke, 2015).
- ❖ The solution is then cooled down or quenched to induce solid-liquid (S-L) or liquid-liquid (L-L) phase separation.
- ❖ After the solvent extraction and drying (typically by evaporation), a microporous polymer with the desired structure is formed.

In the present study, the preparation of microporous polyolefin structures as reservoirs to trap large amounts of repellent via thermally-induced phase separation is discussed. A typical phase diagram showing the phase behaviour of a polymer-liquid repellent combination is shown in Figure 2.10.

The system exhibits an upper critical solution temperature (UCST) showing the stable single-phase region together with the metastable and unstable regions.

The phase diagram indicates that the probability of forming a microporous matrix is high when the polymer is the minority phase. In polymer-repellent mixtures the loci of the phase boundaries can be described by the Flory-Huggins theory (Burghardt, 1989). At temperatures above the UCST, the system is fully miscible for all compositions. Below this temperature, phase separation can occur at a temperature which depends on the concentration of the system components (Charlet and Delmas, 1981). The compositions of the two phases in equilibrium at any temperature are defined by the binodal line. In the metastable region indicated in the phase diagram, the phase separation will occur via a nucleation and growth mechanisms (Nunes and Inoue, 1996). This is the usual scenario for liquid-liquid phase separation (Nunes and Inoue, 1996). If the polymer represents the minority phase, it may initially lead to the undesirable formation of separate polymer particles that are suspended in the continuous liquid repellent phase.

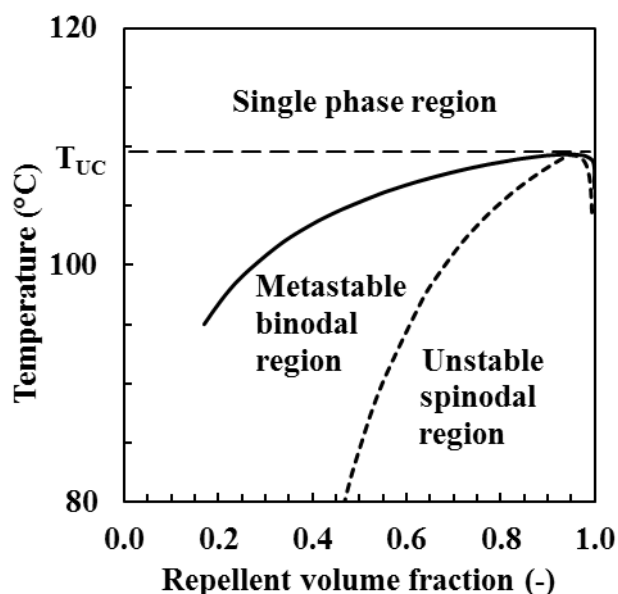


**Figure 2.10:** Phase diagram of a typical miscible polymer-repellent system. The solid line defines the binodal phase boundary and the broken line the spinodal envelope (Akhtar and Focke, 2015)

Inside the two-phase region there is another set of phase envelope, the spinodal curves. In this region of the phase diagram, a homogeneous mixture is thermodynamically completely unstable. In contrast to the metastable bimodal region, the solution will spontaneously split into two phases via spinodal decomposition, a polymer-rich phase and a solvent-rich phase. Phase separation by this mechanism leads to a finely dispersed microstructure via diffusion processes that amplify intrinsic thermodynamic spatial composition fluctuations. Ultimately this co-continuous structure may be fixed by either the subsequent crystallization of the polymer, or by vitrification of the polymer-rich phase. This means that the majority liquid phase is trapped inside a solid polymer-rich phase (which still may contain a minor amount of repellent) with a porous structure. In practice such microporous microstructures are often achieved by rapid quenching of a homogeneous melt in a cold-water bath.

### **2.13 Controlled-release system**

Controlled release is a technology which is used to protect the supply of the reagent and to allow the release of the agent to the target at a controlled rate, and to maintain its concentration in the system within the optimum limits over a prolonged or specified period (Kenawy et al., 1992, Akelah, 1996, Céspedes et al., 2007). The advantages of this technology are listed as: activity prolongation by providing continuous low amounts of a drug at a level sufficient to perform its function over a long period of time; environmental pollution reduction; cost reduction by eliminating the time and cost of repeated and over-applications (Kenawy et al., 1992). This reduces the undesirable side-effects of compound losses such as insecticides or repellents by evaporation and degradation; masking of any odour, since toxic material becomes chemically non-toxic when combined with polymers (Akelah, 1996, Kenawy et al., 1992, Dubey et al., 2011). In order to select the best system to release a sufficient quantity and to achieve the desired effect with minimum biological or ecological adverse risks, the following characteristics need to be considered: (i) the nature of polymer (degree of cross-linking, thermal behaviour, compatibility with the active agent); (ii) stability of the combination during processing; (iii) the desired release rate; (iv) shape and size of the final product; (v) duration of protection time; (vi) seasonal conditions; and (vii) cost and ease of formulation and application (Akelah, 1996). Brade and Davis (1983) investigated the release of chemicals from a porous polymer. They used methyl nonyl ketone (KNK), dimethyl phthalate (DMP) and DEET as repellents. The porous polymer used was made from polypropylene. The results showed that the release rate of DEET from porous polypropylene was constant for 90 days.



For protection against mosquitoes, the concentration of active ingredient in the repellent should have a constant rate of release during a sufficiently prolonged period. However, the efficacy of mosquito repellents is restricted by several factors, such as their fast volatility and their ability to penetrate the skin. For these reasons, new tools have been developed to achieve longer mosquito protection times (Sibanda et al., 2018). The controlled-release technology based on polymer matrices are largely used due their low cost and versatility (Tramon, 2014). The mechanisms involved in controlled release require polymers with a variety of physicochemical properties (Nogueira Barradas et al., 2016).

Previous studies by Akhtar (2015), Sibanda and Focke (2014) and Sibanda (2016) show that polymers have been used as carriers for the controlled release of volatile compounds. A study by Licciardello et al. (2013) incorporated essential oil into packaged food. The effectiveness of coated packaging against red flour beetle (*Tribolium castaneum*) showed repellence results which ranged from 53 to 83% for citronella and rosemary. Arancibia et al. (2014) developed active biodegradable films based on soy protein, lignin and formaldehyde added to citronella. The results showed that the presence of 3 wt-% citronella in polymeric films had good antifungal activity against the pathogen *Fusarium oxysporum* in bananas. Chattopadhyay et al. (2015) evaluated the repellence activity of an essential oil-based polymeric patch against mosquitoes. The product provided up to 3 hours protection. In addition, Islam et al. (2017a) evaluated the stability potential of matrix-type polymeric patches composed of volatile ethyl anthranilate for prophylaxis against vector-borne diseases. The polymeric matrix based on ethyl anthranilate was successful and the optimized polymeric patches remained stable for six months under the conditions studied without significant changes. These earlier studies demonstrated different ways of incorporating mosquito repellent in

polymer matrices and proved their effectiveness against insects. The polymeric materials used for designing different devices not only enhanced the physical-chemical stability but also the safety by entrapping the volatile compounds internally and releasing them at a desired controlled rate (Islam et al., 2017a).

Therefore, kinetic modelling of controlled release systems is necessary to predict the volatile compound release and protection time against insects. If the model is consistent, the behaviour of different combinations of active ingredients of compound and polymeric materials can be simulated at a reduced cost to achieve the desired performance (Tramon, 2014). Mathematical modelling of controlled release systems reduces the time and resources necessary for experimental work in product and process development (Tramon, 2014). In the next section, a model of repellent release from microporous polymer strands is described.

### 2.13.1 Modelling for repellent release from polymer strands

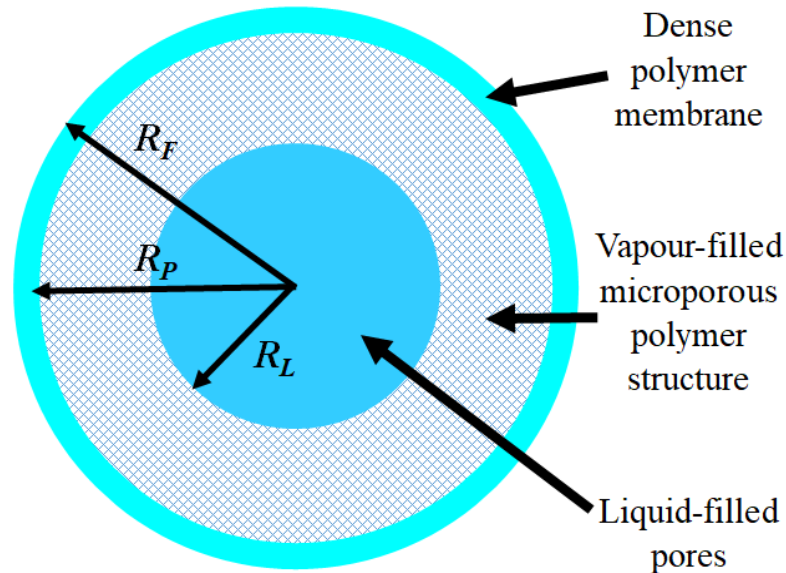


**Figure 2.11:** Model of the microporous strand showing the liquid core location, the vapour-filled microporous region and the outer skin layer that functions like a membrane that limits the rate at which the repellent is released

Figure 2.11 shows a schematic of a long cylindrical microporous strand covered by a thin membrane-like outer skin layer, which serves as a model of the repellent-release characteristics. The geometric features of this model were informed by the FESEM results presented in Chapter IV. The cross-section is assumed to be circular, and the structure of the inner polymer section is assumed to be microporous. Conceptually it corresponds to an open-cell polymer foam which is initially completely filled with the liquid repellent. As the repellent is gradually released into the atmosphere, it is assumed that the outer pores are progressively emptied, and the lost liquid is replaced by air and repellent vapour. In a first approximation, it is assumed that the location of the liquid-vapour boundary is concentric with the outer wall.

In order for the active compound to be released from the strand, a portion of the liquid evaporates and diffuses through the porous matrix towards the outer membrane. The matrix polymer forms both the microporous structure and the outer membrane. The permeability of the repellent through this membrane is defined by the product of its solubility in the membrane and the diffusion coefficient inside the membrane. The implication is that the active ingredient is also dissolved in the rest of the microporous polymer structure. This has several implications, including the fact that the polymer structure could change shape (e.g. shrink) and that it can contribute to the rate of mass transport. However, in this first-cut analysis these effects are ignored. The fact that the active ingredient must diffuse through a porous polymer maze also affects the release rate. Therefore, it is necessary to consider the transport mechanisms of the active ingredient in the porous region in addition to the permeation through the membrane. In reality, surface tension will affect the shape of the liquid meniscus inside partially filled pores. This has implications for the rate at which the liquid transforms into vapour, i.e. the evaporation rate. At present this is not taken into account. Finally, it is assumed that, once the repellent molecules reach the outside surface of the strand, they are rapidly removed by convection air currents so that it can be assumed that the concentration on the outside surface of the strand is negligible.

The mathematical model for the release of the repellent assumes that it is determined by vapour diffusion in the porous regions and by permeation through the outer skin layer. At the inner liquid surface, the repellent evaporates into the porous region. It then diffuses via the air-filled pores towards the membrane where it dissolves in the polymer and permeates to the outside. The assumptions forming the basis of the model can be summarised as follows:

- ❖ The porosity of the microporous region is  $\varepsilon$ .

- ❖ The liquid-filled region is located concentric to the cylindrical strand of the main polymer.
- ❖ The diffusion equation holds for both the porous region as well as for the membrane, but the effective diffusion coefficients differ.
- ❖ The equilibrium vapour concentration at the liquid interface can be estimated from the ideal gas expression given by equation (2.24)

$$\rho_{eq} = \frac{M_A P_A^{sat}}{RT} \quad (2.24)$$

which expresses the equilibrium mass density ( $\rho_{eq}$ ) of the repellent at temperature  $T$  in Kelvin in terms of its molar mass ( $M_A$ ) and its vapour pressure ( $P_A^{sat}$ ), where  $R$  denotes the gas constant.

- ❖ The solubility of the repellent in the membrane is described by Henry's law.
- ❖ The evaporation rate is very slow so that quasi-steady state diffusion may be assumed.

The initial mass of repellent inside a strand, for which the diameter of the porous region is  $R_p$ , is given by equation (2.25):

$$m_o = \rho_L \varepsilon \pi R_p^2 L \quad (2.25)$$

After some time, during which part of the repellent has evaporated, the fraction of remaining repellent will be according to equation (2.26):

$$X = m(t)/m_o \quad (2.26)$$

and the remaining liquid is assumed to be confined to a co-axial cylindrical body with radius  $R_L$ .

The total amount of the repellent remaining in a filament of length  $L$  is given by equation (2.27):

$$X(t) = \frac{2}{R_P^2 C_L} \int_{R_L}^{R_P} r C(r, t) dr + \left(\frac{R_L}{R_P}\right)^2 \quad (2.27)$$

However, the first term is negligible compared to the second term because, compared to the liquid, the repellent vapour density is very low so that instead it is assumed that (equation 2.28) applies:

$$X(t) \approx \left(\frac{R_L}{R_P}\right)^2 \quad (2.28)$$

The governing diffusion equation is given as equation (2.29) as follows:

$$\frac{\partial \rho}{\partial t} = \frac{D_{eff}}{r} \left( \frac{\partial}{\partial r} \left( r \frac{\partial \rho}{\partial r} \right) \right) \quad (2.29)$$

This equation holds for both the outer membrane and the vapour-filled porous region, but the effective diffusion coefficients in these two regions are assumed to be different. The initial and boundary conditions are:

- (1)  $t = 0, \quad 0 < r < R_p \quad \rho = \rho_L$
- (2)  $t > 0, \quad r = R_L \quad \rho = \rho_{eq}$
- (3)  $r = R_P \quad \rho_M(R_P^+) = H \rho_P(R_P^-)$
- (4)  $r = R_P \quad D_P \left( \frac{\partial \rho}{\partial r} \right)_{r=R_P^-} = D_M \left( \frac{\partial \rho}{\partial r} \right)_{r=R_P^+}$

$$(5) \quad r = R_F \quad \rho = 0$$

The assumption of quasi-steady state conditions is justified by the fact that the release rate is very low. This reduces the problem to solving the following differential equation, equation (2.30) as follows:

$$\frac{d}{dr} \left( r \frac{d\rho}{dr} \right) = 0 \quad (2.30)$$

The solution of equation (2.30), subject to the initial and boundary conditions, yields expressions for the concentration profiles in the membrane and the microporous regions for a given value of the stationary liquid core radius  $R_L$ . The rate at which the repellent evaporates is related to the rate at which  $R_L$  decreases. Equation (2.31) describes this phenomenon:

$$\rho_L \frac{dR_L}{dt} = D_P \left. \frac{\partial \rho}{\partial r} \right|_{r=R_L^+} \quad (2.31)$$

Taking this into expression into account, analysis yields an implicit expression that links the amount of repellent released ( $X$ ) to the elapsed time ( $t$ ).

**Model I** is represented by equation (2.32).

$$\kappa_1 t = \kappa_2 (1 - X) + X \ell n X \quad (2.32)$$

where  $\kappa_1$  is obtained by equation (2.33):

$$\kappa_1 = \frac{4D_P \rho_{eq}}{R_P^2 \rho_L} \quad (2.33)$$

and  $\kappa_2$  is obtained by equation (2.34):

$$\kappa_2 = \left[ 1 + \frac{\alpha}{H} \ell n \left( \frac{R_F}{R_P} \right)^2 \right] \quad (2.34)$$

**Model I** provides an approximate expression for the repellent content of the strand for the situation where both the membrane and the porous region influence the rate of release.

Two possible limiting cases can be envisaged. When the outer skin-like membrane fully controls the repellent release, Model I, defined by equation (2.32), simplifies to Model II, which describes the case where permeation through the membrane is rate limiting:

**Model II** is defined by equation (2.35).

$$\kappa_3 t = 1 - X \quad (2.35)$$

where  $\kappa_3$  is represented by equation (2.36):

$$\kappa_3 = \frac{2HD_M}{R_P^2 \ell n \left( \frac{R_F}{R_P} \right)} \left( \frac{\rho_{eq}}{\rho_L} \right) \quad (2.36)$$

Model II also holds at the start of the repellent release when the porous regions of the strand are still filled with liquid.



Another limiting form is represented by Model III, which describes the situation where a rate-controlling membrane layer is completely absent.

**Model III** is given by equation (2.37):

$$\kappa_2 t = X \ell n X + 1 - X \quad (2.37)$$

where  $\kappa_2$  is obtained by equation (2.38):

$$\kappa_2 = 4 \frac{D_P \rho_{eq}}{R_P^2 \rho_L} \quad (2.38)$$

The rate of repellent mass release from a strand of length  $L$ , for which the membrane is rate controlling, is given by equation (2.39):

$$J \approx -\varepsilon \rho_L \pi R_F^2 L \frac{dX}{dt} = \frac{2\varepsilon \rho_{eq} \pi L D_M H \left(\frac{R_F}{R_P}\right)^2}{\ell n\left(\frac{R_F}{R_P}\right)} \quad (2.39)$$

In the more general case, the corresponding expression is represented by equation (2.40):

$$J = \frac{4\varepsilon \rho_{eq} \pi L D_P H \left(\frac{R_F}{R_P}\right)^2}{\ell n\left[X^{-H} \left(\frac{R_F}{R_P}\right)^{2\alpha}\right]} \quad (2.40)$$

## **CHAPTER 3**

### **EXPERIMENTAL**

#### **3.1 Materials**

##### **3.1.1 Chemicals**

In this study the following chemicals were used: N,N-Diethyl-3-methylbenzamide (purity 97%) [CAS-No. 134-62-3], IR3535 (purity  $\geq$  99%) [CAS-No. 52304-36-6], ethyl anthranilate (purity  $\geq$  96 %) [CAS-No. 87-25-2], Citriodiol (70.9% purity) [CAS-No. 1245629-80-4], Icaridin (purity  $\geq$  97%) [CAS-No. 119515-38-7], dimethyl phthalate (purity  $\geq$  99%) [CAS-No. 131-11-3], decanoic acid (purity  $\geq$  98 %) [CAS-No. 334-48-5] and dichloromethane (99% purity) [CAS No. 75-09-2]. The molecular mass, the melting and boiling points, density at 20°C, and suppliers of the chemicals are listed in Table 3.1. All the chemicals were used without further purification.

**Table 3.1:** List of chemicals, their properties and suppliers

Chemical	M <sub>wA</sub> /(g·mol <sup>-1</sup> )	ρ/(g·cm <sup>-3</sup> )	T <sub>b</sub> /(°C)	T <sub>m</sub> /(°C)	Supplier
DEET	191.27	0.998	288	-	Sigma-Aldrich
Ethyl anthranilate	165.19	1.117	268	13-15	Sigma-Aldrich
Dimethyl phthalate	194.18	1.190	282	2	Sigma-Aldrich
Decanoic acid	172.26	0.893	268	27-32	Sigma-Aldrich
Icaridin	229.30	#	296	#	Endura S.pA
IR3535	215.29	0.998	292	#	Merck-KGaA
Citriodiol	*	0.946	267	#	Citrefine International
Dichloromethane	84.93	1.33	40	-95	Merck-KGaA

\* A mixture of components with isomers of *p*-menthane-3,8-diol as major constituents

# No information available.

### 3.1.2 Polymers

Linear low-density polyethylene (LLDPE) (Sasol HR411) was obtained from Sasol. The density was 0.939 g cm<sup>-3</sup> and the MFI was 3.5 g/10 min (190 °C/2.16 kg). Poly(ethylene-co-vinyl acetate) grade Elvax 760A ex DuPont pellets were pulverised by Dreamweaver. The VA content was 9%, the density 0.930 g cm<sup>-1</sup> and the melt flow index (MFI) 2.0 g/10 min at 190 °C.

### 3.1.3 Nanofillers

Fumed silica (HDK<sup>®</sup> N20 pyrogenic silica) was supplied by Wacker silicones. The SiO<sub>2</sub> content (based on the substance heated at 1 000 °C for 2 h) was > 99.8 %; the density at 20 °C (SiO<sub>2</sub>) was approximately 2,2 g·cm<sup>-3</sup>; the refractive index at 20 °C was reportedly 1.46; the BET surface was around 170–230 m<sup>2</sup>·g<sup>-1</sup> and the pH value of a 4% aqueous dispersion was around 3.8–4.3.

Dellite 43B organoclay was supplied by Laviosa Chimica Mineraria S.p.A. According to the supplier, the moisture content was 3% (max). The approximate medium particle size (dry basis) was 7–9 μm and the bulk density was 0.40 g cm<sup>-3</sup>. The clay was organo-modified with dimethyl benzyl hydrogenated tallow ammonium. Figure 3.1. shows the chemical structure of the modifier intercalated in Dellite 43B organoclay.

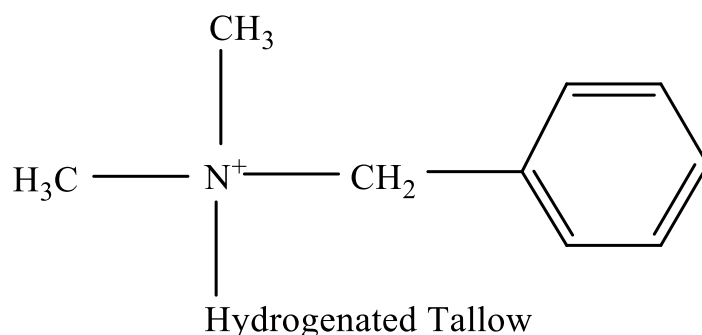


**Figure 3.1:** Chemical structure of the organic modifier intercalated in Dellite 43B organoclay (Majeed et al., 2013)

## **3.2 Sample preparation**

### **3.2.1 Preparation of the polymer-clay nanocomposite films**

Polymer-clay nanocomposites were prepared by first dispersing the clay into the polymer powder with a Sigma spice grinder. The powder blends were then compounded on the TX28P 28 mm co-rotating twin-screw extruder. The extruded strands were cooled by passing them through a water bath. The strands were granulated on a Chen Shin Machinery Co. Ltd model CT-300 pelletizer. The temperature profiles, from hopper to die, were set at 140 /160 /160 /160 °C and 140 /160 /170 /170 °C for EVA- and LLDPE-based compounds respectively. The screw speed was varied in a range of 105 to 150 rpm.

The films used for permeability measurements were blown on a Collin BL 180/400 blown film unit. It comprised a 30 mm  $\phi$  single screw extruder with L/D = 25. The blown film die had a diameter of 60 mm and featured a dual-lip cooling ring. The extruder was operated at a screw speed of 40 rpm. The temperature profiles from hopper to die were 170/190/190/190/190/190/190/190 °C and 190/200/205/205/205/205/205/195 °C for EVA and LLDPE films respectively. The neat LLDPE and EVA films were also compounded before being blown into film to ensure that all the materials were subjected to the same thermal history. These were used as controls for the permeability study. Table 3.2 lists neat polymer and polymer-clay nanocomposite film and film information.

**Table 3.2:** Nanocomposite film samples prepared by melt extrusion method

<b>Film samples</b>	<b>Film information</b>
Control	Neat LLDPE and EVA films
LLDPE-Dellite 43B	LLDPE film loaded with montmorillonite (5 wt.% Dellite 43B)
EVA-Dellite 43B	EVA film loaded with montmorillonite (5 wt.% Dellite 43B)

### **3.3 Mosquito repellent polyolefin strands**

The objective of this study was to produce polyolefin strands impregnated with mosquito repellent (DEET, IR3535, Icaridin and ethyl anthranilate). The concept was to trap the insect repellents inside the polyolefin. Nanofillers (fumed silica and Dellite 43B) were added to assist the compounding into the polymer. It was also thought that, if properly exfoliated and dispersed in the polymer matrix, the presence of the clays could reduce the rate at which the mosquito repellents are released from the strands.

#### **3.3.1 Preparation of mosquito repellent LLDPE strands without a nanofiller**

The purpose of this trial was to compound polymer-repellent combinations. The objective was to compare the effect of the presence of nanofiller on the microstructures obtained using SEM micrographs. Before compounding and extrusion, the setting feeder for LLDPE and pump feed for repellents was calibrated. The calibration results are presented in Appendix V.

Following instrument calibrations, the polymer repellent mixtures (50 wt.% each) were extrusion compounded on a Nanjing Only Extrusion Machinery Co. Ltd (Model TE-30/600-11-40) co-

rotating twin-screw laboratory extruder with diameter of 30 mm, L/D = 40:1. The liquid repellents were dosed via a peristaltic pump (Cole-Parmer with Easy-Load 11 Masterflex L/S head using Masterflex platinum-cured silicone L/S 16 tubing). The temperature profile, from hopper to die, was set at 85/170/210/210/210/210/210 °C, and the screw speed was set at 46.65 rpm. The extruded strands were quenched in an ice-water bath. Additional information is presented in Appendix VI.

### **3.3.2 Preparation of repellent polyolefin strands with added nanofiller**

All polymer-repellent compositions were done on a TX28P 28 mm co-rotating twin-screw laboratory extruder with a screw diameter of 28 mm and an L/D ratio of 18. The screw design of this machine comprised intermeshing kneader blocks that also impart a forward transport action.

The polymer and nanofiller powders were first mixed together in a plastic container. Then the repellent was added and mixed in to obtain a semi-dry consistency that could be fed into the compounding extruder. The exiting polymer strands were quench-cooled in an ice-water bath. After compounding, the repellents did not leak from the polymer strands.

Table 3.3 lists typical compounder settings, i.e. temperature profiles from hopper to die and screw speed. They were used to compound a composition comprising LLDPE (65 wt.%), organoclay (5 wt.%) and Icaridin (30 wt.%). The conditions used for other LLDPE and EVA-compositions are given in Appendix VII.

**Table 3.3:** TX28P extrusion conditions used for compounding LLDPE strands

Conditions	Zone 1 (°C)	Zone 2 (°C)	Zone 3 (°C)	Die (°C)	Speed screw (rpm)
Set	140	160	170	170	150
Read	144.7	157	163.3	169.7	150

### 3.4 Methods of characterizing repellents

#### 3.4.1 Thermal-oxidative stability of repellents by FTIR analysis

Fourier transform infrared (FTIR) spectra were recorded before and after heat exposure in order to determine whether oxidative degradation occurred. A Perkin-Elmer Spectrum 100 fitted with a universal attenuated total reflection (ATR) sampling accessory was used. The FTIR spectra were recorded in absorbance of 4 000–400  $\text{cm}^{-1}$  at a resolution of 4  $\text{cm}^{-1}$ . The reported spectra represent an average of 16 scans.

During the preparation of mock anklets, the mosquito repellents were to be exposed to typical polymer processing temperatures, i.e. exceeding 180 °C. It was deemed necessary to determine whether the repellents could withstand short-time exposure to such high temperatures. Therefore, the heat stability was evaluated using the following procedure: Approximately 6.0 g of repellent was heated for 30 min in an open Polytop glass vial in an EcoTherm-Labcon or a Scientific Series 9000 forced convection oven set at a temperature of 200 °C. In addition, the repellent thermo-oxidative stability testing was conducted at 50 °C in a convection oven. The FTIR spectra were obtained after four months. Approximately 15.0 g of repellent was heated in an open Payne cup in an EcoTherm-Labcon or a Scientific Series 9000 forced convection oven.



### 3.4.2 Determination of chemical composition by X-ray fluorescence (XRF)

The chemical composition of organoclay Dellite 43B was determined using a Thermo Fisher ARL perform'X Sequential XRF instrument with OXSAS software analyses. The samples were milled in a tungsten-carbide milling pot to achieve particles sizes  $< 75 \mu\text{m}$ . The samples were dried at  $100 \text{ }^\circ\text{C}$  and roasted at  $1000 \text{ }^\circ\text{C}$  to determine Loss on Ignition (L.O.I) values. 1 g of sample was mixed with 6 g lithium tetraborate flux and fused at  $1050 \text{ }^\circ\text{C}$  to make a stable fused glass bead.

### 3.4.3 Thermogravimetric analysis and analytical conditions

The TGA instruments, diameters, heights of pans and conditions used to estimate the evaporation of repellents are listed in Table 3.4. The records of mass loss and temperature were obtained and used to calculate the evaporation rate of the mosquito repellents.

**Table 3.4:** TGA instruments and pans used to predict the evaporation rate of the repellents

TGA Instrument	Hitachi STA 7200	Mettler Toledo SDTA851	TA Instrument Q600	Convection oven
Pan material	Alumina	Alumina	Alumina	Alumina
$D_{\text{pan}}/(\text{mm})$	5.2	5.16	6.2	54.91
$H_{\text{pan}}/(\text{mm})$	5	4.56	3.64	19.71
Temperature scan range	50 - 250	30 - 300	50 - 150	50
$\text{N}_2$ flow rate/ $(\text{mL}\cdot\text{min}^{-1})$	200	100	100	-

## 3.5 Methods of characterizing nanocomposite films

### 3.5.1 Fourier transform infrared (FTIR) analysis

FTIR spectra were obtained on a Perkin-Elmer Spectrum 100 instrument fitted with a universal attenuated total reflection (ATR) sampling accessory. FTIR spectra were recorded in the

absorbance range of 4 000 to 400  $\text{cm}^{-1}$  at a resolution of 4  $\text{cm}^{-1}$ . They represent averages of 16 scans. FTIR spectra were taken for the neat polymer film as well as for the polymer-clay nanocomposite films.

### **3.5.2 Thermogravimetric analysis (TGA)**

The thermal stability of the polymer-clay nanocomposite films was explored using thermogravimetric analysis (TGA) on a TA Instruments SDT-Q600 Simultaneous TGA/DSC. Samples weighing approximately 10 mg were heated from ambient temperature up to 900 °C at a rate of 10 °C·min<sup>-1</sup>. The purge gas was nitrogen flowing at 50 mL·min<sup>-1</sup>. The mass loss was recorded as a function of temperature.

### **3.5.3 Measurements of thicknesses**

The final film thicknesses were measured with a micrometer (dial thickness gauge # 013458, Mitutoyo Digital Co., Japan), with a sensitivity of  $\pm 1 \mu\text{m}$ . The reported film thicknesses represent the average of five separate measurements. The instrumentation is shown in Figure 3.2.



**Figure 3.2:** Thickness measurement using a Mitutoyo Digital micrometer

### **3.6 Polymer film permeability tests**

The permeability tests of the blown films were done using Payne permeability cups. The cup dimensions were: diameter 54.9 mm and depth 19.7 mm. They were partially filled with mosquito repellent before clamping the polymer films in place. The cups were placed in convection ovens set at a temperature of at 50 °C. Mass loss was recorded daily over a period of two weeks. The experimental set-up is shown in Figure 3.3.



**Figure 3.3:** Payne permeability cups, rings and polymer nanocomposite films used to study the permeability of the repellents through polymer film

### 3.6.1 Determination of permeability

The permeability of neat polymer and nanocomposite polymer films to the repellents was determined using equation (3.1).

$$P = bL_f/A \tag{3.1}$$

where  $P$  is the permeability coefficient represented as ( $\text{g}\cdot\mu\text{m}\cdot\text{day}^{-1}\cdot\text{mm}^{-2}$ );  $b$  is the slope of the linear mass loss vs. time plot represented as ( $\text{g}\cdot\text{day}^{-1}$ );  $A$  is the area of the film ( $\text{mm}^2$ );  $L_f$  is the film thickness in ( $\mu\text{m}$ ). Reported values are the results obtained from duplicate measurements.

### 3.7 Characterization methods of the polymer strands

#### 3.7.1 Diameter measurement of the polymer strands

The diameters of the polymers strands were measured with a Mitutoyo Digital Vernier caliper with a measurement range up to 150 mm. The instrumentation is shown in Figure 3.4.



**Figure 3.4:** Mitutoyo Digital Vernier calliper

#### 3.7.2 Extraction of repellent from the polymer strands

Polymer strands containing repellent were cut to lengths of approximately 70 mm and weighed using a Radwag Wagi Elektroniczne scale, PS 360/C/2, Nr 263678/09, and placed in Polytop glass vials. Approximately 40 mL dichloromethane was added, and the vials stoppered. The extraction solvent was replaced on a daily basis. After the fifth extraction, the strands were removed and

allowed to dry in a fume hood at ambient temperature. The repellent content was estimated from the recorded mass loss of the strands in the dried form. Reported values are the results obtained from triplicate mass loss determinations. The estimated amount of repellent was calculated using equation (3.2).

$$E(\%) = 100 - \left( \frac{W_f}{W_i} * 100 \right) \quad (3.2)$$

where  $E$  is the estimated repellent amount in per cent (%) that was in the polymer strand;  $W_i$  and  $W_f$  are the weights of the strands before and after extraction of the repellent represented by (g).

### 3.7.3 Estimation of membrane thickness covering the polymer strand

The repellent release data, in combination with the permeability values measured for the films to repellent, allow estimation of the effective thickness of the skin-like membranes covering the strands. From the slope of the linear mass loss vs. time plot of the repellent release rate, the repellent flux was calculated which this passes through the microporous polymer strand. The formula is presented by equation (3.3).

$$J = b/A \quad (3.3)$$

where  $J$  is the repellent flux ( $\text{g}\cdot\text{day}^{-1}\cdot\text{mm}^{-2}$ );  $b$  is the initial slope of repellent release rate from the polymer strand in ( $\text{g}\cdot\text{day}^{-1}$ );  $A$  is the surface area of the polymer strand in ( $\text{mm}^2$ ).

The thickness of the membrane that covered the polymer strand was estimated from the ratio of the permeability coefficient to the measured initial repellent flux (equation (3.4)) as follows:

$$z_{membrane} = P/J \quad (3.4)$$

where  $z$  is the membrane thickness that covers the polymer strand in ( $\mu\text{m}$ );  $P$  is the permeability coefficient represented as ( $\text{g}\cdot\mu\text{m}\cdot\text{day}^{-1}\cdot\text{mm}^{-2}$ );  $J$  is the repellent flux given in ( $\text{g}\cdot\text{day}^{-1}\cdot\text{mm}^{-2}$ ).

#### 3.7.4 Absorption of repellent by the polymers

Approximately 4.0 g of neat EVA and LLDPE pellets were weighed using a Radwag Wagi Elektroniczne scale, PS 360/C/2, Nr 263678/09, and placed in Polytop glass vials containing approximately 16 mL repellent (DEET or Icaridin). The vials were placed in either an EcoTherm-Labcon or a Scientific Series 9000 forced convection oven set at a temperature of 30 °C or 50 °C. After three days the pellets were removed, and the excess repellent was removed using a quick rinse with dichloromethane. The pellets were then allowed to dry for a few minutes on paper towels before weighing. After that the repellent absorption was estimated from the recorded mass gain of the pellets. Reported values represent results obtained from triplicate measurements of the mass gain of the pellets. The swelling of polymer was calculated using equation (3.5) (Mooss et al., 2019).

$$Q(\%) = 100 * \left( \frac{W_s - W_d}{W_d} \right) \quad (3.5)$$

where  $Q$  is the estimated polymer matrix swelling by repellents in (%);  $W_s$  is the weight of the swollen of polymer pellets;  $W_d$  is the weight of the dry polymer pellets represented by (g).

### 3.7.5 Shrinkage of polymer strand

Seven 70 mm lengths were cut from neat polymer strands and polymer strands containing repellents. The initial diameters were measured with a Mitutoyo Digital Vernier calliper with a measurement range up to 150 mm. The strands were placed in either an EcoTherm-Labcon or a Scientific Series 9000 forced convection oven set at a temperature of 50 °C for 23 days. The change in diameter of the strands was measured after twenty days. The rate of shrinkage of the polymer matrix was calculated by equation (3.6) (Li et al., 2008).

$$S_R(\%) = 100 * \left( \frac{D_i - D_f}{D_i} \right) \quad (3.6)$$

where  $S_R$  is the shrinkage of the polymer strands in (%);  $D_i$  and  $D_f$  are the diameters before and after the shrinkage process of the strands in (mm).

### 3.7.6 Thermogravimetric analysis (TGA)

The repellent content of the polymer strands was investigated with a TGA on either a Hitachi STA-7300 or a TA Instruments SDT-Q600 Simultaneous TGA/DSC. Samples weighing approximately 16 mg were heated from ambient temperature to 600 °C at a rate of 10 K·min<sup>-1</sup>. The purge gas was nitrogen flowing at 50 mL·min<sup>-1</sup>. The first weight loss step of the polymer strand was associated with the loss of the repellent by volatilization.

TGA was used to estimate the amount of the repellent initially trapped by the polymer matrix. It was also used to estimate the repellent remaining after the strands were oven-aged for 6 months at



50 °C. The elevated storage temperature, > 15 °C above the ambient, was chosen to accelerate the ageing.

### **3.7.7 Scanning electron microscopy (SEM)**

Scanning electron microscopy was used to observe the microporous structure of the LLDPE strands, those only impregnated with repellents and those containing clay or silica. First the repellents were leached from the polymer matrices and then the repellent-free polymer strands were immersed in liquid nitrogen for approximately 1 hour and then fractured. The fracture surface was coated six times with carbon using an Emitech K950X sputter coater prior to analysis. The samples were viewed through a Zeiss Ultra 55 Field Emission Scanning Electron Microscope at an acceleration voltage of 1, 2 and 5 kV.

### **3.8 Repellent release rate studies**

The time-dependent repellent release of repellent from the strands was determined by ageing at 50 °C in either a Scientific Series 9000 or an EcoTherm-Labcon forced convection oven. The strands were suspended from the inside roof of the ovens in the form of loose coils. They were weighed twice a week. A four-decimal output scale (Radwag Wagi Elektroniczne, PS 360/C/2, Nr 263678/09) was used to measure the mass loss of the strands. The repellent release kinetics from the microporous polymer strands in various formulations were investigated by fitting the release data into the mathematical model previously developed and described in Chapter 2.

### **3.9 Efficacy studies of the repellents**

In this trial the performance of repellents against *Anopheles arabiensis* incorporated in the polymer filaments was investigated. The polymer strands were first aged at 50 °C in forced convection ovens, a model Labcon FSOH 16 and a Scientific Series 9000. Every two weeks samples measuring 3.0 m in length were removed for foot-in-cage bioassay tests as described below. The mass loss testing and repellence testing were done for up to 12 weeks.

#### **3.9.1 Volunteers**

Three human volunteers participated in the mosquito foot-in-cage test. These individuals had different blood groups (A, B and O, all three Rh<sup>+</sup>). No allergic reaction after bioassay was observed.

#### **3.9.2 Ethics approval**

Ethical clearance for the study was obtained from the Faculty of Health Sciences' ethics committee of the University of Pretoria (Protocol No. 82/2016).

#### **3.9.3 Mosquitoes**

For this study, the insectary colony of *Anopheles arabiensis* was obtained from stock material maintained by the South African National Institute for Communicable Diseases (NICD).

### **3.9.4 Exposure of mosquitoes and conditions of insectary in terms of temperature and humidity**

The tests for mosquito repellent efficacy were conducted under controlled insectary conditions. Caged mosquitoes were offered a dual-choice opportunity for feeding on treated and untreated body parts of human volunteers (WHO, 2009, Barnard and Xue, 2004b). Three hundred mixed-gender mosquitoes were placed in a large (1 200 mm × 600 mm × 600 mm) netting cage which had two entry portals on one side for the insertion of legs spaced about 500 mm apart. Every effort was made to ensure minimal disturbance of the mosquitoes prior to each test, and no blood-meals were offered for 72 hours prior to each trial to ensure that female mosquitoes were starved and would readily try to bite and feed. All the mosquitoes were kept and trials conducted inside the insectary, which was maintained at a constant temperature of  $25 \pm 2$  °C and a relative humidity of  $75 \pm 5\%$ . The mosquitoes had access to cotton wool soaked with a 10% sugar solution, which was removed 6 hours prior to commencement of the repellent trials.

### **3.9.5 Application of polyolefin repellent strands on the leg**

Selected strands with a microporous structure were subjected to repellency testing. The test strand, 3.0 m long, was wound around the lower limb region of one leg of a volunteer (see Figure 3.5), leaving the other leg fully exposed. No socks or shoes or any other items of clothing were worn below the knee. Both legs were then inserted into the cage, one leg per entry hole, and the person stood still for five minutes. At the end of the five minutes two other people used flashlights to count the number of mosquitos present on the lower leg of the test person. The number of mosquitoes on the treated and untreated legs was recorded separately. Although in most cases it was possible to feel or see which mosquitoes were feeding, no distinction was made between

feeding or resting mosquitoes. As long as the mosquito was stationary on the foot or lower leg for at least five seconds it was counted. Only mosquitoes below the mid-calf region were counted (halfway between foot and knee. To avoid possible build-up of repellent on any one ankle due to continuous use, each test person used the alternate ankle on every alternative test day. The tests were conducted at least three days apart at 15:00 to allow sufficient time for the mosquitoes not to become accustomed to any odour which may have lingered after each application.



**Figure 3.5:** A treated foot prepared for a foot-in-cage test

Figure 3.6 shows the set-up for the foot -in-cage mosquito repellence test. At the top it has two entry ports for insertion of the feet.



**Figure 3.6:** Photo of the foot-in-cage test

### **3.9.6 Determination of degree of protection**

The degree of protection ( $p$ ) was calculated as the proportion of the number of mosquitoes landing on and/or probing the treated leg ( $N_T$ ) in relation to the number landing on and/or probing the control leg ( $N_C$ ) of the same individual (Pascual-Villalobos and Robledo, 1998, Salari et al., 2012, Licciardello et al., 2013). The formula is given by equation (3.7).

$$p (\%) = \frac{(N_C - N_T)}{(N_C + N_T)} \times 100 \quad (3.7)$$

The degree of protection was reported in percentage units.

### **3.9.7 Statistical analysis**

Data collected during bioassay of the performance of the polymer strands impregnated with mosquito repellents were subjected to a statistical analysis of variance (ANOVA). The statistical analysis was used to check the reliability of the results obtained from the bioassay, such as the factors that affect the efficiency of a mosquito repellent. More details about statistical analysis (ANOVA) are presented in Appendix XVI.

## CHAPTER 4

### RESULTS AND DISCUSSION

#### 4.1 Characterization of repellents

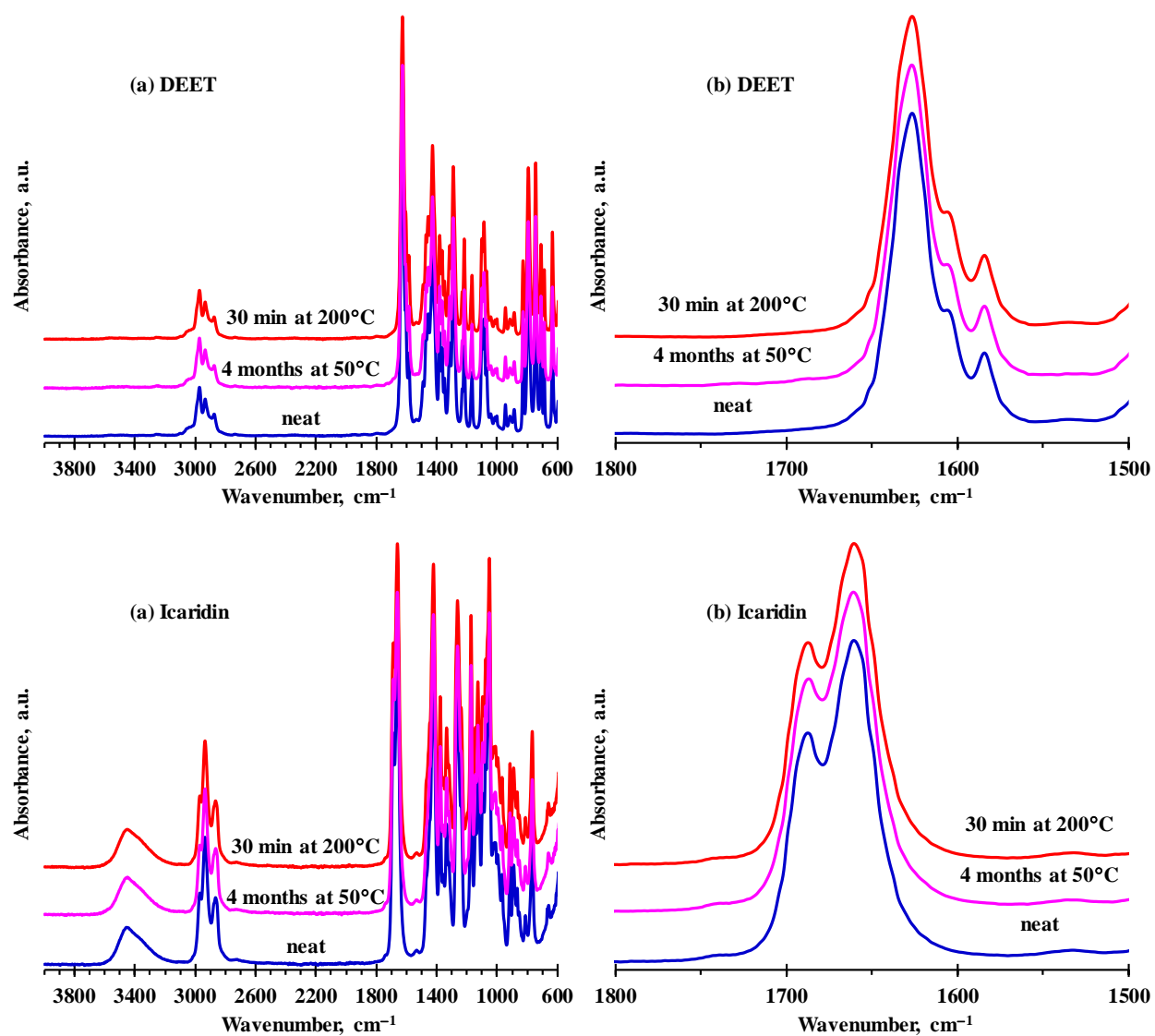
##### 4.1.1 Thermo-oxidative stability of repellents

Figure 4.1, Figure 4.2 and Figure 4.3 show FTIR spectra of DEET, Icaridin, ethyl anthranilate, IR3535 and dimethyl phthalate taken before and after thermo-oxidative stability testing by exposure to air for either 4 months at 50 °C or 30 min at 200 °C. The infrared absorption bands for the repellents were not affected by short-term heat exposure at 200 °C. This suggests that the chemical structures stayed intact or there was no structural degradation of DEET, Icaridin, ethyl anthranilate, IR3535 and dimethyl phthalate. Since the boiling points of these repellents ranged from 267 to 296 °C, this implies that the repellents were stable at elevated temperatures. The presence of the alcohol (—OH stretching) functional group is observed between 3 200 and 3 500  $\text{cm}^{-1}$  for Icaridin, and as expected, is absent in the DEET, IR3535, ethyl anthranilate and dimethyl phthalate spectra since their molecular structures do not contain the (—OH) group.

Additionally, most repellents such as DEET, Icaridin and ethyl anthranilate after long term exposure to air at 50 °C, they were stable. The exceptions were dimethyl phthalate and ethyl butyl acetylaminopropionate. For these two repellents new carbonyl bands developed at ca. 1690  $\text{cm}^{-1}$  and 1685  $\text{cm}^{-1}$ , respectively. However, these new peaks were very small compared to the carbonyl absorption bands of the neat parent molecules. This is illustrated in the FTIR spectra for ethyl butylacetylaminopropionate and dimethyl phthalate shown in Figure (4.3). The indications are that oxidative degradation had commenced when these two repellents were exposed to warm air at 50

°C for four months. The apparently lower thermal-oxidative stability of ethyl butylacetylaminopropionate, compared to the other repellents, is tentatively attributed to its higher aliphatic character. Despite these observations, this study demonstrates that the repellents investigated were able to withstand typical polymer processing temperatures (often exceeding 180 °C) for short periods of time. The fact that they also stayed essentially intact for several months at 50 °C suggests that they may retain repellent activity for comparable lengths of time. Furthermore, in Appendix I are presented the FTIR spectra of decanoic acid and citriodiol.





**Figure 4.1:** (a) FTIR spectra for the mosquito repellents DEET and Icaridin before and after thermal-oxidative stability testing by exposure to air at either 50 °C for four months or for 30 min at 200 °C. (b) Expanded view of the carbonyl absorption region proving the statement of the thermal stability of DEET and Icaridin.

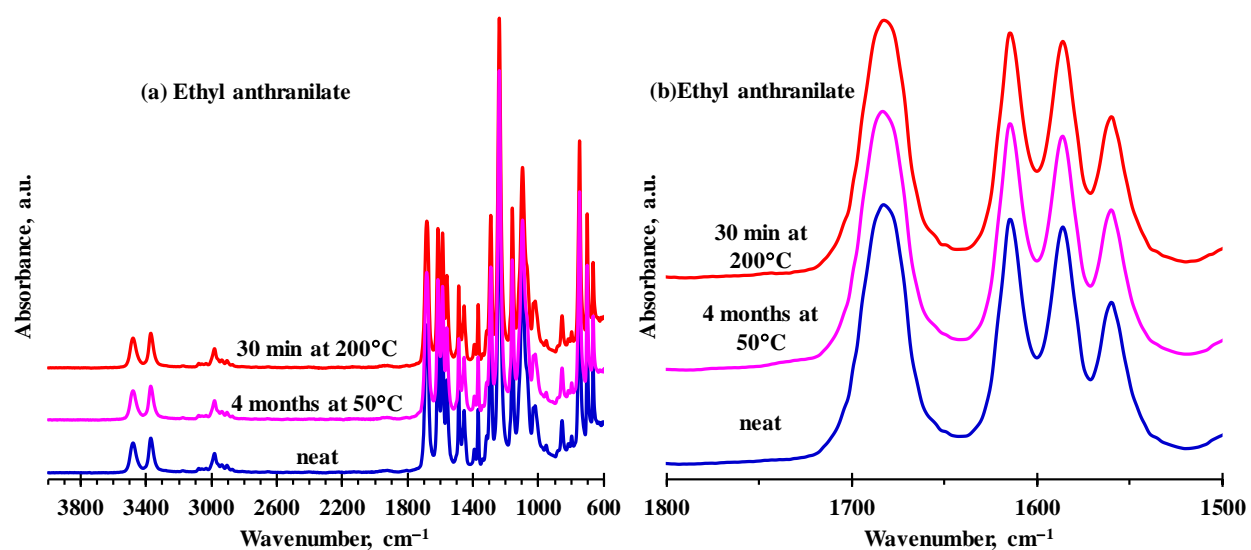


**Figure 4.2:** (a) FTIR spectra for the mosquito repellents ethyl anthranilate before and after thermal-oxidative stability testing by exposure to air at either 50 °C for four months or for 30 min at 200 °C. (b) Expanded view of the carbonyl absorption region proving the statement of the thermal stability of ethyl anthranilate.

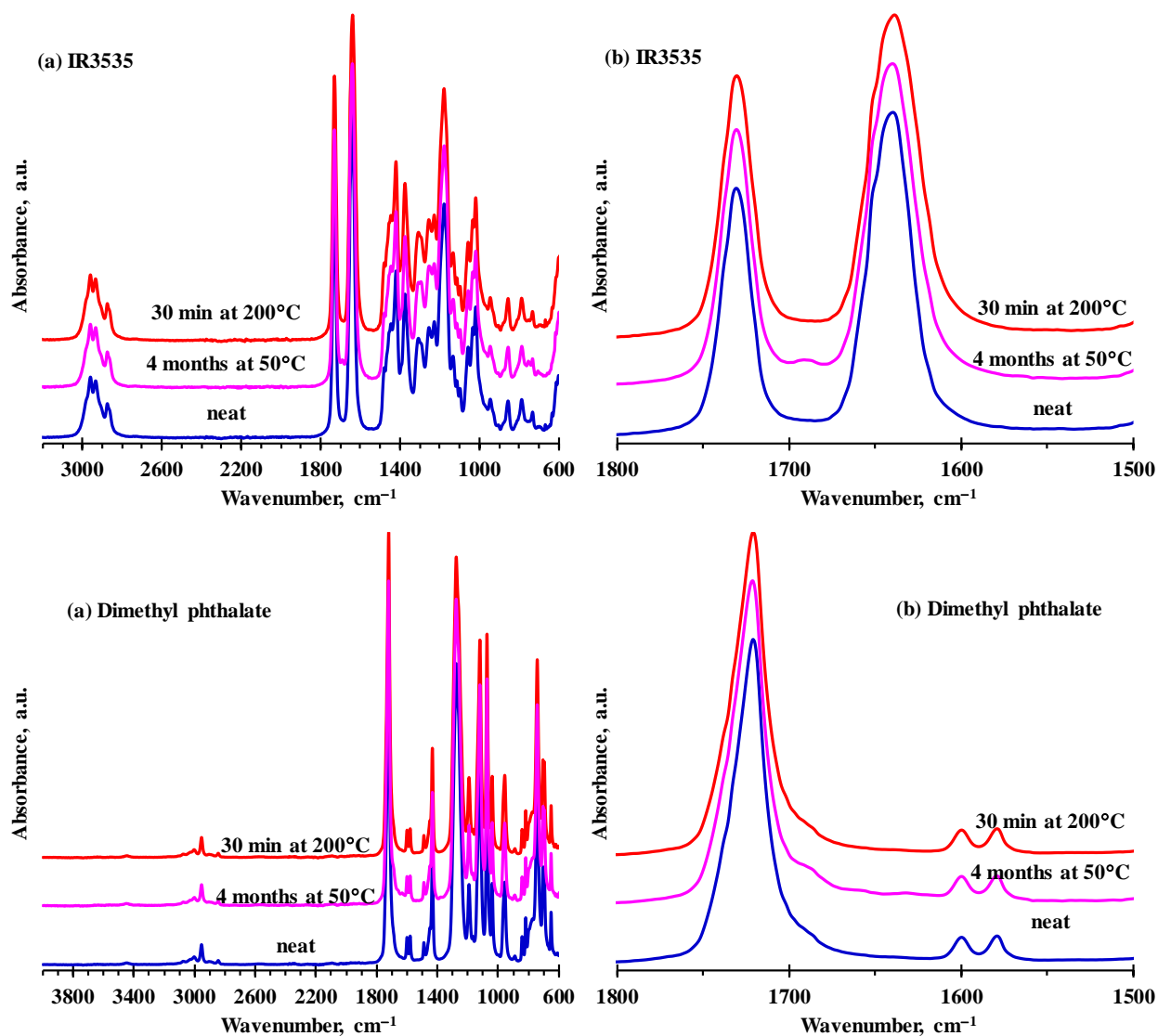


**Figure 4.3:** (a) FTIR spectra for the mosquito repellent ethyl butylacetylaminopropionate (IR3535) and dimethyl phthalate before and after thermal-oxidative stability testing by exposure to air at either 50 °C for four months or for 30 min at 200 °C. (b) Expanded view of the carbonyl absorption region for IR3535 and dimethyl phthalate showing the development of a new band near 1690 cm<sup>-1</sup> and 1685 cm<sup>-1</sup>, respectively.

### 4.1.2 Chemical composition determined by X-ray fluorescence (XRF)

The XRF-determined chemical composition of the Dellite 43B organoclay, in form of the corresponding oxides, is presented in Table 4.1. As expected, these results revealed high Si, Al, Fe and Mg contents consistent with the fact that montmorillonite is a phyllosilicate.

The organoclay analysis also revealed much organic material, shown by the high content of Loss on Ignition (LOI). This is related to the organic modifier (dimethyl benzyl hydrogenated tallow ammonium) of the Dellite 43B clay.

**Table 4.1:** Chemical composition in (%) of Dellite 43B organoclay

SiO <sub>2</sub>	TiO <sub>2</sub>	Al <sub>2</sub> O <sub>3</sub>	Fe <sub>2</sub> O <sub>3</sub>	MgO	CaO	Na <sub>2</sub> O	K <sub>2</sub> O	P <sub>2</sub> O <sub>5</sub>	ZrO <sub>2</sub>	LOI	Total
43.54	0.08	14.29	3.26	1.57	0.47	0.11	0.01	0.37	0.01	36.22	99.93

## 4.2 Determination of the volatility of repellents by thermogravimetric analysis (TGA)

### 4.2.1 Vapour pressure correlations with experimental data in the literature

An effective repellent should have low volatility. Volatility is usually associated with vapour pressure, but in fact the diffusivity in air also contributes (Focke, 2003, Pieterse and Focke, 2003). The volatility controls the duration of the effective action of the repellent. Ambrose and Ghiassee (1987) published vapour pressure data for decanoic acid and Roháč et al. (1999) published data for dimethyl phthalate. Figure 4.4 compares the experimental data for decanoic acid and dimethyl phthalate with predictions made using the Antoine, Wagner, Cox and Myrdal and Yalkowsky equations. Figure 4.4 shows that the performance of the Antoine equation (2.3 and 2.4) was unsatisfactory. This equation can only fit real data well over smaller temperature intervals.

However, the Wagner equation (2.2) gave good predictions for decanoic acid, and the Cox equation (2.5) gave satisfactory results for dimethyl phthalate. The Myrdal and Yalkowsky equation (2.6) performed well for estimating the vapour pressure for dimethyl phthalate but less so for decanoic acid.

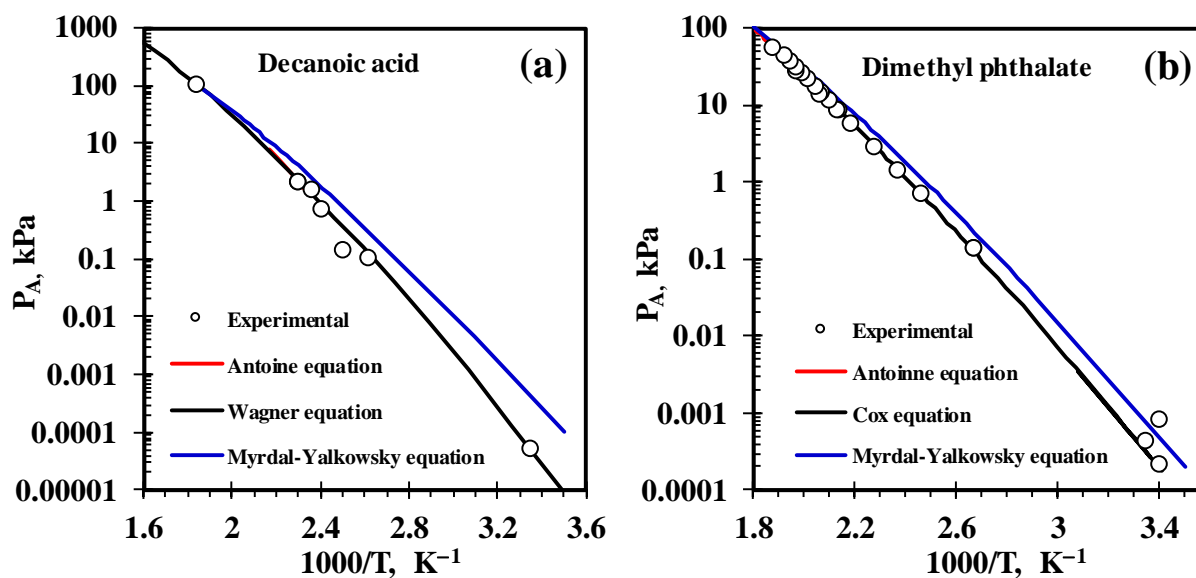


**Figure 4.4:** (a) Comparison of the experimental vapour pressure values reported by Baccanari et al. (1968), Weast and Grasselli (1989) and Lide and David (2009) with the values theoretically determined by equations (2.2), (2.3) and (2.6) for decanoic acid. (b) Comparison of the experimental vapour pressure values reported by Roháč et al. (1999), O'Neil (2013) and Daubert, (1989) with the values theoretically obtained by equations (2.4), (2.5) and (2.6) for dimethyl phthalate.

#### 4.2.2 The Myrdal and Yalkowsky equation

For most repellents, only a few discrete vapour pressure data points were found in the literature. In these cases, the vapour pressure variations with temperature were predicted with the Myrdal and Yalkowsky equation (2.6). A plot of the experimental and predicted vapour pressures is

presented in Figure 4.5. The plot shows small differences between the predicted and experimental curves for Icaridin, DEET, ethyl anthranilate and IR3535. In summary, equation (2.6) proved satisfactory for estimating the vapour pressures of the liquid repellents.

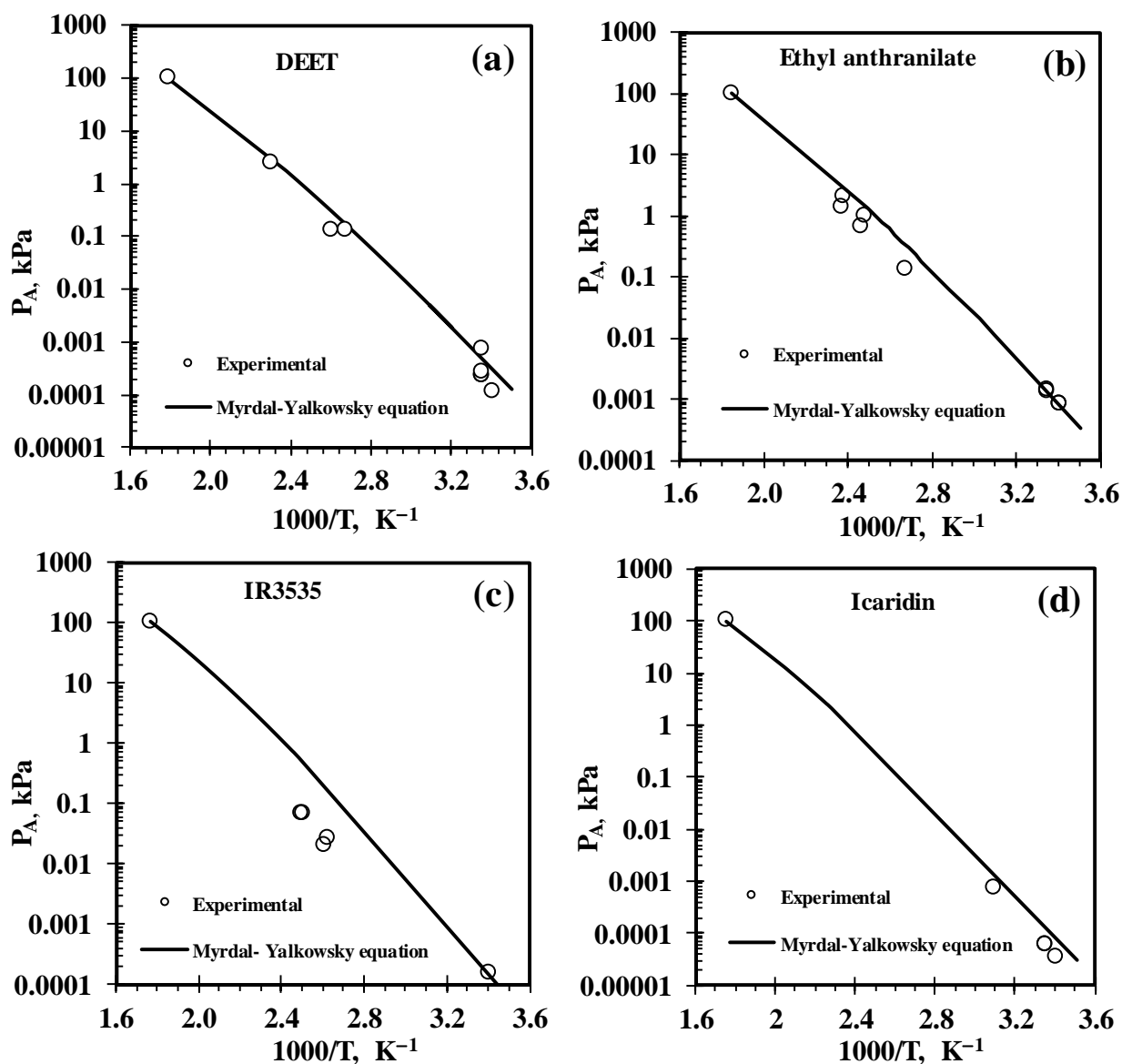


**Figure 4.5:** The experimental vapour pressure values for (a) DEET reported by Drapeau et al. (2011), Haynes (2014) and Blaine (1976); (b) ethyl anthranilate reported by Lide (2004), Api et al. (2015), Weast and Grasselli (1989), Milwaukee (1990), Islam et al. (2017b); (c) IR3535 reported by O'Neil (2013) and (d) Icaridin reported by O'Neil (2013) are compared with the values estimated by equation (2.6).

### 4.2.3 Repellent evaporation

Figures 4.6 and 4.7 show predicted and experimental thermogravimetric evaporation rate data. The experimental data calculated using equation (2.1) and the theoretical prediction determined by equation (2.19) agree over the full temperature range, except for DEET and ethyl anthranilate. The evaporation rates were predicted satisfactorily at high temperatures, i.e. above 100 °C and 120 °C for DEET and ethyl anthranilate respectively. However, at lower temperatures, the experimental values are higher than the predicted values for DEET and ethyl anthranilate.

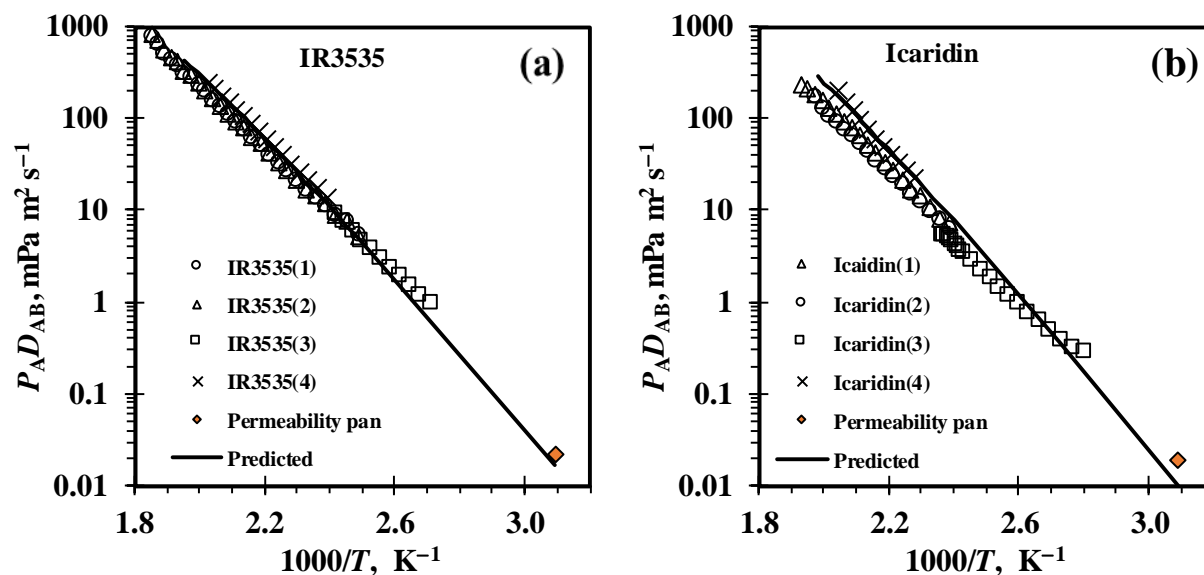


**Figure 4.6:** Comparison of experimentally determined TGA evaporation rates by equation (2.1) and theoretically predicted rates (solid line) by equation (2.19) for: (a) IR3535; and (b) Icaridin

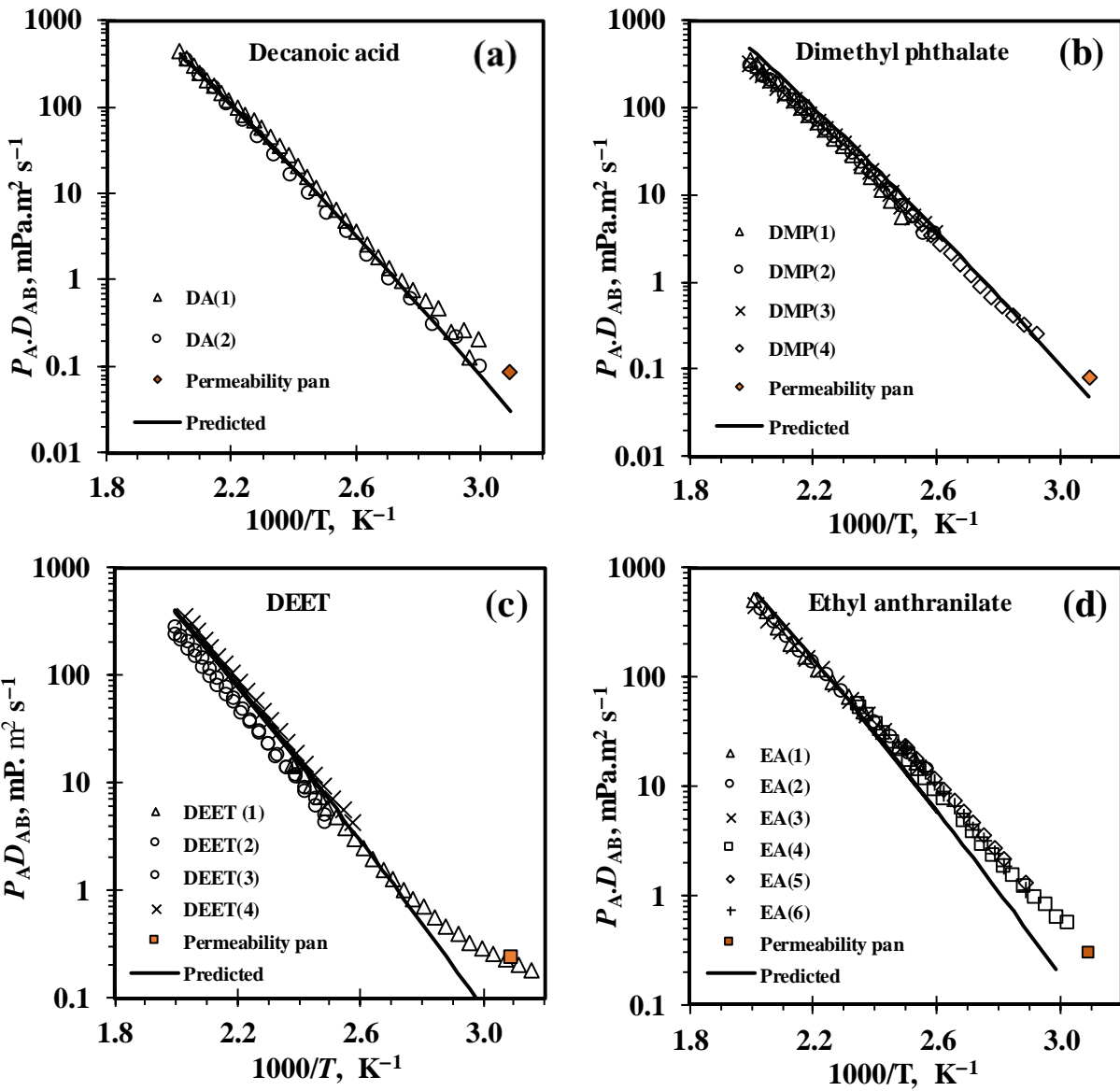


**Figure 4.7:** Comparison of experimentally determined TGA evaporation rates by equation (2.1) and theoretically predicted rates (solid line) by equation (2.19) for: (a) decanoic acid; (b) dimethyl phthalate; (c) DEET; (d) ethyl anthranilate.

Figure 4.8 shows the air permeabilities of the repellents determined with Payne cups at 50 °C. The

$S_A = P_A^{sat} D_A$  values span more than one order of magnitude: Both ethyl anthranilate and citriodiol

are fifty times more volatile than Icaridin. The volatility sequence at 50 °C, i.e. near-ambient



conditions, was as follows: ethyl anthranilate > citriodiol > dimethyl phthalate > DEET > decanoic acid > ethyl butylacetylaminopropionate > Icaridin. Since Icaridin, ethyl butylacetylaminopropionate and DEET had the lowest evaporation rates, it is likely that they would be able to provide longer protection times against mosquitoes. In contrast, ethyl anthranilate and citriodiol showed higher evaporation rates, which may imply a shorter potential protection time depending on the concentration required for effective repellence. The results are reported and described in the next section.

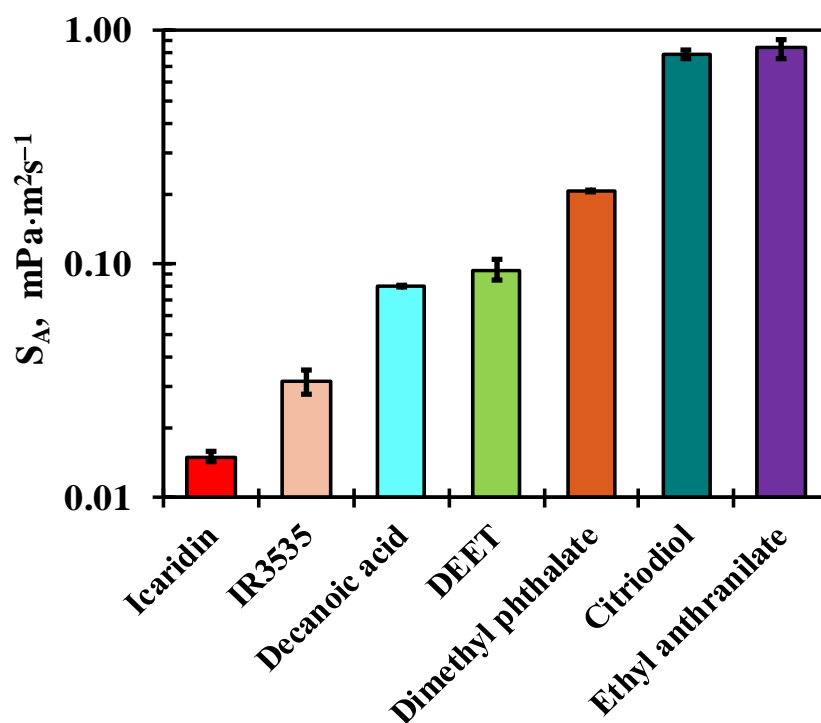


**Figure 4.8:** Air permeabilities of the repellents Icaridin, ethyl butylacetylaminopropionate (IR3535), decanoic acid, DEET, dimethyl phthalate, Citriodiol and ethyl anthranilate measured at 50 °C using Payne cups.

#### **4.2.4 Diffusion coefficient of repellents**

Figures 4.9 and 4.10 show the predicted diffusion coefficients calculated using equation (9). From Figures 4.9 and 4.10 it can be seen that the predicted data correlated well with the experimental data. However, Figure 4.9 (d) revealed a significant difference between the predicted and the experimental data for ethyl anthranilate repellent at low temperatures. In contrast, the Wilke-Lee equation showed good agreement with the result for decanoic acid, dimethyl phthalate, DEET, IR3535 and Icaridin.

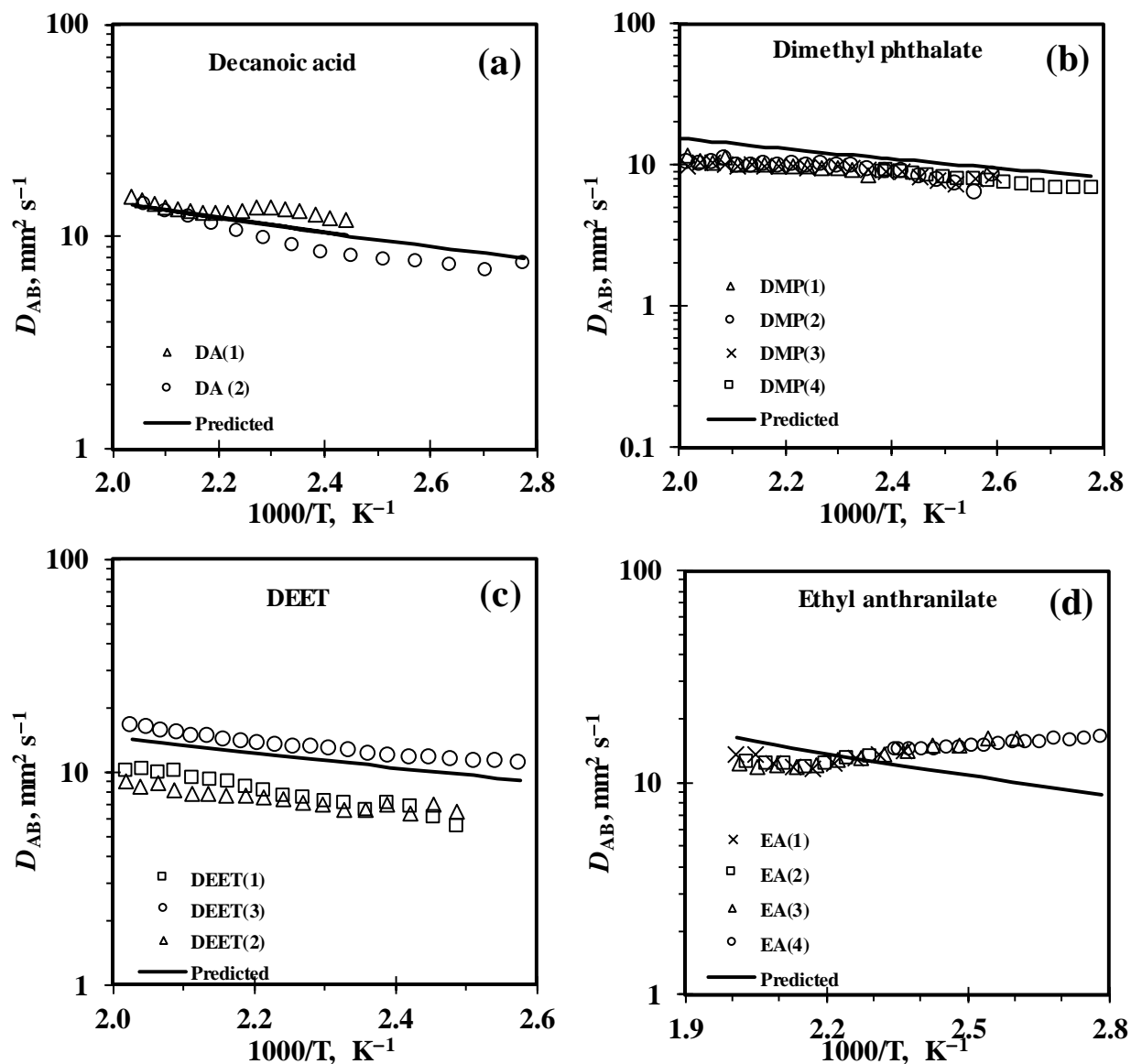


**Figure 4.9:** Comparison of theoretically predicted diffusion coefficients (solid line) obtained by equation (2.9) and experimentally determined TGA diffusion coefficients calculated by equation (2.20) for: (a) decanoic acid; (b) dimethyl phthalate; (c) DEET; and (d) ethyl anthranilate

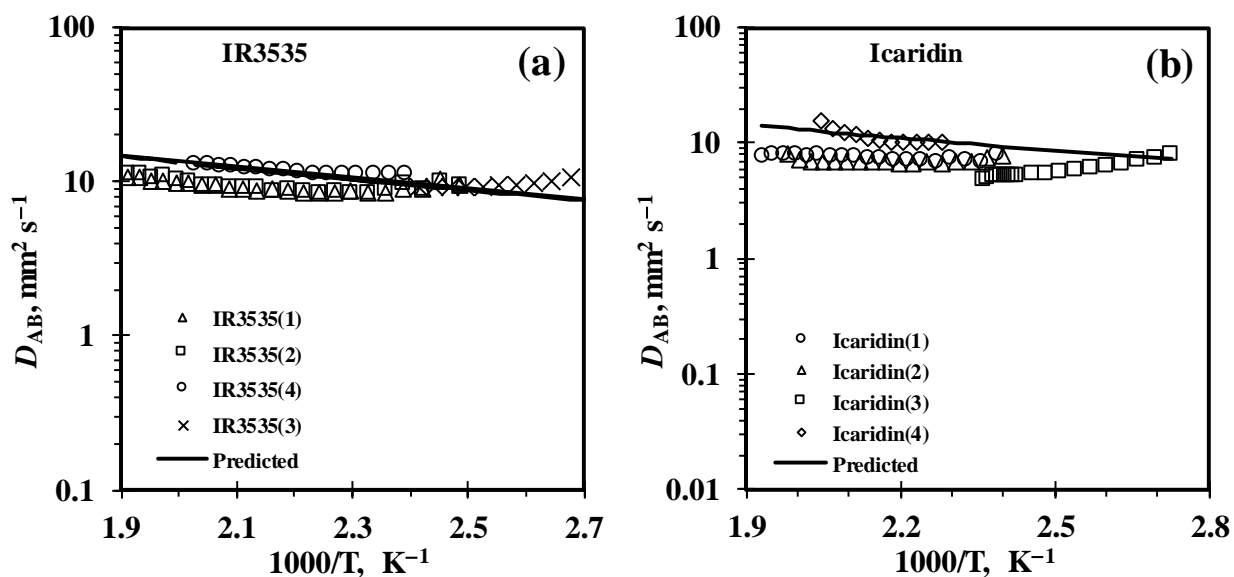


**Figure 4.10:** Comparison of theoretically predicted diffusion coefficients (solid line) obtained by equation (2.9) and experimentally determined TGA diffusion coefficients obtained by equation (2.20) for: (a) IR3535; (b) Icaridin

### 4.3 Characterization of polymer films

#### 4.3.1 Thermogravimetric analysis (TGA)

Figure 4.11 shows TGA and DTG profiles of the neat polymer and its nanocomposite films. The mass loss trace for the neat LLDPE film overlaps with the mass trace for the LLDPE-43B nanocomposite film up to 360 °C. Above this temperature, the mass loss is less for the nanocomposite compared to that of the neat LLDPE. Both the LLDPE and the LLDPE-43B nanocomposite films showed a single degradation step with onset temperature of 364 °C and 409 °C, while the maximum rate occurred at 474 °C and 477 °C respectively. This is attributed to the degradation and volatilization of the LLDPE and an overlap with the degradation of the clay for the nanocomposite filler, i.e. the Dellite 43B organoclay.

Similar behaviour was observed for the neat EVA film. The overlap of the mass loss traces extended to a temperature of 350 °C. Above 350 °C, the thermal stability increased when compared to neat EVA film. However, in this case both films featured a two-step degradation. The first step for the EVA film and EVA - 43B nanocomposite films had onset temperatures of 304 °C and 309 °C respectively, while the maximum rate occurred at 362 °C and 367 °C respectively. This is attributed to the removal of acetate groups (Sefadi and Luyt, 2012). The corresponding values for the second step were 409 °C and 414 °C for the onset temperatures and 474 °C and 478 °C for the maximum mass loss rate for the EVA and the EVA-43B nanocomposite films respectively. This is attributed to the degradation of the polymer backbone and an overlap with the degradation of the 43B Dellite clay for the nanocomposite.

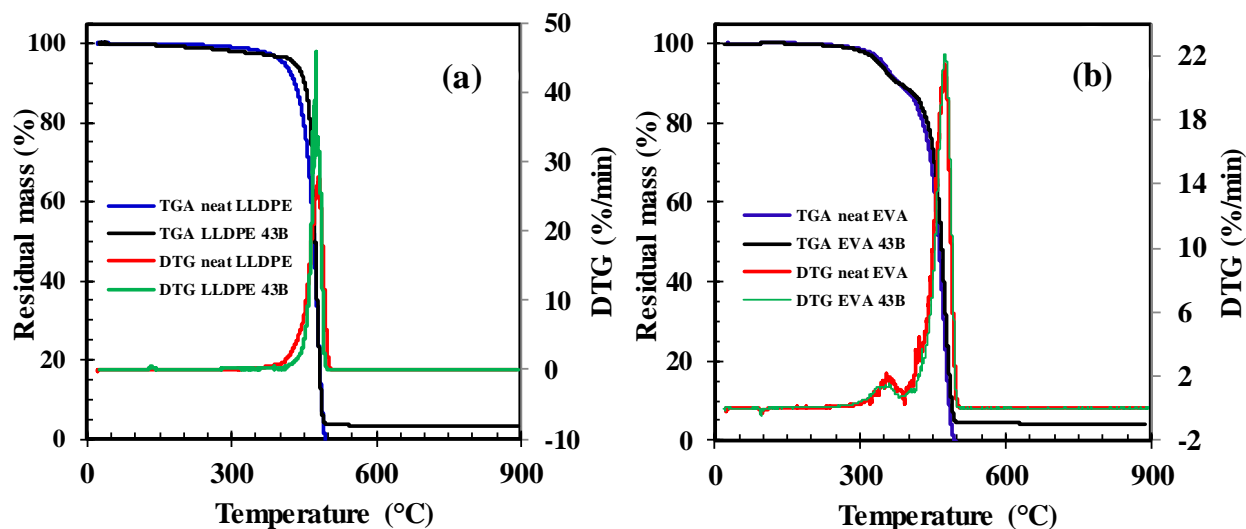


**Figure 4.11:** TGA and DTG profiles of (a) the neat LLDPE and LLDPE-43B nanocomposite films; and (b) the neat EVA and EVA-43B nanocomposite films

### 4.3.2 Fourier transform infrared spectroscopy (FTIR)

Figure 4.12 shows FTIR spectra of the neat polymer and polymer-clay nanocomposite films. The absorption bands of neat LLDPE film are found at 2 850–2 920  $\text{cm}^{-1}$  (C-H stretching), 1 472  $\text{cm}^{-1}$  (C-H bending), 1 366  $\text{cm}^{-1}$  (C-H bending) and 720  $\text{cm}^{-1}$  (C-H rocking). All these absorption bands are also present in LLDPE-clay nanocomposite film with an additional band between 956 and 1 100  $\text{cm}^{-1}$  (Si-O stretching). The FTIR spectra belonging to LLDPE film obtained in the present study were similar to those of previous studies (Tornuk et al., 2018, Morlat-Therias et al., 2008, Durmuş et al., 2007, Ismail et al., 2010).

In addition, the typical absorption bands of EVA were observed at 1 734, 1 234, 1 018, and 607  $\text{cm}^{-1}$  which are assigned to ester groups, while the bands between 2916, 2848, 1460, 1367 and 720  $\text{cm}^{-1}$  are attributed to ethylene groups present in EVA. The absorption bands are in agreement with values in previous reports values (Adelnia et al., 2015, Khodkar and Ebrahimi, 2011). The absorption bands observed in neat EVA films are also present in EVA-clay nanocomposite film with an additional largest band appearing between 944 and 1 100  $\text{cm}^{-1}$  (Si-O stretching). This band overlapped an absorption band of EVA film found at 1 018  $\text{cm}^{-1}$ .

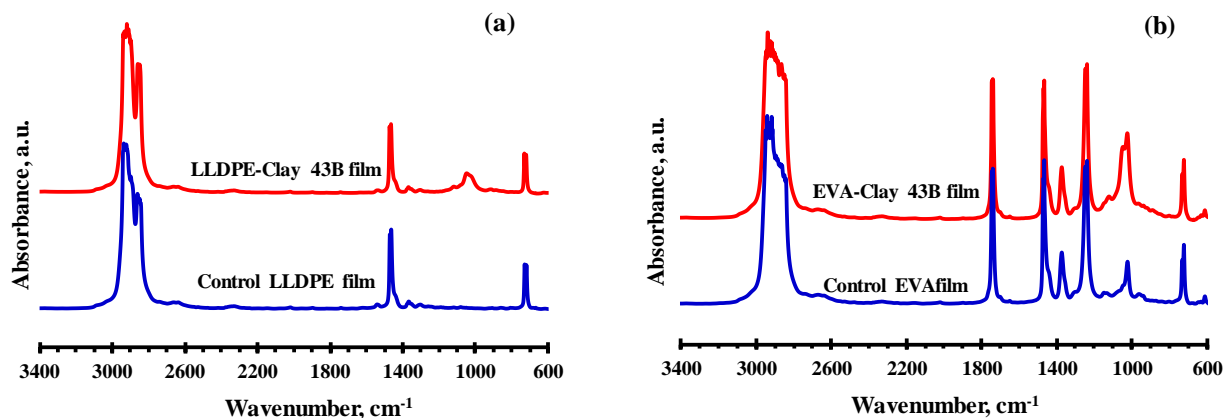


**Figure 4.12:** FTIR spectra of (a) the neat LLDPE and LLDPE-43B nanocomposite films, and (b) the neat EVA and EVA-43B nanocomposite films

#### 4.3.4 Determination of permeability of films to repellents

Table 4.2 lists the polymer film thicknesses used to calculate the permeability to each repellent.

**Table 4.2:** Thickness of neat polymer and polymer-clay nanocomposite films in units of  $\mu\text{m}$

Polymer film	DEET	Icaridin	IR3535	Ethyl anthranilate
Neat LLDPE	55±1	55.3±0.4	54±3	49±3
LLDPE-43B	76±6	74±13	78±7	83±6
Neat EVA	44±2	48±5	51±7	63±5
EVA-43B	47±1	47±2	48±1	49±3

Table 4.3 lists the permeability of the neat polymer and polymer-clay nanocomposite films to the repellents as calculated with equation (3.1). The EVA films had a higher permeability than LLDPE to all the tested repellents. In essence, the permeability is defined as the product of the diffusion

coefficient and the solubility of the permeant in the polymer matrix. The repellents are all polar molecules and should therefore be more soluble in the more polar EVA than in the highly non-polar polyethylene. This behaviour is corroborated by the polymer swelling results shown in Table 4.4. Secondly, permeants are only soluble in the amorphous fraction of a semicrystalline polymer. LLDPE has a higher crystallinity than EVA. These two factors explain the higher permeability shown by the EVA. Noteworthy is the observation that the permeability of Icaridin was lower compared to the other repellents studied in both the EVA and LLDPE films.

Furthermore, Table 4.3 reveals that, compared to neat EVA film, the EVA nanocomposite films presented a higher barrier to all the repellents investigated. However, the same did not hold for the LLDPE nanocomposite films when ethyl anthranilate was the permeant. This behaviour is in contradiction to the conventional wisdom with respect to nanocomposites. It was expected that the impermeable clay platelets, if well dispersed in the matrix, should decrease the permeability by the tortuosity of the diffusion path effect. It is speculated that the observed opposite result could be attributed to poor matrix-filler adhesion which resulted in the formation of a porous structure that increased the mobility of the volatile repellents through the polymer film.

Previous studies conducted by Choudalakis and Gotsis (2009) reported that a crucial factor that affects the permeation properties of the nanocomposites is the aggregation of silicate layers, which leads to a reduction of the aspect ratio of the nanoparticles. Furthermore, Manninen et al. (2005) showed that the processing path taken to prepare the nanocomposites may result in agglomeration of the layers of the organoclay. Such agglomerates may form large-scale holes (pores) in the matrix, which can act as low-resistance pathways for gas transport within the nanocomposite (Choudalakis and Gotsis, 2009). In summary, the present study demonstrated that the Dellite 43B



organoclay was more compatible with the EVA matrix than the LLDPE matrix, but it did not necessarily lead to a lowering of film permeability.

**Table 4.3:** Permeability of the neat polymer and polymer-clay nanocomposite films to the repellents in units of  $\text{g}\cdot\mu\text{m}\cdot\text{day}^{-1}\cdot\text{m}^{-2}$ . Both properties were evaluated at 50 °C.

<b>Polymer film</b>	<b>DEET</b>	<b>Icaridin</b>	<b>IR3535</b>	<b>Ethyl anthranilate</b>
Neat LLDPE	312±64	126±4	140±32	1391±61
LLDPE-43B	304±35	119±3	129±5	2176±31
Neat EVA	400±47	158±6	166±55	3466±54
EVA-43B	370±33	107±21	111±6	2245±27

#### 4.4 Release of repellents from microporous polymer strands

##### 4.4.1 Effect of repellent on swelling and shrinkage of the polymers

Table 4.4 lists the amount of repellent absorbed by the two polymers at 30 and 50 °C determined by equation (3.5). As expected, less of the polar repellents was absorbed by the semicrystalline and nonpolar LLDPE compared to the amorphous and polar EVA matrix. The polar repellents interacted more weakly with the LLDPE matrix compared to EVA. Charara et al. (1992) reported the absorption of essential oils in various polymeric packaging materials. They found that amorphous polymers absorbed more of the essential oils than the ones with higher crystallinity. In the present study, the solubility of Icaridin was just about half of that measured for DEET. This suggests that the latter is less compatible with the polymers than DEET.

**Table 4.4:** Polymer swelling by repellents expressed in wt.% evaluated at 30 and 50 °C

Temperature (°C)	30		50	
	DEET	Icaridin	DEET	Icaridin
LLDPE	0.28±0.01	0.18±0.09	0.79±0.03	0.43±0.06
EVA	1.73±0.20	0.96±0.26	5.49±0.12	3.44±0.29

A polymer matrix swelled by a repellent will shrink over time as the active ingredient is lost by evaporation. Such dimensional instability is undesirable in products such as insect repellent bracelets and anklets (Akhtar and Focke, 2015). Therefore, it was important to determine the potential for shrinkage of polymer strands impregnated with repellents. Table 4.5 shows the shrinkage of neat polymer strands and polymer strands impregnated with DEET and Icaridin. The sample dimensions were measured after ageing for 23 days at 50 °C in a convection oven. The EVA strands showed more extensive shrinkage than LLDPE strands. In addition, DEET-containing strands showed a higher shrinkage than Icaridin-filled polymers irrespective of the matrix polymer (EVA and LLDPE). This is due to the higher solubility of DEET, compared to Icaridin, in the polymers. Even the neat polymer strands showed a degree of shrinkage, indicating that some orientation had occurred during the extrusion process. However, the degree of shrinkage was much less than that of the repellent-filled samples. However, overall the LLDPE matrix showed better dimensional stability than the EVA matrix.

**Table 4.5:** Shrinkage of polymer strands expressed in wt.% evaluated at 50 °C

<b>Polymer strand</b>	<b>Sample No.</b>	<b>Diameter before shrinkage (mm)</b>	<b>Diameter after shrinkage (mm)</b>	<b>Shrinkage (%)</b>
Neat LLDPE	BM00	3.28±0.07	3.25±0.04	0.78
Neat EVA	AS00	3.58±0.05	3.49±0.12	2.64
LLDPE-Icaridin (20)	BM400	3.43±0.07	3.31±0.06	3.59
LLDPE-Icaridin (30)	BM401	4.29±0.05	4.19±0.03	2.31
LLDPE-DEET (20)	BM402	4.24±0.13	4.08±0.19	3.73
LLDPE-DEET (30)	BM403	4.16±0.05	3.96±0.04	4.76
EVA-Icaridin (20)	AS400	3.53±0.25	3.38±0.10	4.43
EVA-Icaridin (30)	AS401	3.65±0.26	3.48±0.06	4.66
EVA-DEET (20)	AS402	3.40±0.12	3.22±0.10	5.23
EVA-DEET (30)	AS403	3.55±0.06	3.20±0.07	9.77

#### 4.4.2 Repellent content of the extruded strands by TGA and solvent extraction

Figure 4.13 shows TGA traces for the repellent, neat polymer and repellent content trapped in the polymer-clay nanocomposite strands. The first of mass loss is assigned to the loss of the volatile repellent component in polymer-based strands in all samples analyzed. Therefore, mass loss of the neat DEET by vaporization commenced just above 105 °C and was complete by 268 °C, while evaporative mass loss of the neat Icaridin commenced just above 126 °C and was complete by 294 °C. However, the DEET and Icaridin mass loss is complete before the LLDPE starts to lose mass in earnest above 400 °C. Therefore, the volatility of the repellents is suppressed

when they are trapped in the LLDPE filaments. Appendix IX lists the results for other LLDPE repellent formulations.

Similar trends were observed for the DEET-filled EVA and the Icaridin-filled EVA. However, the DEET mass loss by evaporation overlapped with the first mass-loss event for the polymer, while this behaviour was not observed for Icaridin and the mass loss by evaporation commenced just above 112 °C.

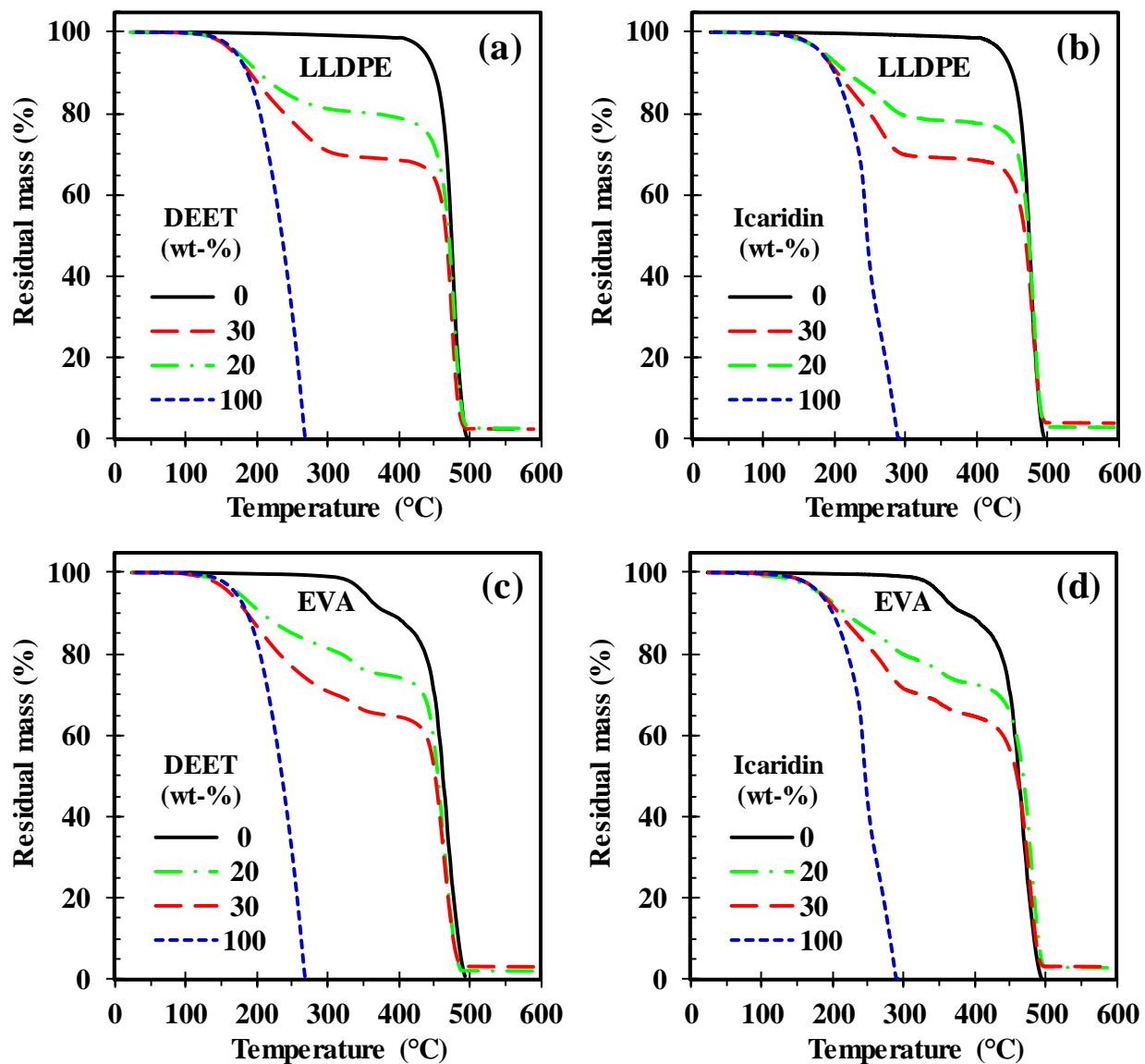


**Figure 4.13:** TGA mass loss traces for DEET, Icaridin, neat polymers and (a) and (b) LLDPE, and (c) and (d) EVA-based strands containing 5 wt.% Dellite 43B clay and either 20 or 30 wt.% DEET and 20 or 30 wt.% Icaridin

In addition, Figure 4.14 shows that trapping IR3535 and ethyl anthranilate in LLDPE strands suppresses their volatilization. Mass loss of the neat IR3535 commenced just above 102 °C and was complete by 270 °C, while evaporative mass loss of the neat ethyl anthranilate commenced

just above 95 °C and was complete by 250 °C before the LLDPE starts to lose mass in earnest above 400 °C.

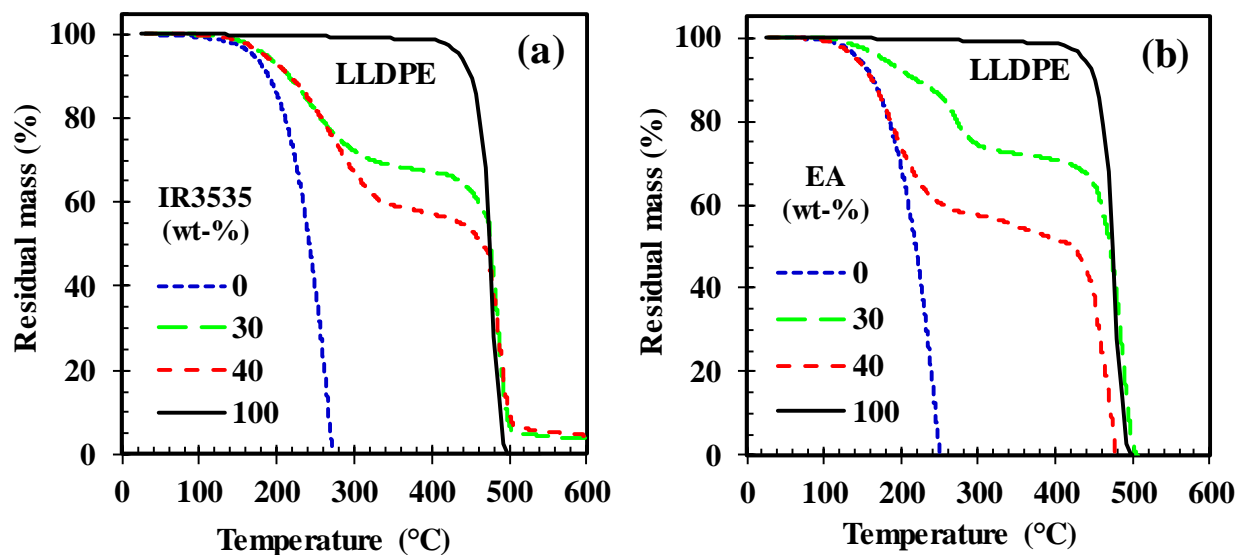


**Figure 4.14.** TGA mass loss traces for IR3535, ethyl anthranilate and neat LLDPE. (a) LLDPE-based strands contained 5 wt.% Dellite 43B clay and either 30 or 40 wt.% IR3535. The formulation 40 wt.% IR3535 was loaded with 5 wt.% fumed silica. (b) LLDPE-based strands contained 5 wt.% Dellite 43B clay and either 30 wt.% ethyl anthranilate and formulation 40 wt.% ethyl anthranilate only contained 5 wt.% fumed silica.

Table 4.6 shows the estimated amount of repellent determined by thermogravimetric analysis (TGA) and solvent extraction, calculated using equation (3.2). The results are in close agreement with the amount of repellent initially loaded in the compounding process. This shows that very little repellent mass was lost by evaporation during the compounding process. Appendix XI lists repellent contents estimated from solvent extraction and thermogravimetric analysis (TGA) experiments for other LLDPE formulations.

**Table 4.6:** Nominal repellent content (in wt.%) and values estimated using solvent extraction and thermogravimetric analysis (TGA)

<b>Polymer strand</b>	<b>Nominal</b>	<b>TGA</b>	<b>Solvent extraction</b>	<b>Sample code</b>
LLDPE-DEET	20	19.8	19.3±0.6	BM402
LLDPE-DEET	30	30.2	30.0±0.9	BM403
LLDPE-Icaridin	20	20.1	20.2±0.6	BM400
LLDPE-Icaridin	30	30.3	29.0±0.2	BM401
EVA-DEET	20	19.7	18.7±0.5	AS402
EVA-DEET	30	29.9	29.0±0.2	AS403
EVA-Icaridin	20	20.3	19.6±0.2	AS503
EVA-Icaridin	30	28.5	30.1±0.5	AS504
LLDPE-IR3535	30	27.8	28.2±0.2	BM204
LLDPE-IR3535	40	37.8	38.2±0.1	BM205
LLDPE-EA	30	27.8	27.6±0.2	BM207
LLDPE-EA	40	40.0	40.1±0.5	BM106

Figure 4.15 shows the TGA curves for the LLDPE-Icaridin and LLDPE-Icaridin-clay strands. The mass loss proceeded stepwise in all samples. The mass loss is less for the nanocomposite strand compared to that of the LLDPE strand without clay. The mass loss of Icaridin by volatilization in the nanocomposite strand without clay is almost complete at approximately 380 °C and 420 °C. Additionally, the TGA curves for the LLDPE nanocomposite strand and the LLDPE strand without

clay initially containing 20 wt.% Icaridin had 19.94% and 17.01% of Icaridin trapped in the LLDPE.

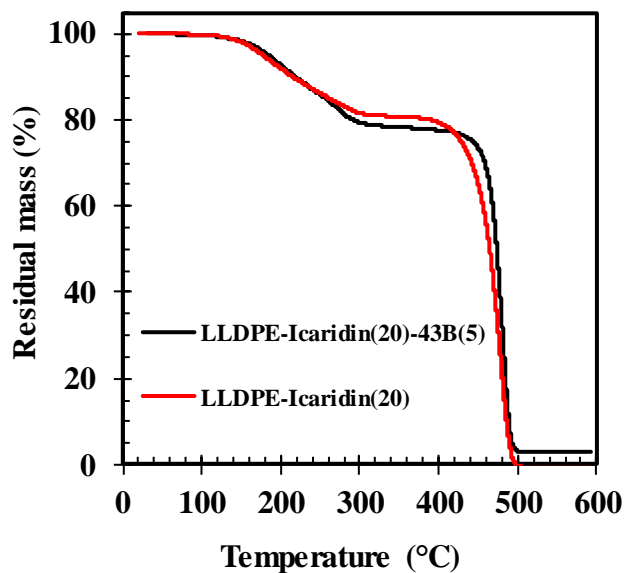


**Figure 4.15:** TGA curves of LLDPE strands initially containing: (—) 20 wt.% Icaridin and loaded with 5 wt.% Dellite 43B organoclay; and (—) 20 wt.% Icaridin with the absence of nanofillers.

Figure 4.16 shows the TGA profiles of the DEET and Icaridin-containing strands, before and after aging in a convection oven at 50 °C. The results present the same structure, demonstrating the stability of the LLDPE repellent strands for six months.



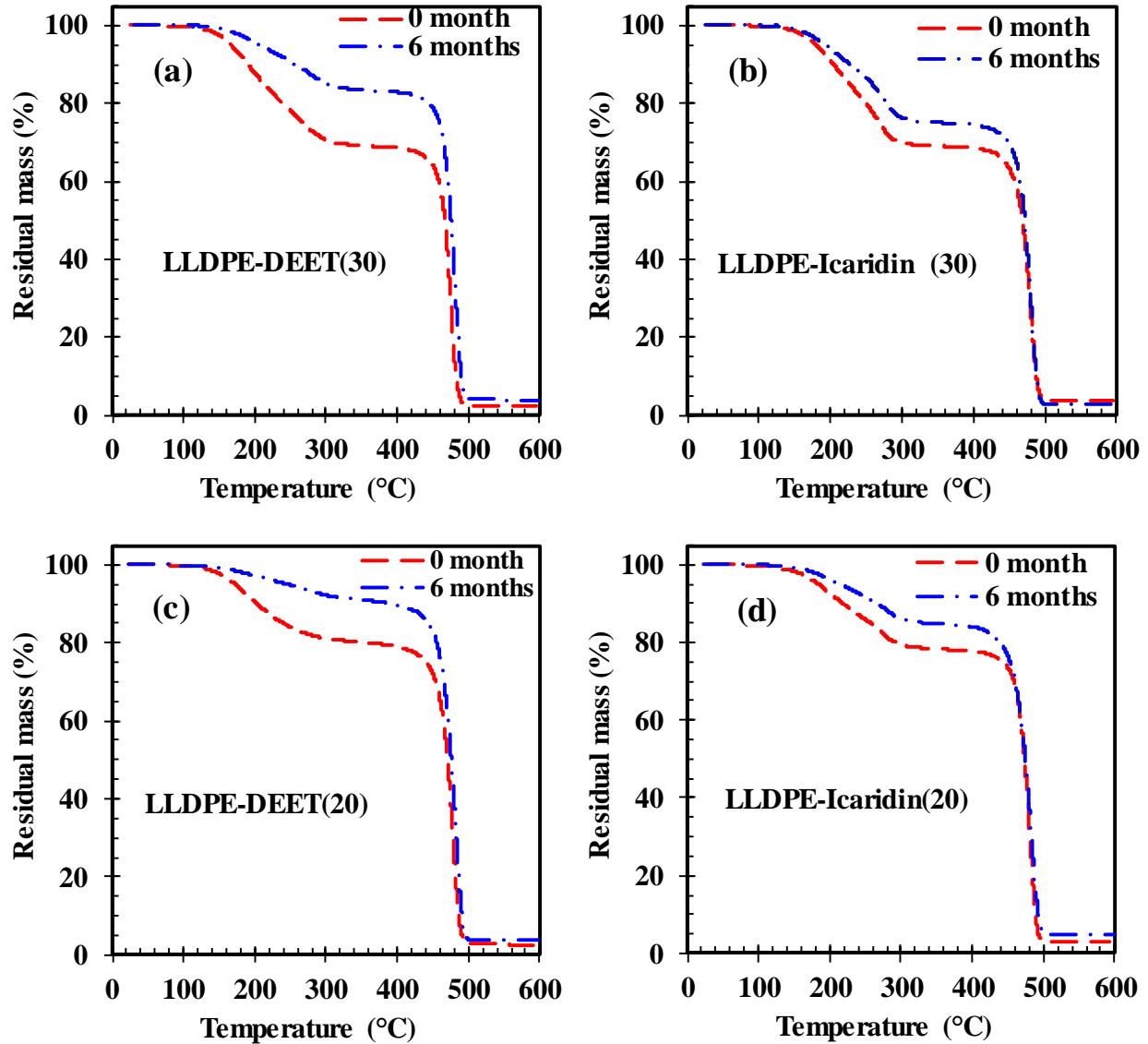


**Figure 4.16:** TGA traces of LLDPE strands initially containing: (a) 30 wt.% DEET; (b) 30 wt.% Icaridin; (c) 20 wt.% DEET; and (d) 20 wt.% Icaridin at 0 month and 6 months. All strands initially contained 5 wt.% Dellite 43B organoclay

Table 4.7 lists the residual repellent present in LLDPE strands oven-aged for six months at 50 °C. It compares the estimates obtained from actual mass loss measurements on full strands to TGA determinations on small samples. The TGA-derived values were found to be somewhat higher than

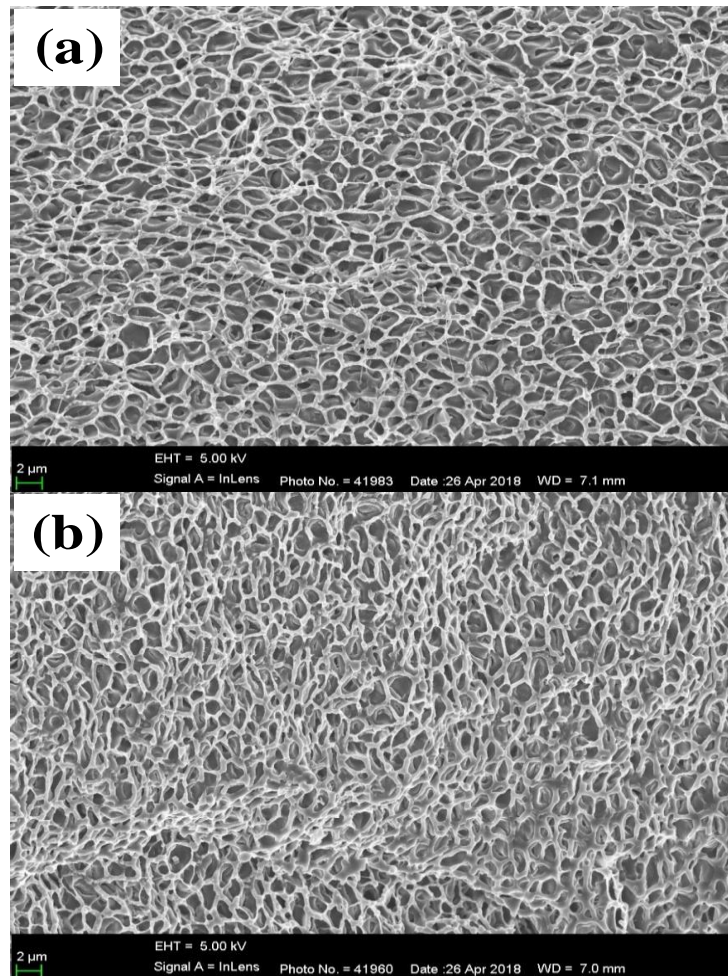
those determined from mass loss measurements on a full coil. It is not clear what the source of the discrepancy is. However, the TGA result reflects the repellent content of a sample taken from the middle of the aged coil, and it could be that the lower value recorded for the full coil reflects additional losses of repellent from the open ends of the strands. In either case the results show that, after six months of aging, more than 50% of the repellent was still present and trapped inside the strands, except for the LLDPE-DEET (20) composition. This demonstrates that the LLDPE strands extended the time of the repellent release.

**Table 4.7:** Nominal repellent content in (wt.%) and estimated values of repellent trapped in LLDPE strands after oven aging for 6 months at 50 °C using thermogravimetric analysis (TGA) and mass loss of repellents from strands

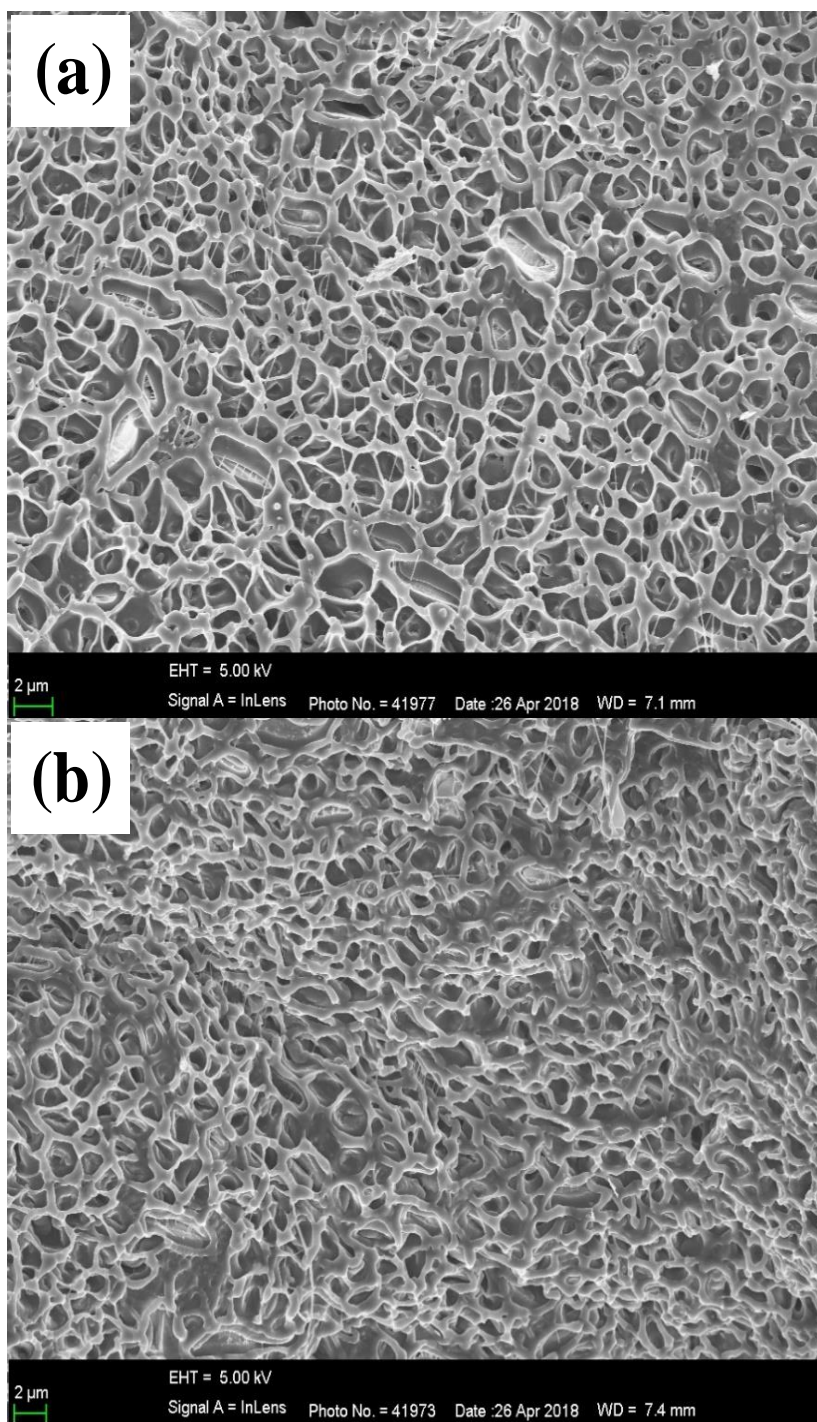
<b>Polymer strand</b>	<b>Nominal</b>	<b>TGA</b>	<b>Mass loss</b>	<b>Sample code</b>
LLDPE-DEET (20)	20	9.0	7.1	BM402
LLDPE-DEET (30)	30	15.9	13.0	BM403
LLDPE-Icaridin (20)	20	14.6	13.5	BM400
LLDPE-Icaridin (30)	30	23.3	22.2	BM401

#### **4.4.3 Structure of the internal region of the extruded polymer strands**

Figures 4.17 and Figure 4.18 show SEM micrographs of LLDPE strands prepared in the absence of the nanofillers (Dellite 43B and fumed silica). The open-cell foam structure of the polymer scaffold comprising the strands is clearly visible. It is clear that the type of repellent did affect the morphology of the strands, as it gave rise to different microporous structures in the interior of the strands.

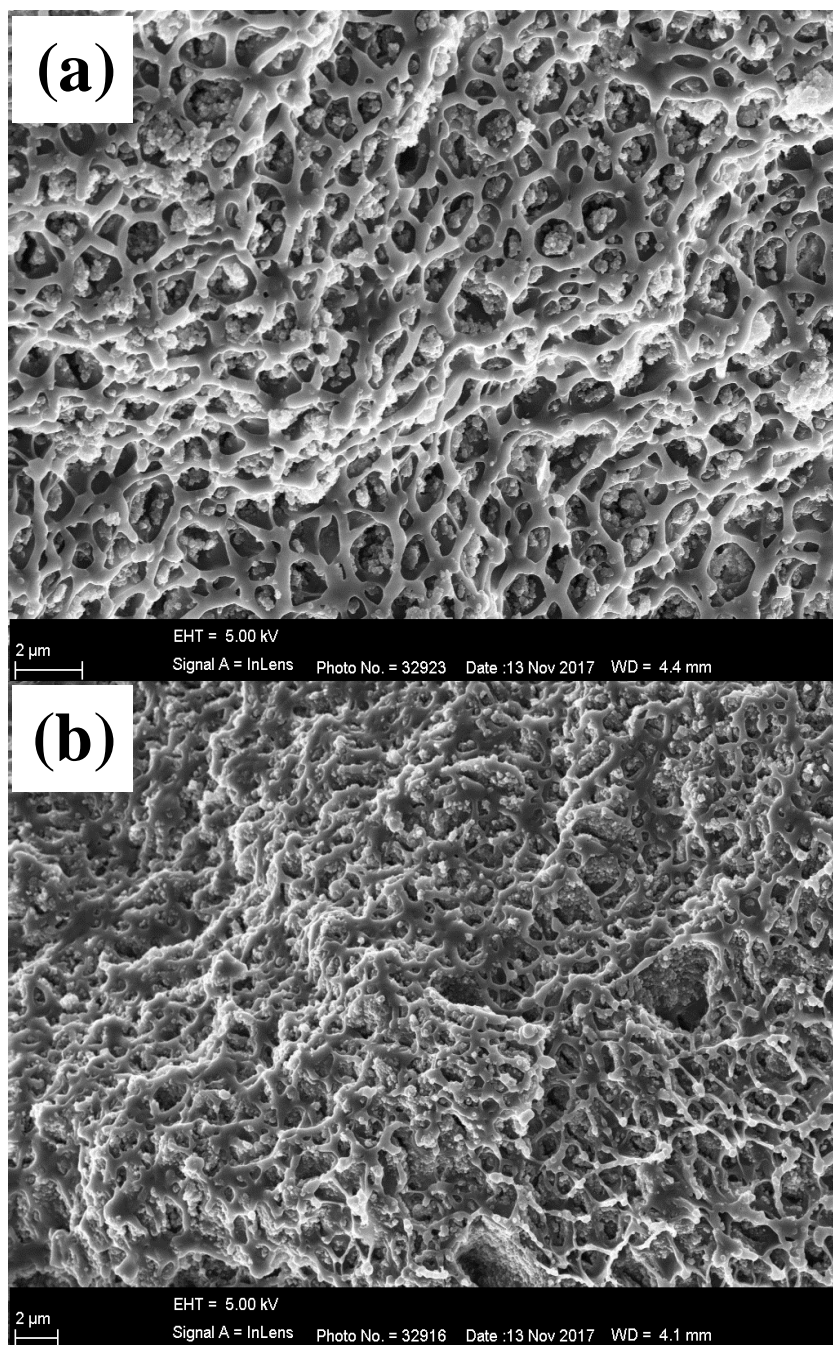


**Figure 4.17:** SEM micrographs of LLDPE strands impregnated with: (a) 41 wt.% of DEET; and (b) 42 wt.% of Icaridin. No fillers were added in the LLDPE strands.

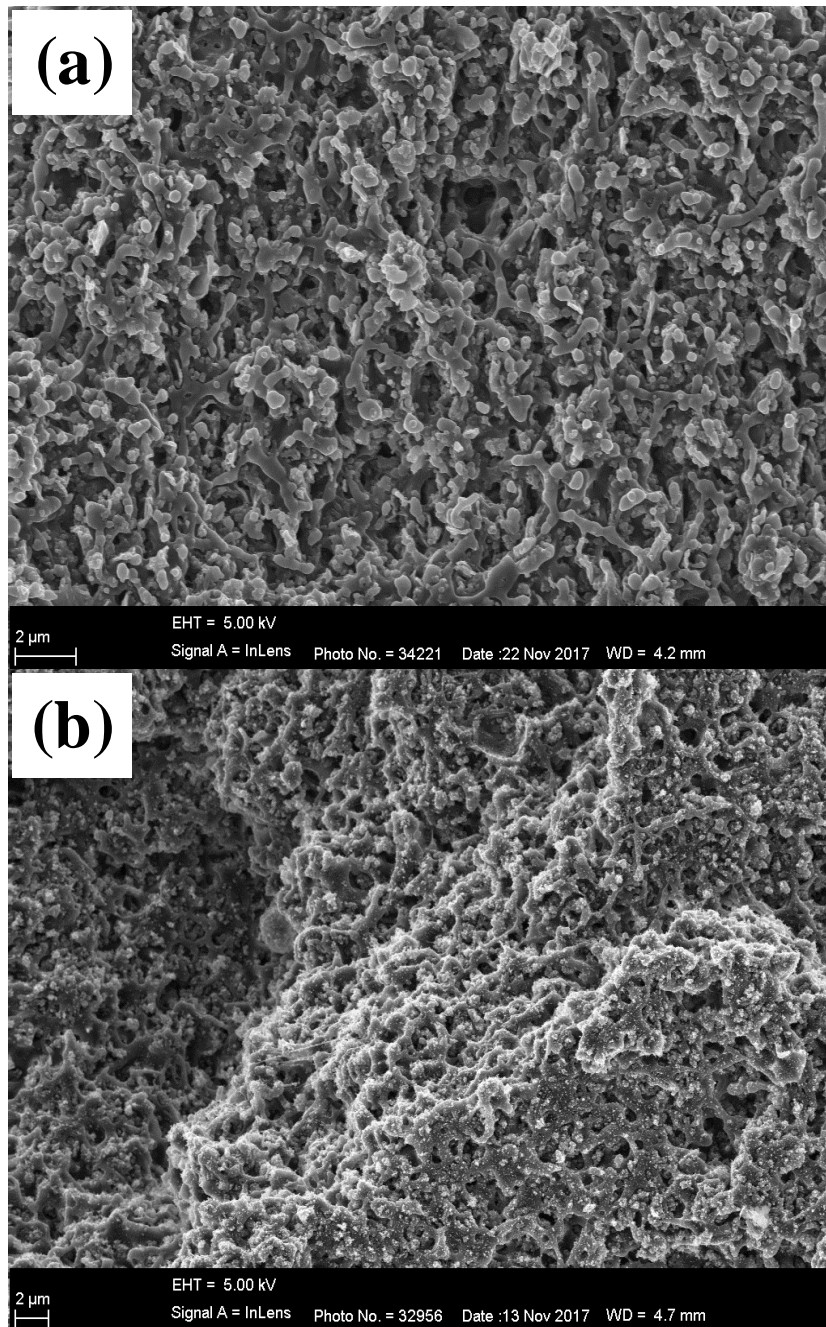


**Figure 4.18:** SEM micrographs of LLDPE strands impregnated with: (a) 41 wt.% of IR3535; and (a) 44 wt.% of ethyl anthranilate. No fillers were added in the LLDPE strands.

Figure 4.19 and Figure 4.20 show the effect of fumed silica and insect repellent type on the structure of the internal microporous region of extruded LLDPE strands. The morphology of polymer strands changed with the incorporation of fumed silica into the microporous polymer strand. The micrographs reveal the presence of agglomerated fumed silica particles inside the cavities. This suggests that the fumed silica was primarily present in the repellent-rich phase after phase separation was complete. This behaviour was most visible in the LLDPE strand impregnated with Icaridin (see Figure 4.19a) where the pore sizes are bigger than those of other LLDPE-repellent systems.



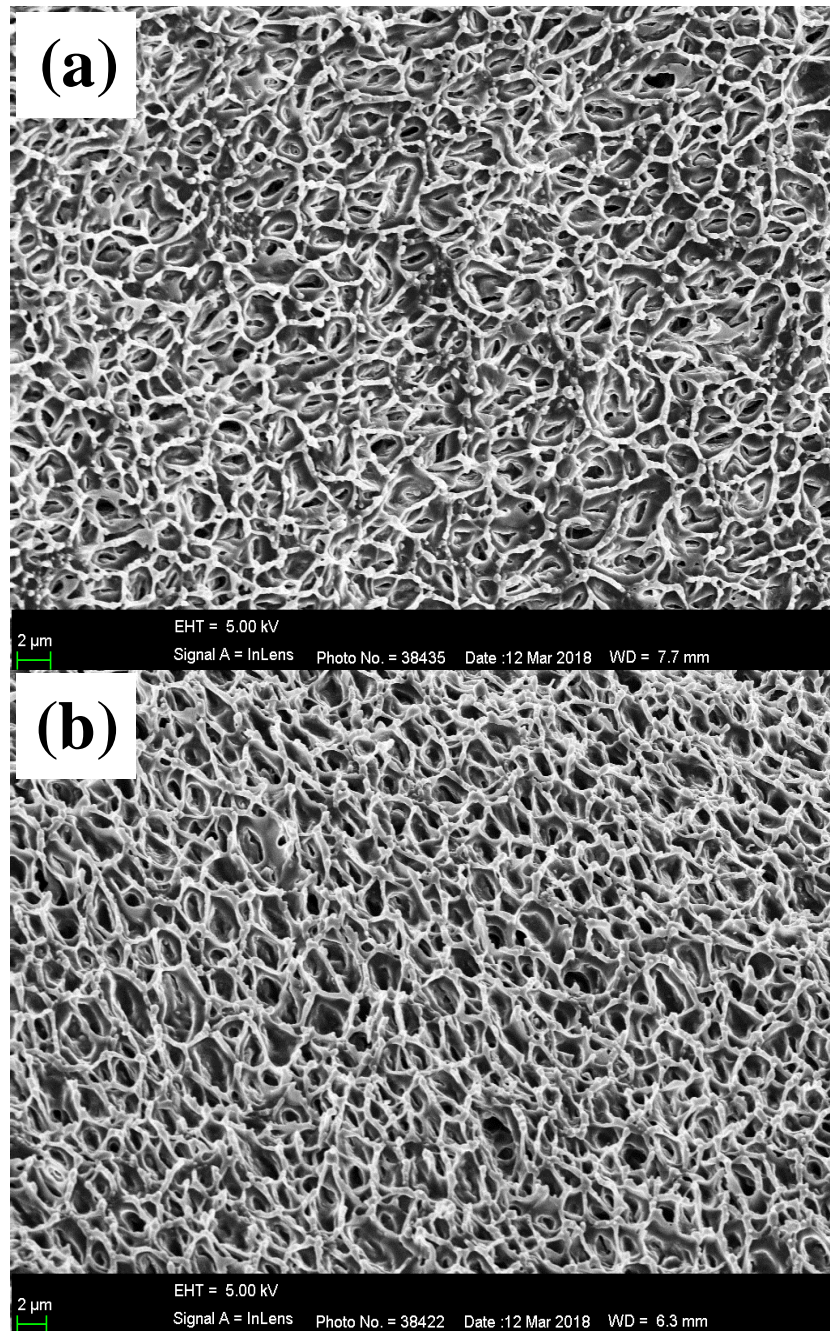
**Figure 4.19:** SEM micrographs showing the effect of silica and insect repellent type on the structure of the internal microporous region of extruded LLDPE strands. (a) 30 wt.% Icaridin; and (b) 30 wt.% DEET. All strands contained 5 wt.% fumed silica.



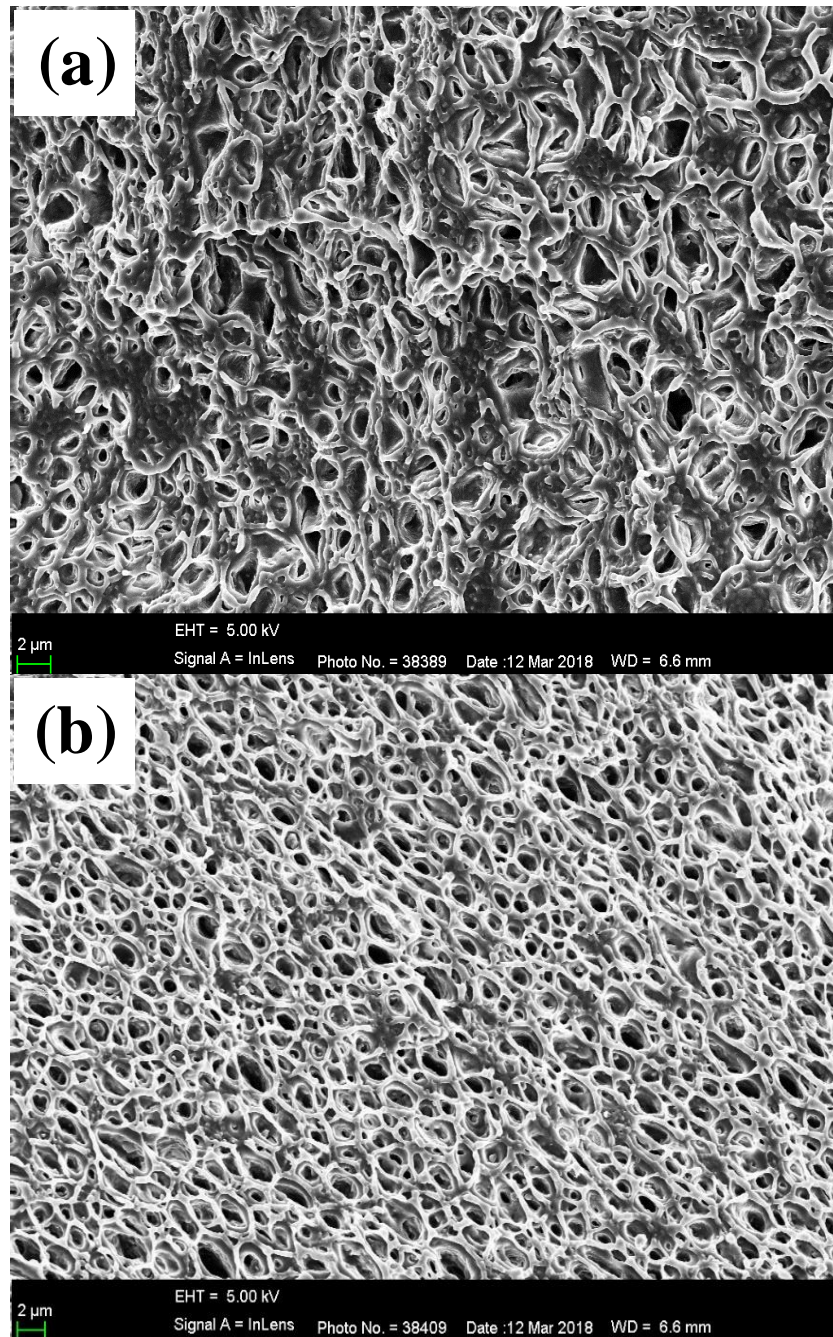
**Figure 4.20:** SEM micrographs showing the effect of silica and insect repellent type on the structure of the internal microporous region of extruded LLDPE strands. (a) 30 wt.% IR3535, and (b) 30 wt.% ethyl anthranilate. All strands contained 5 wt.% fumed silica.

Figure 4.21, Figure 4.22 and Figure 4.23 show the effect of the repellent type (DEET, Icaridin, IR3535 and ethyl anthranilate) and their concentration on the LLDPE clay phase morphology. The observed microporous polymer structure is quite evident on the inner polymer section with the interconnecting pores clearly visible. However, it is clear from the micrographs that the nature of the repellent, as well as the concentration that was used, did affect the final microstructure. For example, the DEET-derived polymer scaffold featured a filamentous structure (Figure 4.21(a) and (b)). It seems that the Icaridin-derived microstructure had a more cellular appearance comprising near-spherical voids interconnected by smaller holes (Figure 4.22(a) and (b)). In both cases, the scale of the voids was in the order of a few microns. No clay platelets were observed, suggesting that they were confined to the polymer-rich phase that formed the microporous scaffold. Additional results are presented in Appendix XIV. This experiment showed that the thermally induced spinodal decomposition route does in fact lead to a microporous polymer structure.





**Figure 4.21:** SEM micrographs showing the effect of insect repellent type and concentration on the structure of the internal microporous region of extruded LLDPE strands. (a) 20 wt.% DEET; and (b) 30 wt.% DEET. All strands contained 5 wt.% Dellite 43B clay.



**Figure 4.22:** SEM micrographs showing the effect of insect repellent type and concentration on the structure of the internal microporous region of extruded LLDPE strands. (a) 20 wt.% Icaridin; and (b) 30 wt.% Icaridin. All strands contained 5 wt.% Dellite 43B clay.

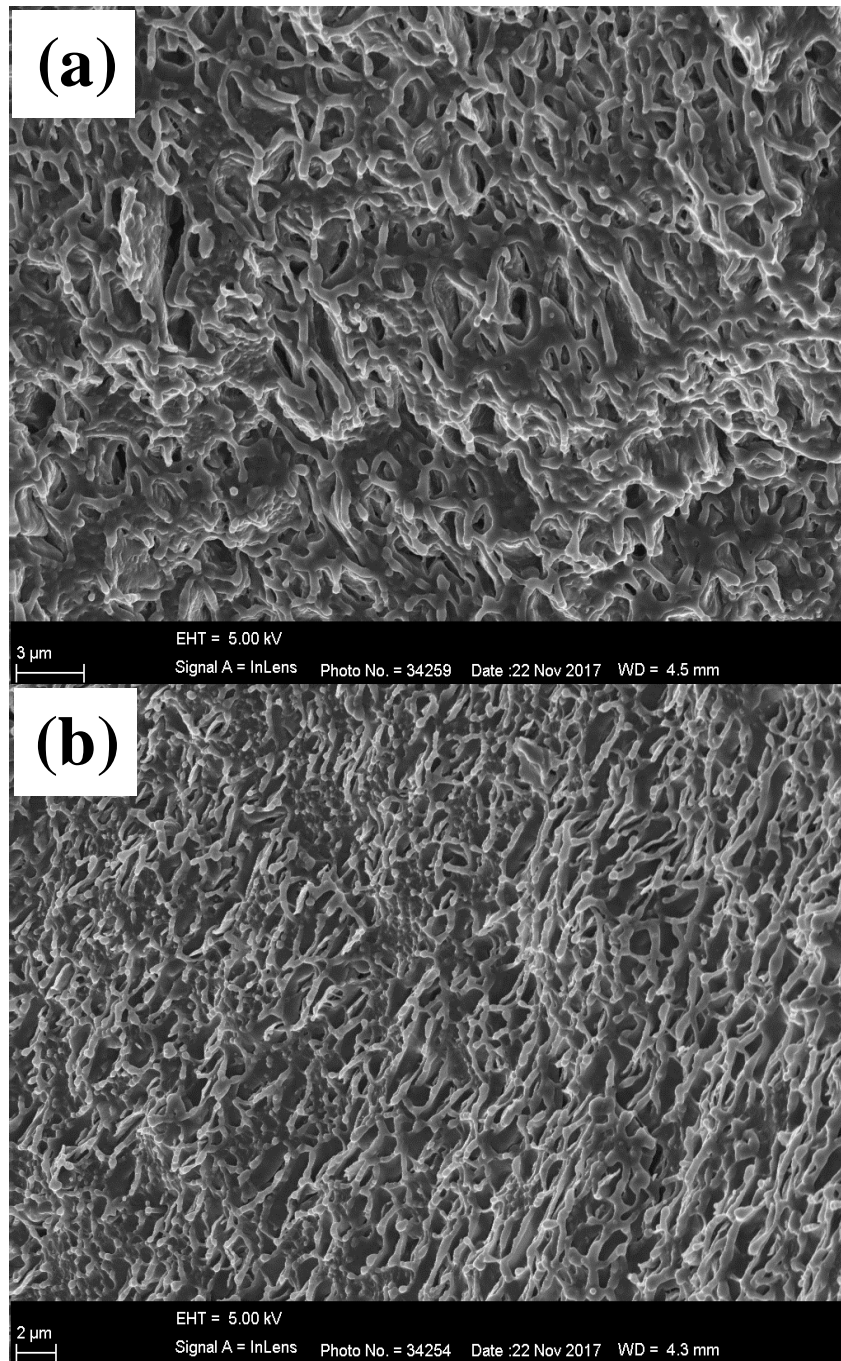


**Figure 4.23:** SEM micrographs showing the effect of insect repellent type on the structure of the internal microporous region of extruded LLDPE strands. (a) 30 wt.% IR3535; and (b) 30 wt.% ethyl anthranilate. All strands contained 5 wt.% Dellite 43B clay.

Figure 4.24 shows SEM micrographs of the internal structure of EVA strands initially containing 30 wt.% DEET or Icaridin. The interior of the strand did not have a uniformly porous structure. The connectivity of the porous structure was poor, showing numerous closed pores. This could have been caused by the shrinkage of the polymer scaffold after extraction of the DEET and Icaridin with dichloromethane.

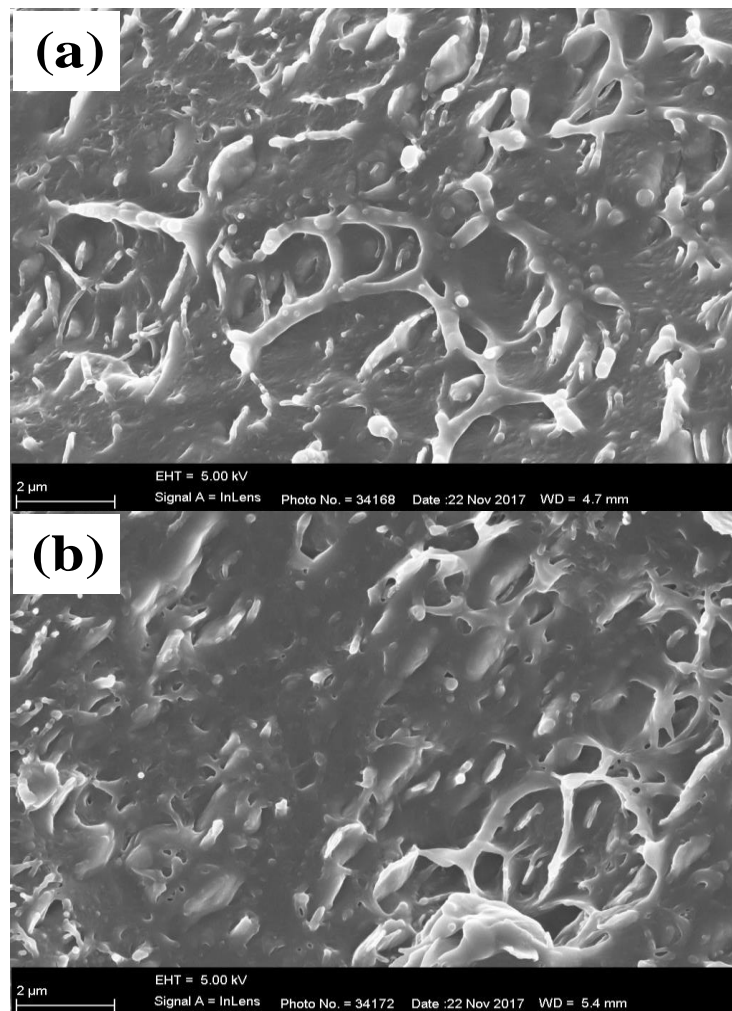


**Figure 4.24:** SEM micrographs showing the internal structure region of extruded EVA strands. (a) 30 wt.% DEET; and (b) 30 wt.% Icaridin. All strands contained 5 wt.% Dellite 43B clay.

#### **4.4.4 Outer surfaces of LLDPE strands**

The outer surfaces of the LLDPE strands were also observed with the scanning electron microscope (SEM). Figure 4.25 shows a cross-section of a strand that clearly reveals the presence of a pronounced dense skin at the edge of the strand. Figure 4.26 provides views of the outer surface structure of the strand. Clearly there is evidence of a dense, smooth outer surface. The presence of a membrane-like skin covering the microporous polymer strands is also visible in Figure 4.27. This suggests that the skin may present a membrane-like barrier to outward migration of the actives. When diffusion of the active ingredient through the membrane is the mass transport limiting step, a more gradual reduction in the release rate over time is realized. The permeability of membranes with respect to an active ingredient can be engineered by adjusting the membrane thickness and judicious selection of the polymer system to be used as a matrix (Akhtar, 2015). Additional results are presented in Appendix XV.

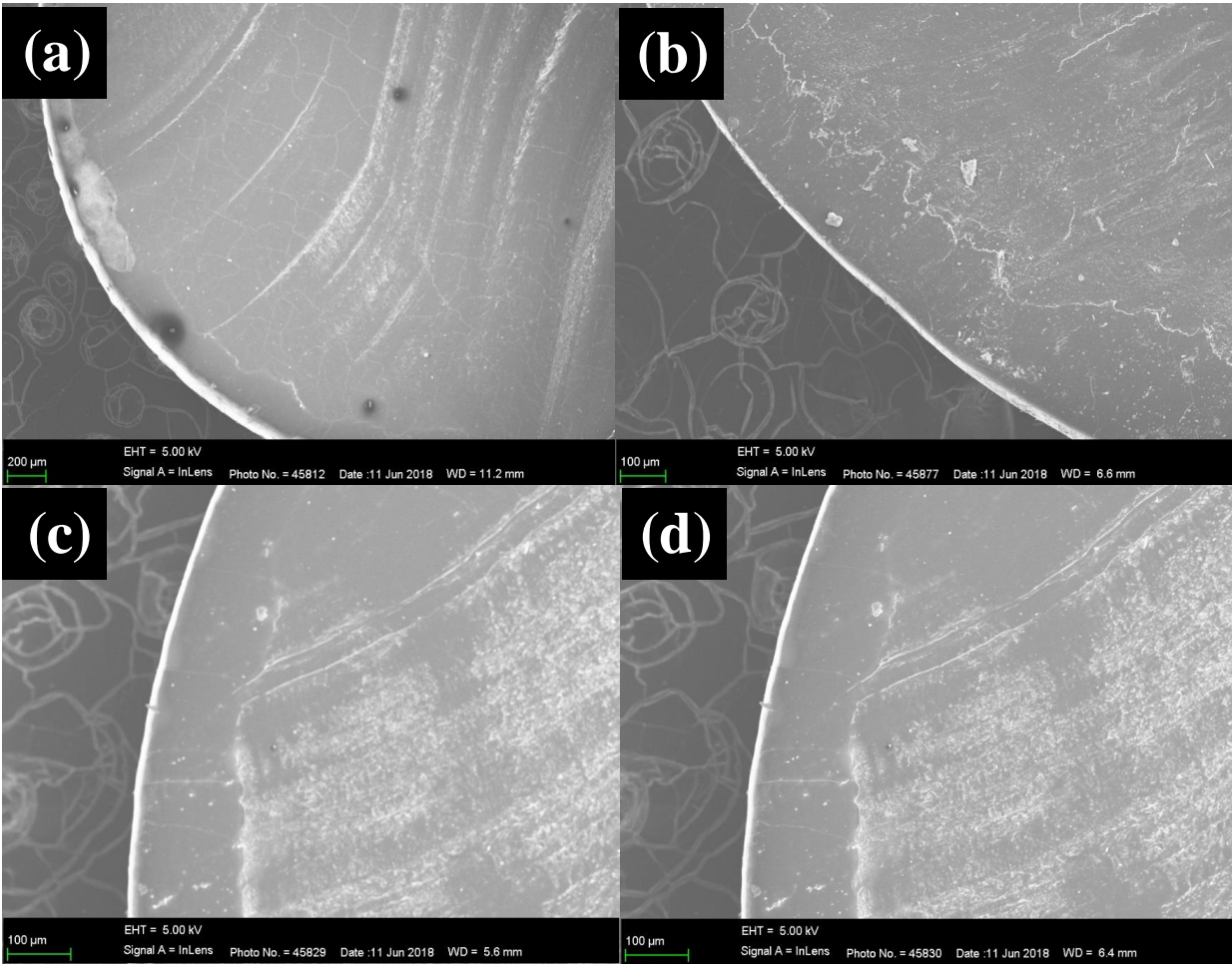


**Figure 4.25:** Cross-section evidently showing an outside skin covering of the strand: (a) 20 wt.% Icaridin; (b) 30 wt.% Icaridin; (c) 20 wt.% DEET; and (d) 30 wt.% DEET. All LLDPE strands contained 5 wt.% Dellite 43B clay.

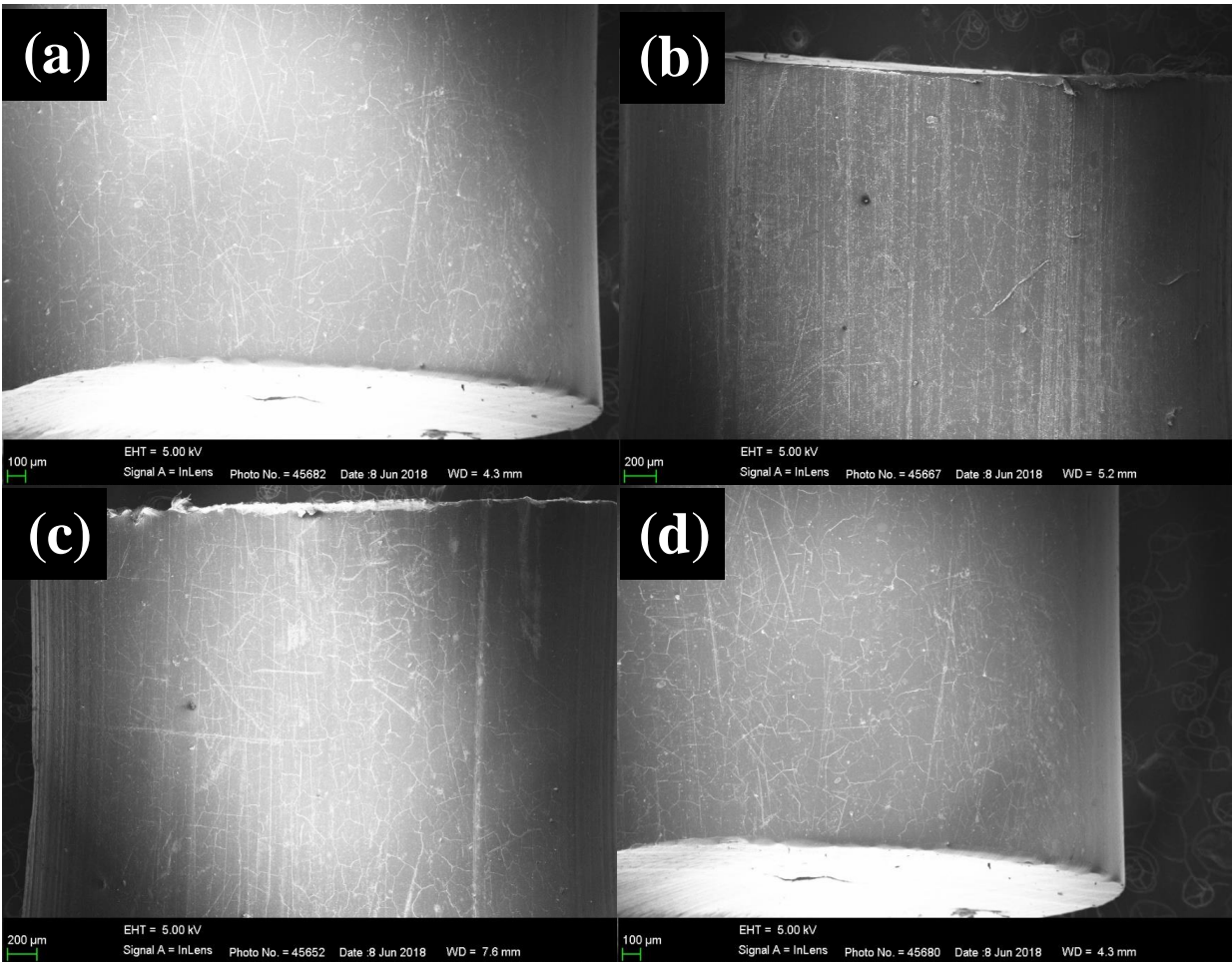


**Figure 4.26:** Side views of the outer surface structure of the strand: (a) 20 wt.% Icaridin; (b) 20 wt.% DEET and (c) and (d) initially containing 30 wt.% DEET. All LLDPE strands contained 5 wt.% Dellite 43B clay.

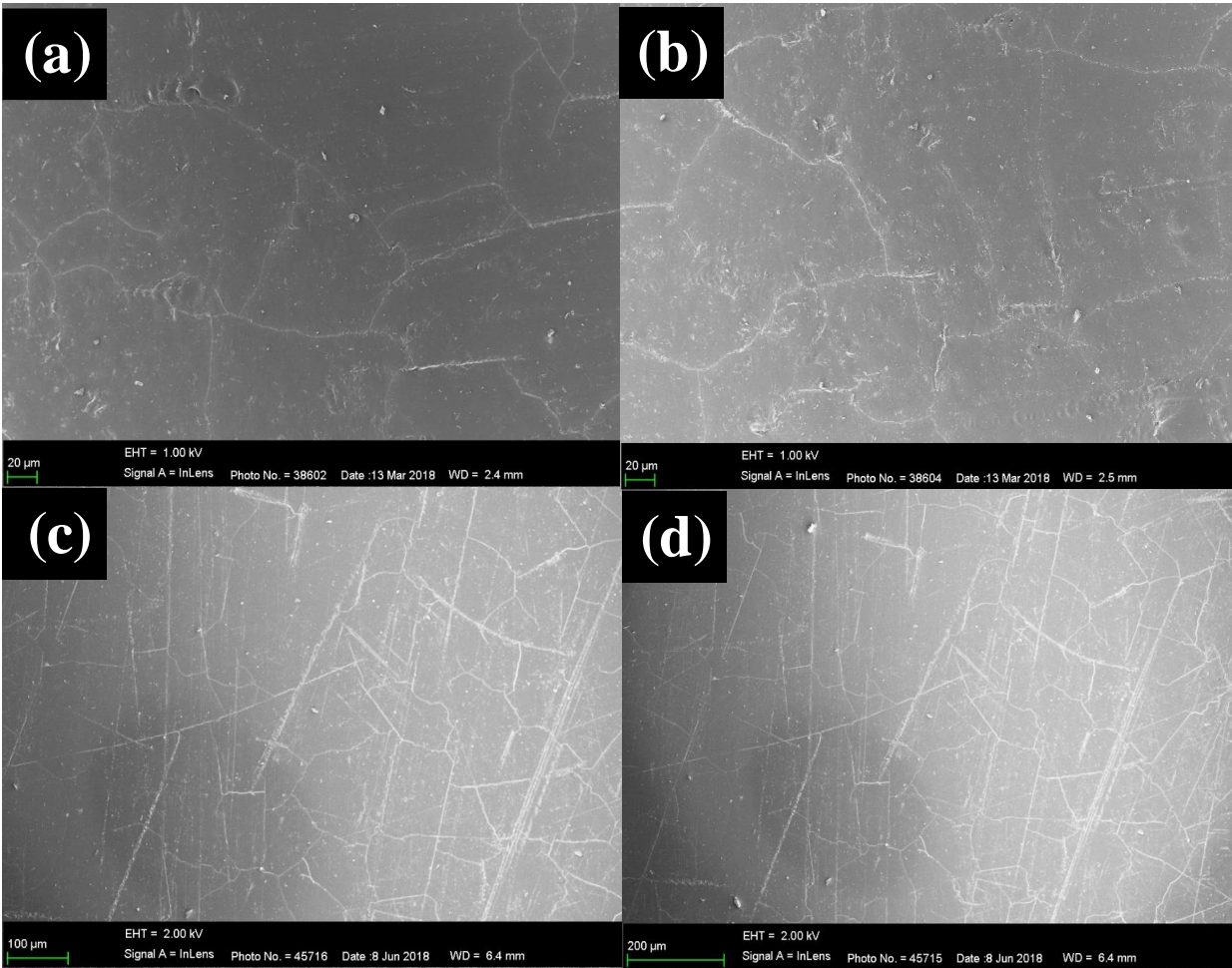


**Figure 4.27:** The outer surface appearance of the skin of the LLDPE strands: (a) and (b) 30 wt.% DEET and (c) and (d) 20 wt.% Icaridin. All the LLDPE strands contained 5 wt.% Dellite 43B clay.



#### 4.4.5 Estimation of the membrane thickness

The assumption was made that the permeability of the membrane covering the strands was the same as that for the blown film samples tested separately. Right at the beginning, all the pores of the strands are filled with liquid so that only the membrane covering presents a diffusion barrier to repellent release. This allowed the thickness of the membrane film covering the strands to be estimated from the initial release rate, i.e. the slope of the mass loss vs. time at time  $t = 0$ . Table 4.8 lists the repellent content, polymer strand diameters, repellent release rate model parameters, initial evaporation rates and the estimated values of the thickness of the skin-like membranes covering the strands determined from the repellent release data in combination with the permeability values measured for the films (equation (3.4)). The estimated membrane thickness varied from 4 to 104  $\mu\text{m}$  for DEET-containing strands and from 12 to 186  $\mu\text{m}$  for the Icaridin-filled strands. These values are in agreement by an order of magnitude with SEM observations as illustrated in Figure 4.25.

The parameter ( $\kappa_2$ ) provides an indication of the effect of the membrane layer on the rate of release of the repellent. In the complete absence of the membrane layer,  $\kappa_2=1$ , the rate is determined solely by the rate at which the repellent diffuses out of the porous polymer scaffold. In this case, the release of repellent will be relatively fast because there is no skin covering the strand. However, if  $\kappa_2 \gg 1$ , the outer skin-like membrane fully controls the repellent release. In this case the repellent will be released slowly and at a constant rate until it is fully depleted. The time to complete repellent loss is proportional to  $1/\kappa_3 = \kappa_2/\kappa_1 = \frac{R_p^2 \ln(R_F/R_P)}{2HD_m} \left( \frac{C_L}{C_{eq}} \right)$ . The link to the membrane thickness ( $z_{membrane}$ ) comes via the expression  $R_F/R_P = 1 + z/R_P$ . Often the relative

thickness is very small and therefore one can use the approximation  $\ln(1 + x) \approx x$ . With this approximation one obtains:

$$t_f = \kappa_1 / \kappa_2 \approx \frac{zR_p}{2HD_m} \left( \frac{C_L}{C_{eq}} \right) \quad (4.1)$$

This indicates that the time to complete depletion of the repellent from a given strand (for the case where a relatively thin membrane controls the release rate) is proportional, not only to the thickness of the membrane, but also to the diameter of the strand.

In the complete absence of a membrane the time to complete depletion of the repellent will be given by equation (4.2):

$$t_f = 1 / \kappa_1 \approx \frac{R_p^2}{4D_p} \left( \frac{C_L}{C_{eq}} \right) \quad (4.2)$$

In this case the total release time is proportional to the square of the strand diameter. Clearly, when both mechanisms together control the release rate, the proportionality will be the intermediate power of the strand diameter.

Table 4.8 shows the range of parameter ( $\kappa_1$  and  $\kappa_2$ ) values of the strands over several orders of magnitude. However, in all cases, reasonable fits to the experimental data were obtained. The adjustable model parameters were determined by least squares data fitting. For ethyl anthranilate based LLDPE strands the parameter  $\kappa_2$  was indeed equal to unity ( $\kappa_2=1$ ) showing that there was, for practical purposes, an absence of a membrane. In contrast, the IR3535, DEET and Icaridin-based strands presented parameter  $\kappa_2 > 1$ , although most of them had values close to unity,

indicating that the strands had relatively thin membrane layers (see Table 4.8). In some cases,  $\kappa_3$  values are also listed in Table 4.8. This parameter ( $\kappa_3$ ) was estimated using a simpler expression (equation (2.35)) which provided adequate data fits. In the next section, the solid lines in curves of the repellents released from strands show the trend lines based on equation (2.32).

**Table 4.8:** Repellent content (wt-%), polymer strand diameters, release model parameters ( $\kappa_1$  and  $\kappa_2$ ), initial evaporation rate (dX/dt) and estimated membrane thicknesses ( $z_{\text{membrane}}$ ) of microporous EVA and LLDPE strands aged at 50 °C.

<b>Polymer strand</b>	<b>Repellent</b>	<b>Repellent content (wt-%)</b>	<b>Strand diameter (mm)</b>	$\kappa_1$	$\kappa_2$	<b>dX/dt (day<sup>-1</sup>)</b>	$z_{\text{membrane}}$ ( $\mu\text{m}$ )	<b>Sample Code</b>
LLDPE	DEET	20.2 ± 0.5	3.42 ± 0.16	0.00295	1.137	0.0215	17	BM302B
LLDPE	DEET	19.3 ± 0.6	4.39 ± 0.17	0.00206	1.308	0.00668	44	BM402
LLDPE	DEET	20.2 ± 0.5	4.61 ± 0.17	0.00185	1.049	0.0376	7	BM302A
LLDPE	DEET	29.3 ± 0.9	2.87 ± 0.15	0.00205	1.087	0.0235	19	BM303B
LLDPE	DEET	30.0 ± 0.8	4.08 ± 0.12	0.00394	2.317	0.00299	104	BM403
LLDPE	DEET	29.3 ± 0.9	4.66 ± 0.21	0.00146	1.079	0.0185	15	BM303A
LLDPE	Icaridin	19.7 ± 0.6	2.26 ± 0.05	0.00143	1.168	0.00850	26	BM300B
LLDPE	Icaridin	18.5 ± 0.8	2.89 ± 0.10	0.00157	1.112	0.0141	12	BM500
LLDPE	Icaridin	20.2 ± 0.5	3.84 ± 0.18	0.164	175.0	0.000944	139	BM400
LLDPE	Icaridin	19.7 ± 0.6	4.54 ± 0.23	0.000545	1.080	0.00680	16	BM300A
LLDPE	Icaridin	31.0 ± 0.6	2.15 ± 0.06	0.000657	1.129	0.00509	46	BM301B
LLDPE	Icaridin	29.5 ± 0.8	2.60 ± 0.09	0.00121	1.128	0.00949	20	BM501

LLDPE	Icaridin	29.0 ± 0.2	3.96 ± 0.17	0.269	397.5	0.000678	186	BM401
LLDPE	Icaridin	31.0 ± 0.6	4.63 ± 0.25	0.000351	1.055	0.00639	17	BM301A
LLDPE	DEET	27.7 ± 0.2	3.17 ± 0.41	0.00889	1.906	0.00981	41	BM103
LLDPE	Icaridin	27.4 ± 0.3	3.74 ± 0.31	0.305	337.9	0.000906	148	BM206
LLDPE	EA	26.6 ± 0.2	3.63 ± 0.73	0.0110	1.000	-	-	BM207
LLDPE	IR3535	25.5 ± 0.2	3.59 ± 0.39	0.847	494.9	0.00171	88	BM208
EVA	DEET	18.72 ± 0.47	3.42±0.20	0.00651	1.262	0.000934	4	AS402
EVA	DEET	29.03 ± 0.21	3.40±0.16	1.782	208.5	0.00844	8	AS403
EVA	Icaridin	19.55± 0.19	4.16±0.21	0.250	65.97	0.000564	47	AS503
EVA	Icaridin	30.11 ± 0.47	2.86±0.18	1.476	318.6	0.000784	26	AS504

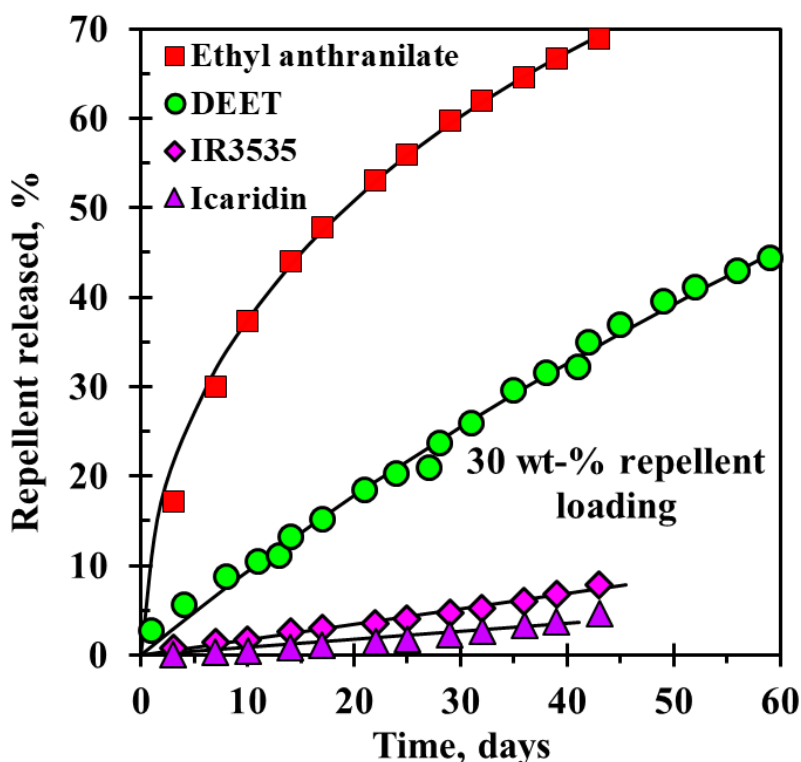
---

This section deals with the following parameters that affect the rate of repellent release from the polymer strands: (i) the nature and concentration of the repellent; (ii) the nature of the nanofiller; (iii) the diameter size of the polymer strand; (iv) the temperature, and (v) the nature of the polymer. The repellent release curves obtained for the various polymer strands are shown and discussed below. It should be mentioned that the extrusion process that was used did not allow control over the thickness of the membrane skin that covered the strands. It is suspected that the rheology of the melt and the shear experienced by the polymer when passing through the shaping die were the most important factors that affected this thickness. In turn, these factors depended on the temperature profile that was used, the flow rate and the nature of the components, as well as the composition. These factors are believed to be highly nonlinearly related. It was not possible, in the present study, to disentangle these intricate connections between the factors. Therefore, the comments and results presented below are, with respect to their validity, limited to the samples that were actually extruded with the characteristics listed in Table 4.8.

#### **4.4.6 Factors affecting the release behaviour**

Figure 4.28 shows the release curves of DEET, Icaridin, IR3535 and ethyl anthranilate based LLDPE strands aged at 50 °C in a convention oven. Both strands contained 5 wt.% clay. Ethyl anthranilate was released fastest from the strands. The ethyl anthranilate-based strand was practically exhausted within the first 40 days of exposure; other repellents were released at an almost constant rate over a longer time. There are two reasons that explain the higher release rate: (i) the ethyl anthranilate release was not limited by the presence of a membrane (see Table 4.8), this means that the difference of membrane thickness covering strands containing repellents explains this reason. And (ii) ethyl anthranilate had a much higher vapour pressure compared to

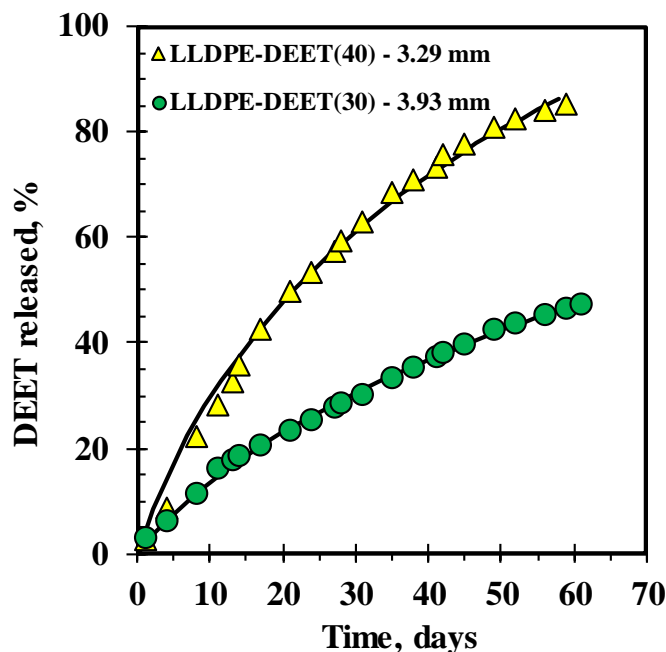
neat DEET, IR3535 and Icaridin. This justified the choice of DEET and Icaridin-based strands for repellence testing against mosquitoes. Additional results on release rate and modelling of IR3535-based LLDPE strands are listed in Appendix XII.



**Figure 4.28:** Release of 30 wt.% DEET (BM103), 30 wt.% Icaridin (BM206), 30 wt.% IR3535 (BM208) and 30 wt.% ethyl anthranilate (BM207) from strands. The LLDPE-based strands initially contained 5 wt.% Dellite 43B organoclay.

Figure 4.29 shows the measured DEET release curves for samples aged in a convection oven at 50 °C. The LLDPE strands contained two different concentrations of DEET (30 wt.% and 40 wt.%) and both strands contained 5 wt.% fumed silica. The repellent depletion happened fastest for the strand with the higher DEET loading. 55.0 g of DEET was originally used in the strands with higher DEET loading, but about 41.1 g was released. In the case of lower DEET loading, 44.8 g

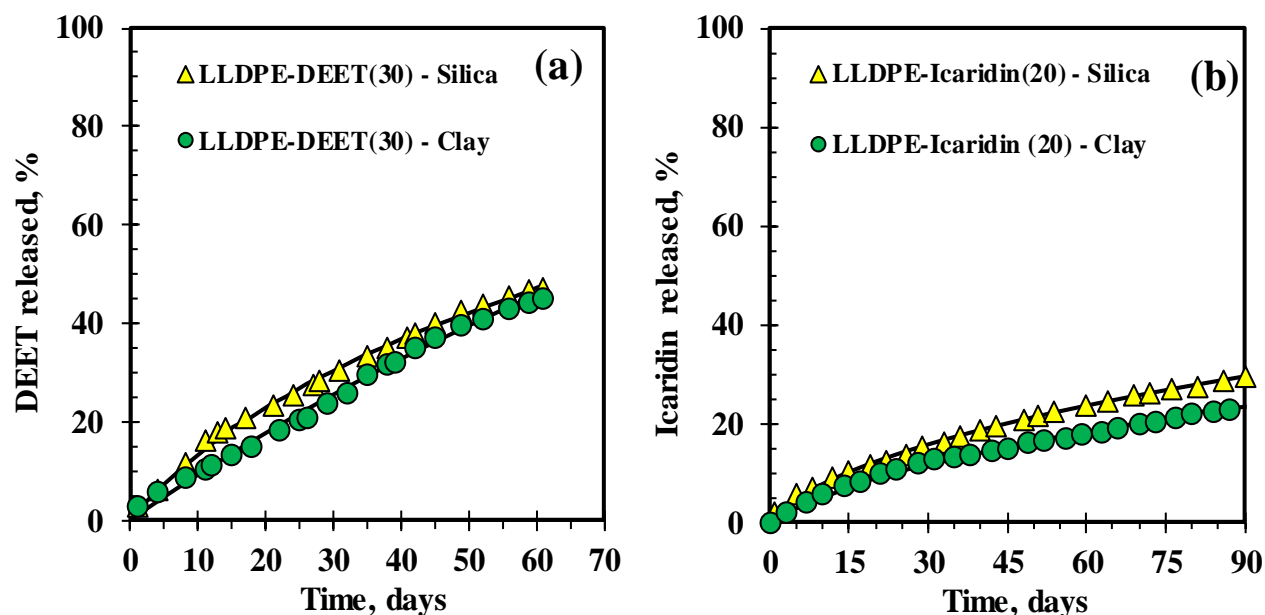
was originally used in strands, but only 23.1 g of repellent was released. This difference in behaviour can be attributed to differences in (i) the membrane thicknesses (see Table 4.8); and (ii) the diameters of the strands (see Figure 4.29).



**Figure 4.29:** Effect of concentration of the DEET on release from the LLDPE strands. The amount of repellent initially incorporated into the LLDPE strands was: ( $\Delta$ ) 40wt.% DEET (BM101) and ( $\bullet$ ) 30wt.% DEET (BM102). Both strands contained 5 wt.% fumed silica.

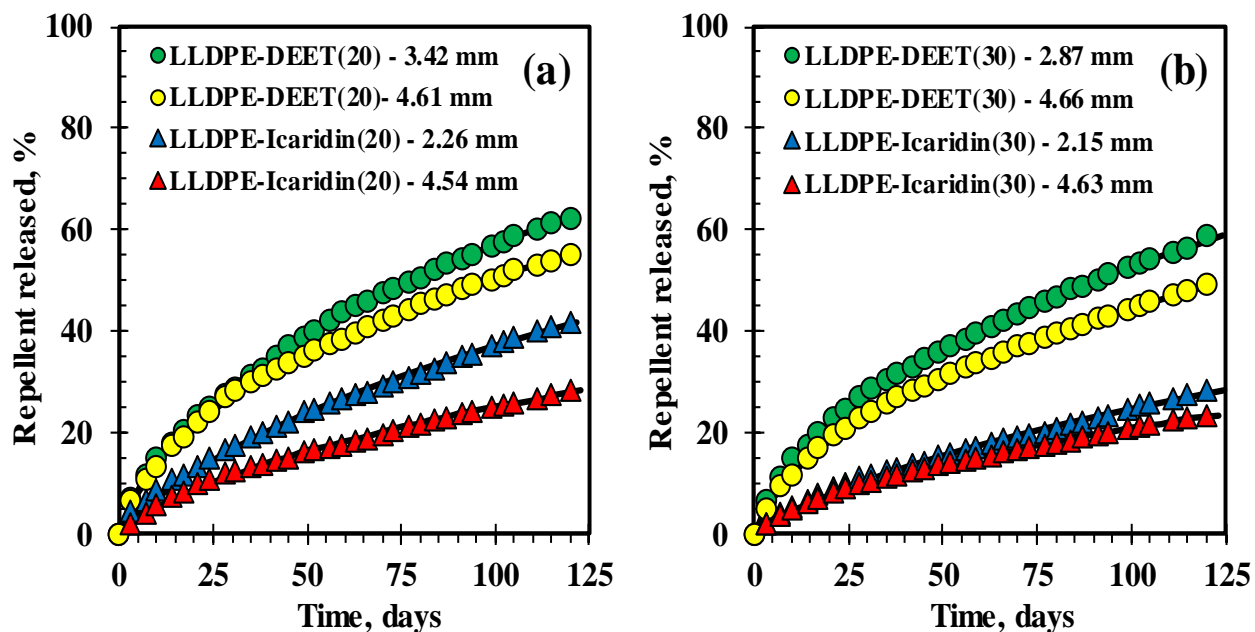
Figure 4.30 shows the effect of nanofiller (silica or Dellite 43B organoclay) on the repellent release from LLDPE strands aged in a convection oven set at a temperature of 50 °C. The release of the repellents was slightly lower for strands containing the clay. The differences in the membrane thickness of the strands may explain this behaviour. The repellent-based strands containing the fumed silica featured thinner membrane thicknesses (see Table 4.8).





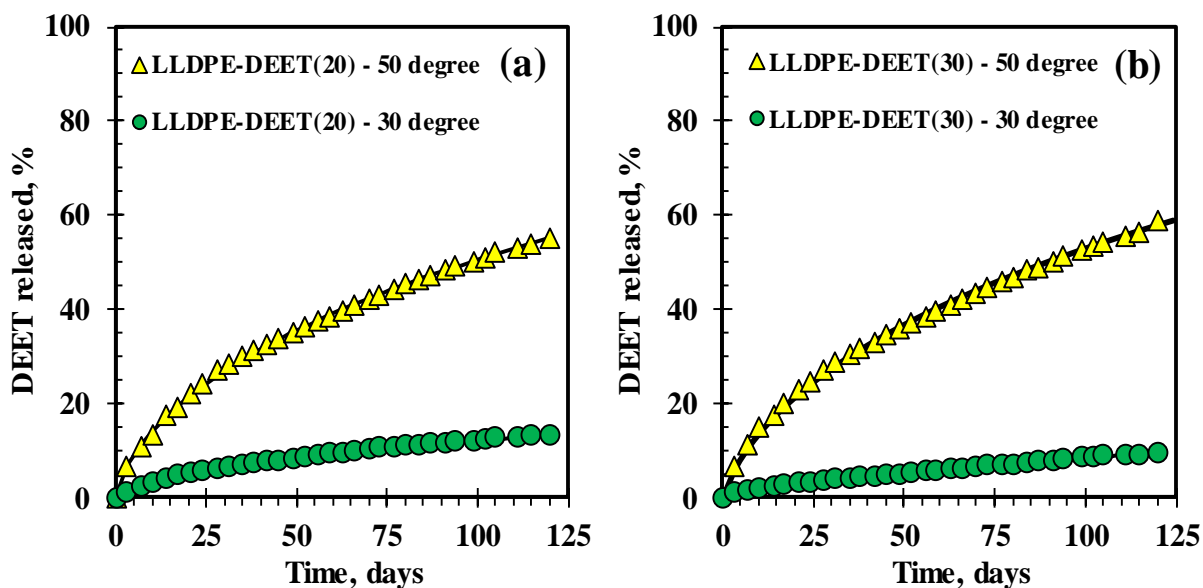
**Figure 4.30:** Effect of nanofiller on repellent release from LLDPE strands. (a) The LLDPE strands initially containing: ( $\blacktriangle$ ) 30 wt.% DEET and 5 wt.% fumed silica (BM102); and ( $\bullet$ ) 30 wt.% DEET and 5 wt.% Dellite 43B clay (BM103); (b) The LLDPE strands initially containing: ( $\blacktriangle$ ) 20 wt.% Icaridin and 5 wt.% fumed silica (BM504) and ( $\bullet$ ) 20 wt.% Icaridin and 5 wt.% Dellite 43B clay (BM300A).

Figure 4.31 shows the effect of the diameter of the strands on the release of Icaridin and DEET aged in a convection oven at a temperature of 50 °C. Strands of different diameter sizes were studied for each repellent-LLDPE composition. The release of DEET and Icaridin occurred fastest for LLDPE strands with a small diameter in contrast to the theoretical expectations. However, the differences in release rate were likely caused by differences in other geometric parameters than those of the strand diameter, e.g. the thickness of the membrane covering or the structure of the internal porous regions (see Table 4.8). This behaviour was observed in all repellent-strand compositions.



**Figure 4.31:** Effect of diameter sizes of LLDPE-strands on release of the repellent. (a) (●) 20 wt.% DEET (BM302B) - diameter size ( $3.42 \pm 0.16$  mm); (●) 20 wt.% DEET (BM302A) - diameter size ( $4.61 \pm 0.17$  mm); (▲) 20 wt.% Icaridin (BM300B) - diameter size ( $2.26 \pm 0.05$  mm); and (▲) 20 wt.% Icaridin (BM300A) - diameter size ( $4.54 \pm 0.23$  mm). (b) (●) 30 wt.% DEET (BM303B) - diameter size ( $2.87 \pm 0.15$  mm); (●) 30 wt.% DEET (BM303A) - diameter size ( $4.66 \pm 0.21$  mm); (▲) 30 wt.% Icaridin (BM301B) - diameter size ( $2.15 \pm 0.06$  mm); and (▲) 30 wt.% Icaridin (BM301A) - diameter size ( $4.63 \pm 0.25$  mm). All strands contained 5 wt.% Dellite 43B clay.

Figure 4.32 and Figure 4.33 show the effect of temperature on the release of repellent from LLDPE strands aged in a convection oven at a temperature of 30 °C and 50 °C. As expected, the repellents were released at a faster rate at the higher temperature. The LLDPE repellent-based strands contained 5 wt.% Dellite 43B clay.



**Figure 4.32:** Effect of temperature on release of DEET-containing LLDPE strands. (a) LLDPE initially containing ( $\blacktriangle$ ) 20 wt.% DEET aged at 50 °C and ( $\bullet$ ) 20 wt.% DEET aged at 30 °C; (b) LLDPE initially containing ( $\blacktriangle$ ) 30 wt.% DEET aged at 50 °C and ( $\bullet$ ) 30 wt.% DEET aged at 30 °C.

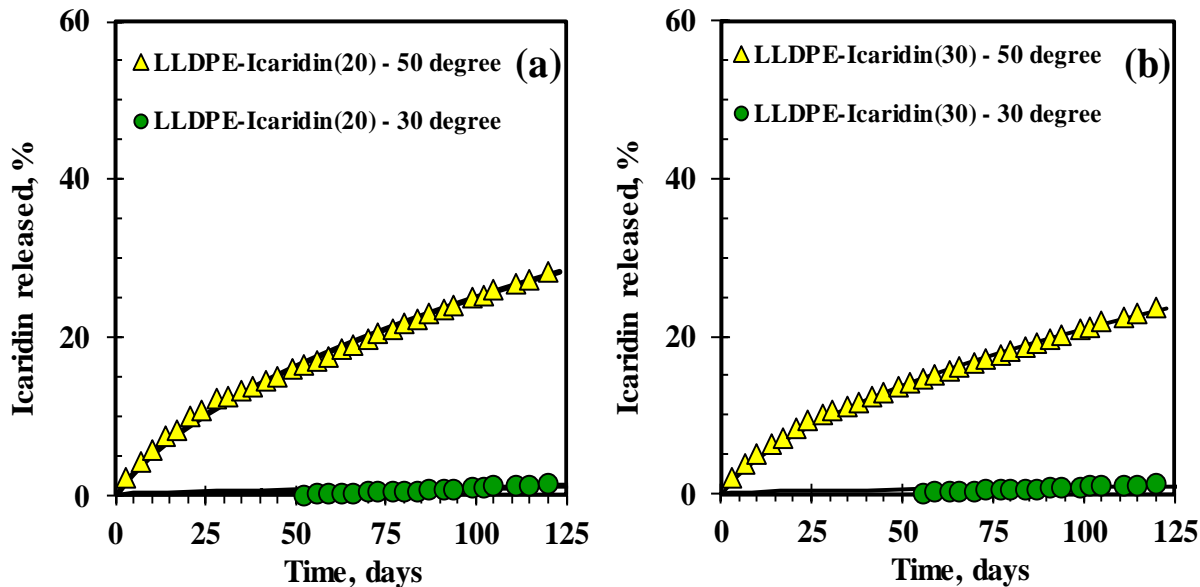


**Figure 4.33:** Effect of temperature on release of Icaridin-based LLDPE strands. (a) LLDPE initially containing ( $\blacktriangle$ ) 20 wt.% Icaridin aged at 50 °C and ( $\bullet$ ) 20 wt.% Icaridin aged at 30 °C; (b) LLDPE initially containing ( $\blacktriangle$ ) 30 wt.% Icaridin aged at 50 °C and ( $\bullet$ ) 30 wt.% Icaridin aged at 30 °C.

Figure 4.34 shows repellent release curves for LLDPE and EVA strands aged in the convection ovens set at a temperature of 50 °C. Figure 4.34 (a) reveals that the release of DEET at similar concentrations occurred faster from EVA strands compared to LLDPE strands. This is in accordance with the much thinner membrane thicknesses estimated for the EVA strands that are reported in Table 4.8. The situation is more complicated for the Icaridin-containing strands. In this case, the fraction repellent release occurred fastest and slowest for the LLDPE strands containing 20 wt.% and 30 wt.% Icaridin respectively. This can be attributed to a complex interplay of the effects of the differences in the strand diameters and membrane thicknesses of the EVA and LLDPE strands containing different loading levels of Icaridin. Besides the difference in the results, the repellents were released at a constant rate for the extended period that was investigated.

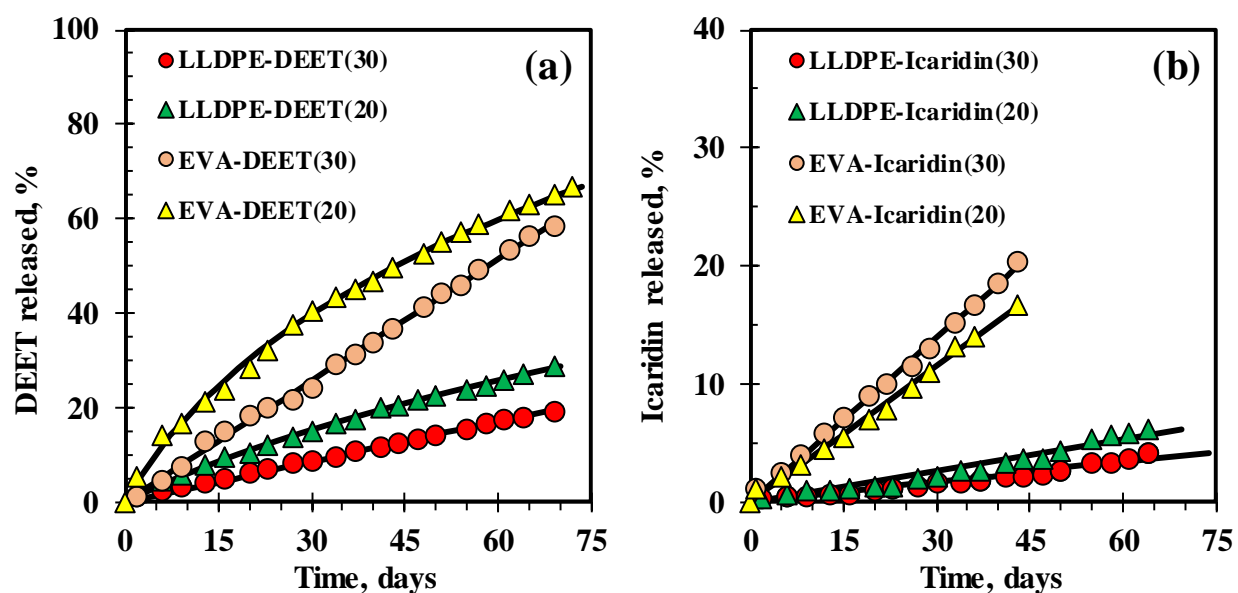


**Figure 4.34:** Repellent release curves during oven ageing at 50 °C. The LLDPE- and EVA-based strands contained 5 wt.% Dellite 43B clay and either DEET or Icaridin as a repellent. (a) 30 wt.% DEET (BM403), 20 wt.% DEET (BM402), 30 wt.% DEET (AS403), 20 wt.% DEET (AS402). (b) 30 wt.% Icaridin (BM401), 20 wt.% Icaridin (BM400), 30 wt.% Icaridin (AS504) and 20 wt.% 30 wt.% Icaridin (AS503)-based strands.

#### 4.5 Repellence testing

The initial foot-in-cage experiments compared untreated feet with feet covered with neat EVA or LLDPE polymer strands. It was observed that the mosquitoes preferred probing the foot covered by repellent-free strands rather than the fully exposed foot. The degree of protection, averaged over both the neat LLDPE and EVA strands, was estimated at  $-19 \pm 8\%$ . This means that the mosquitoes preferred the foot covered by neat, repellent-free strands over the bare foot. The reasons for this behaviour are not currently understood. It is known that acetic acid can act as a mosquito attractant (Allan et al., 2006) and that it is released in small quantities when EVA is processed at high temperatures, e.g. in the extrusion of the strands. This could explain the effect observed for the EVA strands. However, processing LLDPE does not release acetic acid and the reason for the observed attraction therefore remains a mystery. However, the observation that the neat strands acted as attractants informed the decision to conduct all the foot-in-cage tests comparing a covered foot to a bare foot rather than a foot covered by an inert strand.

Table 4.9 gives the results of the foot-in-cage tests. A statistical analysis of the results is presented in the supplementary material (see Appendix XVI). First a parametric analysis of variance (ANOVA) was performed in order to detect significant factors that might have an influence on the protection measurements obtained for the repellents. Following this, a non-parametric ANOVA was performed using the Kruskal-Wallis test, which makes no assumptions of the underlying data structure. In all these tests, the null hypothesis was that no effects were observed. The important conclusions of the statistical analysis were that, at the 95% level of confidence, neither polymer, repellent type, repellent loading level, test person, treated foot, nor ageing time had a significant effect on the level of protection provided. Although no significant effects could be detected

between the different treatments, they all differed significantly from the effects of untreated feet, which indicated that being treated differed significantly from not being treated, i.e. there were significantly fewer mosquito probings. The implication is that all the strands provided a similar level of protection against mosquito bites for up to 12 weeks. The observation that oven ageing time did not have a statistically significant effect on the degree of protection was expected, since the measured mass loss rate of the strands was approximately constant over time. This implies that all the repellence tests conducted over the full oven ageing time for a given strand represent repeat measurements of the protection performance. Figure 4.35 shows the results of the foot-in-cage repellent tests of the LLDPE-based strands, all of which contained 5 wt.% Dellite 43B clay. The results presented in Figure 4.33 suggest that the best repellence performance was obtained with the LLDPE strands which initially contained 30 wt.% Icaridin.

**Table 4.9:** Results of foot-in-cage mosquito repellent tests

Polymer	Repellent	Level	Ageing	Test	Foot	1st bite	Number of bites on foot		Protection
							Untreated	Treated	
		wt. %	weeks	person	(L/R)	s	#	#	%
LLDPE	DEET	20	1	X	R	10	49	6	78
LLDPE	DEET	20	3	Z	L	23	39	4	81
LLDPE	DEET	20	5	Z	L	48	16	0	100
LLDPE	DEET	20	7	Z	R	103	20	6	54
LLDPE	DEET	20	9	Y	R	30	11	0	100
LLDPE	DEET	20	11	Y	L	54	26	6	63
LLDPE	DEET	30	1	Z	R	20	26	8	53
LLDPE	DEET	30	3	Z	R	21	98	12	78
LLDPE	DEET	30	5	X	R	62	7	0	100
LLDPE	DEET	30	7	X	R	79	40	1	95
LLDPE	DEET	30	9	Y	R	27	7	2	56

---

LLDPE	DEET	30	11	X	L	26	47	4	84
LLDPE	Icaridin	20	1	Z	L	13	47	1	96
LLDPE	Icaridin	20	3	X	R	10	24	3	78
LLDPE	Icaridin	20	5	X	L	51	45	0	100
LLDPE	Icaridin	20	7	Z	R	35	18	1	89
LLDPE	Icaridin	20	9	X	R	27	27	6	64
LLDPE	Icaridin	20	11	X	L	43	41	15	46
LLDPE	Icaridin	30	1	X	L	105	18	1	89
LLDPE	Icaridin	30	3	X	L	15	62	0	100
LLDPE	Icaridin	30	5	Z	L	29	24	0	100
LLDPE	Icaridin	30	7	Z	L	57	20	0	100
LLDPE	Icaridin	30	9	X	L	24	7	0	100
LLDPE	Icaridin	30	11	Y	L	54	48	1	96
EVA	DEET	20	2	Z	R	45	36	0	100
EVA	DEET	20	4	X	R	50	33	0	100

---



---

EVA	DEET	20	6	X	L	32	11	0	100
EVA	DEET	20	8	Z	L	115	65	13	67
EVA	DEET	20	10	X	L	57	28	8	56
EVA	DEET	20	12	X	R	21	29	2	87
EVA	DEET	30	2	X	L	25	21	0	100
EVA	DEET	30	4	Z	R	36	17	0	100
EVA	DEET	30	6	Z	L	25	11	1	83
EVA	DEET	30	8	X	R	90	20	1	90
EVA	DEET	30	10	Y	L	75	43	16	46
EVA	DEET	30	12	Y	R	13	55	8	75
EVA	Icaridin	20	2	Z	L	20	22	0	100
EVA	Icaridin	20	4	Z	L	115	7	1	75
EVA	Icaridin	20	6	Z	R	34	78	4	90
EVA	Icaridin	20	8	Z	L	28	24	0	100
EVA	Icaridin	20	10	Y	R	29	13	0	100

---

EVA	Icaridin	20	12	Y	L	6	62	6	82
EVA	Icaridin	30	2	X	L	40	23	0	100
EVA	Icaridin	30	4	X	L	170	7	0	100
EVA	Icaridin	30	6	X	R	40	57	3	90
EVA	Icaridin	30	8	X	R	51	50	0	100
EVA	Icaridin	30	10	X	R	-	24	5	66
EVA	Icaridin	30	12	X	L	6	71	12	71

#### 4.5.1 Statistical analysis

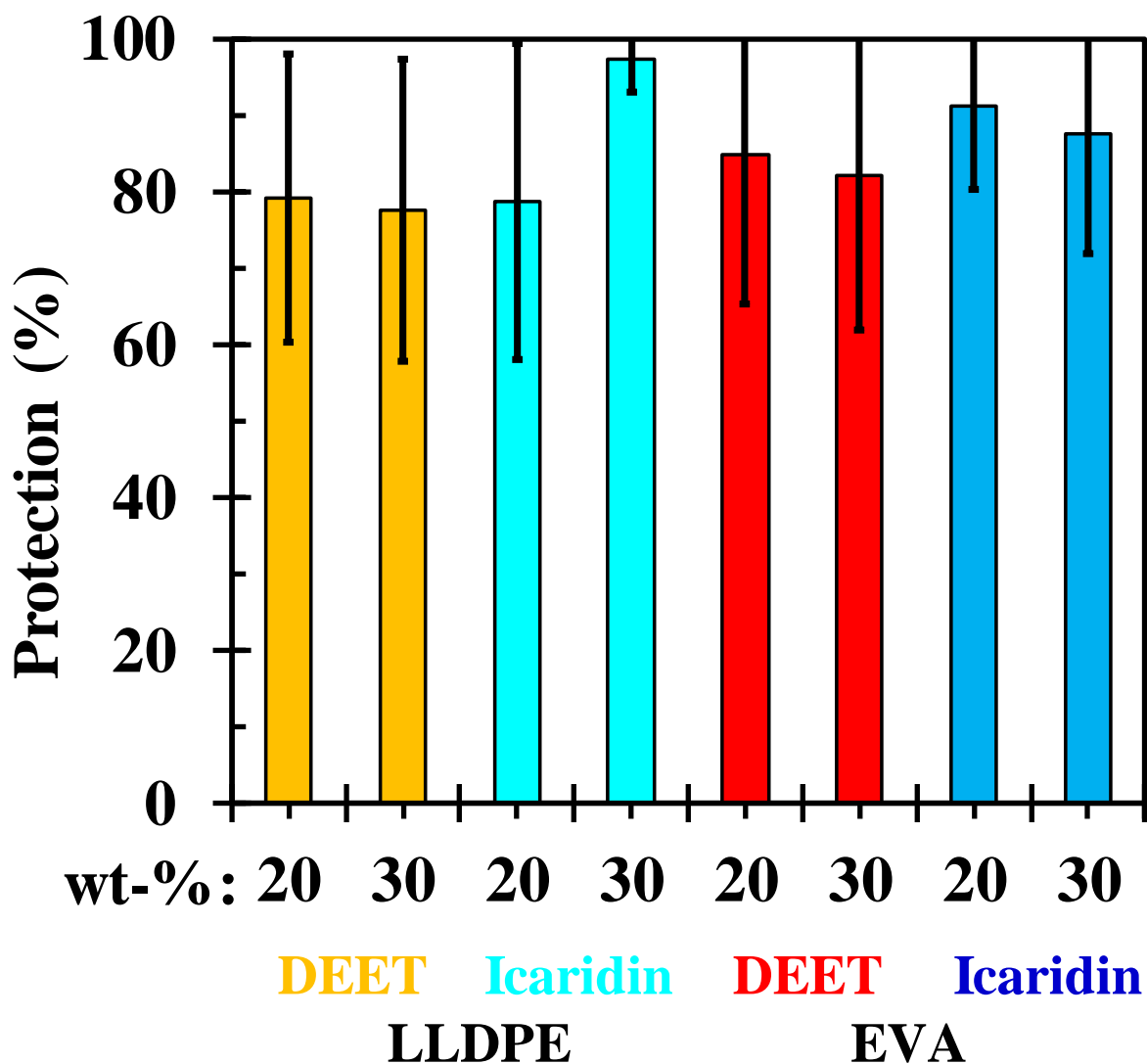


**Figure 4.35:** Bar plot of results of foot-in-cage repellent tests for polymer strands containing either DEET or Icaridin as repellents. All the compositions utilized Dellite 43B clay as the thickening agent. The repellents-based polymer strands used are: 30 wt.% DEET (BM403), 20 wt.% DEET (BM402), 30 wt.% DEET (AS403), 20 wt.% DEET (AS402), 30 wt.% Icaridin (BM401), 20 wt.% Icaridin (BM400), 30 wt.% Icaridin (AS504) and 20 wt.% 30 wt.% Icaridin (AS503)-based strands. The strands were aged at 50 °C in a convection oven and the bioassay tests were done every two weeks for up to 12 weeks.

## CHAPTER 5

### CONCLUSIONS AND RECOMENDATIONS

This study explored the possibility of making long-lasting insect repellent strands for outdoor protection against mosquito bites. The strands were produced by an extrusion-compounding process in which a homogeneous polymer melt, containing large amounts of a dissolved repellent, was rapidly quenched in an ice-water bath. Before compounding, it was ascertained that not only were the repellents sufficiently stable to withstand exposure to the high polymer processing temperatures of 180 °C used, but also that they would survive long-term exposure to the atmosphere in the intended application of anklet or bracelet. This was confirmed by recording FTIR spectra of the repellents after exposure to (a) a temperature of 200 °C in a convection oven for 30 minutes; and (b) after storage in open containers for four months at 50 °C in a convection oven. The repellents investigated were able to withstand typical polymer processing temperatures for short periods of time. The fact that they also stayed essentially intact for several months at 50 °C suggests that they may retain repellent activity for comparable lengths of time. In general, this study proved that all the repellents considered were sufficiently thermally stable for polymer processing and end-use application.

Next, the compatibility of the polymers and repellents was established. The LLDPE and EVA were exposed to the repellents at 50 °C in a convection oven. The LLDPE swelled significantly less than the EVA. The latter absorbed as much as when 5.5 wt.% was exposed to the repellent DEET. As expected, the latter polymer also shrunk more when the absorbed repellent was lost, i.e. it had a poorer dimensional stability.

The permeability of neat and nanocomposite films made from LLDPE and EVA to the repellents was also determined. Compared to the LLDPE films, the EVA-based films had a significantly lower permeability to the repellents, i.e. DEET, Icaridin, IR3535 and ethyl anthranilate.

To be effective, a repellent must be present near the skin of the body part to be protected. This means that the repellent is continuously lost to the atmosphere. Hence it must be continuously replenished, and large amounts are required for long-term protection. The latter requirements were achieved via the high-porosity microstructure of the extruded strands, which allowed significant amounts of the repellents to be trapped. Microporous polyolefin strands, containing significant quantities of mosquito repellent (20, 30, 40 and 50 wt.%) were successfully prepared via the TIPS method. Scanning electron microscopy confirmed an open-cell inner structure of the polymer strands. The type and concentration of repellent, and the nature of the nanofiller (fumed silica or clay), affected the scaffold morphology of the strands. SEM also revealed that, in most cases, the extrusion process also yielded a thin, integral skin-like membrane that covered the extruded strands.

The repellent contents, measured by either solvent extraction or thermogravimetric analysis, were in close agreement with the amount of repellent initially loaded during the compounding process. This means that very little repellent was lost during processing.

The volatilization of the repellents was studied in neat form and also from the extruded strands. For the former, the evaporation rate into air was determined by thermogravimetric analysis (TGA) and with open Payne cups. DEET, IR3535 and Icaridin were found to have the lowest volatility. These experiments also yielded estimates of the air permeability of the repellents. This parameter

is equivalent to the product of the diffusion coefficient and the vapour pressure. The experimental values were compared to the values predicted from calculation based on independent predictions of vapour pressure (using the Myrdal and Yalkowsky equation) and the diffusion coefficient (using the Wilke-Lee equation). The experimental data were only in approximate agreement with the prediction.

The time-dependent volatilization of the repellents from the extruded strands aged at 50 °C in a convection oven was tracked gravimetrically for up to six months. In some cases, and after six months of ageing, more than 50% of the repellent was still present and trapped inside the strands. This is attributed to a thick membrane-like skin that covered the strand and controls the release of the repellent at a low effective rate. This concept was lent support by a simple mathematical model that was developed for fitting data describing the repellent release over time.

Two different repellents (DEET and Icaridin) were incorporated into either the EVA or the LLDPE at two different loading levels (20 and 30 wt.%). These samples were used for repellence testing against *Anopheles arabiensis* mosquitoes. The polymer strands that contained up to 30 wt.% of either DEET or Icaridin provided effective protection against mosquito bites up to 12 weeks of ageing in a convection oven set at a temperature of 50 °C.

The results of this study suggested the possibility of developing long-life mosquito repellent anklets/footlets/bracelets that can be implemented in malaria-endemic regions outdoors. As recommendation, more work will be required to understand the formation and thickness control of the membrane-like skin found on the surface of the extruded strands. It is possible that the trapping of the repellents inside the microporous structures of the strands also reduces direct skin contact.

However, additional experimental exploration will be required to confirm this potential advantage. Clearly, it should be possible to produce strands that will last longer than several months in oven ageing tests at 50 °C and still show repellence. However, when actually worn by an active person, the bracelets will be subjected to both flexing and chafing. The effect of this on performance is unknown but it is likely that it will reduce the effective life. Nevertheless, the results do show that it may be worthwhile to consider development of actual bracelet products based on the microporous strand concept.

Additionally, the study therefore emphasizes the physical and chemical elements and basic entomological impact. Although, more extensive and rigorous entomological and epidemiological testing will be required on products that are more refined before they could become commercially acceptable.

## REFERENCES

- ABDALLA, H., WILDING, C.S., NARDINI, L., PIGNATELLI, P., KOEKEMOER, L.L., RANSON, H. & COETZEE, M., 2014. Insecticide resistance in *Anopheles arabiensis* in Sudan: temporal trends and underlying mechanisms. *Parasites & vectors*, 7(1), 213.
- ADELNIA, H., BIDSORKHI, H. C., ISMAIL, A. & MATSUURA, T. 2015. Gas permeability and permselectivity properties of ethylene vinyl acetate/sepiolite mixed matrix membranes. *Separation and Purification Technology*, 146, 351-357.
- AFIFY, A., HORLACHER, B., ROLLER, J. & GALIZIA, C.G. 2014. Different repellents for *Aedes aegypti* against blood-feeding and oviposition. *PLoS One*, 9(7), e103765.
- ALOU, L.P.A., KOFFI, A.A., ADJA, M.A., ASSI, S.B., KOUASSI, P.K. & N'GUESSAN, R., 2012. Status of pyrethroid resistance in *Anopheles gambiae* ss M form prior to the scaling up of Long Lasting Insecticidal Nets (LLINs) in Adzope, Eastern Cote d'Ivoire. *Parasites & vectors*, 5(1), 289.
- AKELAH, A. 1996. Novel utilizations of conventional agrochemicals by controlled release formulations. *Materials Science and Engineering: C*, 4, 83-98.
- AKHTAR, M. U. 2015. *Towards controlled release of a natural mosquito repellent from polymer matrices*. University of Pretoria.
- AKHTAR, M. U. & FOCKE, W. W. 2015. Trapping citronellal in a microporous polyethylene matrix. *Thermochimica Acta*, 613, 61-65.
- ALLAN, S., BERNIER, U. R. & KLINE, D. 2006. Attraction of mosquitoes to volatiles associated with blood. *Journal of Vector Ecology*, 31, 71-78.



- ALPERN, J. D., DUNLOP, S. J., DOLAN, B. J., STAUFFER, W. M. & BOULWARE, D. R. 2016. Personal protection measures against mosquitoes, ticks, and other arthropods. *Medical Clinics*, 100, 303-316.
- AMBROSE, D. & GHIASSEE, N. 1987. Vapour pressures and critical temperatures and critical pressures of some alkanolic acids: C1 to C10. *The Journal of Chemical Thermodynamics*, 19, 505-519.
- AMER, A. & MEHLHORN, H. 2006. Repellency effect of forty-one essential oils against *Aedes*, *Anopheles*, and *Culex* mosquitoes. *Parasitology research*, 99, 478.
- API, A., BELSITO, D., BHATIA, S., BRUZE, M., CALOW, P., DAGLI, M., DEKANT, W., FRYER, A., KROMIDAS, L. & LA CAVA, S. 2015. RIFM fragrance ingredient safety assessment, ethyl anthranilate, CAS registry number 87-25-2. *Food and Chemical Toxicology*, 82, S97-S104.
- ARANCIBIA, M.Y., LÓPEZ-CABALLERO, M.E., GÓMEZ-GUILLÉN, M.C. & MONTERO, P. 2014. Release of volatile compounds and biodegradability of active soy protein lignin blend films with added citronella essential oil. *Food Control*, 44, 7-15.
- AUYSAWASDI, N., CHUNTRANULUCK, S., PHASOMKUSOLSIL, S. & KEERATINIJAKAL, V. 2016. Improving the effectiveness of three essential oils against *Aedes aegypti* (Linn.) and *Anopheles dirus* (Peyton and Harrison). *Parasitology research*, 115, 99-106.
- BACCANARI, D. P., NOVINSKI, J. A., PAN, Y.-C., YEVITZ, M. M. & SWAIN, H. A. 1968. Heats of sublimation and vaporization at 25° of long-chain fatty acids and methyl esters. *Transactions of the Faraday Society*, 64, 1201-1205.

- BARASA, S. S., NDIEGE, I. O., LWANDE, W. & HASSANALI, A. 2002. Repellent activities of stereoisomers of p-menthane-3, 8-diols against *Anopheles gambiae* (Diptera: Culicidae). *Journal of Medical Entomology*, 39, 736-741.
- BARDAJÍ, A., SIGAUQUE, B., SANZ, S., MAIXENCHS, M., ORDI, J., APONTE, J. J., MABUNDA, S., ALONSO, P. L. & MENÉNDEZ, C. 2011. Impact of malaria at the end of pregnancy on infant mortality and morbidity. *Journal of Infectious Diseases*, 203, 691-699.
- BARNARD, D. & WHO, 2000. Global collaboration for development of pesticides for public health: repellents and toxicants for personal protection: position paper (No. WHO/CDS/WHOPES/GCDPP/2000.5). Geneva: World Health Organization.
- BARNARD, D. R. & XUE, R.-D. 2004a. Laboratory evaluation of mosquito repellents against *Aedes albopictus*, *Culex nigripalpus*, and *Ochlerotatus triseriatus* (Diptera: Culicidae). *Journal of medical entomology*, 41, 726-730.
- BARNARD, D.R., 2005. Biological assay methods for mosquito repellents. *Journal of the American Mosquito Control Association*, 21, 12-17.
- BARNETT, E. D. 2007. Yellow fever: epidemiology and prevention. *Clinical Infectious Diseases*, 44, 850-856.
- BENELLI, G. & MEHLHORN, H. 2016. Declining malaria, rising of dengue and Zika virus: insights for mosquito vector control. *Parasitology research*, 115, 1747-1754.
- BEVERLEY, K., CLINT, J. & FLETCHER, P. I. 1999. Evaporation rates of pure liquids measured using a gravimetric technique. *Physical Chemistry Chemical Physics*, 1, 149-153.
- BHARADWAJ, R. K. 2001. Modeling the barrier properties of polymer-layered silicate nanocomposites. *Macromolecules*, 34, 9189-9192.

- BHATTARAI, A., ALI, A. S., KACHUR, S. P., MÅRTENSSON, A., ABBAS, A. K., KHATIB, R., AL-MAFAZY, A.-W., RAMSAN, M., ROTLLANT, G. & GERSTENMAIER, J. F. 2007. Impact of artemisinin-based combination therapy and insecticide-treated nets on malaria burden in Zanzibar. *PLoS Medicine*, 4, e309.
- BISSINGER, B. W. & ROE, R. M. 2010. Tick repellents: past, present, and future. *Pesticide Biochemistry and Physiology*, 96, 63-79.
- BOUZOUITA, A., NOTTA-CUVIER, D., RAQUEZ, J.-M., LAURO, F. & DUBOIS, P. 2017. Poly (lactic acid)-based materials for automotive applications. *Industrial Applications of Poly (lactic acid)*, 177-219.
- BRAACK, L., HUNT, R., KOEKEMOER, L. L., GERICKE, A., MUNHENGA, G., HADDOW, A. D., BECKER, P., OKIA, M., KIMERA, I. & COETZEE, M. 2015. Biting behaviour of African malaria vectors: 1. where do the main vector species bite on the human body? *Parasites & Vectors*, 8, 76.
- BRADE, W. R. & DAVIS, T. D. 1983. Evaporative release of repellent chemicals from porous polymers. *Journal of Cellular Plastics*, 19, 309-311.
- BROWN, M. & HEBERT, A. A. 1997. Insect repellents: an overview. *Journal of the American Academy of Dermatology*, 36, 243-249.
- BURGHARDT, W. R. 1989. Phase diagrams for binary polymer systems exhibiting both crystallization and limited liquid-liquid miscibility. *Macromolecules*, 22, 2482-2486.
- CARROLL, S. P. 2008. Prolonged efficacy of IR3535 repellents against mosquitoes and blacklegged ticks in North America. *Journal of Medical Entomology*, 45, 706-714.
- CARROLL, S. P. & LOYE, J. 2006. PMD, a registered botanical mosquito repellent with deet-like efficacy. *Journal of the American Mosquito Control Association*, 22, 507-514.

- CASTRO, A. J. 1981. Methods for making microporous products. Google Patents.
- CAUCHEMEZ, S., BESNARD, M., BOMPARD, P., DUB, T., GUILLEMETTE-ARTUR, P., EYROLLE-GUIGNOT, D., SALJE, H., VAN KERKHOVE, M. D., ABADIE, V. & GAREL, C. 2016. Association between Zika virus and microcephaly in French Polynesia, 2013–15: a retrospective study. *The Lancet*, 387, 2125-2132.
- CÉSPEDES, F. F., SÁNCHEZ, M. V., GARCÍA, S. P. & PÉREZ, M. F. 2007. Modifying sorbents in controlled release formulations to prevent herbicides pollution. *Chemosphere*, 69, 785-794.
- CHA, B., CHAR, K., KIM, J.-J., KIM, S. & KIM, C. 1995. The effects of diluent molecular weight on the structure of thermally-induced phase separation membrane. *Journal of Membrane Science*, 108, 219-229.
- CHARARA, Z., WILLIAMS, J., SCHMIDT, R. & MARSHALL, M. 1992. Orange flavor absorption into various polymeric packaging materials. *Journal of Food Science*, 57, 963-968.
- CHARLET, G. & DELMAS, G. 1981. Thermodynamic properties of polyolefin solutions at high temperature: 1. Lower critical solubility temperatures of polyethylene, polypropylene and ethylene-propylene copolymers in hydrocarbon solvents. *Polymer*, 22, 1181-1189.
- CHATTOPADHYAY, P., DHIMAN, S., BORAH, S., RABHA, B., CHAURASIA, A. K. & VEER, V. 2015. Essential oil based polymeric patch development and evaluating its repellent activity against mosquitoes. *Acta tropica*, 147, 45-53.
- CHEN, L. G. & SHANKS, R. 2007. Thermoplastic polymer-dispersed liquid crystals prepared from solvent-induced phase separation with predictions using solubility parameters. *Liquid Crystals*, 34, 1349-1356.

- CHOUDALAKIS, G. & GOTSIS, A. 2009. Permeability of polymer/clay nanocomposites: a review. *European Polymer Journal*, 45, 967-984.
- CHRISOPOULOU, K. & ANASTASIADIS, S. 2011. Polyolefin/layered silicate nanocomposites with functional compatibilizers. *European Polymer Journal*, 47, 600-613.
- CHRISOPOULOU, K. & ANASTASIADIS, S. H. 2010. Polyolefin nanocomposites with functional compatibilizers. *Advances in Polyolefin Nanocomposites*, 365.
- CORCIONE, C. E., PRINARI, P., CANNOLETTA, D., MENSITIERI, G. & MAFFEZZOLI, A. 2008. Synthesis and characterization of clay-nanocomposite solvent-based polyurethane adhesives. *International Journal of Adhesion and Adhesives*, 28, 91-100.
- CUI, Y., KUMAR, S., KONA, B. R. & VAN HOUCKE, D. 2015. Gas barrier properties of polymer/clay nanocomposites. *Rsc Advances*, 5, 63669-63690.
- DA SILVA PORTELA, A., DAS GRACAS ALMEIDA, M., GOMES, A. P. B., CORREIA, L. P., DA SILVA, P. C. D., NETO, A. N. M., DE MEDEIROS, A. C. D. & SIMÕES, M. O. S. 2012. Vapor pressure curve determination of  $\alpha$ -lipoic acid raw material and capsules by dynamic thermogravimetric method. *Thermochimica Acta*, 544, 95-98.
- DAUBERT, T. E. 1989. Physical and thermodynamic properties of pure chemicals: data compilation. *Design Institute for Physacal Property Data (DIPPR)*.
- DE OLIVEIRA, C. E. L. & CREMASCO, M. A. 2014. Determination of the vapor pressure of *Lippia gracilis* Schum essential oil by thermogravimetric analysis. *Thermochimica Acta*, 577, 1-4.
- DEBBOUN, M., STRICKMAN, D., SOLBERG, V. B., WILKERSON, R. C., MCPHERSON, K. R., GOLEND, C., KEEP, L., WIRTZ, R. A., BURGE, R. & KLEIN, T. A. 2000. Field evaluation of deet and a piperidine repellent against *Aedes communis* (Diptera: Culicidae)

- and *Simulium venustum* (Diptera: Simuliidae) in the Adirondack mountains of New York. *Journal of Medical Entomology*, 37, 919-923.
- DELETRE, E., SCHATZ, B., BOURGUET, D., CHANDRE, F., WILLIAMS, L., RATNADASS, A. & MARTIN, T. 2016. Prospects for repellent in pest control: current developments and future challenges. *Chemoecology*, 26, 127-142.
- DIAZ, J. H. 2016. Chemical and plant-based insect repellents: efficacy, safety, and toxicity. *Wilderness & Environmental Medicine*, 27, 153-163.
- DRAPEAU, J., ROSSANO, M., TOURAUD, D., OBERMAYR, U., GEIER, M., ROSE, A. & KUNZ, W. 2011. Green synthesis of para-Menthane-3, 8-diol from *Eucalyptus citriodora*: Application for repellent products. *Comptes Rendus Chimie*, 14, 629-635.
- DUBEY, S., JHELM, V. & PATANJALI, P. 2011. Controlled release agrochemical formulations: a review.
- DUFFY, M. R., CHEN, T.-H., HANCOCK, W. T., POWERS, A. M., KOOL, J. L., LANCIOTTI, R. S., PRETRICK, M., MARFEL, M., HOLZBAUER, S. & DUBRAY, C. 2009. Zika virus outbreak on Yap Island, Federated States of Micronesia. *New England Journal of Medicine*, 360, 2536-2543.
- DUNCAN, T. V. 2011. Applications of nanotechnology in food packaging and food safety: barrier materials, antimicrobials and sensors. *Journal of Colloid and Interface Science*, 363, 1-24.
- DURMUS, A., KASGOZ, A. & MACOSKO, C. W. 2007. Linear low density polyethylene (LLDPE)/clay nanocomposites. Part I: Structural characterization and quantifying clay dispersion by melt rheology. *Polymer*, 48, 4492-4502.
- DURMUŞ, A., WOO, M., KAŞGÖZ, A., MACOSKO, C. W. & TSAPATSI, M. 2007. Intercalated linear low density polyethylene (LLDPE)/clay nanocomposites prepared with

- oxidized polyethylene as a new type compatibilizer: structural, mechanical and barrier properties. *European Polymer Journal*, 43, 3737-3749.
- DYER, O. 2015. Zika virus spreads across Americas as concerns mount over birth defects. *British Medical Journal*, 351:h6983 doi: 10.1136/bmj.h6983.
- FASULO, T. R. 2008. History and insects. *Encyclopedia of Entomology*, 1810-1826.
- FELDMAN, D. 2001. Polymer barrier films. *Journal of Polymers and the Environment*, 9, 49-55.
- FOCKE, W. 2003. A revised equation for estimating the vapour pressure of low-volatility substances from isothermal TG data. *Journal of Thermal Analysis and Calorimetry*, 74, 97-107.
- FORERO G. L. A. & VELÁSQUEZ J. J. A. 2011. Wagner liquid–vapour pressure equation constants from a simple methodology. *The Journal of Chemical Thermodynamics*, 43, 1235-1251.
- FRADIN, M. S. 1998. Mosquitoes and mosquito repellents: a clinician's guide. *Annals of Internal Medicine*, 128, 931-940.
- FRADIN, M. S. & DAY, J. F. 2002. Comparative efficacy of insect repellents against mosquito bites. *New England Journal of Medicine*, 347, 13-18.
- FRANCES, S., EAMSILA, C., PILAKASIRI, C. & LINTHICUM, K. 1996. Effectiveness of repellent formulations containing deet against mosquitoes in north-eastern Thailand. *Journal of the American Mosquito Control Association*, 12, 331.
- FRANCES, S., MACKENZIE, D., ROWCLIFFE, K. & CORCORAN, S. 2009. Comparative field evaluation of repellent formulations containing deet and IR3535 against mosquitoes in Queensland, Australia. *Journal of the American Mosquito Control Association*, 25, 511-513.

- FRANCES, S., WATERSON, D. G. E., BEEBE, N. & COOPER, R. 2004. Field evaluation of repellent formulations containing deet and picaridin against mosquitoes in Northern Territory, Australia. *Journal of Medical Entomology*, 41, 414-417.
- GABEL, M., SPENCER, T. & AKERS, W. 1976. Evaporation rates and protection times of mosquito repellents. *Mosquito News*.
- GILLIJ, Y., GLEISER, R. & ZYGADLO, J. 2008. Mosquito repellent activity of essential oils of aromatic plants growing in Argentina. *Bioresource Technology*, 99, 2507-2515.
- GOBBLE, C., CHICKOS, J. & VEREVKIN, S. P. 2014. Vapor pressures and vaporization enthalpies of a series of dialkyl phthalates by correlation gas chromatography. *Journal of Chemical & Engineering Data*, 59, 1353-1365.
- GOLEBIEWSKI, J., ROZANSKI, A., DZWONKOWSKI, J. & GALESKI, A. 2008. Low density polyethylene–montmorillonite nanocomposites for film blowing. *European Polymer Journal*, 44, 270-286.
- GONÇALVES, J., FIGUEIRA, J., RODRIGUES, F. & CAMARA, J. S. 2012. Headspace solid-phase microextraction combined with mass spectrometry as a powerful analytical tool for profiling the terpenoid metabolomic pattern of hop-essential oil derived from Saaz variety. *Journal of Separation Science*, 35, 2282-2296.
- GONG, J., YANG, L., ZHOU, X., DENG, Z., LEI, G. & WANG, W. 2012. Effects of low atmospheric pressure on combustion characteristics of polyethylene and polymethyl methacrylate. *Journal of Fire Sciences*, 30, 224-239.
- HAMMEN, C. R. 2014. Product having a paper layer and a film layer and methods of forming such a product. Google Patents.
- HAYNES, W. M. 2014. *CRC handbook of chemistry and physics*, CRC press.



- HAZRA, A., DOLLIMORE, D. & ALEXANDER, K. 2002. Thermal analysis of the evaporation of compounds used in aromatherapy using thermogravimetry. *Thermochimica Acta*, 392, 221-229.
- HEINZ, F. X. & STIASNY, K. 2012. Flaviviruses and flavivirus vaccines. *Vaccine*, 30, 4301-4306.
- HELLMAN, D. J., GREENBERG, A. R. & KRANTZ, W. B. 2004. A novel process for membrane fabrication: thermally assisted evaporative phase separation (TAEPS). *Journal of Membrane Science*, 230, 99-109.
- HENNESSEY, M., FISCHER, M. & STAPLES, J. E. 2016. Zika virus spreads to new areas—region of the Americas, May 2015–January 2016. *American Journal of Transplantation*, 16, 1031-1034.
- HONG, S.-I. & RHIM, J.-W. 2012. Preparation and properties of melt-intercalated linear low density polyethylene/clay nanocomposite films prepared by blow extrusion. *Lwt-food Science and Technology*, 48, 43-51.
- HOTTA, S. & PAUL, D. 2004. Nanocomposites formed from linear low density polyethylene and organoclays. *Polymer*, 45, 7639-7654.
- ISHIKAWA, T., YAMANAKA, A. & KONISHI, E. 2014. A review of successful flavivirus vaccines and the problems with those flaviviruses for which vaccines are not yet available. *Vaccine*, 32, 1326-1337.
- ISLAM, J., ZAMAN, K., CHAKRABARTI, S., BORA, N. S., PATHAK, M. P., MANDAL, S., JUNEJO, J. A. & CHATTOPADHYAY, P. 2017a. Exploration of ethyl anthranilate-loaded monolithic matrix-type prophylactic polymeric patch. *Journal of Food and Drug Analysis*, 25, 968-975.

- ISLAM, J., ZAMAN, K., DUARAH, S., RAJU, P. S. & CHATTOPADHYAY, P. 2017b. Mosquito repellents: an insight into the chronological perspectives and novel discoveries. *Acta Tropica*, 167, 216-230.
- ISLAM, J., ZAMAN, K., TYAGI, V., DUARAH, S., DHIMAN, S. & CHATTOPADHYAY, P. 2017c. Protection against mosquito vectors *Aedes aegypti*, *Anopheles stephensi* and *Culex quinquefasciatus* using a novel insect repellent, ethyl anthranilate. *Acta tropica*, 174, 56-63.
- ISMAIL, H., NORDIN, R., AHMAD, Z. & RASHID, A. 2010. Processability and miscibility of linear low-density polyethylene/poly (vinyl alcohol) blends: In situ compatibilization with maleic acid. *Iranian Polymer Journal*, 19 (4), 297-308.
- ISRAEL, C., WENJUN, L., YOUXIN, Y. & ISRAEL, C. 1995. Formation and microstructure of polyethylene microporous membranes through thermally induced phase separation. *Chinese Journal of Polymer Science*, 13, 7-19.
- IZADI, H., FOCKE, W. W., ASAADI, E., MAHARAJ, R., PRETORIUS, J. & LOOTS, M. T. 2017. A promising azeotrope-like mosquito repellent blend. *Scientific Reports*, 7, 10273.
- JAKA, K. and DHARMANI, C., 2003. Global surveillance of DDT and DDE levels in human tissues. *International Journal of Occupational Medicine and Environmental Health*, 16(1), 7-20.
- JAIN, A. & YALKOWSKY, S. H. 2006. Estimation of melting points of organic compounds - II. *Journal of Pharmaceutical Sciences*, 95, 2562-2618.
- JAIN, A., YANG, G. & YALKOWSKY, S. H. 2004. Estimation of melting points of organic compounds. *Industrial & Engineering Chemistry Research*, 43, 7618-7621.

- JANTAN, I. & ZAKI, Z. M. 1998. Development of environment-friendly insect repellents from the leaf oils of selected Malaysian plants. *ASEAN Review of Biodiversity and Environmental Conservation (ARBEC)*, 6, 1-7.
- KAHLBAUM, G. W. 1894. Studien über Dampfspannkraftmessungen. *Zeitschrift für Physikalische Chemie*, 13, 14-55.
- KAIN, P., BOYLE, S.M., THARADRA, S.K., GUDA, T., PHAM, C., DAHANUKAR, A. & RAY, A. 2013. Odour receptors and neurons for DEET and new insect repellents. *Nature*, 502(7472), 507.
- KASMAN, S., EOADHOUSE, L. & WRIGHT, G. 1953. Studies in testing insect repellents. *Mosquito News*, 13, 116-23.
- KATZ, T. M., MILLER, J. H. & HEBERT, A. A. 2008. Insect repellents: historical perspectives and new developments. *Journal of the American Academy of Dermatology*, 58, 865-871.
- KENAWY, E., SHERRINGTON, D. & AKELAH, A. 1992. Controlled release of agrochemical molecules chemically bound to polymers. *European Polymer Journal*, 28, 841-862.
- KHAN, A., MAIBACH, H. & SKIDMORE, D. 1973. A study of insect repellents. 2. Effect of temperature on protection time. *Journal of Economic Entomology*, 66, 437-438.
- KHODKAR, F. & EBRAHIMI, N. G. 2011. Effect of irradiation on mechanical and structural properties of ethylene vinyl acetate copolymer hollow fibers. *Journal of Applied Polymer Science*, 119, 2085-2092.
- KIM, J.-K., TAKI, K. & OHSHIMA, M. 2007. Preparation of a unique microporous structure via two step phase separation in the course of drying a ternary polymer solution. *Langmuir*, 23, 12397-12405.

- KIM, S. & LEE, Y. M. 2015. Rigid and microporous polymers for gas separation membranes. *Progress in Polymer Science*, 43, 1-32.
- KIM, S. S. & LLOYD, D. R. 1991. Microporous membrane formation via thermally-induced phase separation. III. Effect of thermodynamic interactions on the structure of isotactic polypropylene membranes. *Journal of Membrane Science*, 64, 13-29.
- KLEINSCHMIDT, I., SCHWABE, C., SHIVA, M., SEGURA, J. L., SIMA, V., MABUNDA, S. J. A. & COLEMAN, M. 2009. Combining indoor residual spraying and insecticide-treated net interventions. *The American Journal of Tropical Medicine and Hygiene*, 81, 519-524.
- KOREN, G., MATSUI, D. & BAILEY, B. 2003. DEET-based insect repellents: safety implications for children and pregnant and lactating women. *Canadian Medical Association Journal*, 169, 209-212.
- KWEKA, E. J., MUNGA, S., MAHANDE, A. M., MSANGI, S., MAZIGO, H. D., ADRIAS, A. Q. & MATIAS, J. R. 2012. Protective efficacy of menthol propylene glycol carbonate compared to N, N-diethyl-methylbenzamide against mosquito bites in Northern Tanzania. *Parasites & Vectors*, 5, 189.
- LALLOO, D. G., SHINGADIA, D., BELL, D. J., BEECHING, N. J., WHITTY, C. J. & CHIODINI, P. L. 2016. UK malaria treatment guidelines 2016. *Journal of Infection*, 72, 635-649.
- LEAL, W. S. 2014. The enigmatic reception of DEET—the gold standard of insect repellents. *Current Opinion in Insect Science*, 6, 93-98.
- LEBARON, P. C., WANG, Z. & PINNAVAIA, T. J. 1999. Polymer-layered silicate nanocomposites: an overview. *Applied Clay Science*, 15, 11-29.

- LENGELER, C. 2004. Insecticide-treated bed nets and curtains for preventing malaria. *Cochrane Database of systematic reviews*, 2, 1-46.
- LI, X., WANG, Y., LU, X. & XIAO, C. 2008. Morphology changes of polyvinylidene fluoride membrane under different phase separation mechanisms. *Journal of Membrane Science*, 320, 477-482.
- LIANG, H.-Q., WU, Q.-Y., WAN, L.-S., HUANG, X.-J. & XU, Z.-K. 2013. Polar polymer membranes via thermally induced phase separation using a universal crystallizable diluent. *Journal of Membrane Science*, 446, 482-491.
- LICCIARDELLO, F., MURATORE, G., SUMA, P., RUSSO, A. & NERÍN, C. 2013. Effectiveness of a novel insect-repellent food packaging incorporating essential oils against the red flour beetle (*Tribolium castaneum*). *Innovative Food Science & Emerging Technologies*, 19, 173-180.
- LIDE, D. & DAVID, R. 2009. CRC Handbook of Chemistry and Physics, 90th (ed.) CRC Press. *Boca Raton.[Links]*.
- LIDE, D. R. 2004. *CRC Handbook of Chemistry and Physics 2004-2005: A Ready-Reference Book of Chemical and Physical Data*. CRC Press Boca Raton.
- LIM, G. B., KIM, S. S., YE, Q., WANG, Y. F. & LLOYD, D. R. 1991. Microporous membrane formation via thermally-induced phase separation. IV. Effect of isotactic polypropylene crystallization kinetics on membrane structure. *Journal of Membrane Science*, 64, 31-40.
- LIN, Y., TANG, Y., MA, H., YANG, J., TIAN, Y., MA, W. & WANG, X. 2009. Formation of a bicontinuous structure membrane of polyvinylidene fluoride in diphenyl carbonate diluent via thermally induced phase separation. *Journal of Applied Polymer Science*, 114, 1523-1528.

- LIU, S., ZHOU, C. & YU, W. 2011. Phase separation and structure control in ultra-high molecular weight polyethylene microporous membrane. *Journal of Membrane Science*, 379, 268-278.
- LLOYD, D. R., KINZER, K. E. & TSENG, H. 1990. Microporous membrane formation via thermally induced phase separation. I. Solid-liquid phase separation. *Journal of Membrane Science*, 52, 239-261.
- LUPI, E., HATZ, C. & SCHLAGENHAUF, P. 2013. The efficacy of repellents against *Aedes*, *Anopheles*, *Culex* and *Ixodes* spp.—A literature review. *Travel Medicine and Infectious Disease*, 11, 374-411.
- MAIBACH, H. I., AKERS, W. A., JOHNSON, H. L., KHAN, A. & SKINNER, W. 1974. Topical insect repellents. *Clinical Pharmacology & Therapeutics*, 16, 970-973.
- MAJEED, K., JAWAID, M., HASSAN, A., BAKAR, A. A., KHALIL, H. A., SALEMA, A. & INUWA, I. 2013. Potential materials for food packaging from nanoclay/natural fibres filled hybrid composites. *Materials & Design*, 46, 391-410.
- MAKONO, R. & SIBANDA, S. 1999. Review of the prevalence of malaria in Zimbabwe with specific reference to parasite drug resistance (1984–1996). *Transactions of the Royal Society of Tropical Medicine and Hygiene*, 93, 449-452.
- MANNINEN, A. R., NAGUIB, H. E., NAWABY, A. V. & DAY, M. 2005. CO<sub>2</sub> sorption and diffusion in polymethyl methacrylate–clay nanocomposites. *Polymer Engineering & Science*, 45, 904-914.
- MARCHANTE, V. & BELTRÁN, M. 2015. Montmorillonite polyethylene nanocomposites. *Polyethylene-Based Blends, Composites and Nanocomposites*, 257-280.
- MARCHIO, F. 1996. Insect repellent 3535: a new alternative to DEET. *SÖFW. Seifen, Öle, Fette, Wachse*, 122, 478-485.

- MATSUYAMA, H., OKAFUJI, H., MAKI, T., TERAMOTO, M. & KUBOTA, N. 2003. Preparation of polyethylene hollow fiber membrane via thermally induced phase separation. *Journal of Membrane Science*, 223, 119-126.
- MATSUYAMA, H., YANO, H., MAKI, T., TERAMOTO, M., MISHIMA, K. & MATSUYAMA, K. 2001. Formation of porous flat membrane by phase separation with supercritical CO<sub>2</sub>. *Journal of Membrane Science*, 194, 157-163.
- MENG, X., DU, X., WANG, Z., BI, W. & TANG, T. 2008. The investigation of exfoliation process of organic modified montmorillonite in thermoplastic polyurethane with different molecular weights. *Composites Science and Technology*, 68, 1815-1821.
- MESSINA, J. P., BRADY, O. J., SCOTT, T. W., ZOU, C., PIGOTT, D. M., DUDA, K. A., BHATT, S., KATZELNICK, L., HOWES, R. E. & BATTLE, K. E. 2014. Global spread of dengue virus types: mapping the 70 year history. *Trends in Microbiology*, 22, 138-146.
- MILWAUKEE, W. 1990. Catalog Handbook of Fine Chemicals. *Aldrich Chemical Company*, 971.
- MISNI, N., SULAIMAN, S., OTHMAN, H. & OMAR, B. 2009. Repellency of essential oil of *Piper aduncum* against *Aedes albopictus* in the laboratory. *Journal of the American Mosquito Control Association*, 25, 442-447.
- MITTAL, P., SREEHARI, U., RAZDAN, R., DASH, A. & ANSARI, M. 2011. Efficacy of Advanced Odomos repellent cream (N, N-diethyl-benzamide) against mosquito vectors. *The Indian Journal of Medical Research*, 133, 426.
- MOHAMMADZADEH, S. & ZAHEDI, G. 2008. A new vapor pressure equation for pure substances. *Korean Journal of Chemical Engineering*, 25, 1514-1517.
- MONATH, T. P. 2001. Yellow fever: an update. *The Lancet Infectious Diseases*, 1, 11-20.

- MONATH, T. P. & VASCONCELOS, P. F. 2015. Yellow fever. *Journal of Clinical Virology*, 64, 160-173.
- MORLAT-THERIAS, S., FANTON, E., GARDETTE, J.-L., DINTCHEVA, N. T., LA MANTIA, F. P. & MALATESTA, V. 2008. Photochemical stabilization of linear low-density polyethylene/clay nanocomposites: towards durable nanocomposites. *Polymer Degradation and Stability*, 93, 1776-1780.
- MOOSS, V.A., HAMZA, F., ZINJARDE, S.S. & ATHAWALE, A.A. 2019. Polyurethane films modified with polyaniline-zinc oxide nanocomposites for biofouling mitigation. *Chemical Engineering Journal*, 359, 1400-1410.
- MUNHENGA, G., MASENDU, H.T., BROOKE, B.D., HUNT, R.H. & KOEKEMOER, L.K. 2008. Pyrethroid resistance in the major malaria vector *Anopheles arabiensis* from Gwave, a malaria-endemic area in Zimbabwe. *Malaria Journal*, 7(1),.247.
- MYRDAL, P. B. & YALKOWSKY, S. H. 1997. Estimating pure component vapor pressures of complex organic molecules. *Industrial & Engineering Chemistry Research*, 36, 2494-2499.
- NAUCKE, T., KRÖPKE, R., BENNER, G., SCHULZ, J., WITTERN, K., ROSE, A., KRÖCKEL, U. & GRÜNEWALD, H. 2007. Field evaluation of the efficacy of proprietary repellent formulations with IR3535® and Picaridin against *Aedes aegypti*. *Parasitology Research*, 101, 169.
- NERIO, L. S., OLIVERO-VERBEL, J. & STASHENKO, E. 2010. Repellent activity of essential oils: a review. *Bioresource Technology*, 101, 372-378.
- NHLAPO, N. S. 2013. *TGA-FTIR study of the vapours released by volatile corrosion inhibitor model systems*. University of Pretoria.



- NIKKHAH, S. J., SA, A. R., BANIASADI, H. & TAVAKOLZADEH, F. 2009. Investigation of properties of polyethylene/clay nanocomposites prepared by new in situ Ziegler–Natta catalyst. *Materials & Design*, 30, 2309-2315.
- NKUMAMA, I. N., O’MEARA, W. P. & OSIER, F. H. 2017. Changes in malaria epidemiology in Africa and new challenges for elimination. *Trends in Parasitology*, 33, 128-140.
- NOGUEIRA BARRADAS, T., PERDIZ SENNA, J., RICCI JUNIOR, E. & REGINA ELIAS MANSUR, C. 2016. Polymer-based drug delivery systems applied to insect repellent devices: A Review. *Current Drug Delivery*, 13, 221-235.
- NUNES, S. P. & INOUE, T. 1996. Evidence for spinodal decomposition and nucleation and growth mechanisms during membrane formation. *Journal of Membrane Science*, 111, 93-103.
- O’NEIL, M. J. 2013. *The Merck Index: an encyclopedia of chemicals, drugs, and biologicals*. RSC Publishing.
- ODALO, J. O., OMOLO, M. O., MALEBO, H., ANGIRA, J., NJERU, P. M., NDIEGE, I. O. & HASSANALI, A. 2005. Repellency of essential oils of some plants from the Kenyan coast against *Anopheles gambiae*. *Acta Tropica*, 95, 210-218.
- OKUMU, F. O. & MOORE, S. J. 2011. Combining indoor residual spraying and insecticide-treated nets for malaria control in Africa: a review of possible outcomes and an outline of suggestions for the future. *Malaria Journal*, 10, 208.
- OOI, E.-E., GOH, K.-T. & GUBLER, D. J. 2006. Dengue prevention and 35 years of vector control in Singapore. *Emerging Infectious Diseases*, 12, 887.
- PASCUAL-VILLALOBOS, M. & ROBLEDO, A. 1998. Screening for anti-insect activity in Mediterranean plants. *Industrial Crops and Products*, 8, 183-194.

- PAVLACKY, E., RAVINDRAN, N. & WEBSTER, D. C. 2012. Novel in situ synthesis in the preparation of ultraviolet-curable nanocomposite barrier coatings. *Journal of Applied Polymer Science*, 125, 3836-3848.
- PAVLIDOU, S. & PAPASPYRIDES, C. 2008. A review on polymer-layered silicate nanocomposites. *Progress in Polymer Science*, 33, 1119-1198.
- PENG, Z., BECKETT, A. N., ENGLER, R. J., HOFFMAN, D. R., OTT, N. L. & SIMONS, F. E. R. 2004. Immune responses to mosquito saliva in 14 individuals with acute systemic allergic reactions to mosquito bites. *Journal of Allergy and Clinical Immunology*, 114, 1189-1194.
- PETERSEN, E., WILSON, M. E., TOUCH, S., MCCLOSKEY, B., MWABA, P., BATES, M., DAR, O., MATTES, F., KIDD, M. & IPPOLITO, G. 2016. Rapid spread of Zika virus in the Americas-implications for public health preparedness for mass gatherings at the 2016 Brazil Olympic Games. *International Journal of Infectious Diseases*, 44, 11-15.
- PHANG, P. & DOLLIMORE, D. 2001. The calculation of the vapor pressures of antioxidants over a range of temperatures using thermogravimetry. *Thermochimica Acta*, 367, 263-271.
- PHILLIPS, M., BURROWS, J., MANYANDO, C., HOOFT VAN HUIJSDUIJNEN, R. C. VAN VOORHIS, W. & WELLS, T. 2017. Malaria. *Nature Reviews*, 3, 17050.
- PIETERSE, N. & FOCKE, W. W. 2003. Diffusion-controlled evaporation through a stagnant gas: estimating low vapour pressures from thermogravimetric data. *Thermochimica Acta*, 406, 191-198.
- PIETERSE, N., FOCKE, W. W., VUORINEN, E. & RÁCZ, I. 2006. Estimating the gas permeability of commercial volatile corrosion inhibitors at elevated temperatures with thermo-gravimetry. *Corrosion Science*, 48, 1986-1995.

- PLUESS, B., TANSER, F. C., LENGELER, C. & SHARP, B. L. 2010. Indoor residual spraying for preventing malaria. *Cochrane database of systematic reviews*, 4. No.: CD006657. DOI: 10.1002/14651858.CD006657.pub2.
- POLING, B. E., PRAUSNITZ, J. M., JOHN PAUL, O. C. & REID, R. C. 2001. *The properties of gases and liquids*. McGraw-Hill: New York.
- PRICE, D. M. 2001. Vapor pressure determination by thermogravimetry. *Thermochimica Acta*, 367, 253-262.
- RAHNAMA, M. R., BARIKANI, M., BARMAR, M. & HONARKAR, H. 2014. An investigation into the effects of different nanoclays on polyurethane nanocomposites properties. *Polymer-Plastics Technology and Engineering*, 53, 801-810.
- RAJABZADEH, S., YOSHIMOTO, S., TERAMOTO, M., AL-MARZOUQI, M. & MATSUYAMA, H. 2009. CO<sub>2</sub> absorption by using PVDF hollow fiber membrane contactors with various membrane structures. *Separation and Purification Technology*, 69, 210-220.
- RANSON, H., N'GUESSAN, R., LINES, J., MOIROUX, N., NKUNI, Z. & CORBEL, V. 2011. Pyrethroid resistance in African anopheline mosquitoes: what are the implications for malaria control?. *Trends in parasitology*, 27(2), 91-98.
- REDDY, M. R., OVERGAARD, H. J., ABAGA, S., REDDY, V. P., CACCONE, A., KISZEWSKI, A. E. & SLOTMAN, M. A. 2011. Outdoor host seeking behaviour of *Anopheles gambiae* mosquitoes following initiation of malaria vector control on Bioko Island, Equatorial Guinea. *Malaria Journal*, 10, 184.

- REZZA, G., NICOLETTI, L., ANGELINI, R., ROMI, R., FINARELLI, A., PANNING, M., CORDIOLI, P., FORTUNA, C., BOROS, S. & MAGURANO, F. 2007. Infection with chikungunya virus in Italy: an outbreak in a temperate region. *The Lancet*, 370, 1840-1846.
- ROHÁČ, V., MUSGROVE, J. E., RUŽIČKA, K., RUŽIČKA, V., ZÁBRANSKÝ, M. & AIM, K. 1999. Thermodynamic properties of dimethyl phthalate along the (vapour + liquid) saturation curve. *The Journal of Chemical Thermodynamics*, 31, 971-986.
- RONG, Y., GREGSON, C. M. & PARKER, A. 2012. Thermogravimetric measurements of liquid vapor pressure. *The Journal of Chemical Thermodynamics*, 51, 25-30.
- RUEDA, L.M., RUTLEDGE, L.C. and GUPTA, R.K., 1998. Effect of skin abrasions on the efficacy of the repellent DEET against *Aedes aegypti*. *Journal of the American Mosquito Control Association*, 14(2): 178-182.
- SADIKU, R., IBRAHIM, D., AGBOOLA, O., OWONUBI, S. J., FASIKU, V. O., KUPOLATI, W. K., JAMIRU, T., EZE, A. A., ADEKOMAYA, O. S. & VARAPRASAD, K & AGWUNCHA, S.C. 2017. Automotive components composed of polyolefins. *In Polyolefin Fibres*, 449-496.
- SALARI, E., AHMADI, K., DEHYAGHOBI, R. Z., PURHEMATY, A. & TAKALLOOZADEH, H. M. 2012. Toxic and repellent effect of harmal (*Peganum harmala* L.) acetonic extract on several aphids and *Tribolium castaneum* (Herbst). *Chilean Journal of Agricultural Research*, 72, 147.
- SEFADI, J. S. & LUYT, A. 2012. Morphology and properties of EVA/empty fruit bunch composites. *Journal of Thermoplastic Composite Materials*, 25, 895-914.

- SHANG, M., MATSUYAMA, H., TERAMOTO, M., LLOYD, D. R. & KUBOTA, N. 2003. Preparation and membrane performance of poly (ethylene-co-vinyl alcohol) hollow fiber membrane via thermally induced phase separation. *Polymer*, 44, 7441-7447.
- SHEN, L., PENG, M., QIAO, F. & ZHANG, J.-L. 2008. Preparation of microporous ultra high molecular weight polyethylene (UHMWPE) by thermally induced phase separation of a UHMWPE/liquid paraffin mixture. *Chinese Journal of Polymer Science*, 26, 653-657.
- SHIFF, C. 2002. Integrated approach to malaria control. *Clinical Microbiology Reviews*, 15, 278-293.
- SIBANDA, M. & FOCKE, W. 2014. Development of an insecticide impregnated polymer wall lining for malaria vector control. *Malaria Journal*, 13, P80.
- SIBANDA, M., FOCKE, W., BRAACK, L., LEUTERITZ, A., BRÜNIG, H., TRAN, N. H. A., WIECZOREK, F. & TRÜMPER, W. 2018. Bicomponent fibres for controlled release of volatile mosquito repellents. *Materials Science and Engineering: C*, 91, 754-761.
- SIBANDA, M. M. 2016. *Polyolefin copolymers as controlled release devices for insecticides and repellents*. University of Pretoria.
- SINKA, M. E., BANGS, M. J., MANGUIN, S., COETZEE, M., MBOGO, C. M., HEMINGWAY, J., PATIL, A. P., TEMPERLEY, W. H., GETHING, P. W. & KABARIA, C. W. 2010. The dominant Anopheles vectors of human malaria in Africa, Europe and the Middle East: occurrence data, distribution maps and bionomic précis. *Parasites & Vectors*, 3, 117.
- SMITH, C. N. 1963. Factors affecting the protection period of mosquito repellents, US Dept. of Agriculture, 1281.
- SORGE, F., IMBERT, P., LAURENT, C., MINODIER, P., BANERJEE, A., KHELFAOUI, F., GUÉRIN, N. & GENDREL, D. 2007. Children arthropod bites protective measures:

- insecticides and repellents. *Archives de Pediatrie: Organe Officiel de la Societe Francaise de Pediatrie*, 14, 1442-1450.
- SUBRAMANIAN, M. N. 2017. *Basics of Polymer Chemistry*. River Publishers.
- TANSER, F. C., PLUESS, B., LENGELER, C. & SHARP, B. L. 2007. Indoor residual spraying for preventing malaria. *Cochrane Database of Systematic Reviews: Protocols*.
- TAWATSIN, A., ASAVADACHANUKORN, P., THAVARA, U., WONGSINKONGMAN, P., BANSIDHI, J., BOONRUAD, T., CHAVALITTUMRONG, P., SOONTHORNCHAREONNON, N., KOMALAMISRA, N. & MULLA, M. S. 2006. Repellency of essential oils extracted from plants in Thailand against four mosquito vectors (Diptera: Culicidae) and oviposition deterrent effects against *Aedes aegypti* (Diptera: Culicidae). *Southeast Asian Journal of Tropical Medicine and Public Health*, 37, 915.
- TAWATSIN, A., WRATTEN, S. D., SCOTT, R. R., THAVARA, U. & TECHADAMRONGSIN, Y. 2001. Repellency of volatile oils from plants against three mosquito vectors. *Journal of Vector Ecology*, 26, 76-82.
- THAVARA, U., TAWATSIN, A., CHOMPOOSRI, J., SUWONKERD, W., CHANSANG, U. & ASAVADACHANUKORN, P. 2001. Laboratory and field evaluations of the insect repellent 3535 (ethyl butylacetylaminopropionate) and deet against mosquito vectors in Thailand. *Journal of the American Mosquito Control Association - Mosquito News*, 17, 190-195.
- TISGRATOG, R., SANGUANPONG, U., GRIECO, J. P., NGOEN-KLUAN, R. & CHAREONVIRIYAPHAP, T. 2016. Plants traditionally used as mosquito repellents and the implication for their use in vector control. *Acta Tropica*, 157, 136-144.

- TOLOZA, A. C., LUCIA, A., ZERBA, E., MASUH, H. & PICOLLO, M. I. 2008. Interspecific hybridization of Eucalyptus as a potential tool to improve the bioactivity of essential oils against permethrin-resistant head lice from Argentina. *Bioresource Technology*, 99, 7341-7347.
- TORNUK, F., SAGDIC, O., HANCER, M. & YETIM, H. 2018. Development of LLDPE based active nanocomposite films with nanoclays impregnated with volatile compounds. *Food Research International*, 107, 337-345.
- TRAMON, C. 2014. Modeling the controlled release of essential oils from a polymer matrix—a special case. *Industrial Crops and Products*, 61, 23-30.
- TRIGG, J. 1996. Evaluation of a eucalyptus-based repellent against Anopheles spp. in Tanzania. *Journal of the American Mosquito Control Association - Mosquito News*, 12, 243-246.
- TRONGTOKIT, Y., RONGSRIYAM, Y., KOMALAMISRA, N. & APIWATHNASORN, C. 2005. Comparative repellency of 38 essential oils against mosquito bites. *Phytotherapy Research*, 19, 303-309.
- TRONGTOKIT, Y., RONGSRIYAM, Y., KOMALAMISRA, N., KRISADAPHONG, P. & APIWATHNASORN, C. 2004. Laboratory and field trial of developing medicinal local Thai plant products against four species of mosquito vectors. *Southeast Asian Journal of Tropical Medicine and Public Health*, 35, 325-333.
- VENTURA, C. V., MAIA, M., BRAVO-FILHO, V., GÓIS, A. L. & BELFORT, R. 2016. Zika virus in Brazil and macular atrophy in a child with microcephaly. *The Lancet*, 387, 228.
- WANG, Z., YU, W. & ZHOU, C. 2015. Preparation of polyethylene microporous membranes with high water permeability from thermally induced multiple phase transitions. *Polymer*, 56, 535-544.

- WEAST, R. & GRASSELLI, J. 1989. Handbook of Data on Organic Compounds, 2nd Ed., Vol. 2. *CRC Press Inc., Boca Raton, Florida*, 1010, 1070-1115.
- WEAVER, S. C. 2014. Arrival of chikungunya virus in the new world: prospects for spread and impact on public health. *PLoS Neglected Tropical Diseases*, 8, e2921.
- WHO 2009. Guidelines for efficacy testing of mosquito repellents for human skin. Geneva: World Health Organisation.
- WHO 2012. Global strategy for dengue prevention and control, 2012-2020. *WHO Library Cataloguing-in-Publication Data, Switzerland*.
- WHO 2014. Dengue and severe dengue. World Health Organisation, Switzerland, 2014.
- WHO 2016. World Malaria Report 2016, World Health Organisation, Geneva, Switzerland, 2016.
- WHO 2017. World Malaria Report 2017. World Health Organisation, Geneva, Switzerland, 2017.
- WHO 2018. World Malaria Report 2018. World Health Organisation, Geneva, Switzerland, 2018.
- WILKE, C. & LEE, C. 1955. Estimation of diffusion coefficients for gases and vapors. *Industrial & Engineering Chemistry*, 47, 1253-1257.
- WRIGHT, S., DOLLIMORE, D., DUNN, J. & ALEXANDER, K. 2004. Determination of the vapor pressure curves of adipic acid and triethanolamine using thermogravimetric analysis. *Thermochimica Acta*, 421, 25-30.
- WU, J. & LIU, Z. 2005. An accurate vapor pressure equation with good extrapolation characteristics. *International Journal of Thermophysics*, 26, 767-784.
- XIN, Y., FUJIMOTO, T. & UYAMA, H. 2012. Facile fabrication of polycarbonate monolith by non-solvent induced phase separation method. *Polymer*, 53, 2847-2853.
- XU, B., ZHENG, Q., SONG, Y. & SHANGGUAN, Y. 2006. Calculating barrier properties of polymer/clay nanocomposites: effects of clay layers. *Polymer*, 47, 2904-2910.



- YANG, J., LI, D., LIN, Y., WANG, X., TIAN, F. & WANG, Z. 2008. Formation of a bicontinuous structure membrane of polyvinylidene fluoride in diphenyl ketone diluent via thermally induced phase separation. *Journal of Applied Polymer Science*, 110, 341-347.
- YANG, Y.-C., LEE, E.-H., LEE, H.-S., LEE, D.-K. & AHN, Y.-J. 2004. Repellency of aromatic medicinal plant extracts and a steam distillate to *Aedes aegypti*. *Journal of the American Mosquito Control Association*, 20, 146-149.
- YANG, Z., LI, P., XIE, L., WANG, Z. & WANG, S.-C. 2006. Preparation of iPP hollow-fiber microporous membranes via thermally induced phase separation with co-solvents of DBP and DOP. *Desalination*, 192, 168-181.
- YANO, K., USUKI, A., OKADA, A., KURAUCHI, T. & KAMIGAITO, O. 1993. Synthesis and properties of polyimide-clay hybrid. *Journal of Polymer Science Part A: Polymer Chemistry*, 31, 2493-2498.
- ZAIM, M. & GUILLET, P. 2002. Alternative insecticides: an urgent need. *Trends in Parasitology*, 18, 161-163.
- ZAMMARCHI, L., TAPPE, D., FORTUNA, C., REMOLI, M., GÜNTHER, S., VENTURI, G., BARTOLONI, A. & SCHMIDT-CHANASIT, J. 2015. Zika virus infection in a traveller returning to Europe from Brazil, March 2015. *Eurosurveillance*, 20, 21153.
- ZHOU, J., ZHANG, H., WANG, H. & DU, Q. 2009. Effect of cooling baths on EVOH microporous membrane structures in thermally induced phase separation. *Journal of Membrane Science*, 343, 104-109.

## **PUBLICATIONS**

### **Journal Articles**

**Mapossa, A.B.**, Sibanda, M.M., Siteo, A., Focke, W.W., Braack, L., Ndonyane, C., Mouatcho, J., Smart, J., Muiambo, H., Androsch, R. and Loots, M.T., 2019. Microporous polyolefin strands as controlled-release devices for mosquito repellents. *Chemical Engineering Journal*, 360, pp.435-444.

**Mapossa, A. B.**, Siteo, A., Focke, W. W., Izadi, H., Toit, E., Androsch, R., Sungkapreecha, C., Merwe, L. V. 2019. Mosquito repellent thermal stability, permeability and air volatility. *Journal of Pest management science (submitted)*.

### **Conferences participated in**

Siteo, A., Mapossa, A.B., Focke, W.W. Attempts to prepare microporous polymer repellent matrices. *14th Annual UNESCO/IUPAC Workshop & Conference on Macromolecules & Materials*, 11 – 13 April 2017, Stellenbosch, South Africa.

Mapossa, A.B., Siteo, A., Focke, W.W. Designing microporous LLDPE mosquito repellent anklets. *3rd Southern Africa Malaria Research Conference*, 7 – 9 November 2017, Johannesburg, South Africa.

Siteo, A., Mapossa, A.B., Focke, W.W. Designing microporous EVA mosquito repellent anklets. *3rd Southern Africa Malaria Research Conference*, 7 – 9 November 2017, Johannesburg, South Africa.

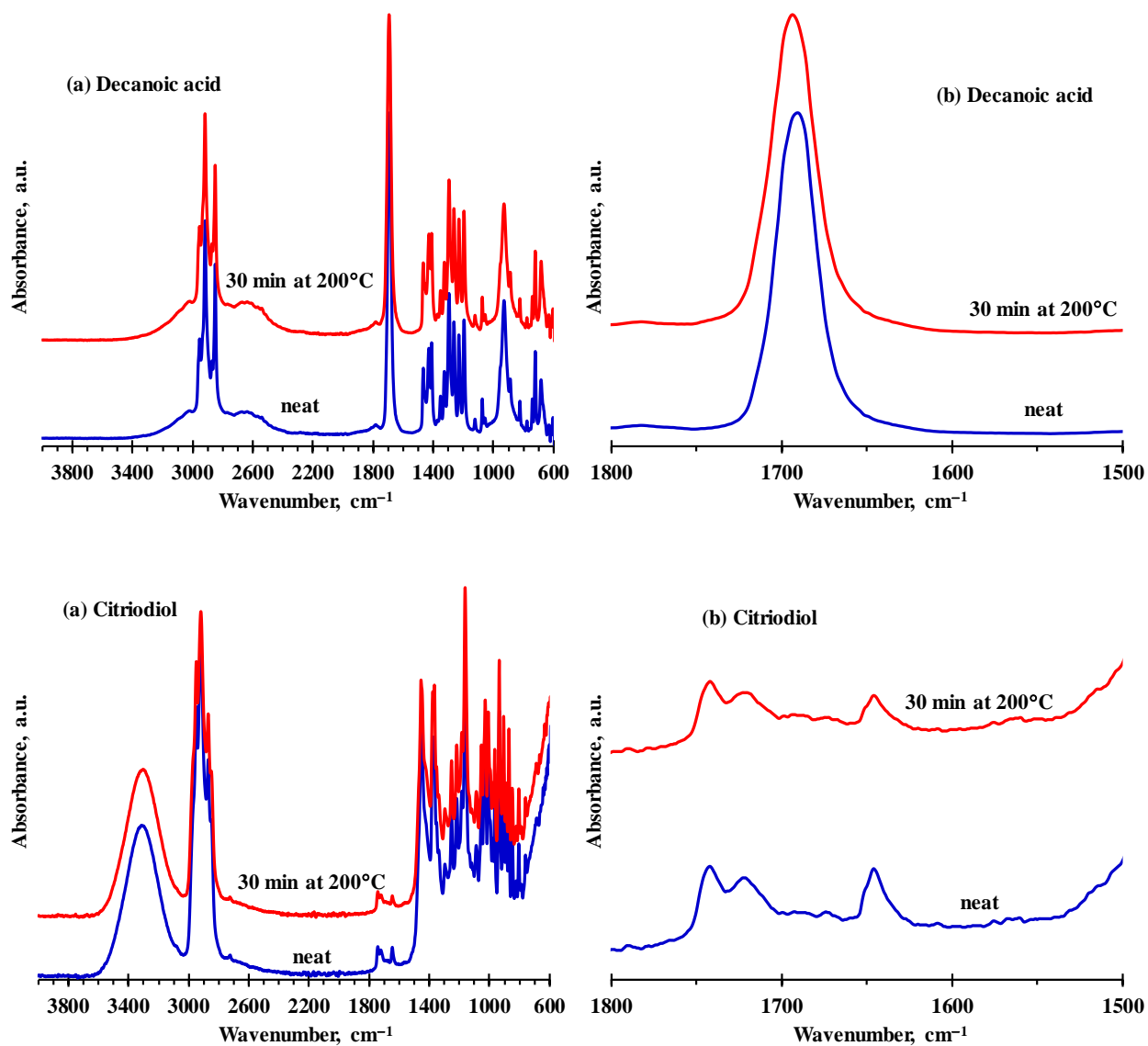
Sitoe, A., Focke, W.W., Mapossa, A.B., Braack, L., Androsch, R., Sibanda, M. Microporous polyolefin long-life insect repellent bracelets. *4th Southern Africa Malaria Research Conference*, 30 July to 1 August 2018, Johannesburg, South Africa.

Mapossa, A.B., Focke, W.W., Sitoe, A., Braack, L., Androsch, R., Sibanda, M.M. Modelling repellent release from long-life bracelets. *4th Southern Africa Malaria Research Conference*, 30 July to 1 August 2018, Johannesburg, South Africa.

Mapossa, A.B., Focke, W.W., Sitoe, A., Braack, L., Androsch, R., Muiambo, H., Salomé, G. Controlled release of volatile mosquito repellents from nano-structured polymers to reduce infectious tropical diseases. *German-African Cooperation Projects in Infectiology Conference*. 5 – 8 September 2018, Entebbe, Uganda.

## APPENDICES

Appendix I: (a) FTIR spectra for the mosquito repellents decanoic acid and citriodiol before and after thermal-oxidative stability testing by exposure to air at 30 min at 200 °C. (b) Expanded view of the carbonyl absorption region proving the statement of the thermal stability of decanoic acid and citriodiol.



## Appendix II: Vapour pressure values reported in the literature for all pure compounds studied

<b>Decanoic acid</b>		
<b>T/K</b>	<b>P<sub>A</sub> (kPa)</b>	<b>Source</b>
298.15	4.88E-05	Baccanari et al., 1968. URL: <a href="https://toxnet.nlm.nih.gov/cgi-bin/sis/search2">https://toxnet.nlm.nih.gov/cgi-bin/sis/search2</a>
381.15	0.100	Lide and David, 2009. URL: <a href="https://wikivividly.com/wiki/Decanoic_acid#cite_note-pubchem-2">https://wikivividly.com/wiki/Decanoic_acid#cite_note-pubchem-2</a>
398.15	0.133	CAMEO Chemicals. <a href="https://cameochemicals.noaa.gov/chemical/17804">https://cameochemicals.noaa.gov/chemical/17804</a>
415.15	0.667	CAMEO Chemicals. <a href="https://cameochemicals.noaa.gov/chemical/17804">https://cameochemicals.noaa.gov/chemical/17804</a>
422.2	1.50	(Weast and Grasselli, 1989). URL: <a href="https://webbook.nist.gov/chemistry/">https://webbook.nist.gov/chemistry/</a>
433.15	2.03	<a href="https://wikivividly.com/wiki/Decanoic_acid#cite_note-pubchem-2">https://wikivividly.com/wiki/Decanoic_acid#cite_note-pubchem-2</a>
541.85	101.325	CAMEO CHEMICALS <a href="https://cameochemicals.noaa.gov/chemical/17804">https://cameochemicals.noaa.gov/chemical/17804</a>
<b>Dimethyl phthalate</b>		
<b>T/K</b>	<b>P<sub>A</sub> (kPa)</b>	<b>Source</b>
293.15	0.0002	CAS-No. 131-11-3, Sigma-Aldrich Co., Dimethyl Phthalate
298.15	0.0004	(Daubert, 1989); URL: <a href="https://toxnet.nlm.nih.gov/cgi-bin/sis/search2/f?./temp/~Ycadp8:2">https://toxnet.nlm.nih.gov/cgi-bin/sis/search2/f?./temp/~Ycadp8:2</a>
373.15	0.1300	CAS-No. 131-11-3, Sigma-Aldrich Co., Dimethyl Phthalate
373.45	0.1333	(Roháč et al., 1999)
404.93	0.6666	(Roháč et al., 1999)
420.76	1.3332	(Roháč et al., 1999)
437.15	2.6664	(Roháč et al., 1999)
455.95	5.3329	(Roháč et al., 1999)
466.106	8.3710	(Roháč et al., 1999)
467.15	7.9993	(Roháč et al., 1999)
474.85	11.1130	(Roháč et al., 1999)
481.441	13.9670	(Roháč et al., 1999)
483.15	13.3322	(Roháč et al., 1999)

487.539	16.8560	(Roháč et al., 1999)
493.754	20.3600	(Roháč et al., 1999)
500.261	24.6530	(Roháč et al., 1999)
505.85	26.6645	(Roháč et al., 1999)
506.556	29.4960	(Roháč et al., 1999)
512.673	34.9410	(Roháč et al., 1999)
518.54	40.9170	(Roháč et al., 1999)
530.95	53.3289	(Roháč et al., 1999)
555.2	101.3250	(Roháč et al., 1999)
556.85	101.3250	(O'Neil, 2013) URL: <a href="https://toxnet.nlm.nih.gov/cgi-bin/sis/search2/f?./temp/~Ycadp8:2">https://toxnet.nlm.nih.gov/cgi-bin/sis/search2/f?./temp/~Ycadp8:2</a>

---

<b>DEET</b>		
<b>T/K</b>	<b>P<sub>A</sub> (kPa)</b>	<b>Source</b>
293.15	1.10E-04	URL: <a href="https://toxnet.nlm.nih.gov/cgi-bin/sis/search2">https://toxnet.nlm.nih.gov/cgi-bin/sis/search2</a>
298.15	7.47E-04	(Drapeau et al., 2011)
298.15	2.67E-04	Blaine R.L. (1976). URL: <a href="https://toxnet.nlm.nih.gov/cgi-bin/sis/search2">https://toxnet.nlm.nih.gov/cgi-bin/sis/search2</a>
298.15	2.30E-04	CAS-No. 134-62-3, Sawyer Co., DEET
298.15	2.27E-04	URL: <a href="https://www.cdpr.ca.gov/docs/risk/rcd/deet.pdf">https://www.cdpr.ca.gov/docs/risk/rcd/deet.pdf</a>
384.15	1.33E-01	CAMEO Chemicals.URL: <a href="https://cameochemicals.noaa.gov/chemical/20199">https://cameochemicals.noaa.gov/chemical/20199</a>
433.15	2.533	(Haynes, 2014). URL: <a href="https://toxnet.nlm.nih.gov/cgi-bin/sis/search2">https://toxnet.nlm.nih.gov/cgi-bin/sis/search2</a>
558.15	101.325	CAMEO Chemicals.URL: <a href="https://cameochemicals.noaa.gov/chemical/20199">https://cameochemicals.noaa.gov/chemical/20199</a>

---

**Ethyl anthranilate**

<b>T/K</b>	<b>P<sub>A</sub> (kPa)</b>	<b>Source</b>
293.15	8.00E-04	URL: <a href="https://toxnet.nlm.nih.gov/cgi-bin/sis/search2">https://toxnet.nlm.nih.gov/cgi-bin/sis/search2</a>
293.15	8.47E-04	(Api et al., 2015)
298.15	1.33E-03	(Islam et al., 2017b)
298.15	1.37E-03	(Api et al., 2015)
373.4	0.13	URL: <a href="https://toxnet.nlm.nih.gov/cgi-bin/sis/search2">https://toxnet.nlm.nih.gov/cgi-bin/sis/search2</a>
402.7	1	(Milwaukee, 1990). URL: <a href="https://webbook.nist.gov/cgi/cbook.cgi?">https://webbook.nist.gov/cgi/cbook.cgi?</a>
404.9	0.67	URL: <a href="https://toxnet.nlm.nih.gov/cgi-bin/sis/search2">https://toxnet.nlm.nih.gov/cgi-bin/sis/search2</a>
419.2	2	(Weast and Grasselli, 1989). URL: <a href="https://webbook.nist.gov/cgi/cbook.cgi?">https://webbook.nist.gov/cgi/cbook.cgi?</a>
420.8	1.33	URL: <a href="https://toxnet.nlm.nih.gov/cgi-bin/sis/search2">https://toxnet.nlm.nih.gov/cgi-bin/sis/search2</a>
541.2	101.325	(Lide, 2004). URL: <a href="https://toxnet.nlm.nih.gov/cgi-bin/sis/search2">https://toxnet.nlm.nih.gov/cgi-bin/sis/search2</a>

---

**IR3535**

<b>T/K</b>	<b>P<sub>A</sub> (kPa)</b>	<b>Source</b>
293.15	1.50E-04	(O'Neil, 2013). URL: <a href="https://toxnet.nlm.nih.gov/cgi-bin/sis/search2">https://toxnet.nlm.nih.gov/cgi-bin/sis/search2</a>
381.15	0.027	(O'Neil, 2013). URL: <a href="https://toxnet.nlm.nih.gov/cgi-bin/sis/search2">https://toxnet.nlm.nih.gov/cgi-bin/sis/search2</a>
383.15	0.02	(O'Neil, 2013). URL: <a href="https://toxnet.nlm.nih.gov/cgi-bin/sis/search2">https://toxnet.nlm.nih.gov/cgi-bin/sis/search2</a>
399.15	0.067	(O'Neil, 2013). URL: <a href="https://toxnet.nlm.nih.gov/cgi-bin/sis/search2">https://toxnet.nlm.nih.gov/cgi-bin/sis/search2</a>
400.15	0.067	(O'Neil, 2013). URL: <a href="https://toxnet.nlm.nih.gov/cgi-bin/sis/search2">https://toxnet.nlm.nih.gov/cgi-bin/sis/search2</a>
565.15	101.325	(O'Neil, 2013). URL: <a href="https://toxnet.nlm.nih.gov/cgi-bin/sis/search2">https://toxnet.nlm.nih.gov/cgi-bin/sis/search2</a>

---

<b>Icaridin</b>		
<b>T/K</b>	<b>P<sub>A</sub> (kPa)</b>	<b>Source</b>
293.15	3.40E-05	(O'Neil, 2013). URL: <a href="https://toxnet.nlm.nih.gov/cgi-bin/sis/search2">https://toxnet.nlm.nih.gov/cgi-bin/sis/search2</a>
298.15	5.90E-05	(O'Neil, 2013). URL: <a href="https://toxnet.nlm.nih.gov/cgi-bin/sis/search2">https://toxnet.nlm.nih.gov/cgi-bin/sis/search2</a>
323.15	7.10E-04	(O'Neil, 2013). URL: <a href="https://toxnet.nlm.nih.gov/cgi-bin/sis/search2">https://toxnet.nlm.nih.gov/cgi-bin/sis/search2</a>
569.15	101.325	(O'Neil, 2013). URL: <a href="https://toxnet.nlm.nih.gov/cgi-bin/sis/search2">https://toxnet.nlm.nih.gov/cgi-bin/sis/search2</a>

---



### Appendix III: Parameters calculated to predict diffusion coefficient for repellents

#### DEET

**WILKE and LEE equation used.** As suggested in the text by (Poling, 2000), for air  $\sigma_{\text{air}} = 3.62 \text{ \AA}$  and  $\varepsilon/k = 97.0 \text{ K}$  and  $M(\text{air}) = 28.97 \text{ g}\cdot\text{mol}^{-1}$ .

For DEET, from, Cameo data sheet: <https://www.chemeo.com/cid/13-6389/Diethyltoluamide>

Parameters	Values	Units	Values	Units
$P_c$	2.520	Mpa	25.2	bar
$T_c$	778.2	K	-	-
$V_c$	0.6	$\text{m}^3\cdot\text{kg}\cdot\text{mol}^{-1}$	600	$\text{cm}^3\cdot\text{mol}^{-1}$
$T_b$	561.15	K	-	-
$M_{(\text{DEET})}$	191.3	$\text{g}\cdot\text{mol}^{-1}$	-	-
$R$	83.14	$\text{bar}\cdot\text{cm}^3\cdot\text{mol}^{-1}\cdot\text{K}^{-1}$	-	-

Thus the parameters for DEET were calculated.

$$Z_c = [(25.2)(600)/(83.14)(778.2)] = 0.234$$

$$\varepsilon(\text{DEET})/k = (1.15)(561.15) = 645.323 \text{ K}$$

$$V_b = (600)(0.234)^{[(1-561.15/778.2)^{2/7}]} = 218.67 \text{ cm}^3 \cdot \text{mol}^{-1}$$

$$\sigma(\text{DEET}) = (1.18)(218.67)^{1/3} = 7.109 \text{ \AA}$$

Then, parameters for DEET combined with air as illustrated (DEET-air) were calculated:

$$\varepsilon(\text{DEET-air})/k = [(645.323)(97.0)]^{1/2} = 250.193 \text{ K}$$

$$\sigma(\text{DEET-air}) = (7.109+3.62)/2 = 5.363 \text{ \AA}$$

$$\text{As } M(\text{DEET}) = 191 \text{ g}\cdot\text{mol}^{-1}, \text{ then, } M(\text{DEET-air}) = [(1/191)+(1/28.97)]^{-1} = 50.319$$

## Dimethyl phthalate

**WILKE and LEE equation used.** As suggested in the text by (Poling, 2000), for air  $\sigma_{\text{air}} = 3.62 \text{ \AA}$  and  $\varepsilon/k = 97.0 \text{ K}$  and  $M(\text{air}) = 28.97 \text{ g}\cdot\text{mol}^{-1}$ .

For DMP, from, Cameo data sheet: <https://www.chemeo.com/cid/21-7208/Dimethyl%20phthalate>

Parameters	Values	units	Values	units
$P_c$	3.190	Mpa	31.9	bar
$T_c$	831.5	K	-	-
$V_c$	0.54	$\text{m}^3\cdot\text{kg}^{-1}\cdot\text{mol}^{-1}$	540	$\text{cm}^3\cdot\text{mol}^{-1}$
$T_b$	555.15	K	-	-
$M_{(\text{DMP})}$	194.18	$\text{g}\cdot\text{mol}^{-1}$	-	-
$R$	83.14	$\text{bar}\cdot\text{cm}^3\cdot\text{mol}^{-1}\cdot\text{K}^{-1}$	-	-

Thus the parameters for DMP were calculated.

$$Z_c = [(31.9)(540)/(83.14)(831.5)] = 0.249$$

$$\varepsilon(\text{DMP})/k = (1.15)(555.15) = 638.423 \text{ K}$$

$$V_b = (540)(0.249)^{[(1-555.15/831.5)^{2/7}]} = 195.82 \text{ cm}^3 \cdot \text{mol}^{-1}$$

$$\sigma(\text{DMP}) = (1.18)(195.82)^{1/3} = 6.852 \text{ \AA}$$

Then, parameters for DMP combined with air as illustrated (DMP-air) were calculated.

$$\varepsilon(\text{DMP-air})/k = [(638.423)(97.0)]^{1/2} = 248.851 \text{ K}$$

$$\sigma(\text{DMP-air}) = (6.852+3.62)/2 = 5.235 \text{ \AA}$$

$$\text{As } M(\text{DMP}) = 194.18 \text{ g}\cdot\text{mol}^{-1}, \text{ then, } M(\text{DMP-air}) = [(1/194.18)+(1/28.97)]^{-1} = 50.418$$

## Ethyl anthranilate

**WILKE and LEE equation used.** As suggested in the text by (Poling, 2000), for air  $\sigma_{\text{air}} = 3.62 \text{ \AA}$  and  $\varepsilon/k = 97.0 \text{ K}$  and  $M(\text{air}) = 28.97 \text{ g}\cdot\text{mol}^{-1}$ .

For EA, from, Cameo data sheet: <https://www.chemeo.com/cid/32-146-4/Benzoic%20acid%2C%202-amino-%2C%20ethyl%20ester>

Parameters	Values	units	Values	units
$P_c$	3.620	Mpa	36.2	bar
$T_c$	812.1	K	-	-
$V_c$	0.48	$\text{m}^3\cdot\text{kg}^{-1}\cdot\text{mol}^{-1}$	480	$\text{cm}^3\cdot\text{mol}^{-1}$
$T_b$	541.15	K	-	-
$M_{(\text{EA})}$	165.19	$\text{g}\cdot\text{mol}^{-1}$	-	-
$R$	83.14	$\text{bar}\cdot\text{cm}^3\cdot\text{mol}^{-1}\cdot\text{K}^{-1}$	-	-

Thus the parameters for EA were calculated.

$$Z_c = [(36.2)(480)/(83.14)(812.2)] = 0.257$$

$$\varepsilon(\text{EA})/k = (1.15)(541.15) = 622.323 \text{ K}$$

$$V_b = (480)(0.257)^{[(1-541.15/812.1)^{2/7}]} = 178.017 \text{ cm}^3 \cdot \text{mol}^{-1}$$

$$\sigma(\text{EA}) = (1.18)(178.017)^{1/3} = 6.638 \text{ \AA}$$

Then the parameters for EA combined with air as illustrated (EA-air) were calculated.

$$\varepsilon(\text{EA-air})/k = [(622.323)(97.0)]^{1/2} = 245.694 \text{ K}$$

$$\sigma(\text{EA-air}) = (6.638+3.62)/2 = 5.127 \text{ \AA}$$

$$\text{As } M(\text{EA}) = 165.19 \text{ g}\cdot\text{mol}^{-1}, \text{ then } M(\text{EA-air}) = [(1/165.19)+(1/28.97)]^{-1} = 49.295.$$

## Decanoic acid

**WILKE and LEE equation used.** As suggested in the text by (Poling, 2000), for air  $\sigma_{\text{air}} = 3.62 \text{ \AA}$  and  $\varepsilon/k = 97.0 \text{ K}$  and  $M(\text{air}) = 28.97 \text{ g}\cdot\text{mol}^{-1}$ .

For DA, from Cameo data sheet: <https://www.chemeo.com/cid/13-6389/Diethyltoluamide>

Parameters	Values	units	Values	units
$P_c$	2.1617	Mpa	21.617	bar
$T_c$	720.53	K	-	-
$V_c$	0.62	$\text{m}^3\cdot\text{kg}^{-1}\cdot\text{mol}^{-1}$	620	$\text{cm}^3\cdot\text{mol}^{-1}$
$T_b$	541.85	K	-	-
$M_{(\text{DA})}$	172.27	$\text{g}\cdot\text{mol}^{-1}$	-	-
$R$	83.14	$\text{bar}\cdot\text{cm}^3\cdot\text{mol}^{-1}\cdot\text{K}^{-1}$	-	-

Thus the parameters for DA were calculated.

$$Z_c = [(21.617)(620)/(83.14)(720.53)] = 0.224$$

$$\varepsilon(\text{DA})/k = (1.15)(541.85) = 623.128 \text{ K}$$

$$V_b = (620)(0.224)^{[(1-541.85/720.53)^{2/7}]} = 226.882 \text{ cm}^3 \cdot \text{mol}^{-1}$$

$$\sigma(\text{DA}) = (1.18)(226.882)^{1/3} = 7.197 \text{ \AA}$$

Then the parameters for DA combined with air as illustrated (DA-air) were calculated.

$$\varepsilon(\text{DA-air})/k = [(623.128)(97.0)]^{1/2} = 245.852 \text{ K}$$

$$\sigma(\text{DA-air}) = (7.197+3.62)/2 = 5.407 \text{ \AA}$$

$$\text{As } M(\text{DA}) = 172.27 \text{ g}\cdot\text{mol}^{-1}, \text{ then, } M(\text{DA-air}) = [(1/172.27)+(1/28.97)]^{-1} = 49.599$$

### IR3535

**WILKE and LEE equation used.** As suggested in the text by (Poling, 2000), for air  $\sigma_{\text{air}} = 3.62 \text{ \AA}$  and  $\varepsilon/k = 97.0 \text{ K}$  and  $M(\text{air}) = 28.97 \text{ g}\cdot\text{mol}^{-1}$ .

Parameters	Values	Units
$T_b$	565.15	K
$M$	215.29	$\text{g}\cdot\text{mol}^{-1}$

Thus the parameters for IR3535 were calculated.

$$\varepsilon(\text{IR3535})/k = (1.15)(565.15) = 649.922 \text{ K}$$

$$V_b = 7*(11+21+3+1+2) = 266 \text{ cm}^3\cdot\text{mol}^{-1}$$

$$\sigma(\text{IR3535}) = (1.18)(266)^{1/3} = 7.589 \text{ \AA}$$

Then the parameters for IR3535 combined with air as illustrated (IR3535-air) were calculated.

$$\varepsilon(\text{IR3535-air})/k = [(649.922)(97.0)]^{1/2} = 251.083 \text{ K}$$

$$\sigma(\text{IR3535-air}) = (7.589+3.62)/2 = 5.603 \text{ \AA}$$

$$\text{As } M(\text{IR3535}) = 215.29 \text{ g}\cdot\text{mol}^{-1}, \text{ then, } M(\text{IR3535-air}) = [(1/215.29)+(1/28.97)]^{-1} = 51.068$$

## Icaridin

**WILKE and LEE equation used.** As suggested in the text by Poling (2000), for air  $\sigma_{\text{air}} = 3.62 \text{ \AA}$  and  $\varepsilon/k = 97.0 \text{ K}$  and  $M(\text{air}) = 28.97 \text{ g}\cdot\text{mol}^{-1}$ .

Parameters	Values	Units
$T_b$	569.15	K
$M$	229.3	$\text{g}\cdot\text{mol}^{-1}$

Thus the parameters for Icaridin<sup>®</sup> were calculated.

$$\varepsilon(\text{Icaridin})/k = (1.15)(569.15) = 654.523 \text{ K}$$

$$V_b = 7*(12+23+3+1+1)-7 = 273 \text{ cm}^3\cdot\text{mol}^{-1}$$

$$\sigma(\text{Icaridin}) = (1.18)(273)^{1/3} = 7.655 \text{ \AA}$$

Then the parameters for Icaridin<sup>®</sup> combined with air as illustrated (Icaridin<sup>®</sup>-air) were calculated.

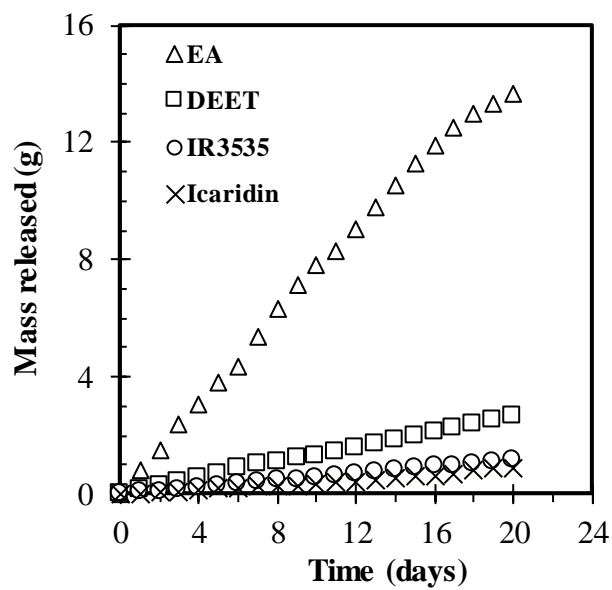
$$\varepsilon(\text{Icaridin-air})/k = [(654.523)(97.0)]^{1/2} = 251.969 \text{ K}$$

$$\sigma(\text{Icaridin-air}) = (7.655+3.62)/2 = 5.636 \text{ \AA}$$

$$\text{As } M(\text{Icaridin}) = 229.3 \text{ g}\cdot\text{mol}^{-1}, \text{ then } M(\text{Icaridin-air}) = [(1/229.3)+(1/28.97)]^{-1} = 51.441$$

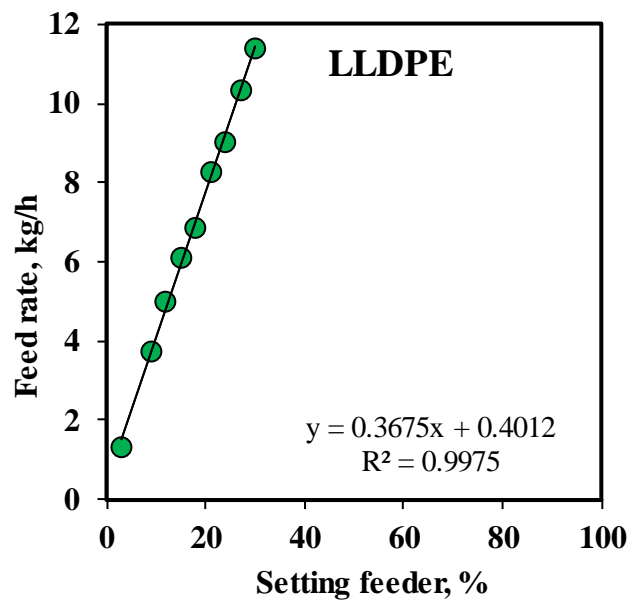
#### Appendix IV: Isothermal repellent evaporation from open cups

The isothermal evaporation of the repellents from open Payne cups was conducted at 50 °C in a convection oven for 20 days. Ethyl anthranilate was the most volatile repellent followed by DEET, IR3535 and lastly Icaridin.



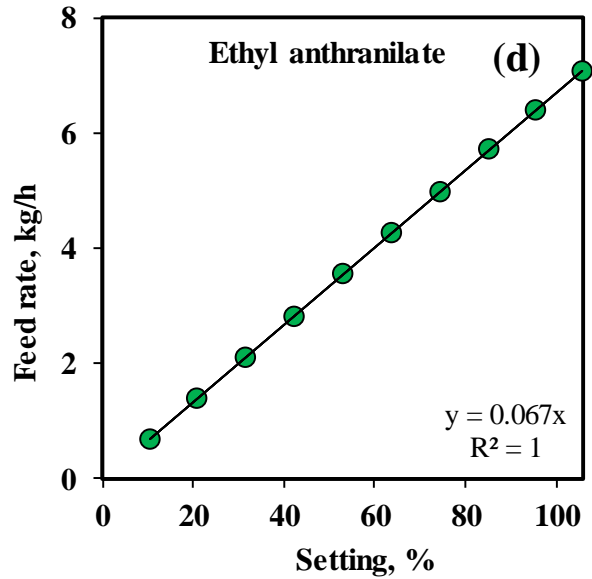
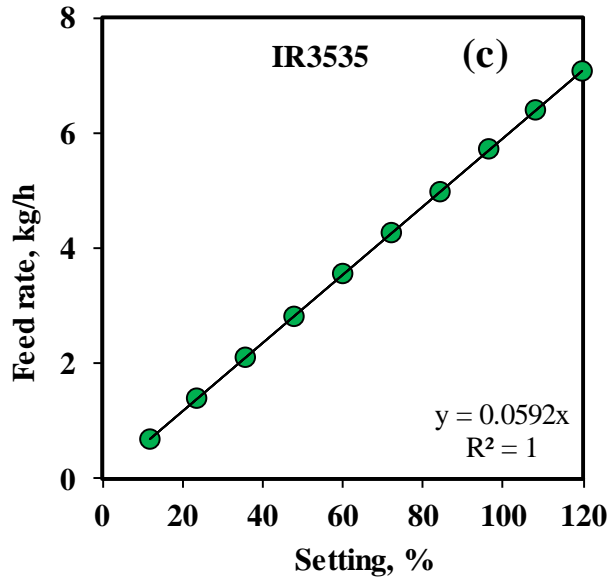
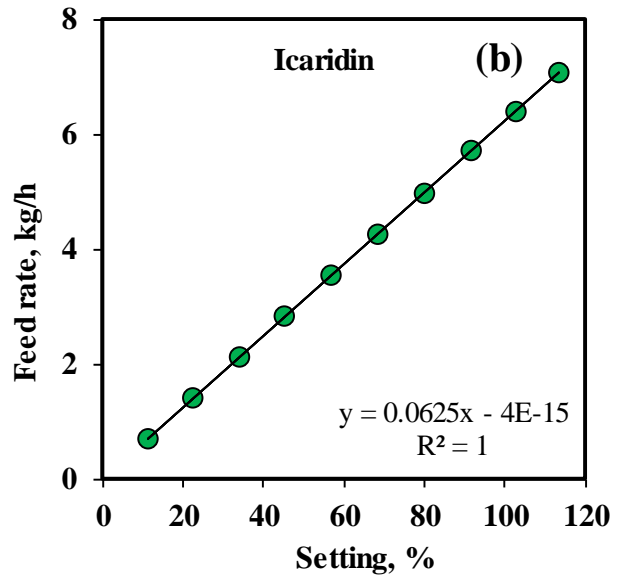
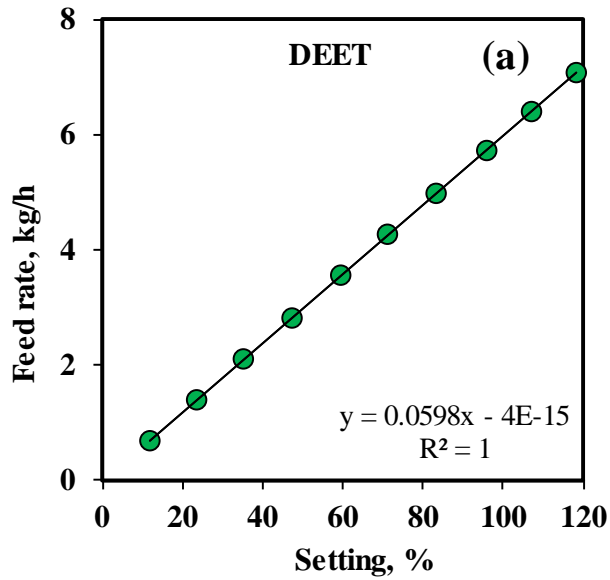
**Appendix V: Calibration of setting feeder for LLDPE and pump feed for (a) DEET; (b) Icaridin; (c) IR3535; and (d) ethyl anthranilate**

The calibration setting feeder for the LLDPE was studied. However, the  $R^2$  value on the chart is 0.9975, indicating accurate calibration.





The pump feed calibration for the DEET, Icaridin, IR3535 and ethyl anthranilate repellents was studied. The  $R^2$  value on the chart is one (1) for all repellents. These values on the chart indicate accurate calibration.



**Appendix VI: Conditions of compounding of the LLDPE strands impregnated with repellent without clay**

---

<b>Samples</b>	<b>Setting Feeder</b>	<b>Kg/h</b>	<b>Pump Feed</b>	<b>Kg/h</b>	<b>LLDPE (wt %)</b>	<b>Repellent (wt %)</b>	<b>Screw speed (rpm)</b>	<b>T/(°C)</b>
LLDPE Virgin	4	1.87212	0	0	100	0	147.74	210
LLDPE/IR3535	4	1.87212	20	1.3404	58	42	46.65	210
LLDPE/DEET	4	1.87212	20	1.324	59	41	46.65	210
LLDPE/EA	4	1.87212	20	1.4763	56	44	46.65	210
LLDPE/Icaridin	4	1.87212	20	1.3359	58	42	46.65	210

---

**Appendix VII: Typical compounder settings, i.e. temperature profiles from hopper to die and screw speed used to compound polymer strands**

TX28P extrusion conditions used to compound a composition comprising LLDPE (60 wt.%), fumed silica (5 wt.%), organoclay (5 wt.%) and DEET (30 wt.%).

<b>Conditions</b>	<b>Zone 1 (°C)</b>	<b>Zone 2 (°C)</b>	<b>Zone 3 (°C)</b>	<b>Die (°C)</b>	<b>Screw speed (rpm)</b>
Set	140	175	180	190	150
Read	140.6	175.2	178.6	190.5	150

TX28P extrusion conditions used to compound a composition comprising LLDPE (50 wt.%), fumed silica (5 wt.%), organoclay (5 wt.%) and DEET (40 wt.%).

<b>Conditions</b>	<b>Zone 1 (°C)</b>	<b>Zone 2 (°C)</b>	<b>Zone 3 (°C)</b>	<b>Die (°C)</b>	<b>Screw speed (rpm)</b>
Set	140	175	180	190	150
Read	138.6	175	180.1	190	150

TX28P extrusion conditions used to compound a composition comprising LLDPE (60 wt.%), fumed silica (5 wt.%), organoclay (5 wt.%) and Icaridin (30 wt.%).

<b>Conditions</b>	<b>Zone 1 (°C)</b>	<b>Zone 2 (°C)</b>	<b>Zone 3 (°C)</b>	<b>Die (°C)</b>	<b>Speed screw (rpm)</b>
Set	140	175	180	190	150
Read	141.3	174.3	179.5	189.6	150

TX28P extrusion conditions used to compound a composition comprising LLDPE (50 wt.%), fumed silica (5 wt.%), organoclay (5 wt.%) and Icaridin (40 wt.%).

<b>Conditions</b>	<b>Zone 1 (°C)</b>	<b>Zone 2 (°C)</b>	<b>Zone 3 (°C)</b>	<b>Die (°C)</b>	<b>Screw speed (rpm)</b>
Set	140	160	170	170	150
Read	148.5	157.8	165.3	172.1	150

TX28P extrusion conditions used to compound a composition comprising LLDPE (60 wt.%), fumed silica (5 wt.%), organoclay (5 wt.%) and IR3535 (30 wt.%).

<b>Conditions</b>	<b>Zone 1 (°C)</b>	<b>Zone 2 (°C)</b>	<b>Zone 3 (°C)</b>	<b>Die (°C)</b>	<b>Screw speed (%)</b>
Set	140	160	170	170	150
Read	142.6	154.6	170.5	169.8	150

TX28P extrusion conditions used to compound a composition comprising LLDPE (50 wt.%), fumed silica (5 wt.%), organoclay (5 wt.%) and IR3535 (40 wt.%).

<b>Conditions</b>	<b>Zone 1 (°C)</b>	<b>Zone 2 (°C)</b>	<b>Zone 3 (°C)</b>	<b>Die (°C)</b>	<b>Screw speed (rpm)</b>
Set	140	160	170	170	150
Read	142.6	154.6	170.5	169.8	150

TX28P extrusion conditions used to compound a composition comprising LLDPE (65 wt.%), organoclay (5 wt.%) and IR3535 (30 wt.%).

<b>Conditions</b>	<b>Zone 1 (°C)</b>	<b>Zone 2 (°C)</b>	<b>Zone 3 (°C)</b>	<b>Die (°C)</b>	<b>Screw speed (%)</b>
Set	140	160	170	170	150
Read	142.6	158.6	171.5	169.8	150

TX28P extrusion conditions used to compound a composition comprising LLDPE (65 wt.%), organoclay (5 wt.%) and ethyl anthranilate (30 wt.%).

<b>Conditions</b>	<b>Zone 1 (°C)</b>	<b>Zone 2 (°C)</b>	<b>Zone 3 (°C)</b>	<b>Die (°C)</b>	<b>Screw speed (rpm)</b>
Set	140	160	170	170	150
Read	142.6	159.6	170.5	170.8	150

TX28P extrusion conditions used to compound a composition comprising LLDPE (75 wt.%), organoclay (5 wt.%) and DEET (20 wt.%).

<b>Conditions</b>	<b>Zone 1 (°C)</b>	<b>Zone 2 (°C)</b>	<b>Zone 3 (°C)</b>	<b>Die (°C)</b>	<b>Screw speed (rpm)</b>
Set	140	175	180	190	150
Read	140.6	175.2	178.6	190.5	150

TX28P extrusion conditions used to compound a composition comprising LLDPE (65 wt.%), organoclay (5 wt.%) and DEET (30 wt.%).

<b>Conditions</b>	<b>Zone 1 (°C)</b>	<b>Zone 2 (°C)</b>	<b>Zone 3 (°C)</b>	<b>Die (°C)</b>	<b>Screw speed (rpm)</b>
Set	140	175	180	190	150
Read	141.6	175.2	178.6	190.5	150

TX28P extrusion conditions used to compound a composition comprising LLDPE (75 wt.%), organoclay (5 wt.%) and Icaridin (20 wt.%).

<b>Conditions</b>	<b>Zone 1 (°C)</b>	<b>Zone 2 (°C)</b>	<b>Zone 3 (°C)</b>	<b>Die (°C)</b>	<b>Screw speed (%)</b>
Set	140	160	170	170	150
Read	148.5	157.8	165.3	172.1	150

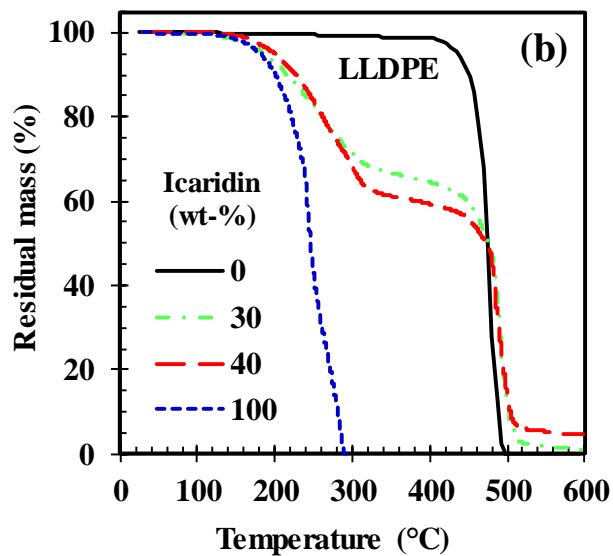
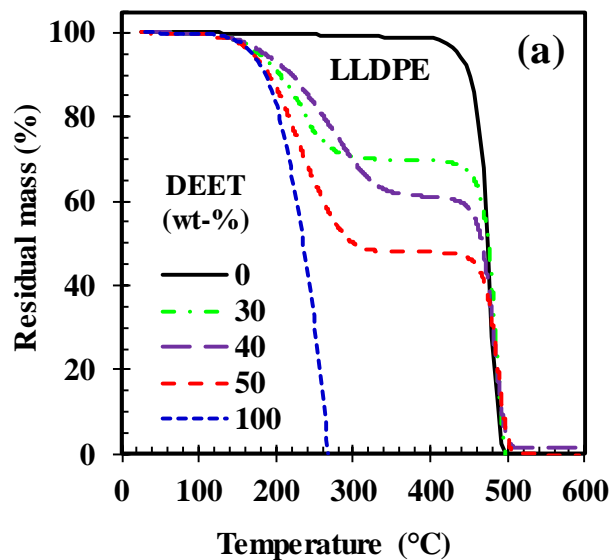
TX28P extrusion conditions used to compound a composition comprising EVA (65 wt.%), organoclay (5 wt.%) and Icaridin (30 wt.%).

<b>Conditions</b>	<b>Zone 1 (°C)</b>	<b>Zone 2 (°C)</b>	<b>Zone 3 (°C)</b>	<b>Die (°C)</b>	<b>Screw speed (rpm)</b>
Set	140	160	160	160	100
Read	143.4	160.2	159.1	160.4	100

TX28P extrusion conditions used to compound a composition comprising EVA (65wt.%), organoclay (5 wt.%) and DEET (30 wt.%).

<b>Conditions</b>	<b>Zone 1 (°C)</b>	<b>Zone 2 (°C)</b>	<b>Zone 3 (°C)</b>	<b>Die (°C)</b>	<b>Screw speed (rpm)</b>
Set	140	160	160	160	100
Read	146.5	159.7	160.7	160.3	100

**Appendix VIII: Thermogravimetric analysis (TGA) of neat DEET and Icaridin, neat LLDPE and LLDPE nanocomposite strands impregnated with repellents**





**Appendix IX: Repellent content by solvent extraction and thermogravimetric analysis**

<b>Samples</b>	<b>Repellent content by TGA (%)</b>	<b>Repellent content by solvent extraction (%)</b>	<b>Sample No.</b>
LLDPE-DEET (50)-SiO <sub>2</sub> (5)	50.55	49.07±0.05	BM100
LLDPE-DEET (40)- SiO <sub>2</sub> (5)	39.25	36.89±0.05	BM101
LLDPE-DEET (30)-SiO <sub>2</sub> (5)	30.67	27.56±0.34	BM102
LLDPE-Icaridin (30)-43B (5)- SiO <sub>2</sub> (5)	29.69	29.42±0.08	BM202
LLDPE-Icaridin (40)-43B (5)- SiO <sub>2</sub> (5)	35.24	36.00±0.07	BM203
LLDPE-Icaridin (42)	-	39.41±0.70	-
LLDPE-DEET (41)	-	40.41±0.63	-
LLDPE-IR3535 (41)	-	38.10±0.55	-
LLDPE-EA (44)	-	41.50±0.65	-

**Appendix X: Diameter size of the LLDPE strands measured by Mutotoyo Vernier caliper**

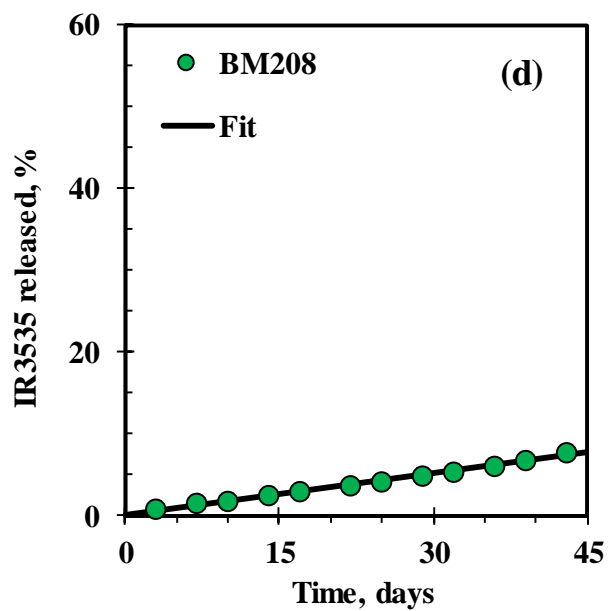
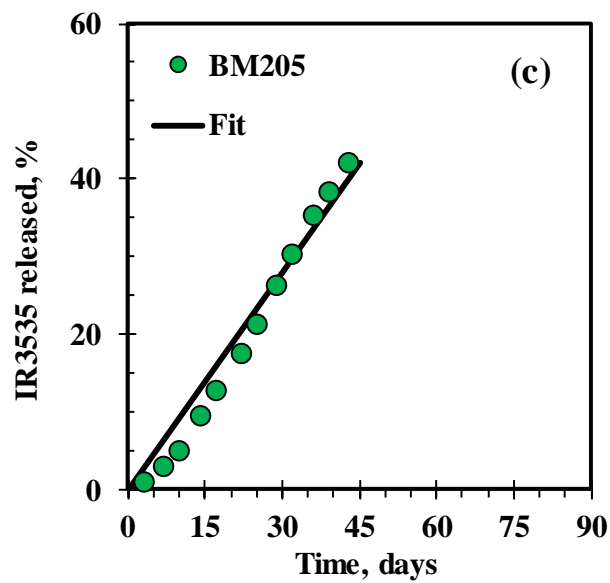
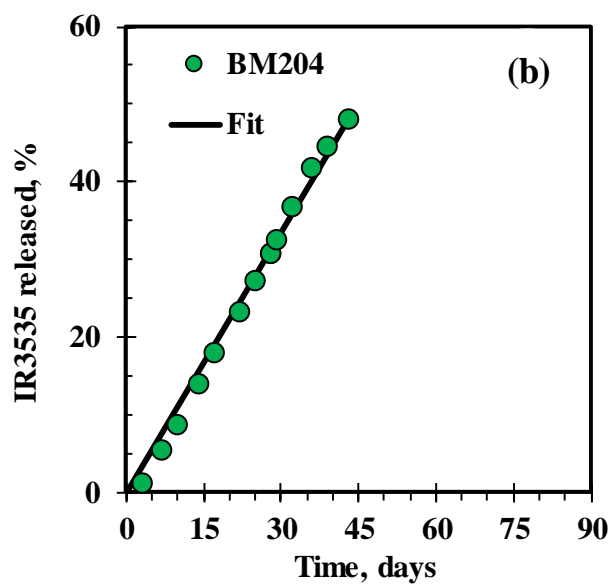
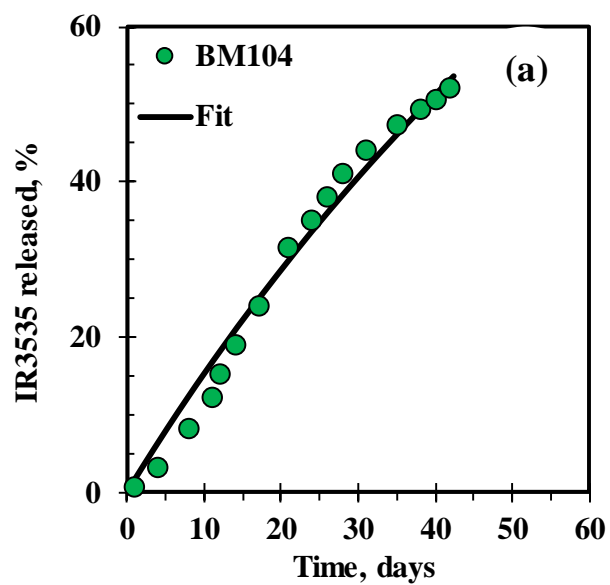
<b>Samples</b>	<b>Diameter size (mm)</b>	<b>Sample No.</b>
LLDPE-DEET (50)-SiO <sub>2</sub> (5)	3.21±0.34	BM100
LLDPE-DEET (40)- SiO <sub>2</sub> (5)	3.29±0.52	BM101
LLDPE-DEET (30)-SiO <sub>2</sub> (5)	3.93±0.54	BM102
LLDPE-DEET (30)-SiO <sub>2</sub> (5)	3.17±0.41	BM103
LLDPE-IR3535 (40)-SiO <sub>2</sub> (5)	3.31±0.44	BM104
LLDPE-Icaridin (40)-SiO <sub>2</sub> (5)	3.74±0.66	BM105
LLDPE-EA (40)-SiO <sub>2</sub> (5)	3.34±0.51	BM106
LLDPE-DEET (30)- 43B (5)- SiO <sub>2</sub> (5)	3.64±0.54	BM200
LLDPE-DEET (40)- 43B (5)- SiO <sub>2</sub> (5)	3.64±0.41	BM201
LLDPE-Icaridin (30)-43B (5)- SiO <sub>2</sub> (5)	3.64±0.25	BM202
LLDPE-Icaridin (40)-43B (5)- SiO <sub>2</sub> (5)	3.24±0.33	BM203
LLDPE-IR3535 (30)-43B (5)-SiO <sub>2</sub> (5)	3.39±0.44	BM204
LLDPE-IR3535 (40)-43B (5)-SiO <sub>2</sub> (5)	3.38±0.29	BM205
LLDPE-Icaridin (30)-43B (5)	3.74±0.21	BM206
LLDPE-EA (30)-43B (5)-SiO <sub>2</sub> (5)	2.63±0.73	BM207
LLDPE-IR3535 (30)-43 (5)	3.59±0.39	BM208

**Appendix XI: Strand diameters, release model parameters ( $\kappa_1$ ,  $\kappa_2$ ,  $\kappa_3$ ) and estimated membrane thickness ( $z_{\text{membrane}}$ ) for LLDPE microporous strands aged at 50 °C**

<b>Polymer</b>	<b>DEET (wt.%)</b>	<b>Diameter (mm)</b>	<b><math>\kappa_1 \times 10^3</math> (day<sup>-1</sup>)</b>	<b><math>\kappa_2</math> (-)</b>	<b><math>\kappa_3 \times 10^3</math> (day<sup>-1</sup>)</b>	<b><math>z_{\text{membrane}}</math> (<math>\mu\text{m}</math>)</b>	<b>Sample No.</b>
LLDPE	40	3.29±0.50	15.493	1.359	-	10	BM101
LLDPE	30	3.93±0.54	3.992	1.221	-	25	BM102
LLDPE	30	3.47±0.41	10.52	2.048	-	29	BM103
LLDPE	20	4.61±0.17	1.899	1.056	-	109	BM302A
LLDPE	20	3.42±0.16	2.911	1.132	-	94	BM302B
LLDPE	20	4.64±0.30	0.094	1.088	-	405	BM302C
LLDPE	20	3.34±0.08	0.135	1.027	-	390	BM302D
LLDPE	30	4.66±0.21	1.300	1.049	-	88	BM303A
LLDPE	30	2.87±0.15	1.968	1.075	-	94	BM303B
LLDPE	30	5.06±0.20	0.057	1.018	-	448	BM303C
LLDPE	30	3.50±0.14	0.060	1.028	-	374	BM303D
<b>Polymer</b>	<b>Icaridin (wt.%)</b>	<b>Diameter (mm)</b>	<b><math>\kappa_1 \times 10^3</math> (day<sup>-1</sup>)</b>	<b><math>\kappa_2</math> (-)</b>	<b><math>\kappa_3 \times 10^3</math> (day<sup>-1</sup>)</b>	<b><math>z_{\text{membrane}}</math> (<math>\mu\text{m}</math>)</b>	<b>Sample No.</b>
LLDPE	20	4.54±0.23	0.454	1.052	-	85	BM300A
LLDPE	20	2.26±0.05	1.105	1.099	-	60	BM300B
LLDPE	30	4.63±0.25	0.289	1.032	-	74	BM301A
LLDPE	30	2.15±0.06	0.469	1.067	-	40	BM301B

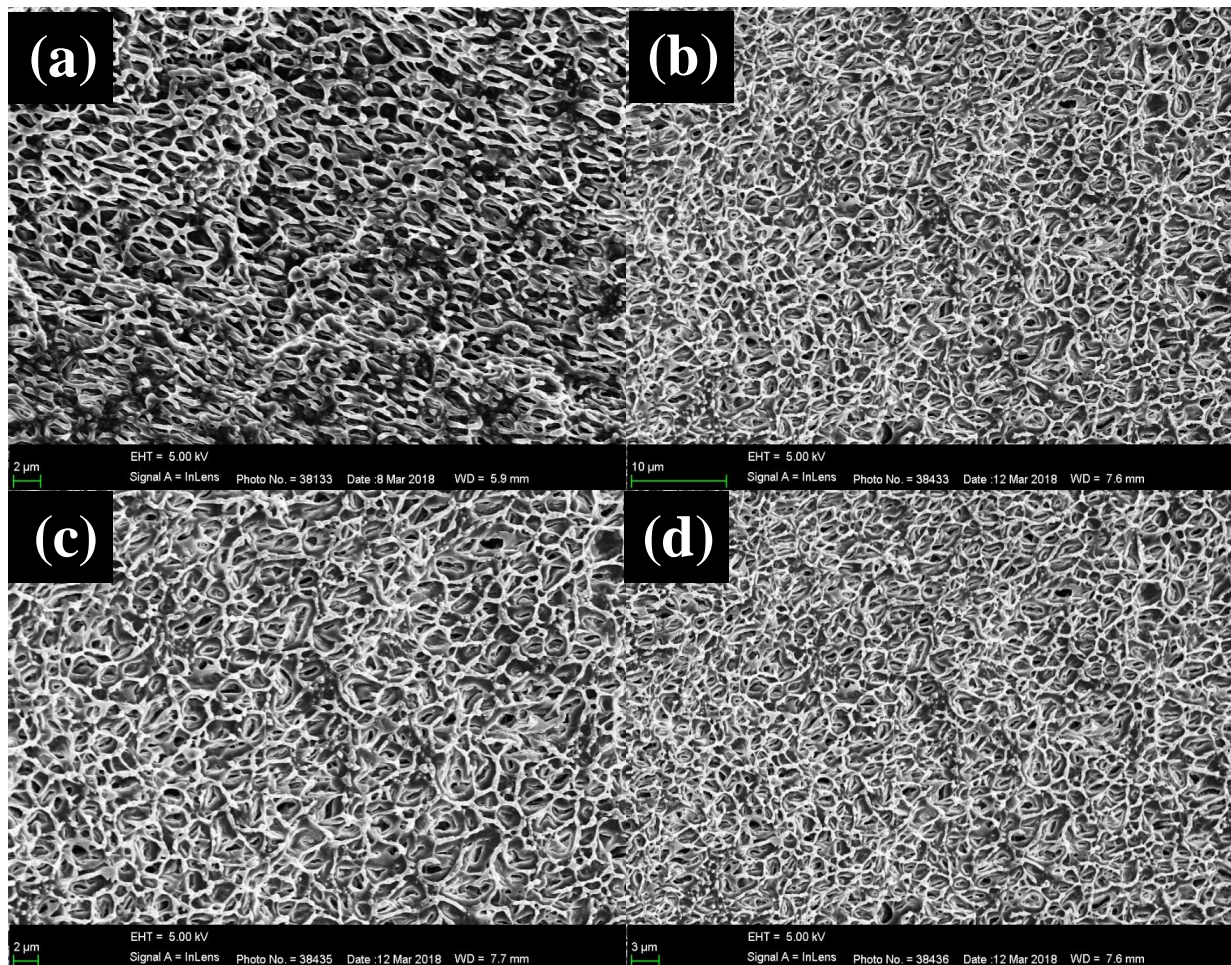
**Appendix XII: Modelling for IR3535 released from LLDPE strands. Release model parameters are also listed**

	Sample <b>BM104</b>	<b>BM204</b>	<b>BM208</b>	<b>BM205</b>	Sample
Oven temperature (°C)	<b>50</b>	<b>50</b>	<b>50</b>	<b>50</b>	Oven temperature (°C)
IR3535 (wt-%)	39.96	<b>28.16</b>	<b>26</b>	<b>37</b>	IR3535 (wt-%)
Average of IR3535	0.28	<b>0.19</b>	<b>0.194</b>	<b>0.09</b>	Average of IR3535
Dellite 43B (wt.%)	0	5	5	5	Dellite 43B (wt.%)
Fumed silica (wt.%)	5	5	0	5	Fumed silica (wt.%)
Strand diameter (mm)	3.31	3.39	3.59	3.38	Strand diameter (mm)
Std. of strand diameter	0.44	0.44	0.39	0.29	Average of strand diameter
IR3535 (wt)	0.20	0.28	0.26	0.37	IR3535 (wt)
<b><math>k_1 =</math></b>					
	<b>1.90E-02</b>	<b>6.44E+00</b>	<b>7.65E-02</b>	<b>5.87E+00</b>	
<b><math>k_2 =</math></b>					
	<b>2.159</b>	<b>576.3298</b>	<b>45.5989</b>	<b>629.911</b>	

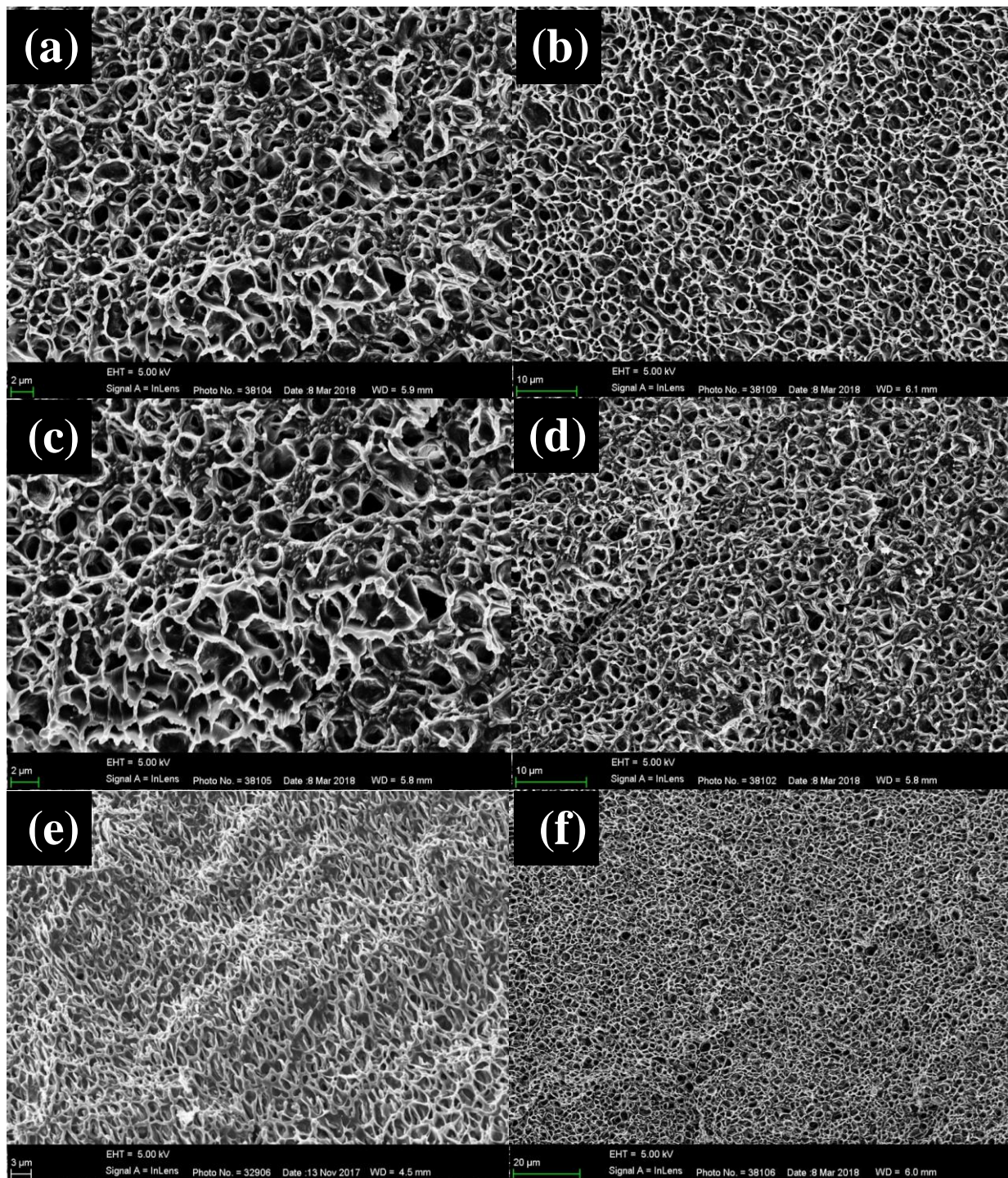


**Appendix XIII: Microporous structures of LLDPE impregnated with repellents and Dellite 43B organoclay**

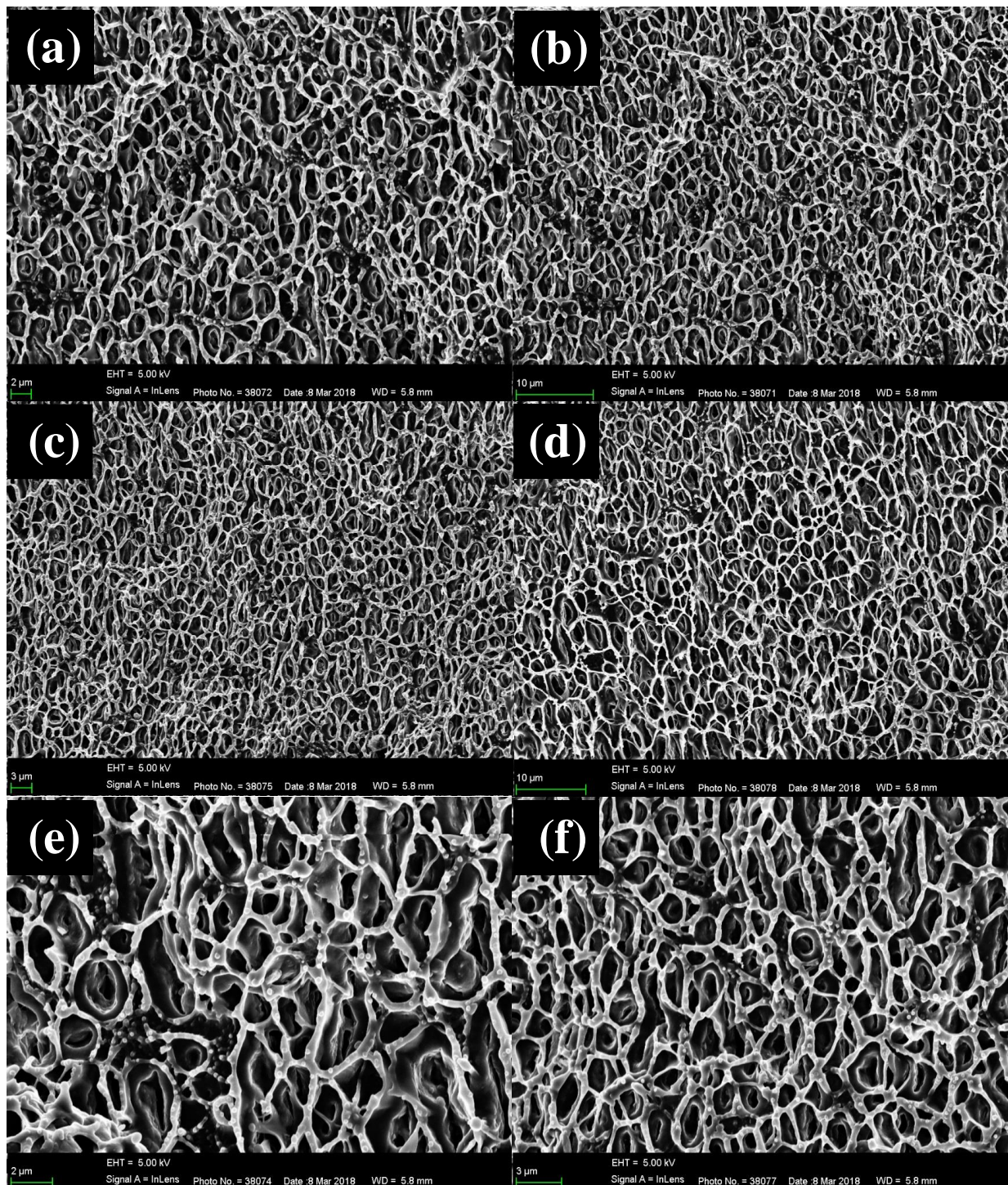
**LLDPE microporous structures formed with 20 wt.% DEET**



## LLDPE microporous structures formed with 30 wt.% DEET

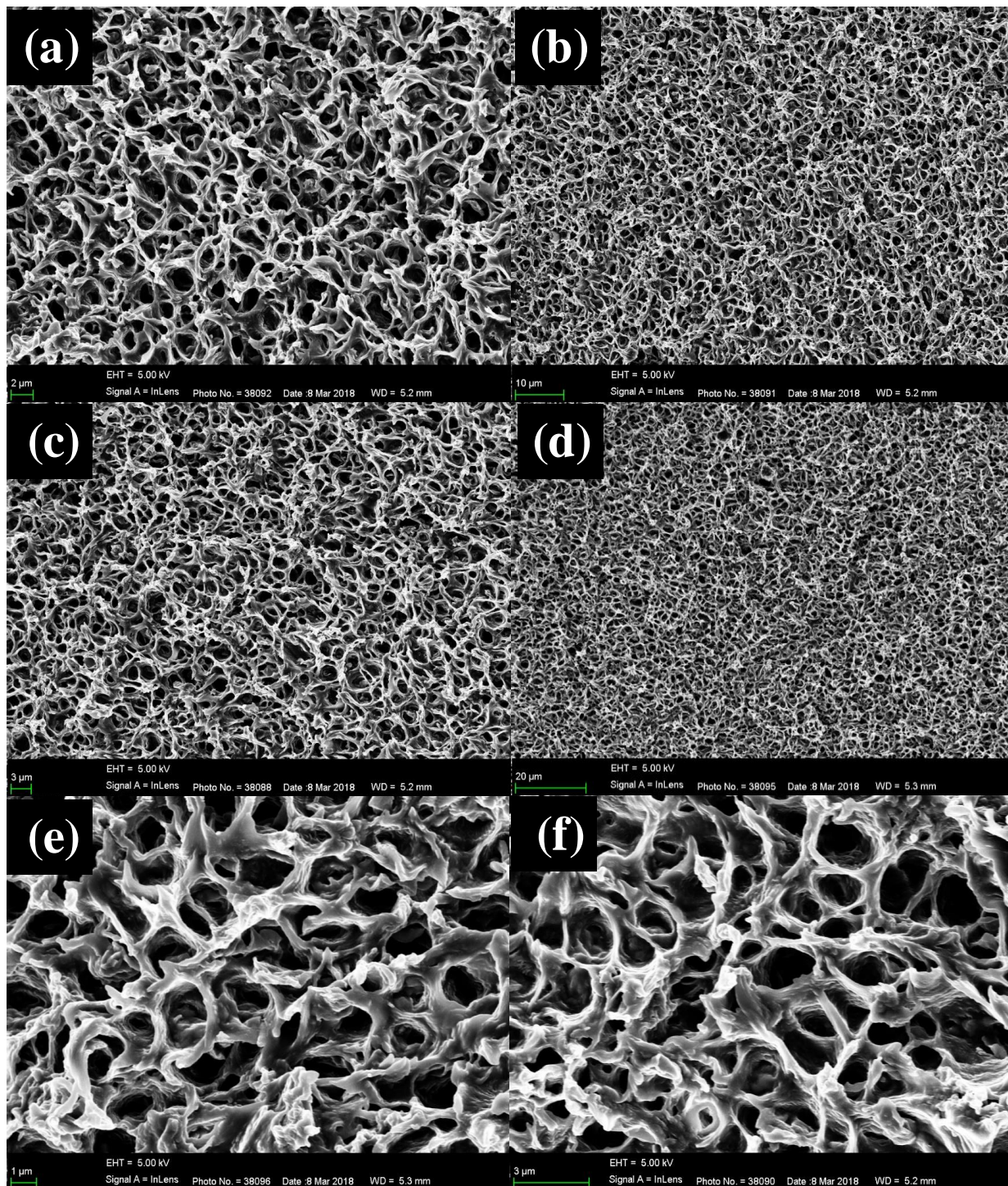


## LLDPE microporous structures formed with 20 wt.% Icaridin

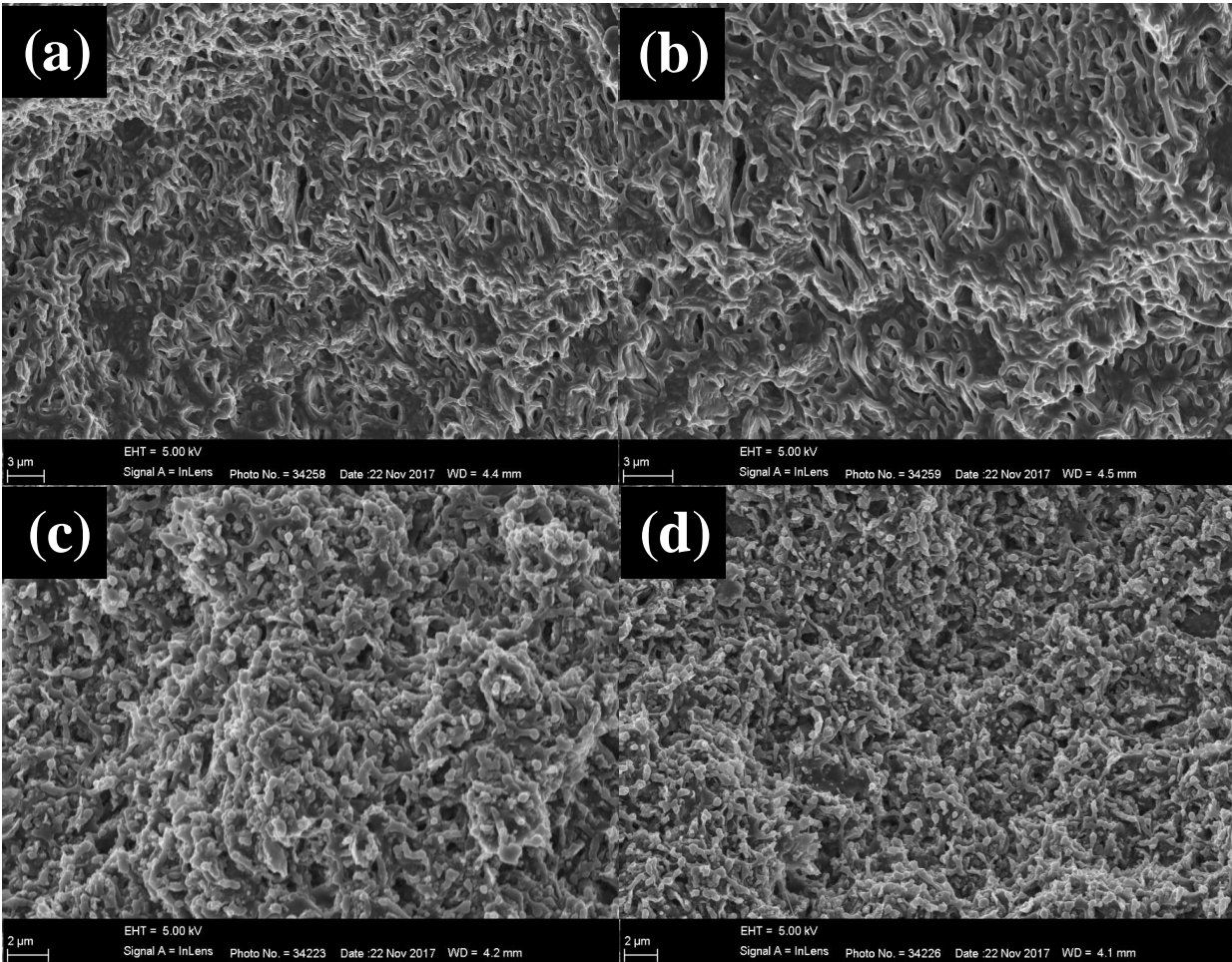




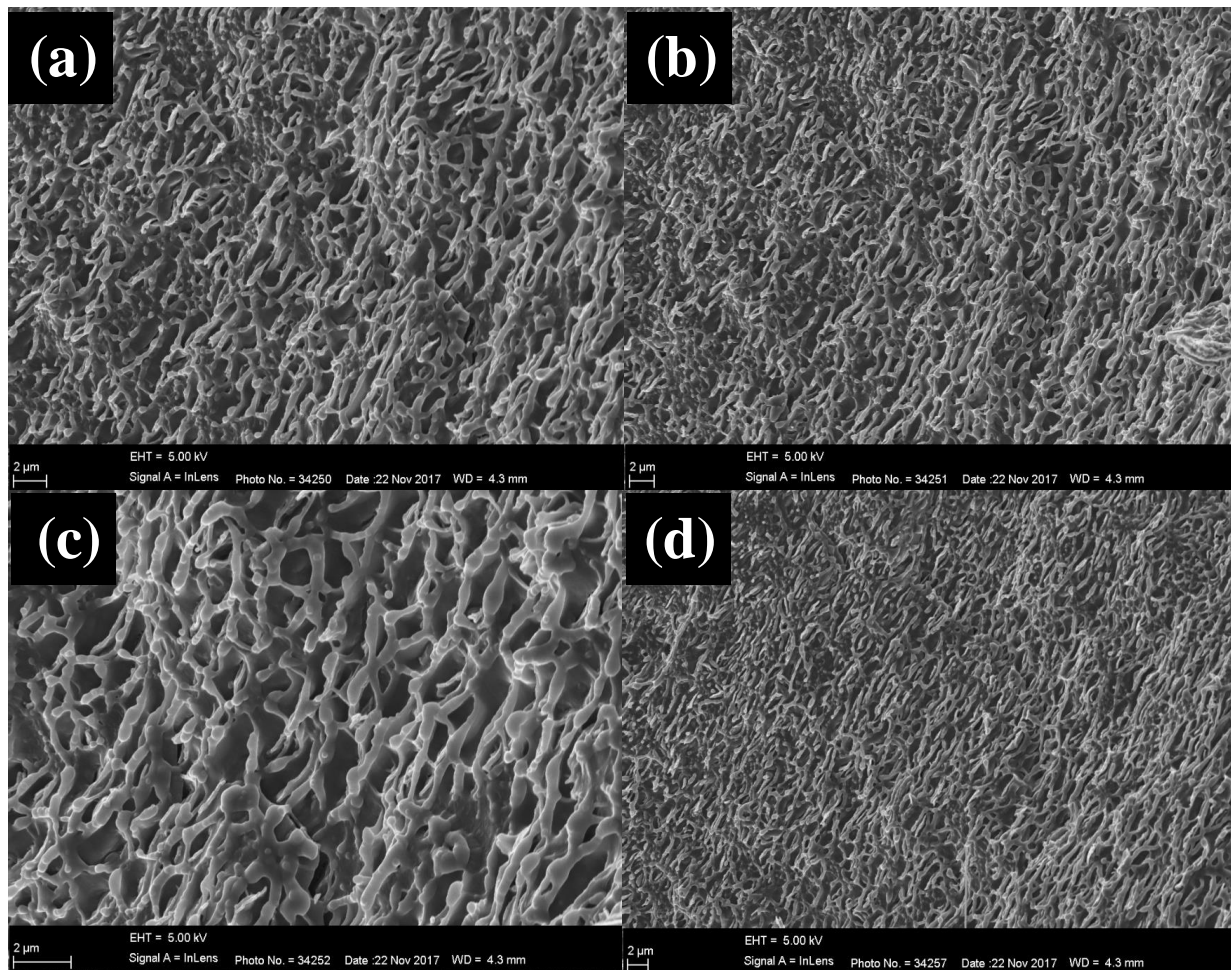
## LLDPE microporous structures formed with 30 wt.% Icaridin



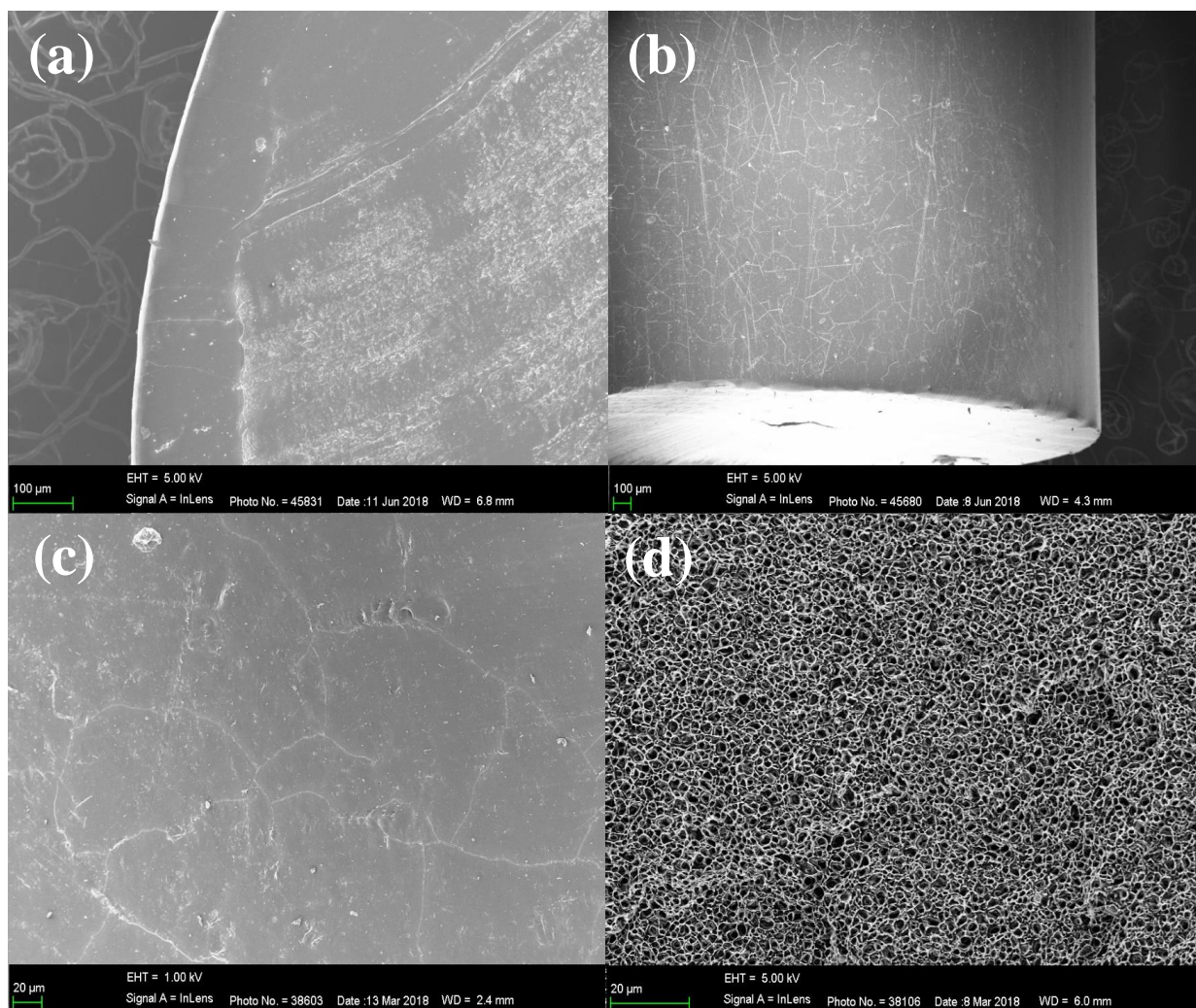
## LLDPE microporous structures formed with 30 wt.% IR3535



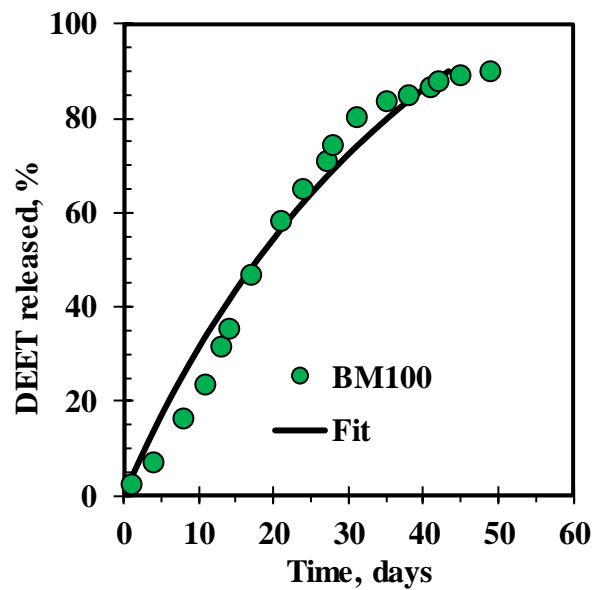
## LLDPE microporous structures formed with 30 wt.% ethyl anthranilate



## Appendix XIV: Comparison of the inner and outer surfaces of the polymer strands



Appendix XV: DEET released from polymer strands aged at 50 °C. Initially 5 wt.% Dellite 43B organoclay was added to the strand



## Appendix XVI: Protection Analysis

*Mr. Theodor Loots*

*Department of Statistics, Faculty of Natural and Agricultural Sciences, University of Pretoria*

*17 September 2018*

The factors influencing the efficiency of a mosquito repellent are analyzed below. All the analyses were performed using R Core Team (2018), and in particular the ANOVA functionality from the *car* package by Fox and Weisberg (2011).

The following data were received (See Table below):

```
'data.frame': 48 obs. of 11 variables:
 $ Product      : Factor w/ 8 levels "A","B","C","D",...: 1 1 1 1 1 1 2 2 2 2 ...
 $ Polymer      : Factor w/ 2 levels "EVA","LLDPE": 2 2 2 2 2 2 2 2 2 2 ...
 $ Repellent    : Factor w/ 2 levels "DEET", "Icaridin": 1 1 1 1 1 1 1 1 1 1 ...
 $ Level       : int 20 20 20 20 20 20 30 30 30 30 ...
 $ Week        : int 1 3 5 7 9 11 1 3 5 7 ...
 $ Test.person  : Factor w/ 3 levels "AS","BM","RT": 2 1 1 1 3 3 1 1 2 2 ...
 $ Treated.foot: Factor w/ 2 levels "L","R": 2 1 1 2 2 1 2 2 2 2 ...
 $ Time.1st.bite: int 10 23 48 103 30 54 20 21 62 79 ...
 $ Untreated.foot: int 49 39 16 20 11 26 26 98 7 40 ...
 $ Treated.foot.1: int 6 4 0 6 0 6 8 12 0 1 ...
 $ Protection: num 0.78 0.81 1 0.54 1 0.63 0.53 0.78 1 0.95 ...
```

Summary statistics for the measurement variable:

Min.	1st Qu.	Median	Mean	3rd Qu.	Max.
------	---------	--------	------	---------	------

0.4600	0.7500	0.9000	0.8496	1.0000	1.0000
--------	--------	--------	--------	--------	--------

A parametric analysis of variance (ANOVA) was performed in order to detect significant factors that might have an influence on the protection measurement of the repellent. This insures that the effect of multiple testing is sufficiently dealt with, i.e. that the probability of detecting an effect does not increase simply because more tests are performed. Following this, a non-parametric ANOVA was performed using the Kruskal-Wallis test, which makes no assumptions of the underlying data structure. In all these tests, the null hypothesis was that no effect was observed.

### ANOVA Models

	<b>Sum Sq</b>	<b>Df</b>	<b>F value</b>	<b>Pr(&gt;F)</b>
(Intercept)	0.98	1	36.39	0.0000
Polymer	0.05	1	1.70	0.1997
Repellent	0.08	1	2.83	0.1005
Level	0.01	1	0.50	0.4817
Week	0.11	1	4.05	0.0514
Test.person	0.01	2	0.13	0.8761
Treated.foot	0.00	1	0.01	0.9330
Time.1st.bite	0.02	1	0.61	0.4378
Residuals	1.02	38		

All the variables were tested simultaneously to minimize the effect of multiple testing. The product was not included as a variable, since it leads to an inversion problem of the hessian matrix. From this the following conclusions were possible: Neither product, polymer, repellent, level, test person, treated foot, nor time to first bite had a significant effect on the level of protection. The week seemed to indicate a slight relation to the level of protection. This was damped somewhat by the addition of “time to 1st bite”, which is not really an input variable to the model and may be excluded.

These variables were now analyzed separately in a non-parametric model.



### Kruskal-Wallis Test

	Kruskal.Wallis.chi.squared	df	p.value
Product	7.05	7	0.42
Polymer	0.59	1	0.44
Repellent	2.10	1	0.15
Level	0.32	1	0.57
Week	18.90	11	0.06
Test person	1.67	2	0.43
Treated foot	0.51	1	0.47

These results confirm the results of the ANOVA tests, and furthermore show that the “Week” effect is not significant at a 5% level of significance.

### Analysing pre-post data

Since the treated foot did not appear to be a significant effect in the model, the untreated foot was regarded as a control group. Here the number of probes were entered as a dependent variable, and not the protection measurement.

#### Paired t-test

Data: Count by Group  $t = 34.417$ ,  $df = 47$ ,  $p\text{-value} < 2.2e\text{-}16$

Alternative hypothesis: true difference in means is greater than 0

95% confidence interval:

0.8082174 Inf

Sample estimates:

Mean of the differences

0.84964

Wilcoxon signed rank test with continuity correction

Data: Count by Group

V = 1176, p-value = 6.335e-10

Alternative hypothesis: true location shift is greater than 0

95% confidence interval:

0.8125206 Inf

Sample estimates:

(pseudo)median

0.8729766

Therefore, although no significant effects could be detected between the different treatments, they all differed significantly from the untreated feet, indicating that being treated differed significantly from not being treated, i.e. had significantly fewer probes.

Fox, John and Sanford Weisberg. 2011. *An R Companion to Applied Regression*. 2nd edition. Thousand Oaks CA: Sage. <http://socserv.socsci.mcmaster.ca/jfox/Books/Companion>

R Core Team. 2018. *R: A language and environment for statistical computing*. Vienna, Austria: R Foundation for Statistical Computing. <https://www.R-project.org/>.

Data

Product	Polymer	Repellent	Level wt.%	Ageing weeks	Test person	Treated foot (L/R)	Time to 1st bite (s)	Number of bites		Protection
								Untreated foot #	Treated foot #	
A	LLDPE	DEET	20	1	X	R	10	49	6	0.78
A	LLDPE	DEET	20	3	Z	L	23	39	4	0.81
A	LLDPE	DEET	20	5	Z	L	48	16	0	1.00
A	LLDPE	DEET	20	7	Z	R	103	20	6	0.54
A	LLDPE	DEET	20	9	Y	R	30	11	0	1.00
A	LLDPE	DEET	20	11	Y	L	54	26	6	0.63
B	LLDPE	DEET	30	1	Z	R	20	26	8	0.53
B	LLDPE	DEET	30	3	Z	R	21	98	12	0.78
B	LLDPE	DEET	30	5	X	R	62	7	0	1.00
B	LLDPE	DEET	30	7	X	R	79	40	1	0.95
B	LLDPE	DEET	30	9	Y	R	27	7	2	0.56
B	LLDPE	DEET	30	11	X	L	26	47	4	0.84
C	LLDPE	Icaridin	20	1	Z	L	13	47	1	0.96
C	LLDPE	Icaridin	20	3	X	R	10	24	3	0.78
C	LLDPE	Icaridin	20	5	X	L	51	45	0	1.00
C	LLDPE	Icaridin	20	7	Z	R	35	18	1	0.89
C	LLDPE	Icaridin	20	9	X	R	27	27	6	0.64
C	LLDPE	Icaridin	20	11	X	L	43	41	15	0.46
D	LLDPE	Icaridin	30	1	X	L	105	18	1	0.89
D	LLDPE	Icaridin	30	3	X	L	15	62	0	1.00
D	LLDPE	Icaridin	30	5	Z	L	29	24	0	1.00
D	LLDPE	Icaridin	30	7	Z	L	57	20	0	1.00
D	LLDPE	Icaridin	30	9	X	L	24	7	0	1.00
D	LLDPE	Icaridin	30	11	Y	L	54	48	1	0.96

E	EVA	DEET	20	2	Z	R	45	36	0	1.00
E	EVA	DEET	20	4	X	R	50	33	0	1.00
E	EVA	DEET	20	6	X	L	32	11	0	1.00
E	EVA	DEET	20	8	Z	L	115	65	13	0.67
E	EVA	DEET	20	10	X	L	57	28	8	0.56
E	EVA	DEET	20	12	X	R	21	29	2	0.87
F	EVA	DEET	30	2	X	L	25	21	0	1.00
F	EVA	DEET	30	4	Z	R	36	17	0	1.00
F	EVA	DEET	30	6	Z	L	25	11	1	0.83
F	EVA	DEET	30	8	X	R	90	20	1	0.90
F	EVA	DEET	30	10	Y	L	75	43	16	0.46
F	EVA	DEET	30	12	Y	R	13	55	8	0.75
G	EVA	Icaridin	20	2	Z	L	20	22	0	1.00
G	EVA	Icaridin	20	4	Z	L	115	7	1	0.75
G	EVA	Icaridin	20	6	Z	R	34	78	4	0.90
G	EVA	Icaridin	20	8	Z	L	28	24	0	1.00
G	EVA	Icaridin	20	10	Y	R	29	13	0	1.00
G	EVA	Icaridin	20	12	Y	L	6	62	6	0.82
H	EVA	Icaridin	30	2	X	L	40	23	0	1.00
H	EVA	Icaridin	30	4	X	L	170	7	0	1.00
H	EVA	Icaridin	30	6	X	R	40	57	3	0.90
H	EVA	Icaridin	30	8	X	R	51	50	0	1.00
H	EVA	Icaridin	30	10	X	R		24	5	0.66
H	EVA	Icaridin	30	12	X	L	6	71	12	0.71

---

**Appendix XVII: Specification sheets of polymers, fumed silica and Dellite 43B organoclay considered in this study**  
**Specification of LLDPE (HR411)**

**LLDPE - Product Data Sheet**

**HR 411**

**LLDPE**

Date of issue: February 2002

Print Date: July 2002

**Information**  
 Polymer technology centre  
 P O Box 72  
 Modderfontein 1645  
 South Africa

Tel: +27 (0) 11 458 0700  
 Fax: +27 (0) 11 458 0734

**Polyethylene sales**  
 Sasol Polymers  
 Johannesburg  
 Tel: +27 (0) 11 790 1250  
 Cape Town  
 Tel: +27 (0) 21 686 7740  
 Durban  
 Tel: +27 (0) 31 267 0777

www.sasol.com/polymers



**Sasol Polymers**  
**Polythene Business**

**Rotational moulding/injection moulding**

**Melt index: 3.5 Density: 0.939**

Features	Additives	Applications
High rigidity Excellent impact strength Excellent chemical resistance Good ESCR Tough and abrasion resistant Colourable Hexene copolymer	Antioxidant	Large mouldings Thick walled containers Articles for indoor use

**Performance properties - HR 411**

Test	Value	Unit	Test method
MFI (190°C/2.16kg)	3.5	g/10min	ASTM D1238
Nominal density	0.939	g/cm <sup>3</sup>	ASTM D1505
Tensile strength at yield	19	MPa	ASTM D638 <sup>1)</sup>
Tensile strength at break	24	MPa	ASTM D638 <sup>1)</sup>
Elongation at break	820	%	ASTM D638 <sup>1)</sup>
Flexural modulus	846	MPa	ASTM D790
ESCR F <sub>50</sub>	>500	hr	ASTM D1693 <sup>2)</sup>
Impact energy at -40°C	35	J/mm	ASTM D3029 <sup>3)</sup>
Vicat softening temperature	121	°C	ASTM D1525
Shore D hardness	61	Shore D	ASTM D2240

<sup>1)</sup> Crosshead speed 50mm/min  
<sup>2)</sup> 100% Igepal C0630  
<sup>3)</sup> Tested on rotomoulded product



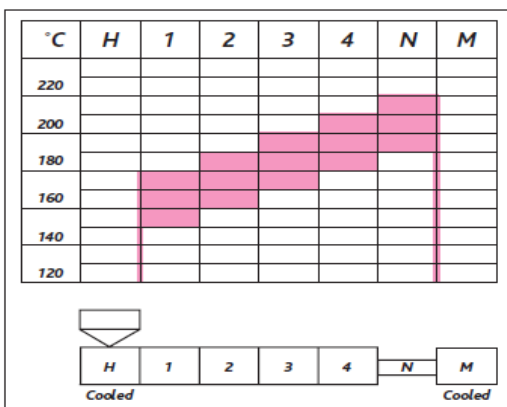
**Processing (Rotomoulding)**

An air temperature of 270 °C to 300 °C is recommended for processing of HR 411. Temperatures above 300 °C should be avoided as this would narrow the processing window considerably and could result in poor physical properties.

**Processing (Injection moulding)**

HR 411 has a medium melt viscosity making it unsuitable for moulds with long flow paths. Typical melt temperatures would be 200 °C - 280 °C. Parts can be demoulded at relatively high temperatures due to the material's high melting point and rigidity.

**Typical temperature profile (Injection moulding)**



**Presentation**

Supplied in pellet form packed in 25kg bags. Grinding of pellets is required to make it suitable for rotomoulding.

**Handling**

Workers should be protected from the possibility of skin or eye contact with molten polymer. Safety glasses are suggested as a minimal precaution to prevent possible mechanical or thermal injury to the eyes. Fabrication areas should be ventilated to carry away fumes or vapours.

**Combustibility**

Polyethylene resins will burn when supplied with adequate heat and oxygen. They should be handled and stored away from contact with direct flames and/or other ignition sources. In burning, polyethylene resins contribute high heat and may generate a dense black smoke. Fires can be extinguished by conventional means, with water and water mist preferred. In enclosed areas, fire fighters should be provided with self-contained breathing apparatus.

**Pigmentation (Rotomoulding)**

For colouring purposes inorganic pigments should be added at the lowest possible concentration and mixed in using a high speed mixer or a tumble blender, prior to moulding. Pigment preparations should contain only minimal amounts of dispersants.

**Food Packaging**

This material complies with F&DA regulation 177.1520 when used unmodified and according to good manufacturing practices for food contact applications. Accordingly, this material may be used in all food contact applications (except holding food during cooking).

**Conveying**

Conveying equipment should be designed to prevent accumulation of fines and dust particles that are contained in all polyethylene resins. These fines and dust particles can, under certain conditions, pose an explosion hazard. We recommend the conveying system used:

1. be equipped with adequate filters;
2. is operated and maintained in such a manner to ensure no leaks develop;
3. that adequate grounding exists at all times.

We further recommend good housekeeping be practised throughout the facility.

**Storage**

As ultraviolet light may cause a change in the material, all resins should be protected from direct sunlight during storage.

This information is based on our current knowledge and experience. In view of many factors that may affect processing and application, this data does not relieve processors from the responsibility of carrying out their own tests and experiments, neither does it imply any legally binding assurance of certain properties or of suitability for a specific purpose. It is the responsibility of those to whom we supply our products to ensure that any proprietary rights and existing laws and legislation are observed.

# Specification of Pyrogenic Silica (HDK® N20)



## HDK® N20 PYROGENIC SILICA

### Product description

Synthetic, hydrophilic amorphous silica, produced via flame hydrolysis.

### Special features

White colloidal powder of high purity.

### Application

HDK® N20 is applied as a thickening and thixotropic agent in many organic systems, e.g. in unsaturated polyesters, coatings, printing inks, adhesives, cosmetics and others. It is used as a reinforcing filler in elastomers, mainly silicone-elastomers. HDK® N20 acts as a free flow additive in the production of technical powders, in food and feed and in pharmaceutical products.

### Processing

A good dispersion of HDK® N20 is a must to assure optimum performance.

More detailed information about the application and processing of HDK® N20 is available in our HDK-brochures and on the WACKER web site (<http://www.wacker.com/hdk>).

### Storage

The 'Best use before end' date of each batch is shown on the shipping label and the certificate of analysis.

HDK® N20 should be stored in the original packaging in dry storage areas.

Storage beyond the date specified on the label does not necessarily mean that the product is no longer usable. In this case however, the properties required for the intended use must be checked for quality assurance reasons.

### Packaging

HDK® N20 is offered in following packaging:

- paper bags on pallet:  
10 kg bags
- Big bags:  
150 kg (big bags on pallets)
- Silotruck:  
depending on size of truck, approx. 3.5 to 5 tons

Details about packaging and handling:  
(<http://www.wacker.com/hdk>).

### Safety notes

Comprehensive instructions are given in the corresponding Material Safety Data Sheets. They are available on request from WACKER subsidiaries or may be printed via the WACKER web site (<http://www.wacker.com/hdk>).

During transportation and processing HDK® N20 may cause electrostatic charges. Like other amorphous silicas HDK® N20 does not show either carcinogenic (IARC classification, Volume 68, 1997) or mutagenic properties.



**Product data**

Typical general characteristics	Inspection Method	Value
SiO <sub>2</sub> content (based on the substance heated at 1000 °C for 2 h)	DIN EN ISO 3262-19	> 99,8 %
Loss of weight at 1000 °C / 2h (based on the substance dried at 105 °C for 2 h)	DIN EN ISO 3262-19	< 2 %
Density at 20 °C (SiO <sub>2</sub> )	DIN 51757	approx. 2,2 g/cm <sup>3</sup>
Refraction index at 20 °C		1,46
Silanol group density		2 SiOH/nm <sup>2</sup>
INCI name		Silica
<b>Physical-chemical properties</b>		
BET surface	DIN ISO 9277/ DIN 66132	170 - 230 m <sup>2</sup> /g
pH-Value (in 4 % aqueous dispersion)	DIN EN ISO 787-9	3,8 - 4,3
Tamped density	DIN EN ISO 787-11	approx. 40 g/l
Loss on drying , ex works (2h at 105 °C)	DIN EN ISO 787-2	< 1,5 %
Sieve residue , acc. to Mocker > 40 µm	DIN EN ISO 787-18	< 0,04 %

The data presented in this leaflet are in accordance with the present state of our knowledge, but do not absolve the user from carefully checking all supplies immediately on receipt. We reserve the right to alter product constants within the scope of technical progress or new developments. The recommendations made in this leaflet should be checked by preliminary trials because of conditions during processing over which we have no control, especially where other companies' raw materials are also being used. The recommendations do not absolve the user from the obligation of investigating the possibility of infringement of third parties' rights and, if necessary, clarifying the position. Recommendations for use do not constitute a warranty, either express or implied, of the fitness or suitability of the products for a particular purpose.

The management system has been certified according to DIN EN ISO 9001 and DIN EN ISO 14001

WACKER is a trademark of Wacker Chemie AG.  
HDK® is a trademark of Wacker Chemie AG.

For technical, quality, or product safety questions, please contact:

Wacker Chemie AG  
Hanns-Seidel-Platz 4  
81737 München, Germany  
hdk@wacker.com

[www.wacker.com/hdk](http://www.wacker.com/hdk)

## Specification of Organoclay DELLITE® 43B

Additives Business Unit/Plastics

### DELLITE® 43B Nanoclay for nanocomposites

**Description**  
DELLITE® 43B is a nanoclay deriving from a naturally occurring montmorillonite especially purified and modified with a quaternary ammonium salt (dimethyl benzylhydrogenated tallow ammonium). DELLITE® 43B is an additive for polymer application, used to improve various physical and thermo-mechanical properties.

**Applications**

- Polyolefins
- Polyester
- Polystyrene
- Ethylene Vinyl Acetate
- Polyamides
- Epoxy and acrylic resins
- Rubbers and Elastomers
- (...)

**Advantages of Dellite® 43B in Polymeric Systems**

- Oxygen, CO<sub>2</sub> and water vapour barrier
- Thermal stability
- Stiffness
- Melt fracture reduction
- Solvent/Chemical resistance
- Weight reduction
- Fibreglas reduction
- Rheology control
- UV transmission
- Flame retardant and Antidropping
- (...)

**Chemical and physical data**

		DELLITE® 43B
Colour		off white
Moisture	%	3 (max)
Loss of ignition	weight %	32 - 35
Particle size (dry)	micron	7-9 (medium)
Particle size after dispersion	nm	1x500 (medium)
Modifier		dimethyl benzylhydrogenated tallow ammonium
Specific weight	g/cc	1.6
Bulk density	g/cc	0.40


**Incorporation**

- **Thermoplastic Systems**  
According to the application the incorporation of Dellite® 43B into a thermoplastic system is usually carried out as follows:
  - a) Adding up to 50% of Dellite® 43B in a masterbatch and diluting the master in the final compound
  - b) Adding directly the Dellite® 43B to the compound.
- **Thermoset Systems**  
The incorporation of Dellite® 43B into a thermoset system may be obtained using the following methods:
  - a) Mixing the desired amount of Dellite® with the resin. Then the curing agent and other additives may be added.
  - b) Mixing the desired amount of Dellite® with the curing agent. Then the resin and other additives may be added.
  - c) Resin, curing agent and additives are mixed and then Dellite® 43B is added.

**Dosage**  
The typical levels of use are included in the range 1-5% based on total system weight.

**Storage Stability and Packing**  
Product does not deteriorate in a significant way in a twelve months period.  
Storage is advisable in a dry sheltered place in closed bags.  
Packing is 25kg net paper bags on wood pallets of 1200kg each. Different packing is possible if required.

All information contained here in is believed to be accurate but is not warranted. It doesn't represent any assurance of properties and fitness for use of the product. Above mentioned specifications may be changed without any notice.



**LAVIOSA CHIMICA MINERARIA S.p.A.**

I-57123 LIVORNO • Via Leonardo da Vinci, 21  
Tel. (+39) 0586 434000 - Fax (+39) 0586 410852  
www.laviosa.it • E-mail: [additives@laviosa.it](mailto:additives@laviosa.it)

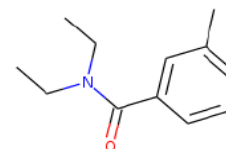
**COMPANY  
WITH QUALITY SYSTEM  
CERTIFIED BY DNV**

Pag. 1 of 1 = **ISO 9001/2000** =

## Appendix XVIII: Physical properties of mosquito repellents

## Diethyltoluamide

**Other names:** 3-Methyl-N,N-diethylbenzamide; A.I. 3-22542; AI 3-22542; Amincene C 140; Amincene C-EM; Autan; Benzamide, N,N-diethyl-3-methyl-; Chemform; DEET; DET; DET (insect repellent); DETA; DETA-20; Delphene; Detamide; Dieltamid; Diethyl-m-toluamide; ENT 20,218; ENT 22542; Flypel; M-DET; MGK diethyltoluamide; Metadelphene; N,N-Diethyl-3-methylbenzamide; N,N-Diethyl-m-Toluamide; NSC 33840; Naugatuck DET; Off; Repel; Repper-DET; Repudin-Special; m-DETA; m-Delphene; m-Toluamide, N,N-diethyl-; m-Toluic Acid diethylamide.



**InChI:** InChI=1S/C12H17NO/c1-4-13(5-2)12(14)11-8-6-7-10(3)9-11/h6-9 H,4-5H2,1-3H3

**InChI Key:** MMOXZBCLCQITDF-UHFFFAOYSA-N

**Formula:** C<sub>12</sub>H<sub>17</sub>NO

**SMILES:** CCN(CC)C(=O)c1cccc(C)c1

**Molecular Weight:** 191.27

**CAS:** 134-62-3

### Physical Properties

Property	Value	Unit	Source
$\Delta_f G^\circ$	134.80	kJ/mol	Joback Method
$\Delta_f H^\circ_{\text{gas}}$	-111.00	kJ/mol	Joback Method
$\Delta_{\text{fus}} H^\circ$	25.11	kJ/mol	Joback Method
$\Delta_{\text{vap}} H^\circ$	54.03	kJ/mol	Joback Method
$\log P_{\text{oct/wat}}$	2.48		Crippen Method
$P_c$	2517.59	kPa	Joback Method
$T_{\text{boil}}$	433.20	K	NIST Webbook
$T_{\text{boil}}$	384.20	K	NIST Webbook
$T_c$	778.19	K	Joback Method
$T_{\text{fus}}$	346.34	K	Joback Method
$V_c$	0.62	m <sup>3</sup> /kg-mol	Joback Method

### Temperature Dependent Properties

Property	Value	Unit	Temperature (K)	Source
$C_{p,gas}$	404.24	J/mol×K	571.93	Joback Method

## Sources

**Joback Method:** [https://en.wikipedia.org/wiki/Joback\\_method](https://en.wikipedia.org/wiki/Joback_method)

**NIST Webbook:** [http://webbook.nist.gov/cgi/inchi/InChI=1S/C12H17NO/c1-4-13\(5-2\)12\(14\)11-8-6-7-10\(3\)9-11/h6-9H,4-5H2,1-3H3](http://webbook.nist.gov/cgi/inchi/InChI=1S/C12H17NO/c1-4-13(5-2)12(14)11-8-6-7-10(3)9-11/h6-9H,4-5H2,1-3H3)

**Crippen Method:** <http://pubs.acs.org/doi/abs/10.1021/ci9903071>

## Legend

$C_{p,gas}$ : Ideal gas heat capacity (J/mol×K).

$\Delta_f G^\circ$ : Standard Gibbs free energy of formation (kJ/mol).

$\Delta_f H^\circ_{gas}$ : Enthalpy of formation at standard conditions (kJ/mol).

$\Delta_{fus} H^\circ$ : Enthalpy of fusion at standard conditions (kJ/mol).

$\Delta_{vap} H^\circ$ : Enthalpy of vaporization at standard conditions (kJ/mol).

$logP_{oct/wat}$ : Octanol/Water partition coefficient .

$P_c$ : Critical Pressure (kPa).

$T_{boil}$ : Normal Boiling Point Temperature (K).

$T_c$ : Critical Temperature (K).

$T_{fus}$ : Normal melting (fusion) point (K).

$V_c$ : Critical Volume (m<sup>3</sup>/kg-mol).

Latest version available from:

<https://www.cheméo.com/cid/13-638-9/Diethyltoluamide>

Generated by Cheméo on Sun, 13 May 2018 20:54:42 +0000.

**Cheméo** (<https://www.cheméo.com>) is the biggest free database of chemical and physical data for the process industry.

## Benzoic acid, 2-amino-, ethyl ester

**Other names:** Benzoic acid, 2-amino-, ethyl ester.

**InChI:**

InChI=1S/C9H11NO2/c1-2-12-9(11)7-5-3-4-6-8(7)10/h3-6H,2,10H2,1H3

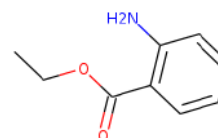
**InChI Key:** TWLLPUMZVVGILS-UHFFFAOYSA-N

**Formula:** C9H11NO2

**SMILES:** CCOC(=O)c1ccccc1N

**Molecular Weight:** 165.19

**CAS:** 87-25-2



### Physical Properties

Property	Value	Unit	Source
$\Delta_f G^\circ$	-39.79	kJ/mol	Joback Method
$\Delta_f H^\circ_{\text{gas}}$	-215.04	kJ/mol	Joback Method
$\Delta_{\text{fus}} H^\circ$	20.70	kJ/mol	Joback Method
$\Delta_{\text{vap}} H^\circ$	58.36	kJ/mol	Joback Method
$\log P_{\text{oct/wat}}$	1.446		Crippen Method
$P_c$	3615.89	kPa	Joback Method
$T_{\text{boil}}$	541.20	K	NIST Webbook
$T_{\text{boil}}$	540.00 ± 1.00	K	NIST Webbook
$T_{\text{boil}}$	402.70	K	NIST Webbook
$T_{\text{boil}}$	419.20	K	NIST Webbook
$T_{\text{boil}}$	419.00 ± 1.00	K	NIST Webbook
$T_c$	812.12	K	Joback Method
$T_{\text{fus}}$	286.00	K	NIST Webbook
$T_{\text{fus}}$	287.50 ± 0.02	K	NIST Webbook
$V_c$	0.484	m <sup>3</sup> /kg-mol	Joback Method

### Temperature Dependent Properties

Property	Value	Unit	Temperature (K)	Source
$C_{p,\text{gas}}$	310.15	J/mol×K	585.8	Joback Method
$\Delta_{\text{vap}}H$	59.60	kJ/mol	513.0	NIST Webbook

## Sources

**Joback Method:** [https://en.wikipedia.org/wiki/Joback\\_method](https://en.wikipedia.org/wiki/Joback_method)

**NIST Webbook:**

[http://webbook.nist.gov/cgi/inchi/InChI=1S/C9H11NO2/c1-2-12-9\(11\)7-5-3-4-6-8\(7\)10/h3-6H,2,10H2,1H3](http://webbook.nist.gov/cgi/inchi/InChI=1S/C9H11NO2/c1-2-12-9(11)7-5-3-4-6-8(7)10/h3-6H,2,10H2,1H3)

**Crippen Method:** <http://pubs.acs.org/doi/abs/10.1021/ci9903071>

## Legend

$C_{p,\text{gas}}$ : Ideal gas heat capacity (J/mol×K).

$\Delta_f G^\circ$ : Standard Gibbs free energy of formation (kJ/mol).

$\Delta_f H^\circ_{\text{gas}}$ : Enthalpy of formation at standard conditions (kJ/mol).

$\Delta_{\text{fus}} H^\circ$ : Enthalpy of fusion at standard conditions (kJ/mol).

$\Delta_{\text{vap}} H^\circ$ : Enthalpy of vaporization at standard conditions (kJ/mol).

$\Delta_{\text{vap}} H$ : Enthalpy of vaporization at a given temperature (kJ/mol).

$\log P_{\text{oct/wat}}$ : Octanol/Water partition coefficient .

$P_c$ : Critical Pressure (kPa).

$T_{\text{boil}}$ : Normal Boiling Point Temperature (K).

$T_c$ : Critical Temperature (K).

$T_{\text{fus}}$ : Normal melting (fusion) point (K).

$V_c$ : Critical Volume ( $\text{m}^3/\text{kg}\cdot\text{mol}$ ).

Latest version available from:

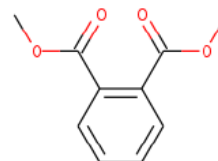
<https://www.cheméo.com/cid/32-146-4/Benzoic%20acid%2C%202-amino-%2C%20ethyl%20ester>

Generated by Cheméo on Sun, 13 May 2018 20:51:25 +0000.

**Cheméo** (<https://www.cheméo.com>) is the biggest free database of chemical and physical data for the process industry.

## Dimethyl phthalate

**Other names:** 1,2-Benzenedicarboxylic acid, 1,2-dimethyl ester; 1,2-Benzenedicarboxylic acid, dimethyl ester; 1,2-dimethyl phthalate; 64441-70-9; Avolin; DMF, Insect repellent; DMP; Dimethyl 1,2-benzenedicarboxylate; Dimethyl 1,2-benzenedicarboxylate; Dimethyl benzene-o-dicarboxylate; Dimethyl benzeneorthodicarboxylate; Dimethyl o-phthalate; Dimethyl orthophthalate; ENT 262; Fermine; Kemester DMP; Kodaflex DMP; Mipax; NSC 15398; NTM; Palatinol M; Phthalic acid, dimethyl ester; Phthalsaeuredimethylester; Repeftal; Solvanom; Solvarone; Unimoll DM; Uniplex 110.



**InChI:**

InChI=1S/C10H10O4/c1-13-9(11)7-5-3-4-6-8(7)10(12)14-2/h3-6H,1-2H3

**InChI Key:** NIQCNGHVCWTJSM-UHFFFAOYSA-N

**Formula:** C<sub>10</sub>H<sub>10</sub>O<sub>4</sub>

**SMILES:** COC(=O)c1ccccc1C(=O)OC

**Molecular Weight:** 194.18

**CAS:** 131-11-3

## Physical Properties

Property	Value	Unit	Source
$\Delta_c H^\circ_{\text{liquid}}$	-4702.00	kJ/mol	NIST Webbook
$\Delta_c H^\circ_{\text{solid}}$	-4680.40 ± 2.40	kJ/mol	NIST Webbook
EA	0.55	eV	NIST Webbook
$\Delta_f G^\circ$	-331.74	kJ/mol	Joback Method
$\Delta_f H^\circ_{\text{gas}}$	-606.10 ± 2.70	kJ/mol	NIST Webbook
$\Delta_f H^\circ_{\text{solid}}$	-683.80 ± 2.70	kJ/mol	NIST Webbook
$\Delta_{\text{fus}} H^\circ$	20.88	kJ/mol	Joback Method
$\Delta_{\text{sub}} H^\circ$	77.70	kJ/mol	NIST Webbook
$\Delta_{\text{vap}} H^\circ$	59.10	kJ/mol	Joback Method
IE	9.64 ± 0.07	eV	NIST Webbook
$\log P_{\text{oct/wat}}$	1.26		Crippen Method
$P_c$	3191.93	kPa	Joback Method
$S^\circ_{\text{liquid}}$	365.50	J/mol×K	NIST Webbook
$T_{\text{boil}}$	555.20	K	NIST Webbook

Property	Value	Unit	Source
$T_{\text{boil}}$	555.50	K	NIST Webbook
$T_{\text{boil}}$	$389.30 \pm 0.30$	K	NIST Webbook
$T_{\text{c}}$	831.50	K	Joback Method
$T_{\text{fus}}$	273.00	K	NIST Webbook
$T_{\text{fus}}$	$273.20 \pm 0.20$	K	NIST Webbook
$T_{\text{triple}}$	$274.18 \pm 0.02$	K	NIST Webbook
$V_{\text{c}}$	0.54	$\text{m}^3/\text{kg-mol}$	Joback Method

### Temperature Dependent Properties

Property	Value	Unit	Temperature (K)	Source
$C_{\text{p,gas}}$	338.80	J/mol×K	612.44	Joback Method
$C_{\text{p,liquid}}$	303.80	J/mol×K	300.0	NIST Webbook
$\eta$	0.00	Pa×s	612.44	Joback Method
$\Delta_{\text{fus}}H$	16.95	kJ/mol	274.18	NIST Webbook
$\Delta_{\text{fus}}H$	16.95	kJ/mol	274.2	NIST Webbook
$\Delta_{\text{fus}}H$	16.95	kJ/mol	274.2	NIST Webbook
$\Delta_{\text{vap}}H$	$74.50 \pm 0.30$	kJ/mol	326.0	NIST Webbook
$\Delta_{\text{vap}}H$	78.70	kJ/mol	337.5	NIST Webbook
$\Delta_{\text{vap}}H$	$72.50 \pm 0.60$	kJ/mol	344.0	NIST Webbook
$\Delta_{\text{vap}}H$	$69.40 \pm 0.10$	kJ/mol	365.0	NIST Webbook
$\Delta_{\text{vap}}H$	68.60	kJ/mol	408.5	NIST Webbook
$\Delta_{\text{vap}}H$	63.70	kJ/mol	459.0	NIST Webbook
$\Delta_{\text{vap}}H$	61.50	kJ/mol	492.0	NIST Webbook
$\Delta_{\text{fus}}S$	61.80	J/mol×K	274.18	NIST Webbook

### Sources

Joback Method: [https://en.wikipedia.org/wiki/Joback\\_method](https://en.wikipedia.org/wiki/Joback_method)



**NIST Webbook:**

[http://webbook.nist.gov/cgi/inchi/InChI=1S/C10H10O4/c1-13-9\(11\)7-5-3-4-6-8\(7\)10\(12\)14-2/h3-6H,1-2H3](http://webbook.nist.gov/cgi/inchi/InChI=1S/C10H10O4/c1-13-9(11)7-5-3-4-6-8(7)10(12)14-2/h3-6H,1-2H3)

**Crippen Method:** <http://pubs.acs.org/doi/abs/10.1021/ci9903071>

## Legend

$\Delta_c H^\circ_{\text{liquid}}$ : Standard liquid enthalpy of combustion (kJ/mol).

$\Delta_c H^\circ_{\text{solid}}$ : Standard solid enthalpy of combustion (kJ/mol).

$C_{p,\text{gas}}$ : Ideal gas heat capacity (J/mol×K).

$C_{p,\text{liquid}}$ : Liquid phase heat capacity (J/mol×K).

$\eta$ : Dynamic viscosity (Pa×s).

**EA**: Electron affinity (eV).

$\Delta_f G^\circ$ : Standard Gibbs free energy of formation (kJ/mol).

$\Delta_f H^\circ_{\text{gas}}$ : Enthalpy of formation at standard conditions (kJ/mol).

$\Delta_f H^\circ_{\text{solid}}$ : Solid phase enthalpy of formation at standard conditions (kJ/mol).

$\Delta_{\text{fus}} H^\circ$ : Enthalpy of fusion at standard conditions (kJ/mol).

$\Delta_{\text{fus}} H$ : Enthalpy of fusion at a given temperature (kJ/mol).

$\Delta_{\text{sub}} H^\circ$ : Enthalpy of sublimation at standard conditions (kJ/mol).

$\Delta_{\text{vap}} H^\circ$ : Enthalpy of vaporization at standard conditions (kJ/mol).

$\Delta_{\text{vap}} H$ : Enthalpy of vaporization at a given temperature (kJ/mol).

**IE**: Ionization energy (eV).

**logP<sub>oct/wat</sub>**: Octanol/Water partition coefficient.

$P_c$ : Critical Pressure (kPa).

$\Delta_{\text{fus}} S$ : Entropy of fusion at a given temperature (J/mol×K).

$S^\circ_{\text{liquid}}$ : Liquid phase molar entropy at standard conditions (J/mol×K).

$T_{\text{boil}}$ : Normal Boiling Point Temperature (K).

$T_c$ : Critical Temperature (K).

$T_{\text{fus}}$ : Normal melting (fusion) point (K).

$T_{\text{triple}}$ : Triple Point Temperature (K).

$V_c$ : Critical Volume (m<sup>3</sup>/kg-mol).

Latest version available from:

<https://www.cheméo.com/cid/21-720-8/Dimethyl%20phthalate>

Generated by Cheméo on Sun, 13 May 2018 15:10:17 +0000.

**Cheméo** (<https://www.cheméo.com>) is the biggest free database of chemical and physical data for the process industry.

## Decanoic acid

**Other names:** 1-Decanoic acid; 1-Nonanecarboxylic acid; Capric acid; Caprinic acid; Caprynic acid; Decanoic acid; Decanoic acid (capric acid); Decoic acid; Decylic acid; Emery 659; Hexacid 1095; NSC 5025; Nonane-1-carboxylic acid; Prifrac 296; n-Capric acid; n-Decoic acid; n-Decylic acid; neo-Fat 10.

**InChI:**

InChI=1S/C10H20O2/c1-2-3-4-5-6-7-8-9-10(11)12/h2-9H2,1H3,(H,11,12)

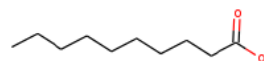
**InChI Key:** GHVNFZFCNZKVNT-UHFFFAOYSA-N

**Formula:** C10H20O2

**SMILES:** CCCCCCCCC(=O)O

**Molecular Weight:** 172.26

**CAS:** 334-48-5



### Physical Properties

Property	Value	Unit	Source
$\Delta_c H^\circ_{\text{liquid}}$	-6079.30 ± 0.90	kJ/mol	NIST Webbook
$\Delta_f G^\circ$	-232.42	kJ/mol	Joback Method
$\Delta_f H^\circ_{\text{gas}}$	-624.20 ± 5.10	kJ/mol	NIST Webbook
$\Delta_{\text{fus}} H^\circ$	27.34	kJ/mol	Joback Method
$\Delta_{\text{sub}} H^\circ$	130.00 ± 5.00	kJ/mol	NIST Webbook
$\Delta_{\text{sub}} H^\circ$	119.00 ± 2.00	kJ/mol	NIST Webbook
$\Delta_{\text{sub}} H^\circ$	118.80 ± 2.20	kJ/mol	NIST Webbook
$\Delta_{\text{vap}} H^\circ$	61.28	kJ/mol	Joback Method
$\log P_{\text{oct/wat}}$	3.212		Crippen Method
$P_c$	2100.00 ± 400.00	kPa	NIST Webbook
$P_c$	2161.74 ± 90.00	kPa	NIST Webbook
$P_{\text{triple}}$	0.00 ± 0.00	kPa	NIST Webbook
$T_{\text{boil}}$	422.20	K	NIST Webbook
$T_{\text{boil}}$	543.20	K	NIST Webbook
$T_{\text{boil}}$	541.00 ± 2.00	K	NIST Webbook
$T_{\text{boil}}$	542.15 ± 3.00	K	NIST Webbook

Property	Value	Unit	Source
$T_{\text{boil}}$	$541.95 \pm 1.00$	K	NIST Webbook
$T_{\text{boil}}$	$435.65 \pm 3.00$	K	NIST Webbook
$T_{\text{boil}}$	$535.65 \pm 5.00$	K	NIST Webbook
$T_{\text{boil}}$	$540.15 \pm 4.00$	K	NIST Webbook
$T_{\text{boil}}$	$544.15 \pm 3.00$	K	NIST Webbook
$T_{\text{boil}}$	$541.65 \pm 3.00$	K	NIST Webbook
$T_{\text{boil}}$	$542.15 \pm 4.00$	K	NIST Webbook
$T_{\text{c}}$	$726.00 \pm 4.00$	K	NIST Webbook
$T_{\text{c}}$	$720.53 \pm 3.00$	K	NIST Webbook
$T_{\text{fus}}$	$304.70 \pm 0.05$	K	NIST Webbook
$T_{\text{fus}}$	$304.00 \pm 1.60$	K	NIST Webbook
$T_{\text{fus}}$	$303.90 \pm 1.00$	K	NIST Webbook
$T_{\text{fus}}$	$305.00 \pm 3.00$	K	NIST Webbook
$T_{\text{fus}}$	$303.40 \pm 0.50$	K	NIST Webbook
$T_{\text{fus}}$	$304.00 \pm 2.00$	K	NIST Webbook
$T_{\text{fus}}$	$303.65 \pm 2.00$	K	NIST Webbook
$T_{\text{fus}}$	$302.90 \pm 1.50$	K	NIST Webbook
$T_{\text{fus}}$	$304.40 \pm 0.20$	K	NIST Webbook
$T_{\text{fus}}$	$304.15 \pm 2.00$	K	NIST Webbook
$T_{\text{fus}}$	$300.10 \pm 1.00$	K	NIST Webbook
$T_{\text{fus}}$	$304.60 \pm 2.00$	K	NIST Webbook
$T_{\text{triple}}$	$304.55 \pm 0.02$	K	NIST Webbook
$T_{\text{triple}}$	$303.95 \pm 0.50$	K	NIST Webbook
$V_{\text{c}}$	0.621	$\text{m}^3/\text{kg}\cdot\text{mol}$	Joback Method

## Temperature Dependent Properties

Property	Value	Unit	Temperature (K)	Source
$C_{p,gas}$	402.78	J/mol×K	574.25	Joback Method
$C_{p,solid}$	361.10	J/mol×K	285.0	NIST Webbook
$C_{p,solid}$	475.59	J/mol×K	298.15	NIST Webbook
$\eta$	0.0001043	Pa×s	574.25	Joback Method
$\Delta_{fus}H$	29.22	kJ/mol	300.1	NIST Webbook
$\Delta_{fus}H$	28.30	kJ/mol	303.8	NIST Webbook
$\Delta_{fus}H$	27.99	kJ/mol	304.4	NIST Webbook
$\Delta_{fus}H$	27.82	kJ/mol	304.5	NIST Webbook
$\Delta_{fus}H$	27.99	kJ/mol	304.5	NIST Webbook
$\Delta_{sub}H$	117.00 ± 2.00	kJ/mol	289.8	NIST Webbook
$\Delta_{sub}H$	117.10 ± 1.70	kJ/mol	295.5	NIST Webbook
$\Delta_{vap}H$	88.60	kJ/mol	314.0	NIST Webbook
$\Delta_{vap}H$	71.40	kJ/mol	418.0	NIST Webbook
$\Delta_{vap}H$	76.40	kJ/mol	470.5	NIST Webbook
$\Delta_{fus}S$	97.40	J/mol×K	300.1	NIST Webbook
$\Delta_{fus}S$	92.00	J/mol×K	304.4	NIST Webbook

## Sources

**Joback Method:** [https://en.wikipedia.org/wiki/Joback\\_method](https://en.wikipedia.org/wiki/Joback_method)

**NIST Webbook:**

[http://webbook.nist.gov/cgi/inchi/InChI=1S/C10H20O2/c1-2-3-4-5-6-7-8-9-10\(11\)12/h2-9H2,1H3,\(H,11,12\)](http://webbook.nist.gov/cgi/inchi/InChI=1S/C10H20O2/c1-2-3-4-5-6-7-8-9-10(11)12/h2-9H2,1H3,(H,11,12))

**Crippen Method:** <http://pubs.acs.org/doi/abs/10.1021/ci9903071>

## Legend

$\Delta_c H^\circ_{liquid}$ : Standard liquid enthalpy of combustion (kJ/mol).

$C_{p,gas}$ : Ideal gas heat capacity (J/mol×K).

$C_{p,solid}$ : Solid phase heat capacity (J/mol×K).

$\eta$ : Dynamic viscosity (Pa×s).

$\Delta_f G^\circ$ : Standard Gibbs free energy of formation (kJ/mol).

$\Delta_f H^\circ_{gas}$ : Enthalpy of formation at standard conditions (kJ/mol).

$\Delta_{\text{fus}}H^\circ$ : Enthalpy of fusion at standard conditions (kJ/mol).  
 $\Delta_{\text{fus}}H$ : Enthalpy of fusion at a given temperature (kJ/mol).  
 $\Delta_{\text{sub}}H^\circ$ : Enthalpy of sublimation at standard conditions (kJ/mol).  
 $\Delta_{\text{sub}}H$ : Enthalpy of sublimation at a given temperature (kJ/mol).  
 $\Delta_{\text{vap}}H^\circ$ : Enthalpy of vaporization at standard conditions (kJ/mol).  
 $\Delta_{\text{vap}}H$ : Enthalpy of vaporization at a given temperature (kJ/mol).  
 $\log P_{\text{oct/wat}}$ : Octanol/Water partition coefficient .  
 $P_c$ : Critical Pressure (kPa).  
 $P_{\text{triple}}$ : Triple Point Pressure (kPa).  
 $\Delta_{\text{fus}}S$ : Entropy of fusion at a given temperature (J/mol×K).  
 $T_{\text{boil}}$ : Normal Boiling Point Temperature (K).  
 $T_c$ : Critical Temperature (K).  
 $T_{\text{fus}}$ : Normal melting (fusion) point (K).  
 $T_{\text{triple}}$ : Triple Point Temperature (K).  
 $V_c$ : Critical Volume (m<sup>3</sup>/kg-mol).

Latest version available from:

<https://www.chemeo.com/cid/39-862-2/Decanoic%20acid>

Generated by Cheméo on Sun, 13 May 2018 20:59:21 +0000.

**Cheméo** (<https://www.chemeo.com>) is the biggest free database of chemical and physical data for the process industry.